NONLINEAR ANALYSIS OF REINFORCED CONCRETE FLAT-PLATE STRUCTURES SUBJECTED TO LATERAL LOADING

by

Husam Anwar Omar

A thesis
presented to the University of Manitoba
in fulfillment of the
thesis requirement for the degree of
Doctor of Philosophy
in
Civil Engineering

Winnipeg, Manitoba

ISBN 0-315-44194-1

NON-LINEAR ANALYSIS OF REINFORCED CONCRETE FLAT-PLATE STRUCTURES SUBJECTED TO LATERAL LOADING

BY

HUSAM ANWAR OMAR

A thesis submitted to the Faculty of Graduate Studies of the University of Manitoba in partial fulfillment of the requirements of the degree of

DOCTOR OF PHILOSOPHY

I hereby declare that I am the sole author of this thesis.

I authorize the University of Manitoba to lend this thesis to other institutions or individuals for the purpose of scholarly research.

Husam Anwar Omar

I further authorize the University of Manitoba to reproduce this thesis by photocopying or by other means, in total or in part, at the request of other institutions or individuals for the purpose of scholarly research.

Husam Anwar Omar

The University of Manitoba requires the signatures of all persons using or photocopying this thesis. Please sign below, and give address and date.

Signature	Address	Date

ABSTRACT

Flat-plate structures tend to experience excessive drifts when subjected to lateral loads. This is due mainly to the nonlinear deformations at the plate-to-column connections. Most of the analysis methods available today do not account for these deformations. Therefore they tend to underestimate the lateral drifts. Several models have been developed to predict the nonlinear behaviour of this type of structure. However they are too complex to be incorporated into a routine structural analysis program.

In this study, a simple-to-use computer program is developed for analyzing laterally-loaded flat-plate structures, with or without shear walls. The nonlinear moment-rotation behaviour at the plate-to-column connections is accounted for by incorporating standardized moment-rotation functions into the computer program. The functions are derived using available experimental data and a modified Ramberg-Osgood function. Several examples are included to demonstrate the capabilities of the program and to compare the results obtained from the nonlinear analysis with results published in the literature.

ACKNOWLEDGEMENT

I would like to express my sincere thanks to Professor Glenn Morris for his continous support and guidance throughout this project. Thanks are also due to Professors John Glanville, Ray Han, and Bob Loov for their assistance in reviewing this thesis.

I wish to thank my family and wife for their support, patience and continous encouragement during this project.

NOMENCLATURE

A = cross-sectional area

a_j = dimensionless exponent which indicates the influence of the jth connection parameter on the moment-rotation relationship

B_i = width of interior plate strip

B_i' = interior equivalent beam width

B_e = width of edge plate strip

B_e' = edge equivalent beam width

C = square column dimension

C_1, C_2, C_3, C_4 = constants used in evaluating Lagrange interpolation function

D = vector of local end displacements

E = modulus of elasticity

f_c' = concrete 28 day compressive strength

G = shear modulus

h = flexural rigidity of flat-plate floor

$$= \frac{E\, t^3}{12\,(1 - \nu^2)}$$

H' = translation transformation matrix

I_1 = second moment of area about the local X_1 axis

I_2 = second moment of area about the local X_2 axis

I_3 = second moment of area about the local X_3 axis

J = St. Venant torsion constant

k_{ij} = stiffness coefficients relating degrees of freedom i and j

K_α = stiffness matrix corresponding to column-depth-to-plate-span ratio = $1/\alpha$

K_p = panel condensed stiffness matrix

K = stiffness matrix of a structural component expressed in local system

K' = stiffness matrix of a structural component, expressed in the global system

L_1 = plate span parallel to the applied moment

L_2 = plate span normal to the applied moment

L = square plate panel span

L_h = storey height

L_g = distance from center of column to location of concentrated gravity load

L_s = span of specimens used in testing plate-column connections

M_g = gravity-load moment at the column face

M = moment due to lateral loading

M' = normalized moment due to lateral loading

M_c = plate cracking moment at the column face

m = number of connection parameters considered in deriving the standardized moment-rotation functions

p_j = numerical value of paramenter p for connection j

P = force vector expressed in local system

P' = force vector expressed in global system

q = rigidity ratio of the spring at beam end b

R = rotational transformation matrix

r = factor that scales the ordinates on the standardized moment-rotation curve, according to their dependence upon the connection parameters

SF = flexibility of flexural spring

S_a = flexural spring stiffness at beam end a

S_b = flexural spring stiffness at beam end b

t = plate total thickness

t_w = shear wall total thickness

T = translation transformation matrix

W = shear wall width

β = angle between local and global axes

ν = Poisson ratio

ϕ = plate-to-column connection rotation

ϕ_c = portion of plate-to-column connection rotation caused by column deformation

ϕ_s = portion of plate-to-column connection rotation caused by spring rotation

ρ = plate steel ratio in the immediate vicinity of the column

ρ_t = sum of plate top and bottom steel ratios in the column immediate vicinity

CONTENTS

LIST OF FIGURES

LIST OF TABLES

Chapter I

INTRODUCTION

1.1 NATURE OF THE PROBLEM

A flat-plate concrete frame is a structure composed of columns and flat-plate floors without drop panels, beams or column capitals as illustrated in Figure 1.1. In some cases the structure may incorporate shear walls, as illustrated in Figure 1.2. The flat plate frame has several advantages for multistorey residential and office buildings. It requires only relatively simple and repetitive formwork, thus minimizing construction costs. The absence of beams minimizes the overall depth of structural components, thus facilitating the installation of mechanical and electrical services. Columns can be easily incorporated into the walls, so it is easy to make the final structure aesthetically pleasing. Finally, the rectangular grid of columns is well suited to office and residential requirements.

The resistance of this type of structure to lateral loads is normally provided by the combination of the three-dimensional frame, composed of the flat-plate floors and the supporting columns, and shear walls. It has been observed that while they possess sufficient strength to resist lateral loads, reinforced-concrete flat-plate frames sometimes tend

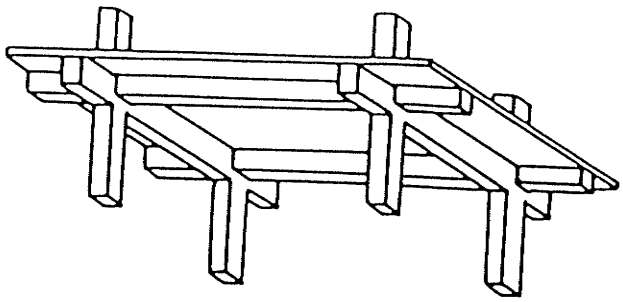

(a) 2-way slab with beams

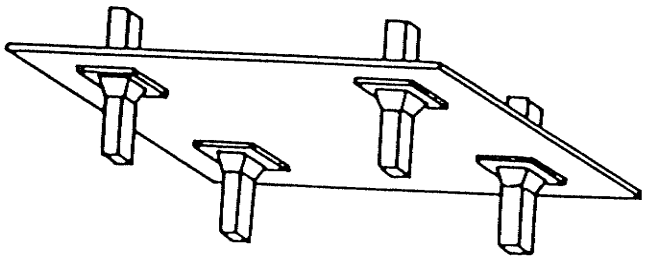

(b) 2-way slab without beams
(drop panels and column capitals)

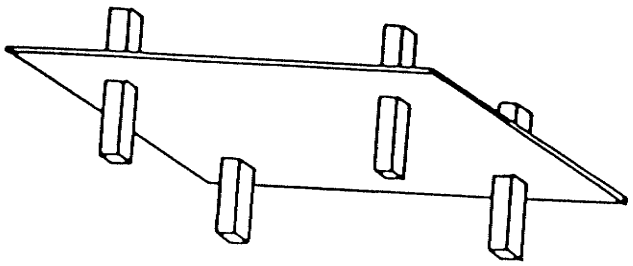

(c) 2-way slab without beams
(flat plate)

Figure 1.1: Types of Two-Way Slab Systems

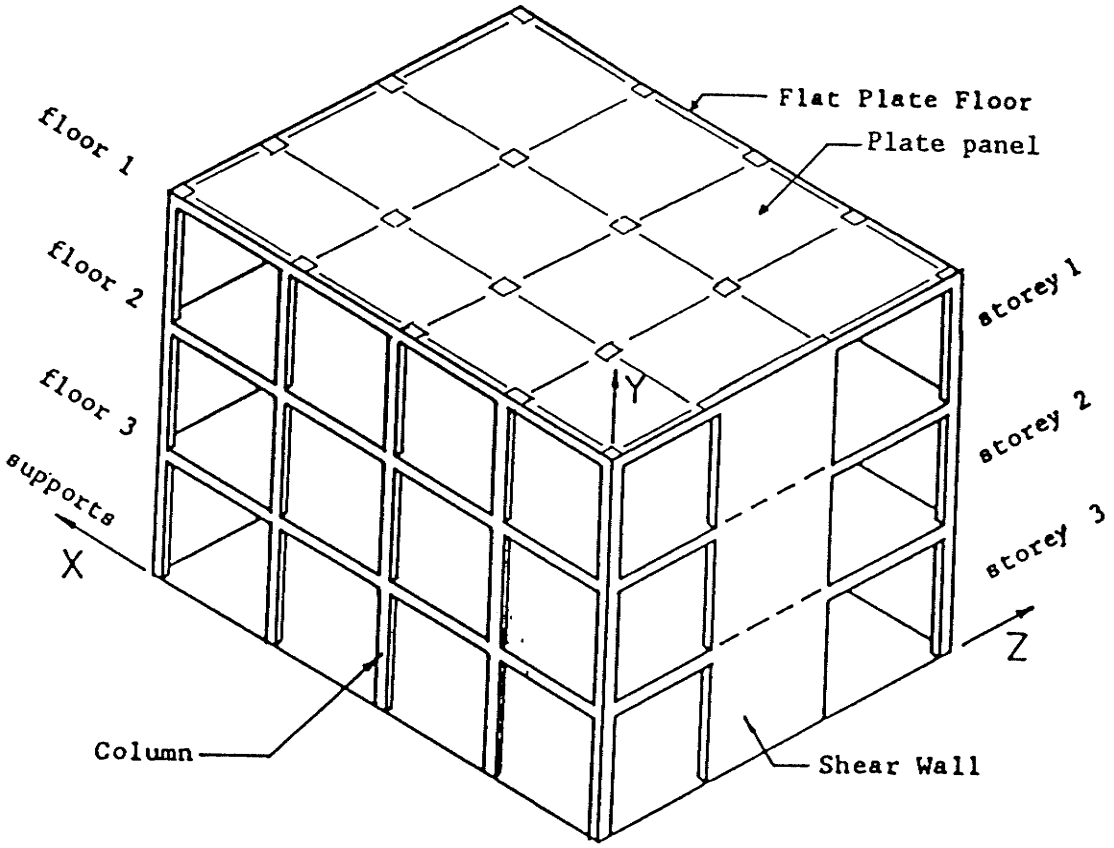

Figure 1.2: Typical Flat-Plate Structure With Shear Wall

to experience excessive lateral drift. A large proportion of the drift is associated with deformations in the plate immediately adjacent to the columns. These deformations result primarily from cracking of the concrete and bond slip of the reinforcement, and they cause the structure to behave nonlinearly starting at low stages of loading. In this study, the junction between a column and a flat-plate floor will be referred to as a "plate-to-column connection", and the deformations referred to above will be assumed to be concentrated at the connections.

Several linear, elastic models have been developed to analyze the load-displacement behaviour of flat-plate structures under lateral load. The results obtained using these models have been found to vary considerably depending upon the model used and the parameters considered. In general, the linear models do not represent the true behaviour of the structure, and in some instances they produce results that are not conservative. Thus, there is an apparent need for a rational, simple-to-use model that can account for the nonlinear behaviour at the plate-to-column connections. The difficulty in developing such a model stems from the mathematical complexities involved when dealing with plate equations, especially for support conditions which realistically approximate multipanel floor plates.

1.2 SCOPE AND OBJECTIVES

The current practice when designing flat-plate structures is to perform separate analyses for gravity loading and lateral loading, and to design for appropriate combinations of the internal forces computed in the analyses. The gravity-load analysis of flat-plate floors has been studied extensively. Analysis procedures have been incorporated into design specifications (CSA A23.3-M84) and (ACI 318-84). Efficient finite element computer programs are available to perform the gravity-load analysis of flat-plate floor systems (Hrabok and Hrudy, 1981).

On the other hand, the lateral-load analysis of flat-plate building structures has received relatively little attention. Available computer programs for performing lateral-load analysis assume linear load-deformation behaviour, even though nonlinear behaviour begins at the plate-to-column connections at low load levels. Consequently, the objective of this study was to develop an economical, easy-to-use computer program which accounts for the nonlinear moment-rotation behaviour at the plate-to-column connections when analyzing laterally loaded flat-plate structures.

The program performs nonlinear lateral-load analysis only; it cannot be used for gravity-load analysis. Thus, in accordance with the current state of practice, it is anticipated that the program will be used in conjunction with a

gravity-load analysis program, when designing flat-plate building structures. It is recognized that because the lateral-load analysis program accounts for the nonlinear behaviour, results obtained from it theoretically cannot be superimposed onto those obtained from a gravity-load analysis program. Nonetheless, it is asserted that the use of a nonlinear lateral-load analysis program in the manner described here represents an improvement over a strictly linear analysis. It is a necessary step toward the development of a program to perform the nonlinear analysis of flat-plate structures under combined gravity and lateral loading.

The development of the nonlinear lateral-load analysis program occured in three phases. The first involved the modelling of the nonlinear moment-rotation behaviour of the plate-to-column connections at an interior column, at an edge column, and at a corner column. For each connection type, simple, normalized expressions were derived as functions of the geometric and material parameters that influence most strongly the connection moment-rotation behaviour. The expressions were derived using a modified Ramberg-Osgood function and calibrated using all available experimental results.

The normalized functions were incorporated into the computer program. The latter reads the appropriate geometric and material parameters for any given connection, selects the normalized function for the connection type specified,

and substitutes the parameters to generate the specific, dimensional moment-rotation function for the connection. This procedure has the advantage that connection moment-rotation behaviour can be incorporated into the structural analysis computer program without having to store moment-rotation data for a large number of connections with different geometric and material parameters.

The second phase involved the development of a procedure for modelling the flat-plate floor panels, which accounts for the nonlinear moment-rotation behaviour at the plate-to-column connections. As illustrated in Figure 1.3, the flat-plate floor is subdivided into interior, edge and corner panels. Only square panels supported on square columns are considered in this study. The plate panel is assumed to be linearly elastic, homogenous, and isotropic, the nonlinear moment-rotation behaviour being concentrated in the plate-to-column "connections". As illustrated in Figure 1.4, the plate panels are connected to the supporting column elements by rigid beam elements, each of which has a nonlinear flexural spring at the end connected to the flat-plate and a rigid connection at the column. The beam elements are used to simulate the column cross-section, which is assumed to remain plane and normal to the column axis. They therefore account for the influence of the cross-sectional dimensions of the column on the stiffness of the plate element. The flexural springs have nonlinear moment-rotation characteris-

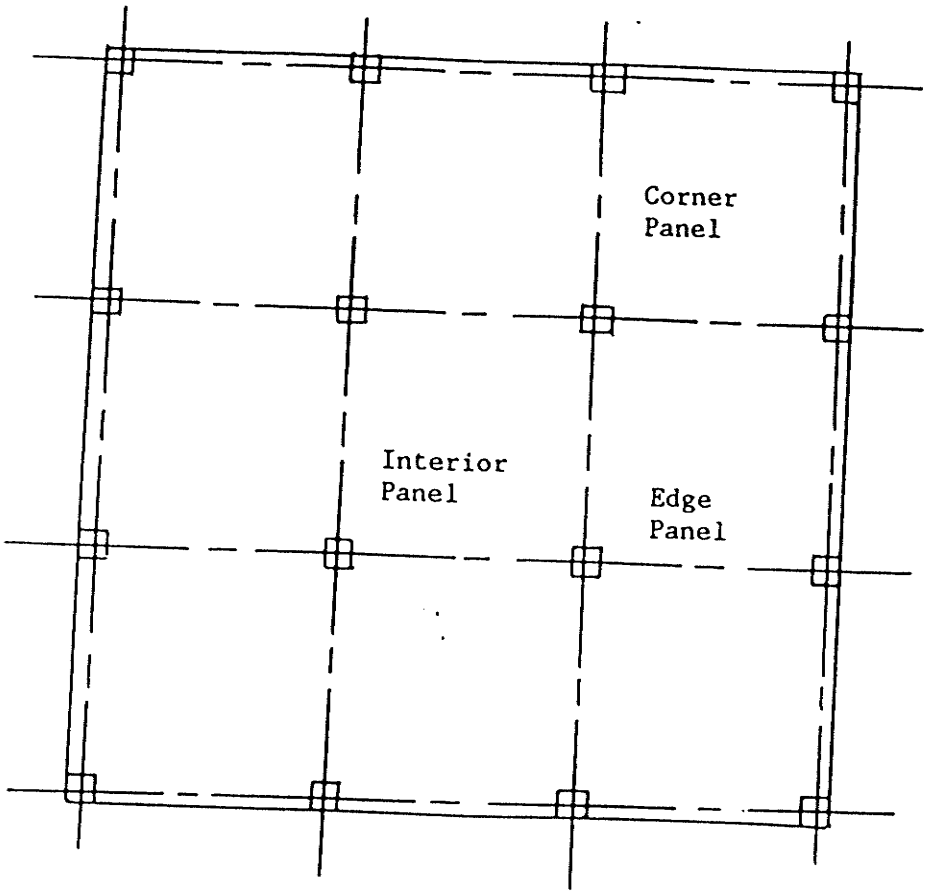

Figure 1.3: Typical Flat-Plate Floor

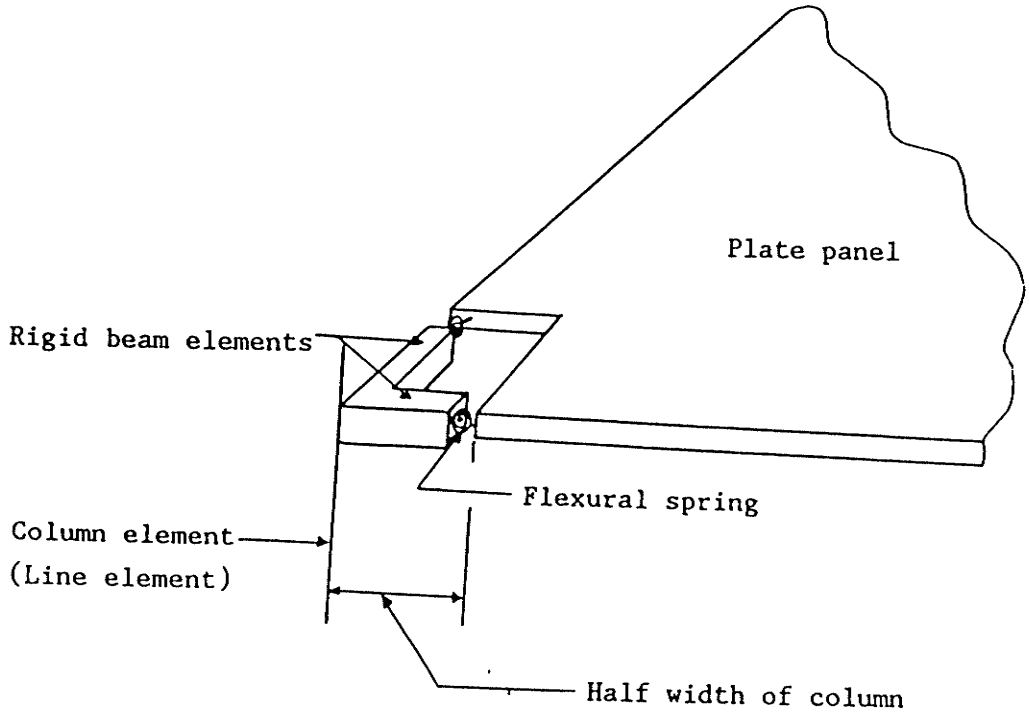

Figure 1.4: Model of the plate-column connection

tics identical to those of the plate-to-column connections, which they model.

The third and final phase of the study involved the incorporation of the features described above into a computer program to perform the nonlinear analysis of a three-dimensional reinforced-concrete flat-plate structure with or without shearwalls. The nonlinear analysis involves repeated cycles of linear analyses to determine the appropriate secant flexibility characteristics for the various plate-to-column connections. The final linear analysis, employing the appropriate connection secant flexibilities, yields the correct structural displacements and forces. The advantage of this analysis procedure is the saving realized in running costs and storage requirements. In developing the program, extensive data generation capabilities were incorporated to reduce the amount of data preparation required.

1.3 ASSUMPTIONS AND LIMITATIONS

A number of assumptions were made when developing the computer analysis program. The assumptions, and the consequent limitations on the use of the program follow.

1. All of the structural elements are linearly elastic except for the flexural springs that connect the rigid beam elements to the plate elements.
2. The plate elements are linearly elastic, homogeneous, and isotropic everywhere.

3. All of the floors in the structure have identical plan geometries and dimensions.
4. The floor plates provide rigid in-plane diaphram action.
5. Lateral loads are applied at floor levels only.
6. Only square plate panels supported by square columns are considered. This was done for two reasons. The first is that most flat-plate structures have square, or nearly square, plate panels. The second is that the effort required to develop the program, and the program storage requirements, would both increase dramatically if more than one plate panel aspect ratio were to be incorporated. It is suggested that it would be appropriate to use the program to analyze structures with approximately square floor panels.
7. Only static lateral loading is considered.
8. All floor panels have the same thickness and reinforcement ratios in the two orthogonal directions.
9. All connections of the same type have the same reinforcement ratios in a given floor. The ratios may vary from floor to floor.
10. All columns in a given storey have the same cross-sectional dimensions. However, the column sizes may vary from storey to storey.

1.4 ORGANIZATION OF REPORT

This report is divided into six chapters. A brief summary of their content is presented in this section.

The first chapter provides an introduction to the problem and a general description of the method used and the assumptions made in the solution.

In the second chapter, a review of the literature relevant to the analysis of flat-plate structures is presented. The chapter is divided into two sections. The first deals with the general methods used to analyze flat-plate structures. The second deals with the nonlinear models that have been developed to predict the moment-rotation behaviour of plate-to-column connections.

Chapter three deals with the modelling of the plate-to-column moment-rotation behaviour. The various parameters that influence the behaviour of the plate-to-column connections are discussed. Then, the standardization procedure used to model the nonlinear moment-rotation behaviour of the connections is described. Finally, a description of the physical model of the connection is presented

In chapter four, the modelling of the various structural components is discussed. The concepts used to model the overall structure are presented first. Then, the modelling of columns, shear walls and flat-plate panels is discussed. Finally, the nonlinear analysis procedure is described.

In chapter five, examples are presented to demonstrate the capabilities of the structural analysis computer program, and to compare the results obtained with published values.

The conclusions and recommendations for further work are presented in chapter six.

Chapter II

LITERATURE REVIEW

2.1 INTRODUCTION

A review of research work related to the analysis of flat-plate structures is presented in this chapter. The chapter is divided into two sections. The first deals with the methods currently used to analyze flat-plate structures. The second deals with the modelling of the rotational behaviour of concrete plate-to-column connections.

2.2 METHODS OF ANALYSIS

To date, only linear structural analysis methods have been developed and used widely for laterally loaded flat-plate structures. Most of them assume a two dimensional structure in which the plates are modelled by equivalent beams. The others assume a three-dimensional structure and represent the floor plates by finite element arrays.

2.2.1 Equivalent Beam Models

These models idealize the structure as a series of linearly elastic planar frames, each comprising a row of columns, associated portions of the flat-plate floors and, where appropriate, shear walls. The flat-plate floors are normally

subdivided into interior and edge strips as illustrated in Figure 2.1. The interior strips are defined by the centerlines of the adjacent panels, while the edge strips are defined by the edge columns and the edge panel centerline. Usually, only a fraction of the plate strip is considered effective in bending. The width of that part is termed the effective width, B', as illustrated on Figure 2.2. Thus, for lateral load analysis purposes strips are replaced by beams with the same thickness as the plate, but with width B'. The resulting planar frame is then analyzed. A summary of the bases of derivation and the parameters considered in the various equivalent beam models is presented in Table 2.1. In the table, and as illustrated in Figure 2.2, C is the column width or depth, L_1 is the plate span parallel to the direction of moment transfer and L_2 is the span normal to the direction of moment transfer. An X in the column headed GL in Table 2.1 indicates that gravity loading is applied to the plate prior to the application of the lateral loads. Since only square plate panels are considered in this study, henceforth the plate span will be referred to as L .

Khan and Sbarounis (1964) presented one of the first equivalent beam representations of the flat-plate floor. It was based on a grid analogy and tests on small scale metal models. The models were excessively flexible because the correct boundary conditions were not enforced during testing. The plate strip aspect ratio was considered as a variable.

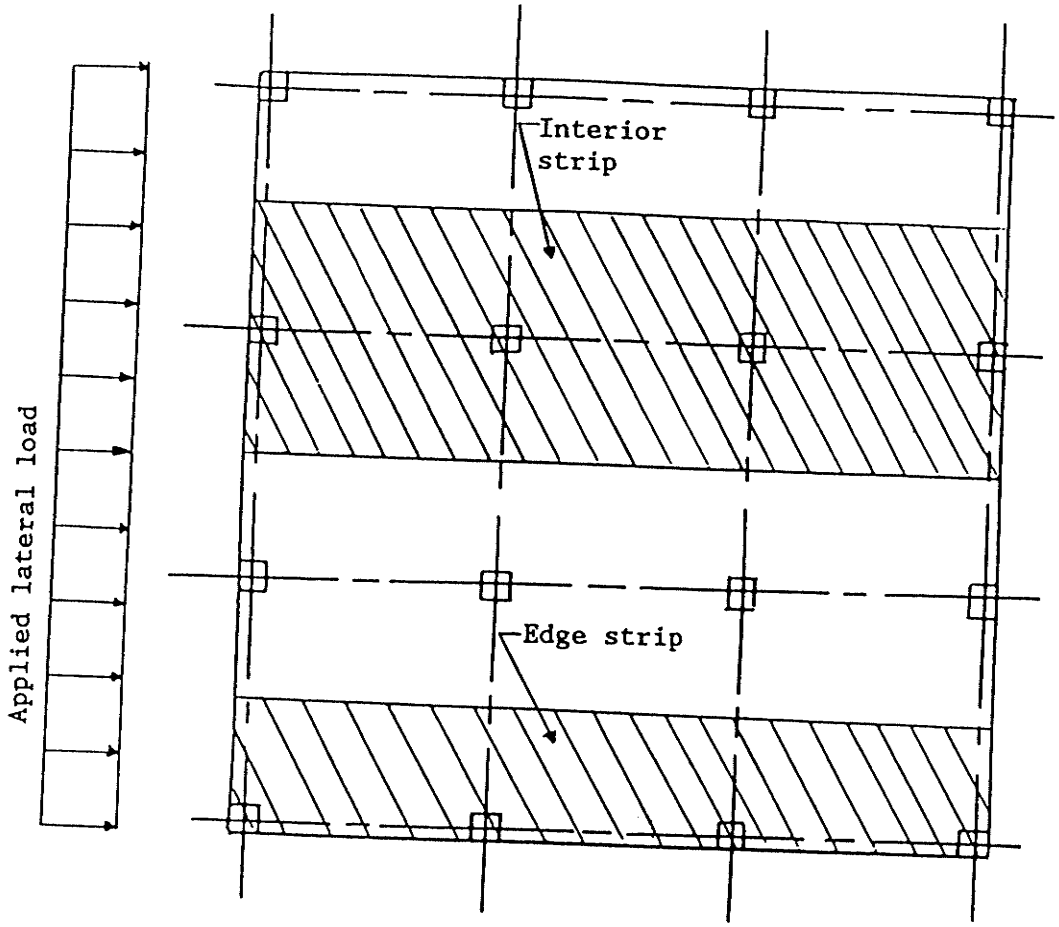

Figure 2.1: Typical Flat-Plate Floor

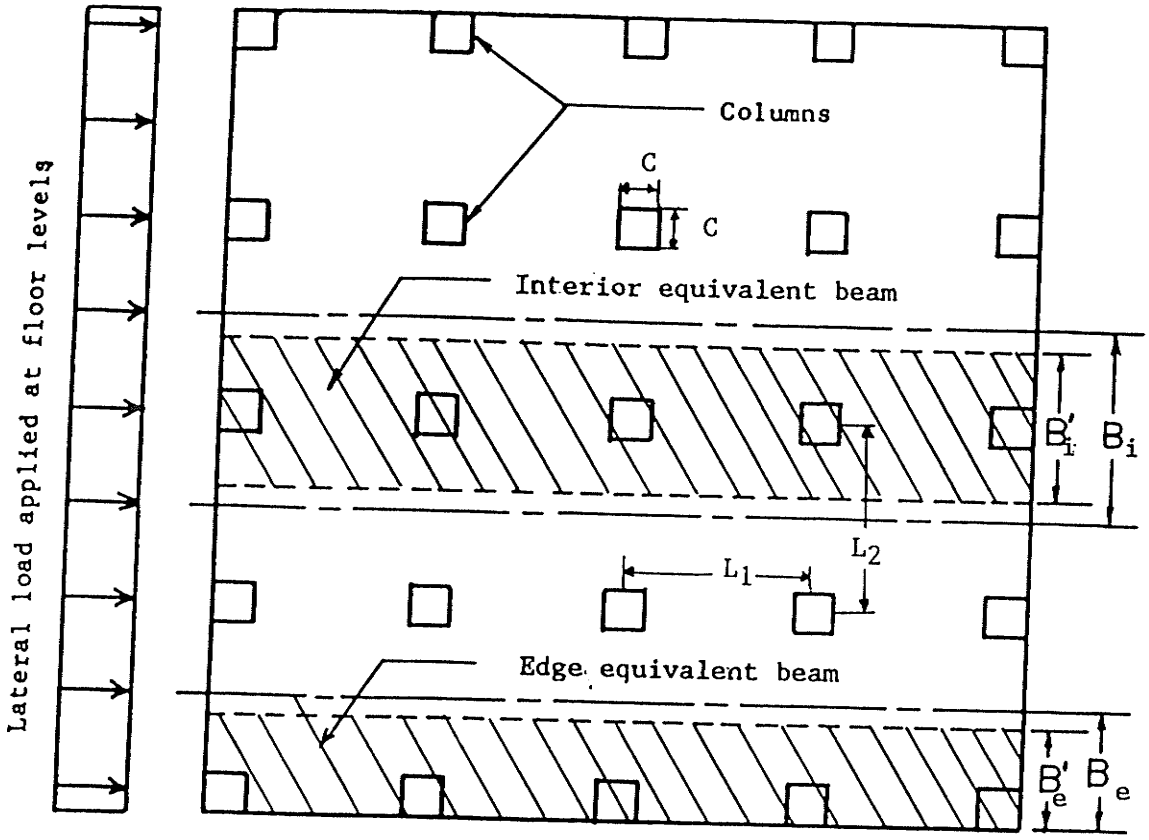

B_i = width of interior plate strip

B_i' = width of interior equivalent beam

B_e = width of edge plate strip

B_e' = width of edge equivalent beam

Figure 2.2: Equivalent Beam Representation

TABLE 2.1

Equivalent Beam Models

Researcher	Basis of Derivation	C/L	L_1/L_2	GL
Khan and Sbarounis	Grid Analogy and Test Models	X		
Pecknold	Elastic Theory	X	X	
Allan and Dervall	Elastic Theory	X		
Wong and Coull	Plate Theory	X	X	
Frazer	Finite Element	X	X	
Long and Kirk	1/3 Scale Models	X		X
Elias and Georgiadis	Energy Methods	X	X	

Pecknold (1975) and Allen and Darvall (1977) developed similar representations based on elastic plate theory. They considered the column-depth-to-plate-span ratio and the aspect ratio of the plate as variables. Only interior strips were considered and no recommendations were given for edge strips.

Elias and Georgiadis (1978) developed a method for determining the stiffness matrix of an equivalent beam using complementary energy methods and an assumed stress distribution in the plate. Both interior and edge strips were considered.

Wong and Coull (1980) presented an equivalent beam representation based on the influence coefficient method for determining the width of the equivalent beam. Two parameters, the column-depth-to-plate-span ratio and the aspect ratio of the plate strip,were considered. Only interior strips were dealt with.

Based upon his finite element studies, Frazer (1983) developed simple equations for determining the effective width. These equations were expressed in terms of the transverse column dimension and the plate strip span. Both interior and edge strips were considered.

Long and Kirk (1980) tested one-third scale concrete models. They observed that a significant reduction in the stiffness of the plate- to-column connection resulted from the cracking of the concrete around the column. They recom-

mended an effective width of 0.3 time the width of the plate strip for column-depth-to-plate-span ratios between 0.08 and 0.12.

The equivalent beam methods all have the shortcoming that they do not force compatibility of displacements among the planar frames. Most of them lack provisions for accommodating edge strips and shear walls. Also, they yield effective widths that vary considerably depending upon the basis of the derivation and the parameters considered. Finally,they do not give a realistic representation of the actual behaviour of the frame, and tend to overestimate the stiffness of the structure in resisting lateral loads.

2.2.2 Equivalent Frame Method

In this method, which has been incorporated into both the American (American Concrete Institute, 1983) and Canadian (Canadian Standards Association, 1983) standards, the full width of the panel is assumed to be effective in resisting lateral loads. The columns are replaced by equivalent columns to account for the two-dimensional behaviour of the plate. The equivalent column consists of the actual column plus torsional elements that connect it to the plate and simulate the stiffness of the column-to-plate connection. The equivalent frame method was originally developed for the analysis of individual floors under gravity loading only. Although it has been used for lateral load analysis, its use

can result in gross overestimations of the stiffness of the structure. Thus, it is not recommended for lateral load analysis.

2.2.3 Finite Element Methods

French, Kabaila and Pulmano (1975) developed a three-dimensional representation of the flat-plate structure in which the flat-plate floor panels were modelled by rectangular finite element arrays. Three degrees of freedom - a vertical displacement and rotations about two horizontal axes - were provided at the corner of the rectangular elements. Inter-element displacement compatibility was enforced at the corner nodes only. The column-depth-to-plate-span ratio and the aspect ratio of the plate panels were the parameters considered.

Ma (1976) modified the TABS program (Wilson, 1975), by adding a finite element representation of the flat-plate floors. Plate bending elements were used to model the floors. The stiffness matrix was then assembled and the internal and edge node stiffness contributions were condensed off, leaving the column node contributions. Ma's model was excessively flexible because he did not account for the finite cross-sectional dimensions of the column. As well, the interaction between floors and shear walls was not incorporated. The program was moderately expensive to use.

Hrabok and Hrudy (1981) developed a linear finite element program for the gravity load analysis of flat-plate floors. The plate bending elements used were derived using the hybrid stress method. The program accounts for both the finite size of the column and the presence of floor beams. The program is a comprehensive one, but it permits the gravity load analysis of flat-plate floors only, and cannot perform lateral load analysis.

Chislet and Morris (1985) developed a linear, three-dimensional analysis program, in which the floor panels were modelled using elastic plate elements with sixteen nodes, four at the corners and three along each panel edge. Three degrees of freedom - a vertical displacement and two horizontal rotations - were assumed at each node. Inter-element displacement compatibility was provided at the corner and edge nodes. The finite size of the column was accounted for by assuming the column elements to be attached to the plate by rigid beam elements. The stiffness matrix for the plate element was derived numerically in a nondimensional form, as a function of the column-depth-to-plate-span ratio. Only square panels supported on square columns were considered. The program is easy and inexpensive to use and the results obtained were in good agreement with those obtained using other linear, elastic models.

The main drawbacks to the use of linear finite element methods such as most of those described in this section, are

the high cost involved in running the programs and the time required to prepare and input the data. Also, because they model the structure linearly elastically, they tend to overestimate its stiffness. Thus the improved accuracy compared to that obtained from equivalent beam models does not justify the extra effort and expense involved in using these programs.

2.3 BEHAVIOUR OF CONCRETE SLAB-COLUMN CONNECTIONS

Observations made on full scale reinforced concrete flat-plate structures under load show that a large proportion of the structural deflections are the result of deformations at the plate-to-column connections. Several experimental and analytical research programs have been carried out to study and model the behaviour of those connections.

2.3.1 Experimental Research

As shown in Figure 2.3 four distinct plate-column connection types can be identified in a typical building. They are interior connections, corner connections, edge connections transferring moment parallel to the edge, and edge connections transferring moment normal to the edge. Most of the available experimental work deals with the behaviour of interior connections, as only a few studies have been done on corner and edge connections.

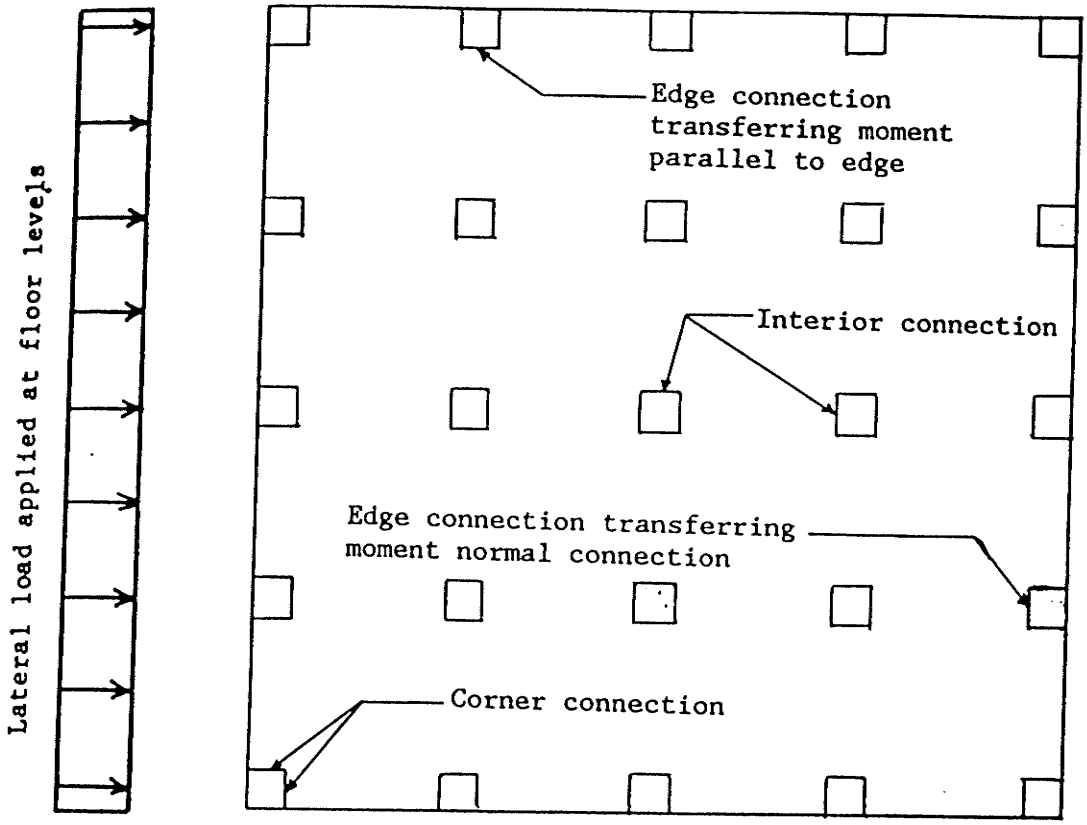

Figure 2.3: Slab-column connection types

To study the influence of different parameters, such as the amount and distribution of the plate reinforcement in the column region, the concrete compressive strength and the loading history, on the behaviour of interior connections, twenty interior plate-column specimens were tested at the University of Washington. Details of tests to destruction on four specimens without shear reinforcement and two with shear reinforcement were presented by Hawkins et al (1974). In the tests, the influence of concrete compressive strength, reinforcement ratio and distribution in the plate, and the presence of shear reinforcement were studied. Hanna (1976) tested three specimens with shear reinforcement to study the influence of the lateral load history of the connection and the type of loading applied. Symonds (1976) tested five specimens subjected to large gravity loads and relatively small lateral load. The parameters considered were the amount and distribution of the flexural reinforcement in the plate, the gravity load level applied to the plate prior to the application of the lateral loads, the concrete compressive strength, and the presence of shear reinforcement in the plate in the region of the column. Simpson (1976) tested six specimens to study the influence of changing the proportions and aspect ratio of the column.

Morrison et al (1983) reported tests to destruction of five interior connections. The influence of the flexural steel ratio and concrete strength were examined. Mulcahy

and Rotter (1983) tested six one-fifth scale specimens, and studied the influence of the steel ratio and concrete strength on the stiffness of the connections.

Chaichanavong (1979) tested five edge connections transferring moment parallel to the edge. Three specimens had shear reinforcement, while the other two had none. In the tests, the influence of the shape and size of the columns was studied, as were the effects of loading history and reinforcement ratio and distribution.

Wong and Yang (1978) tested eight edge connections transferring moments normal to the edge. Five specimens had shear reinforcement while the other five had none. The effects of the column dimension, the concrete strength and the amount and distribution of reinforcement were studied.

Yu (1979) tested five corner connections, Three without shear reinforcement and two with it. The influence of the amount and distribution of reinforcement, the column size and concrete strength were studied.

The experimental research described above has established that a large number of parameters influence the behaviour of plate-to-column connections. The most significant of them are the level of gravity loading applied to the plate prior to the application of lateral loads, the flexural reinforcement ratio in the immediate vicinity of the column, the concrete compressive strength, the column-depth-to-plate-span

ratio, and the bond slip of the plate reinforcement within the column. Of only minor influence are the presence of stirrups in the plate around the column, the yield strength of the reinforcement, the bar diameter, the column aspect ratio and the plate aspect ratio.

2.3.2 Analytical Research

Only a few analytical models have been developed for predicting the nonlinear moment-rotation behaviour of plate-to-column connections. All of them are based on either finite element representations, a beam grid analogy, or a stub beam representation of the flat-plate floors.

Yamazaki and Hawkins (1975) reported one of the first attempts to model the rotational behaviour of an interior plate-to-column connection. The plate was modelled using a general purpose finite element program. The loads were applied incrementally and the stiffnesses were varied according to the magnitude of the major principal moment in each element. The stiffness of the connection was considerably overestimated because no provisions were made to account for the rotations caused by bond slip of the reinforcing bars or the cracking of concrete around the column.

Shue and Hawkins (1980) presented a grid model to predict the stiffness of plate-interior column connections. The plate was modelled as an orthogonal grid of beams with rigid connections. The properties of the beams were determined on

a trial and error basis by correlating elastic predictions for the grid model with the results of finite element analyses. The flexural and torsional stiffnesses of the grid beams were varied to account for the change in stiffnesses with increasing loading.

Morrison et al (1983) developed a similar model in which the properties of the grid beams were derived by matching the curvature of a portion of the plate under a given force with that of beams representing the plate, under a statically equivalent force.

Although results obtained using the beam grid models are in relatively good agreement with experimental results, the models are too complex to be applied directly in design or to be incorporated into a computer analysis program.Thus, they remain of academic interest only.

Akiyama (1984) presented a model in which the plate was assumed to be attached to the column through a series of stub beam elements. The properties of the beams were varied with loading, to model the cracking of the concrete and bond slip of the reinforcement. The results obtained using this model were in good agreement with experimental results. Unfortunately, again the model is too complex to be applied directly in design.

Chapter III

MODELLING OF PLATE-COLUMN CONNECTION BEHAVIOUR

3.1 INTRODUCTION

Observations made on existing structures and on experimental models show that the rotational behaviour of plate-to-column connections greatly influences the behaviour of the entire structure under lateral loading. Therefore, in order to correctly represent the behaviour of the flat-plate structure, provision should be made in the analysis to account for the influence of connection deformation on the overall stiffness of the structure.

The models developed to date to predict the nonlinear behaviour of plate-to-column connections are rather complex and not suitable for incorporation into a structural analysis computer program. In this chapter, a procedure is described for standardizing experimental moment-rotation behaviour so that it can be efficiently incorporated into a nonlinear structural analysis computer program. Also presented is a physical model of the column region, capable of incorporating the influence of connection deformations on the behaviour of the structure.

3.2 FACTORS INFLUENCING CONNECTION BEHAVIOUR

There are several factors that influence the behaviour of plate-to-column connections. The more significant ones are described below, in decreasing order of significance.

3.2.1 Gravity Moment

Experimental studies have shown that the gravity-load moment, M_g, acting on the column face has a large influence on the behaviour of plate-to-column connections. For example, as illustrated in Figure 3.1, Akiyama (1984) found that an increase in gravity loading resulted in a decrease in both the stiffness and the strength of the connection, with regard to lateral load resistance. The reason is that the gravity-load moment causes the initiation of concrete cracking along the boundary where the column intersects the flat plate. Moreover, the rate of crack propagation is a function of the magnitude of the gravity-load moments. It has been observed also that the influence of gravity loading is larger for connections without shear reinforcement than for those with it (Akiyama, 1984).

In tests of plate-to-column specimens under combined gravity and transverse loading, the gravity loading has been simulated by two vertical loads P_g applied at a distance L_g from the column center, as illustrated in Figure 3.2 (Akiyama, 1984). Accordingly, the gravity load moment that has

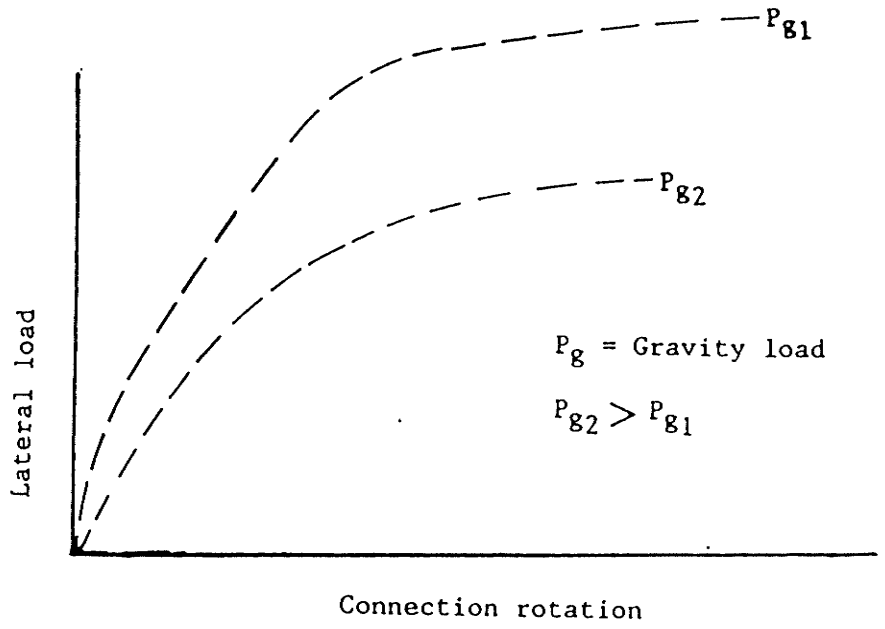

Figure 3.1: Influence of gravity loads on connection behaviour

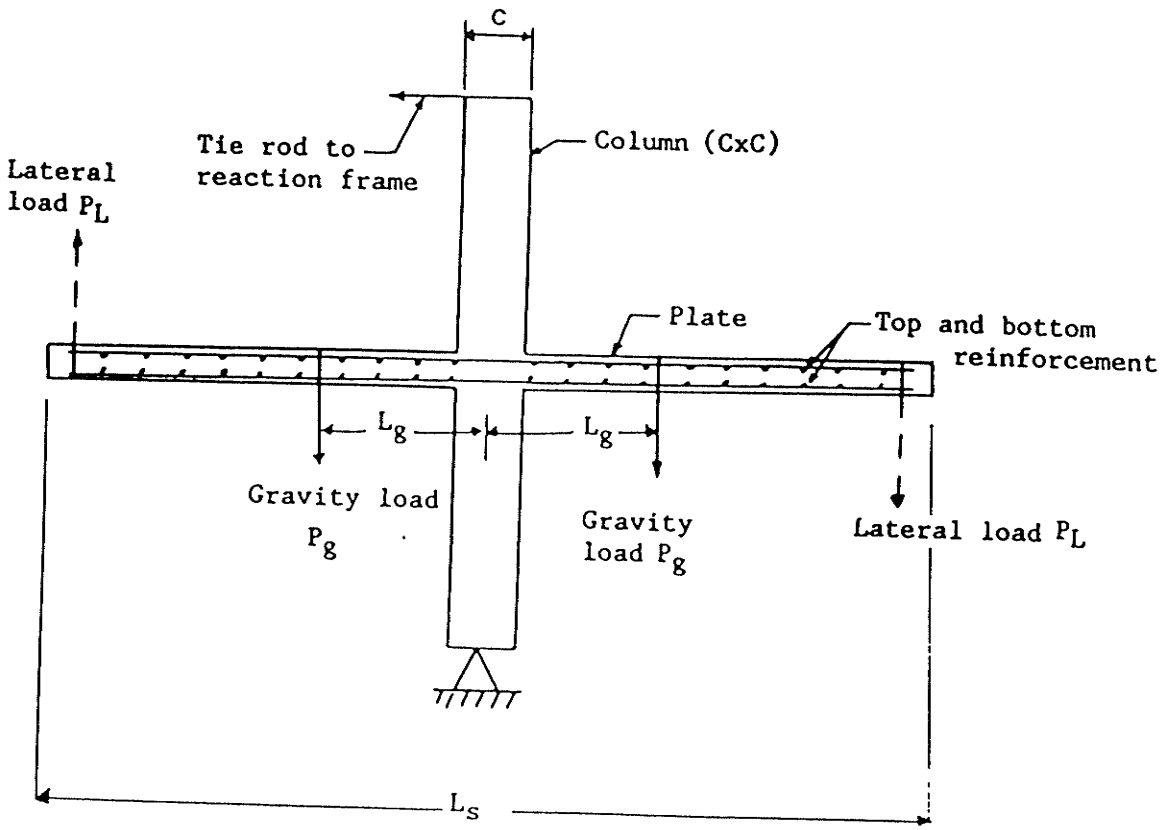

Figure 3.2: Interior connection test specimen

been assumed to be transmitted from the plate to each side of the column is :

$$M_g = P_g\ (L_g - C/2)\ (C/L_s) \qquad (3.1)$$

Where,

M_g = gravity-load moment at the column face

P_g = applied gravity load

L_s = width of test specimen plate

L_g = distance from column center to point of application of gravity load

C = column depth

In the tests, the gravity load was applied to the plate first, then the lateral load was applied in repeated reversed cycles until the specimen failed. The combined effects of the gravity and lateral loads on the moment-rotation behaviour of the plate-to-column connections were determined. No attempt was made to differentiate between the connection behaviour on the side of the column where gravity-load and transverse-load moments were additive, and that on the side where they were in opposite directions.

For interior plate-to-column connections, test results have been reported for specimens subjected to "low gravity load", where plate self weight was the only gravity load applied (Morrison, 1983) and (Mulcahy et al, 1981), for "moderate gravity load" where the average value of the applied gravity load P_g was about four times the plate self

weight (Akiyama, 1984), and for "high gravity load" where the average value of the applied gravity load P_g was about eight times the plate self weight (Akiyama, 1984).

The method used in this study to account for the effects of gravity-load moment on plate-to-column connection behaviour parallels that used in measuring the behaviour experimentally. Thus, for a given level of gravity-load moment, a single standardized moment-rotation function has been derived. No attempt has been made to differentiate between the moment-rotation behaviour on the side of the column that is unloading as transverse load is applied and that on the opposite side of the column, where the moments due to gravity and transverse loads are additive. For interior plate-to-column connections, three such standardized moment-rotation functions have been derived, one corresponding to each of "low", "moderate" and "high" gravity-load moments. To derive the standardized functions, all available experimental data were examined and for each specimen, the ratio of the gravity-load moment, M_g, to the cracking moment, M_c, at the column face was determined. The cracking moment was computed as :

$$M_C = \frac{7.5 \sqrt{f_c'} \; C \; t^2}{6} \qquad (3.2)$$

Where,

f_c' = 28 day compressive strength of concrete

t = total plate thickness

It was found that the ratio M_g/M_c for specimens subjected to high gravity loads, as defined above, was always greater than 4.0. That for specimens subjected to moderate gravity loads was normally between 1.0 and 4.0, and that for specimens subjected to low gravity loads was smaller than 1.0.

For edge connections transferring moments parallel to the edge, for edge connections transferring moments normal to the edge, and for corner connections, test data were available for "moderate" gravity-load moment only. Thus, only a single standardized moment-rotation function was derived for each of them.

Although the procedure described here accounts only approximately for the effect of gravity-load moment, it is asserted that it provides a more realistic model of the actual behaviour of the connection than does the commonly-used assumption of a linearly elastic connection.

3.2.2 Connection Flexural Reinforcement

The strength and stiffness of plate-to-column connections are greatly influenced by the connection flexural reinforcement ratio, ρ, in the immediate vicinity of the column. As illustrated in Figure 3.3, an increase in the reinforcement ratio results in an increase in both the strength and stiffness of the connection. Thus, for example, Akiyama (1984) found that increasing the connection reinforcement ratio in

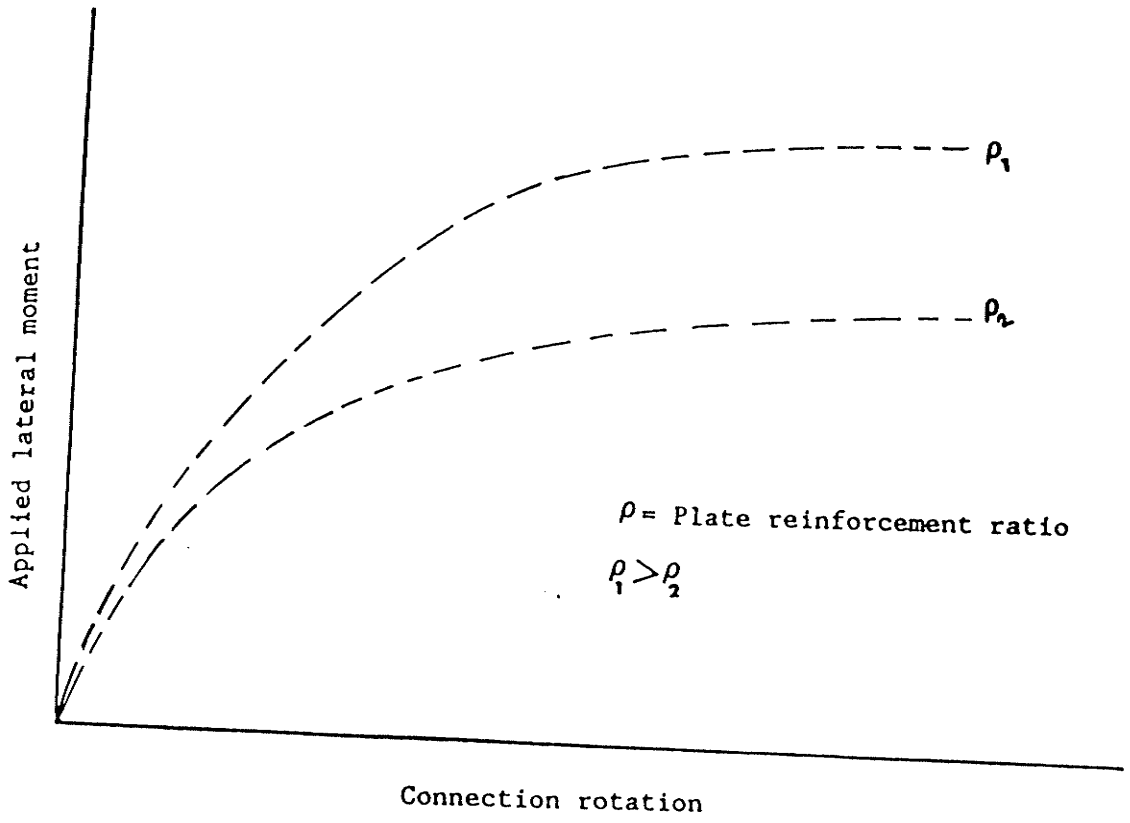

Figure 3.3: Influence of reinforcement ratio on connection behaviour

the vicinity of the column from 0.30% to 1.0% produced an increase in the connection stiffness of more than 40%. The magnitude of the increase depended in part on the specimen geometry and the concrete strength. It has been found also that the distribution of the reinforcement is as important as the reinforcement ratio. Akiyama (1984) recommended that in order to be effective in increasing the connection stiffness, the connection reinforcement should be concentrated in a region extending a distance of at least (C+3t) from the column face.

In this study, the total reinforcement ratio , ρ_t , in the connection region was defined as the sum of the top and bottom plate reinforcement ratios. The total reinforcement ratio was used in developing the standardized moment-rotation functions for all connection types considered. It is assumed that the distribution of the connection reinforcement is consistent with Akiyama's recommendations.

3.2.3 Concrete Strength

Mulcahy et al (1981) observed that an increase in the plate concrete compressive strength, f'_c , resulted in an increase in the strength and stiffness of the connection, as illustrated in Figure 3.4. He found that an increase in the concrete compressive strength is accompanied by an increase in its tensile strength, and therefore by a reduction in the extent of crack propagation and the consequent loss of

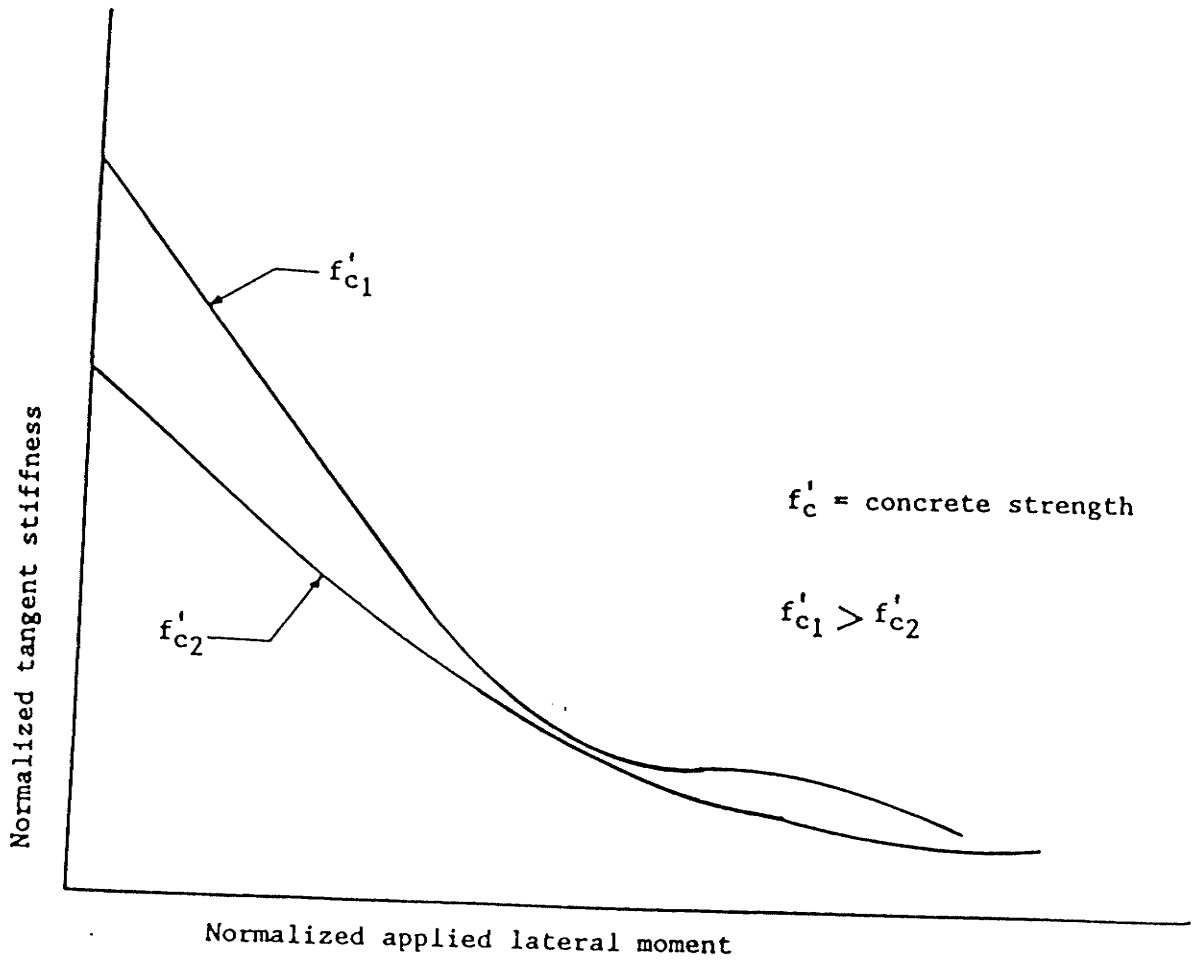

Figure 3.4: Influence of concrete compressive strength on connection behaviour

stiffness. Thus, for example, an increase in the concrete compressive strength from 30 MPA to 45 MPA resulted in an increase in the connection tangent stiffness of as much as 30%, depending on the magnitude of the applied moment.

In this study, the concrete strength was used to compute a dimensionless moment, M', which was used to develop the standardized moment-rotation functions for the various connection types. The dimensionless moment is defined as:

$$M' = \frac{M}{f_c' \quad L \quad t^2} \qquad (3.3)$$

Where,

M' = dimensionless moment transmitted from the floor plate to the column

M = moment transmitted from the floor plate to the column

3.2.4 Column-To-Plate Stiffness Ratio

Pavlovic et al (1985) found that as the ratio of the column stiffness to the plate stiffness is increased, there is an increase in both the strength and the stiffness of the connection. Normaly, the column-depth-to-plate-span ratio, C/L, is used to represent the column-to-plate stiffness ratio. Walker found that an increase in the column-depth-to-plate-span ratio from 0.08 to 0.12 resulted in an increase in the connection secant stiffness of as much as 20%, depending upon other connection parameters.

In this study, the column-depth-to-plate-span ratio,C/L, was incorporated into the standardized moment-rotation functions for all of the connection types considered.

3.2.5 Bond Slip of Plate Reinforcement

Sheu et al (1980) found experimentally that the bond slip of the plate reinforcement within the column produced a concentrated rotation at the column-to-plate boundary, thus reducing the stiffness of the connection. The experimentally measured moment-rotation curves used in developing the standardized moment-rotation functions account, among other things, for the bond slip effects. Thus, the influence of bond slip is automatically accounted for in the standardized moment-rotation functions.

3.2.6 Other Parameters

Akiyama (1984) observed in tests of plate-to-column specimens that while the presence of shear reinforcement in the connection region increased the strength and ductility of the connection, it had very little influence on its stiffness. It has also been observed that other parameters such as the reinforcement yield strength and bar diameter have virtually no influence on the stiffness of plate-to-column connections. Consequently, for the standardized moment-rotation functions derived in this study no attempt was made to account for these parameters.

3.2.7 Summary

The moment-rotation behaviour of plate-to-column connections is influenced by several parameters. In this study, only the four that affect connection behaviour most significantly have been incorporated into the standardized moment-rotation functions. The ratio of gravity-load moment to cracking moment at the column face, M_g/M_c, has been accounted for by deriving different standardized functions for low, moderate and high gravity-load moments for interior connections. Only a single standardized function, for moderate gravity-load moments, has been developed for each of edge and corner connections. The total reinforcement ratio for the plate, ρ_t, the column-depth-to-plate-span ratio, C/L, and the concrete compressive strength, f_c', have all been incorporated explicitly into the standardized functions.

Other parameters which have less significant effects on the connection behaviour were excluded from the standardized functions. They include the presence of shear reinforcement in the plate adjacent to the column, the reinforcement yield strength and the bar diameter.

3.3 STANDARDIZED MOMENT-ROTATION FUNCTIONS

There are two ways in which the nonlinear connection moment-rotation relationships can be incorporated into a structural analysis computer program. One is to store a large family of functions, one for each of the many combinations of the physical parameters associated with the connections, such as reinforcement ratio, concrete strength,etc. This procedure would require a prohibitively large amount of storage. The second alternative, used in this study, is to derive and store standardized connection moment-rotation functions for the various types of connections. These functions are expressed in terms of the several connection parameters. Thus, when the physical parameters are known for a given plate-to-column connection in the structure, they can be substituted into the standardized function in order to generate the specific moment-rotation relationship for that connection.

The first step in the standardization procedure is to express the flexural moment at the plate-to-column connection in dimensionless form as described in Equation (3.3). Next, a Ramberg-Osgood function (1943), which was modified by Ang (1983) to describe the moment-rotation behaviour of steel connections, is used for the standardized function. The modified function is in the following form.

$$\frac{\phi}{\phi_o} = \frac{r\ M'}{(rM_o)} \left[1 + \left\{ \frac{r\ M'}{(rM_o)} \right\}^{n-1} \right] \qquad (3.4)$$

Where,

ϕ = relative rotation between the column axis and the normal to the plate midsurface at the column.

ϕ_o, (rM_o) and n = constants that define the shape of the standardized function

As illustrated in Figure 3.5, ϕ_o and (rM_o) define the position of point 1, through which a family of Ramberg-Osgood curves pass. Constant n defines the sharpness of the curvature for any one of the curves.

In Equation (3.4), factor r scales the ordinates on the curve, according to their dependence upon the connection parameters. It has the form

$$r = \prod_{j=1}^{m} (p_j)^{a_j} \qquad (3.5)$$

Where,

p_j = numerical value of the jth connection parameter

a_j = dimensionless exponent which indicates the influence of the jth connection parameter on the moment-rotation relationship

m = number of connection parameters considered

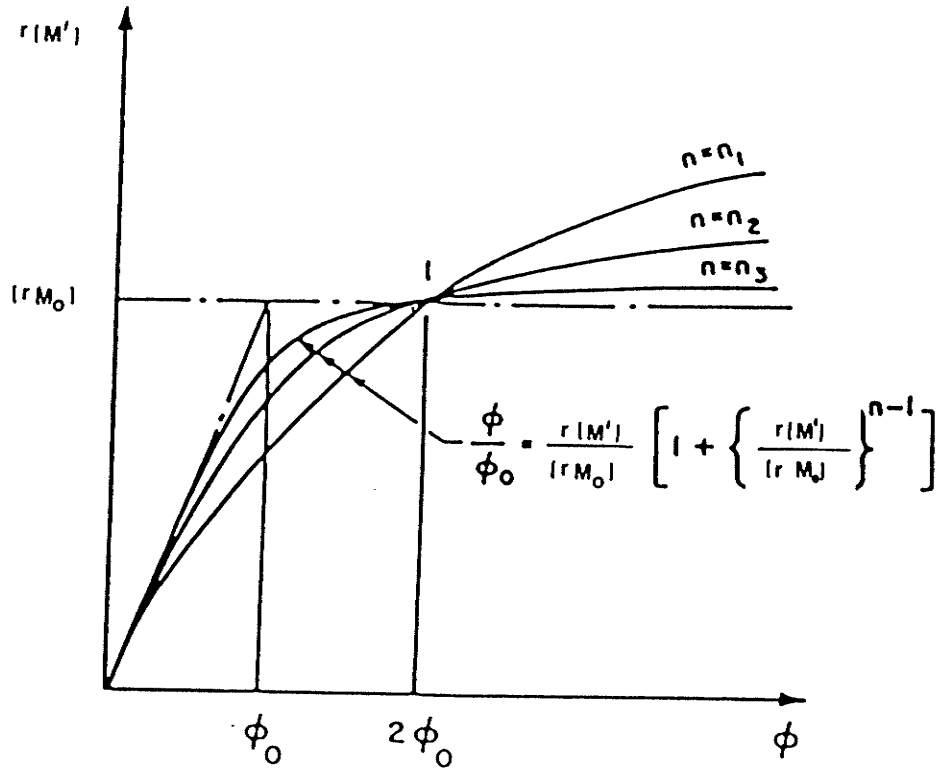

Figure 3.5: Standardized Moment-Rotation Function

The evaluation of the exponent a_j in Equation (3.5) is illustrated by considering a family of experimentally determined moment-rotation curves, as shown in Figure 3.6, for plate-to-column connections that are identical except for parameter p_j. A pair of curves is considered and the relationship between moments M'_1 and M'_2 at a particular rotation Ø is assumed to have the form

$$\frac{M'_1}{M'_2} = \left(\frac{p_{j2}}{p_{j1}} \right)^{a_j} \qquad (3.6)$$

Where p_{j1} and p_{j2} are the numerical values of parameter p_j for connections 1 and 2 (corresponding to curves 1 and 2) respectively.

Equation (3.6) can be rewritten and solved for a_j, as follows

$$a_j = \frac{\log (M'_1 / M'_2)}{\log (p_{j2} / p_{j1})} \qquad (3.7)$$

Equation (3.7) is used to compute a_j values corresponding to several values of rotation Ø, for each combination of experimental curves, such as 1 and 2, 1 and 3, 2 and 3,etc. The mean of the a_j values thus obtained is then used in Equation (3.5).

When mean values have been computed for all m exponents a in Equation (3.5), they are plotted on a standardized moment-rotation (r M' vs Ø) diagram. Finally, a least squares curve fitting procedure is used to evaluate coefficients $Ø_0$,(rM_0) and n in Equation (3.4).

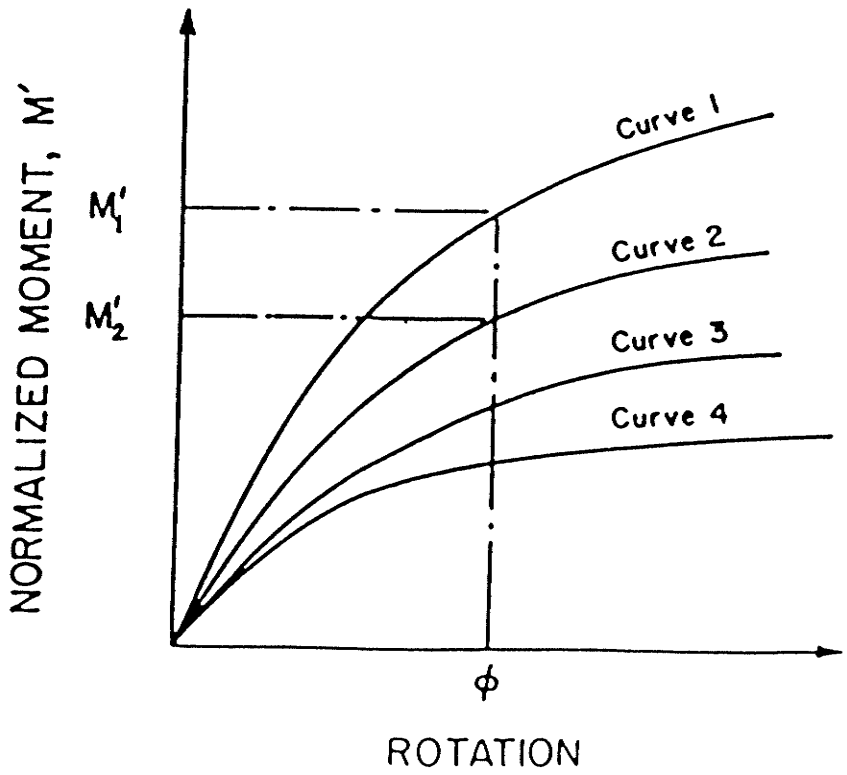

Figure 3.6: Family of experimental moment rotation curves

As illustrated in Table 3.1, 36 tests of plate-to-column specimens, performed in 10 different investigations, were considered in deriving standardized moment-rotation functions in the form of Equation (3.4). Twenty one of the specimens were for interior plate-to-column connections, four were for edge connections transferring moment parallel to the edge, six were for edge connections transferring moment normal to the edge and five were for corner connections. The table shows the reference for each test specimen and the specimen designation used by the original authors. Also included are the values of the parameters ρ_t, C/L, M_g/M_c, and the connection type (interior, corner, etc.) for all of the test specimens used in deriving the standardized moment-rotation functions.

The six standardized moment-rotation functions derived in this study are presented in Table 3.2. Also included in the table are the number of test specimens used in deriving each of the functions, the references for the data on which the functions are based, and the maximum percentage deviations of the derived functions from the experimental values. The deviations were computed by substituting the parameters for a particular test specimen into the appropriate standardized function, computing the connection rotations corresponding to several applied moments, and comparing them with the experimental values.

TABLE 3.1

Test Specimens Used in
Deriving Standardized Moment-Rotation Functions

REFERENCE	SPECIMEN DESIGNATION	ρ_T	C/L	M_g/M_c	PANEL TYPE
Morrison et al. (1983)	S1	0.0130	0.167	0.0	Interior/ Low Grav.
	S2	0.0196	0.167	0.0	Interior/ Low Grav.
	S3	0.0262	0.167	0.0	Interior/ Low Grav.
	S4	0.0196	0.167	2.23	Interior/ Mod. Grav.
	S5	0.0196	0.167	5.39	Interior/ High Grav.
Mulcahy Rotter (1981)	M02	0.0117	0.0571	0.0	Interior/ Low Grav.
	M03	0.0117	0.0571	0.0	Interior/ Low Grav.
	M05	0.0160	0.0571	0.0	Interior/ Low Grav.
	M06	0.0072	0.0571	0.0	Interior/ Low Grav.
Hawkins et al. (1974)	SS1	0.0188	0.077	2.83	Interior/ Mod. Grav.
	SS2	0.0139	0.077	3.01	Interior/ Mod. Grav.
Hanna et al. (1975)	SS3	0.0166	0.0077	2.96	Interior/ Mod. Grav.
	SS5	0.0139	0.077	2.63	Interior/ Mod. Grav.
Symmonds et al. (1976)	SS6	0.0139	0.077	6.54	Interior/ High Grav.
	SS7	0.0173	0.077	6.21	Interior/ High Grav.
Simpson et al. (1976)	SS8	0.0215	0.103	2.95	Interior/ Mod. Grav.
	SS9	0.0215	0.103	5.86	Interior/ High Grav.
	SS10	0.0174	0.125	5.70	Interior/ High Grav.
	SS11	0.0176	0.125	2.44	Interior/ Mod. Grav.
	SS12	0.0176	0.0513	3.31	Interior/ Mod. Grav.
	SS13	0.0174	0.0513	6.76	Interior/ High Grav.

Table 3.1 (continued)

REFERENCE	SPECIMEN DESIGNATION	ρ_T	C/L	M_g/M_c	PANEL TYPE
Chaichanavong (1979)	EL1	0.0121	0.077	2.63	Edge Parallel
	EL2	0.0126	0.103	2.53	Edge Parallel
	ELS1	0.0140	0.077	2.55	Edge Parallel
	ELS2	0.0140	0.077	2.60	Edge Parallel
Hawkins et al. (1978)	E1	0.0133	0.154	2.72	Edge Normal
	E2	0.0191	0.205	2.56	Edge Normal
	E3	0.0227	0.103	2.64	Edge Normal
	ES2	0.0230	0.154	2.58	Edge Normal
	ES4	0.0227	0.250	2.66	Edge Normal
	ES5	0.0236	0.103	2.63	Edge Normal
Yu (1979)	C1	0.0083	0.143	2.58	Corner
	C2	0.0083	0.143	2.61	Corner
	C3	0.0125	0.190	2.71	Corner
	CS1	0.0125	0.43	2.52	Corner
	CS2	0.0150	0.232	2.68	Corner

TABLE 3.2

Standardized Moment-Rotation Functions

Connection Type		Reference	Number of specimens	r	Standardized Function	Maximum Percent Deviation
Interior	$\frac{M_g}{M_c} \leq 1.0$	Mulcahy et. al Morrison et. al.	7	$(\rho)^{-0.042}(\frac{C}{L})^{-0.61}$	$\frac{\phi}{0.0065} = \frac{r M'}{1.25}\left[1 + (\frac{r M'}{1.25})^{4.58}\right]$	15
	$1.0 < \frac{M_g}{M_c} \leq 4.0$	Hawkins et. al. Hanna et. al. Simpson et. al.	8	$(\rho)^{-1.24}(\frac{C}{L})^{-0.11}$	$\frac{\phi}{0.0101} = \frac{r M'}{22.8}\left[1 + (\frac{r M'}{22.8})^{4.86}\right]$	13
	$\frac{M_g}{M_c} > 4.0$	Symmonds et. al. Simpson et. al.	6	$(\rho)^{-3.51}(\frac{C}{L})^{-1.07}$	$\frac{\phi}{5.4\times10^{-3}} = \frac{r M'}{1.6\times10^{6}}\left[1 + (\frac{r M'}{1.6\times10^{6}})^{4.86}\right]$	7
Edge	Parallel to Edge	Chaichanavong et. al.	4	$(\rho)^{-3.02}(\frac{C}{L})^{-2.16}$	$\frac{\phi}{2.1\times10^{-3}} = \frac{r M'}{1.04\times10^{7}}\left[1 + (\frac{r M'}{1.04\times10^{7}})^{5.32}\right]$	9
	Normal to Edge	Hawkins et. al.	6	$(\rho)^{-0.77}(\frac{C}{L})^{-0.59}$	$\frac{\phi}{5.6\times10^{-3}} = \frac{r M'}{2.47}\left[1 + (\frac{r M'}{2.47})^{5.68}\right]$	18
Corner		Yu et. al.	5	$(\rho)^{-2.03}(\frac{C}{L})^{-0.39}$	$\frac{\phi}{9.5\times10^{-3}} = \frac{r M'}{8.1\times10^{2}}\left[1 + (\frac{r M'}{8.1\times10^{2}})^{6.92}\right]$	20

As described previously, the rotational stiffness of the plate-to-column connections was affected most significantly by the the level of gravity loading acting on the structure. Therefore, as shown in Table 3.2, three standardized functions were derived for an interior connection, one each for low gravity loading ($M_g / M_c \leq 1.0$), for moderate gravity loading ($1.0 < M_g/M_c \leq 4.0$), and for high gravity loading ($M_g/M_c > 4.0$). Limited experimental data were available for edge connections transmitting moment parallel to the edge, for those transmitting moment normal to the edge, and for corner connections. Consequently, only one standardized function was derived for each of these cases.

Typical plots of experimentally determined moment-rotation curves and the corresponding curves obtained from the standardized functions are presented in appendix A. It can be seen that in most cases the standardized functions approximate closely the shapes of the experimental curves, while smoothing them somewhat.

As can be seen in Table 3.2 and the plots in Appendix A, in a few instances the standardized functions deviate significantly from the experimental data. This can be attributed to three factors. The first is that the standardization procedure used is an averaging process, capable of describing the behaviour of specimens having parameters that are well within the ranges considered in the standardization process. However, results obtained from the standardized

functions for specimens having parameters that are close to the extremes of the ranges considered in the derivation, tend to deviate significantly from the experimentally measured results.

Secondly, in order to account for the influence of a given connection parameter, several specimens should be available that are identical except for the parameter under consideration. Unfortunately, because of the non-homogeneous nature of concrete, and the limited amount of experimental data available, it was impossible to achieve the latter condition. Therefore, in order to facilitate comparisons among the different specimens available, it was assumed that specimens with parameters that differed by less than five percent were identical. As a consequence, inaccuracies were built into the derived functions. The third factor is that the small number of experimental tests available, especially for edge and corner plate-to-column connections, meant that only a very small number of data values were available.

The Ramberg-Osgood curve fitting function requires that experimental moment-rotation curves start at the origin. On the other hand, most of the available test data included an initial rotation caused by the application of gravity load to the plate prior to the application of the lateral load. The initial rotations due to the gravity load were deducted from the total connection rotations when developing the standardized moment-rotation functions. This is justified on

the basis that the derived functions and the analysis program are applicable to transverse loading only. Gravity loading is not dealt with, except for its effects on the moment-rotation behaviour of interior connections under transverse loads.

3.4 PHYSICAL MODEL OF COLUMN AND CONNECTION

When a flat-plate structure is subjected to transverse loading, nonlinear load-deformation behaviour occurs at the column-to-plate connections beginning at relatively low load levels. The primary source of the nonlinear behaviour is early flexural cracking of the plate, as illustrated in Figure 3.7.

Based upon experimental observations, Hawkins (1980) described the connection moment-rotation behaviour, as follows. As transverse load is applied to the structure, the moment-rotation behaviour at the typical plate-to-column connection is approximately linear, as illustrated in Figure 3.8. When the flexural moment at the plate-to-column boundary reaches the cracking moment, the connection stiffness decreases abruptly as cracking propagates. With increasing load, torsional cracking occurs in the plate at the sides of the column. As the loading is increased further, yielding of the flexural reinforcement commences and the stiffness again decreases. Finally, with a further load increase, the concrete crushes in flexure and the connection fails.

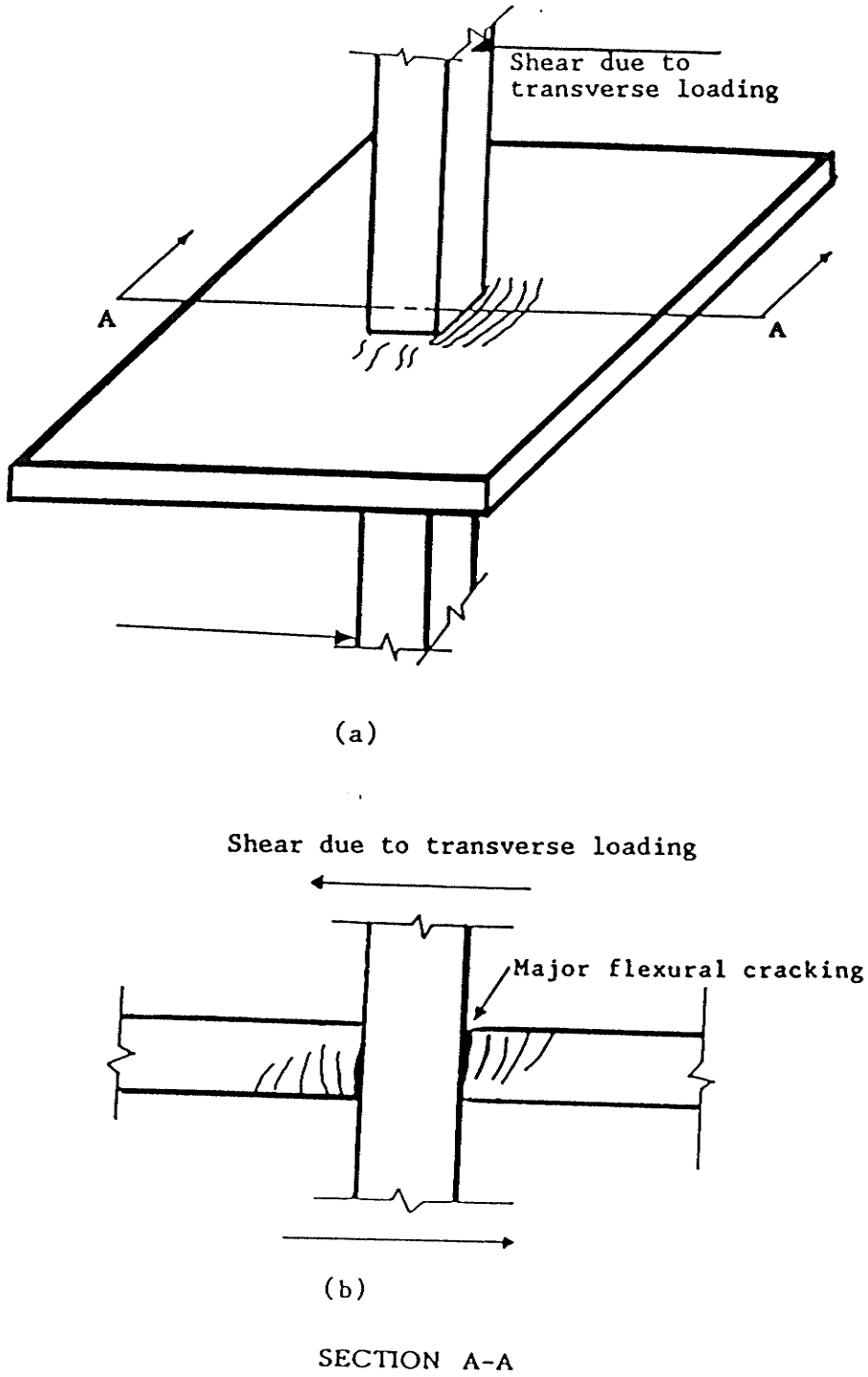

Figure 3.7: Flexural cracking at the plate-column boundary

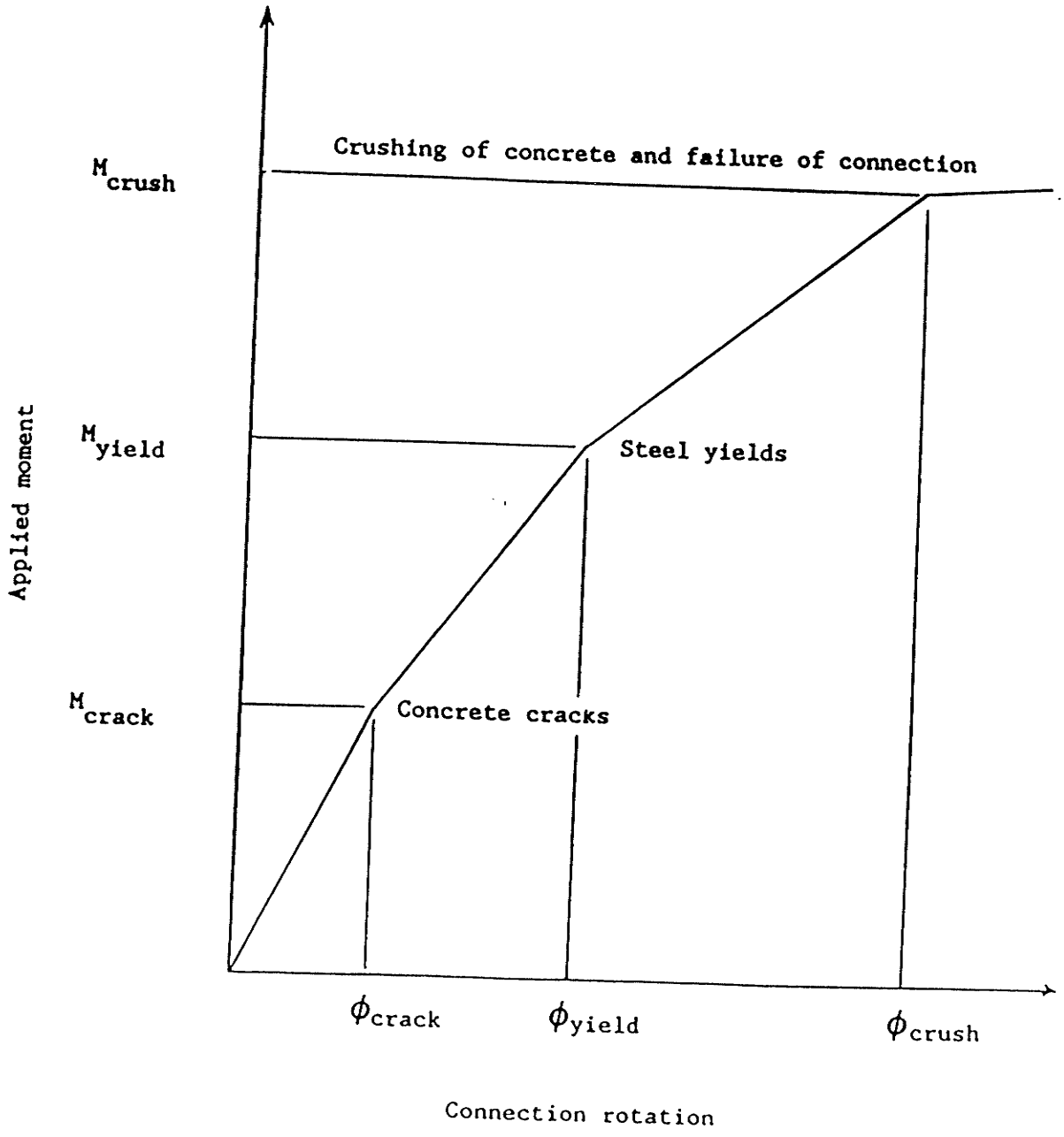

Figure 3.8: Typical plate-column moment-rotation behaviour

In this study, the finite cross-sectional dimensions of the column and the nonlinear behaviour of the plate-to-column connection were modelled using the arrangement shown in Figure 3.9. The column was modelled as a line element extending from one floor plate to the next higher one. To represent the finite cross-sectional dimensions of the column, rigid beam elements, B1 in Figure 3.9, each with a length of half the column width, were assumed to be connected rigidly to the column, at the elevation of the floor plate.

The moment-rotation behaviour of the plate-to-column connection was modelled by flexural springs FS_1 and FS_2, which allow rotations in the two orthogonal directions, and which connect the beam elements to the plate. In order to maintain a constant plate slope normal to the face of the column, torsionally rigid beam elements, B2, were connected to the plate where it intersects the column face. The beam elements were connected to the torsional springs at the column centre lines, and to each other by ball-and-socket joints at the column corners.

Jamieson (1984) derived the stiffness matrix for a beam element with fexural springs at both ends as illustrated in Figure 3.10a. The stiffness coefficients were functions of the rotational stiffnesses, S_a and S_b, of the flexural springs at ends a and b, respectively. In this study, the stiffness matrix for beam elements B1, which have a flexural

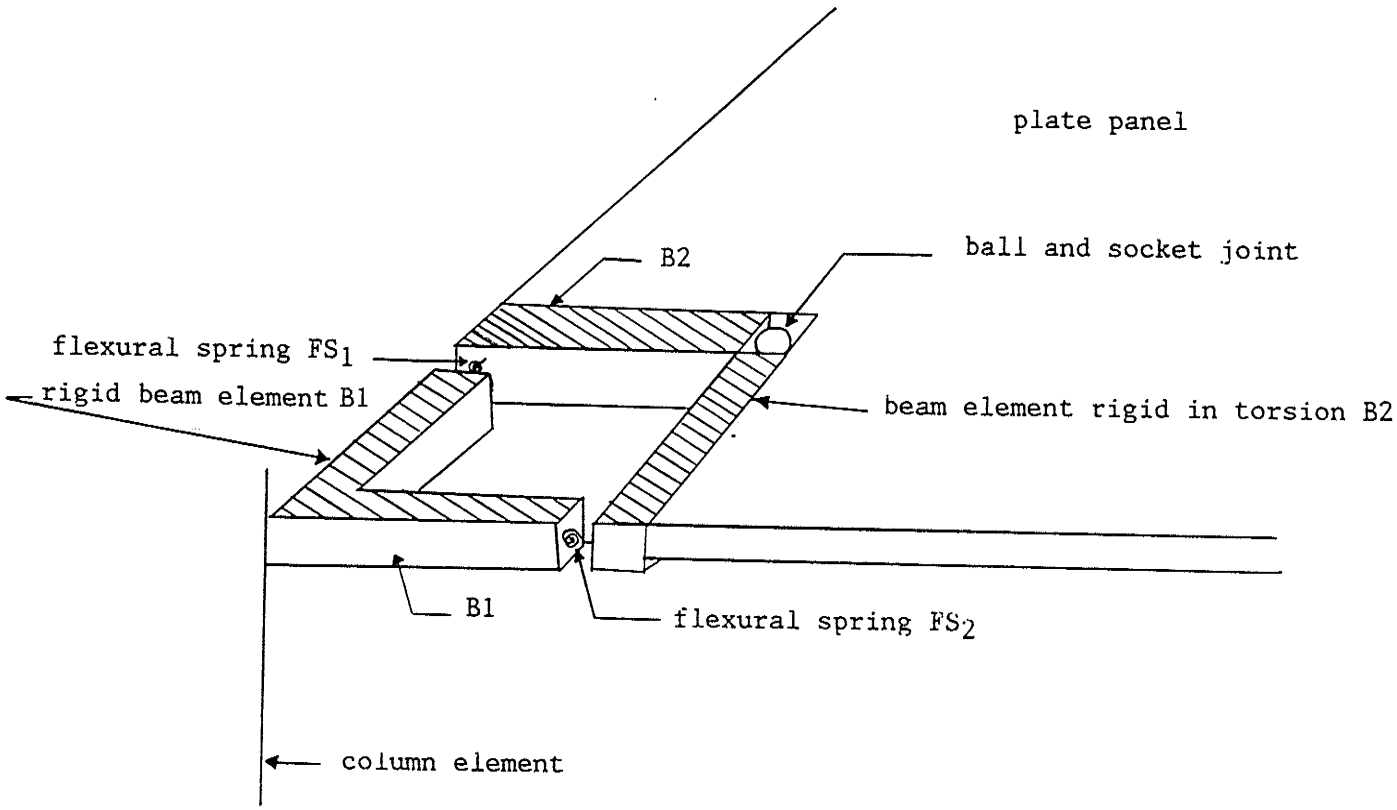

Figure 3.9 : Plate-to-column connection model

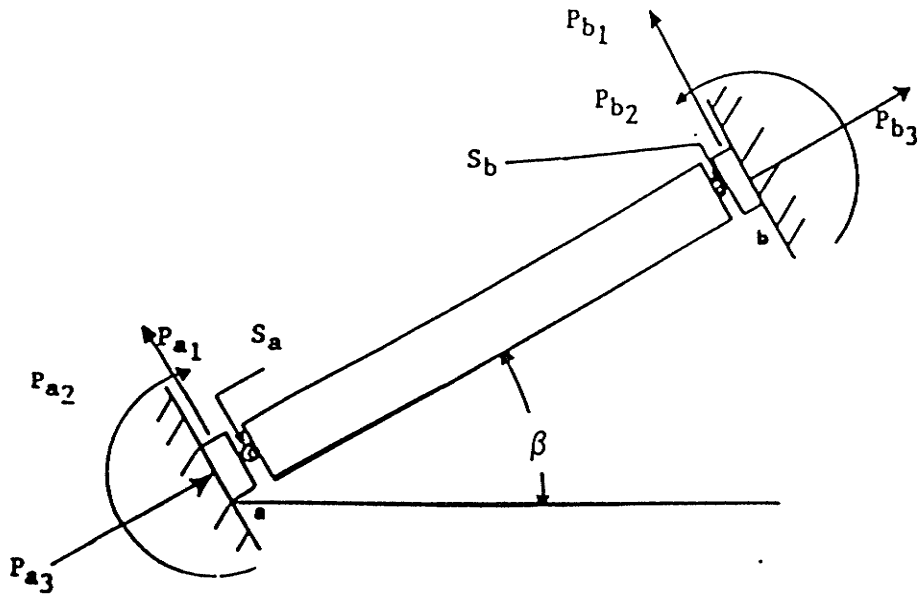

a) Original beam element with flexible ends

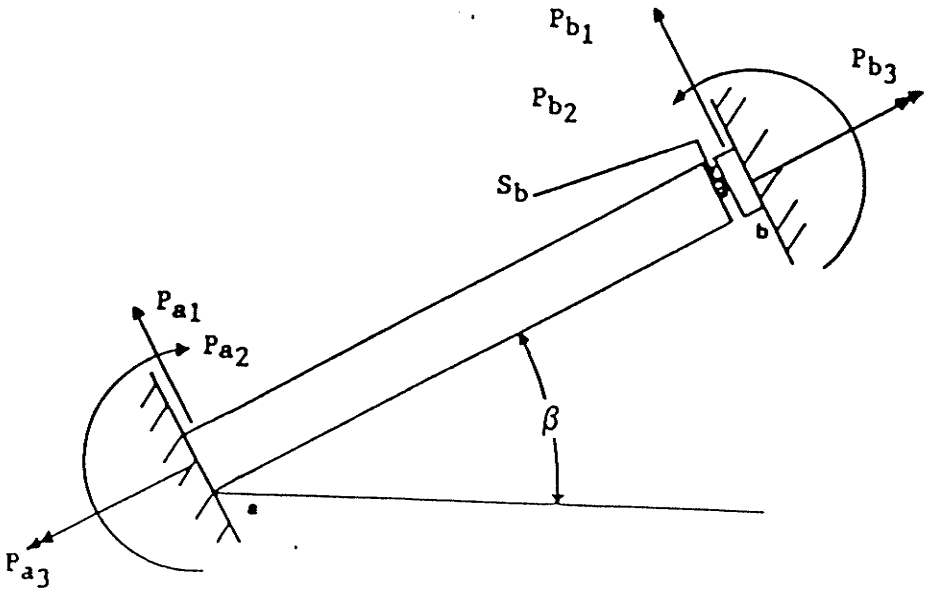

b) Modified beam element

Figure 3.10

spring at end b only, was derived by modifying Jamieson's stiffness matrix by assigning a large value to the spring stiffness S_a. As well, the beam end force vector was modified by including the torsional, instead of the axial, effects. For convenience, the beam stiffness matrix was derived in terms of the rigidity ratio, q, rather than the stiffness, of the spring. The rigidity ratio is defined as

$$q = \frac{1}{1 + \left(\frac{4 E I_3}{S_b (C/2)} \right)} \qquad (3.8)$$

Where,

E = modulus of elasticity

I_3 = second moment of area about the local X_3 axis of the beam

C = twice length of connecting beams B1 and B2 = column width

S_b = spring flexural stiffness

Consequently, the modified stiffness matrix is :

$$\begin{Bmatrix} Pa_1 \\ Pa_2 \\ Pa_3 \\ Pb_1 \\ Pb_2 \\ Pb_3 \end{Bmatrix} = \begin{bmatrix} B_{11} & B_{12} & B_{13} & B_{14} & B_{15} & B_{16} \\ S & B_{22} & B_{23} & B_{24} & B_{25} & B_{26} \\ y & & & & & \\ m & & B_{33} & B_{34} & B_{35} & B_{36} \\ m & & & & & \\ e & & & B_{44} & B_{45} & B_{46} \\ t & & & & & \\ r & & & & B_{55} & B_{56} \\ i & & & & & \\ c & & & & & B_{66} \end{bmatrix} \begin{Bmatrix} Da_1 \\ Da_2 \\ Da_3 \\ Db_1 \\ Db_2 \\ Db_3 \end{Bmatrix} \qquad (3.9)$$

Where,

$B_{11} = (12EI_3/(C/2)^3)e_1$

$B_{12} = (6EI_3/(C/2)^2)\sin(\beta)e_2$

$$B_{13} = (6EI_3/(C/2)^2)\cos(\beta)e_2$$

$$B_{14} = -(12EI_3/(C/2)^3)e_1$$

$$B_{15} = (6EI_3/(C/2)^2)\sin(\beta)e_3$$

$$B_{16} = (6EI_3/(C/2)^2)\cos(\beta)e_3$$

$$B_{22} = (GJ/(C/2))\cos^2(\beta) + (4EI_3/(C/2))\sin^2(\beta)e_4$$

$$B_{23} = (4EI_3/(C/2))\cos(\beta)\sin(\beta)e_4-(GJ/(C/2))\cos(\beta)\sin(\beta)$$

$$B_{24} = -(6EI_3/(C/2)^2)\sin(\beta)e_2$$

$$B_{25} = (2EI_3/(C/2))\sin^2(\beta)e_5 + (GJ/(C/2))\cos^2(\beta)$$

$$B_{26} = (2EI_3/(C/2))\cos(\beta)\sin(\beta)+(GJ/(C/2))\sin(\beta)\cos(\beta)$$

$$B_{33} = (4EI_3/(C/2))\cos^2(\beta)e_4 + (GJ/(C/2))\sin^2(\beta)$$

$$B_{34} = -(6EI_3/(C/2)^2)\cos(\beta)e_2$$

$$B_{35} = (2EI_3/(C/2))\cos(\beta)\sin(\beta)+(GJ/(C/2))\cos(\beta)\sin(\beta)$$

$$B_{36} = (2EI_3/(C/2))\cos^2(\beta)e_5 - (GJ/(C/2))\sin^2(\beta)$$

$$B_{44} = (12EI_3/(C/2)^3)e_1$$

$$B_{45} = -(6EI_3/(C/2)^2)\sin(\beta)e_3$$

$$B_{46} = -(6EI_3/(C/2)^2)\cos(\beta)e_3$$

$$B_{55} = (4EI_3/(C/2))\sin^2(\beta)e_6 + (GJ/(C/2))\cos^2(\beta)$$

$$B_{56} = (4EI_3/(C/2))\cos(\beta)\sin(\beta)-(GJ/(C/2))\cos(\beta)\sin(\beta)$$

$$B_{66} = (4EI_3/(C/2))\cos^2(\beta)e_6 + (GJ/(C/2))\sin^2(\beta)$$

$$e_1 = (3q + 1)/4$$

$$e_2 = (q + 1)/2$$

$$e_3 = q$$

$$e_4 = (q + 3)/4$$

$$e_5 = q$$

$$e_6 = q$$

and,

β = Angle between beam local X_3 axis and the global X_3' axis

G = Shear modulus

J = Polar moment of inertia

Figure 3.11 illustrates the behaviour of the plate-to-column connection model. As the column rotates through angle $\emptyset_c$ under lateral loading of the structure, beam elements B1 rotate through the same angle. This satisfies the small deflection requirement that plane cross-sectional surfaces in the column remain plane after deformation. As the rotation of the column is resisted by the surrounding plate panels, moments are induced in the flexural springs connecting beam elements B1 to the plate. As a consequence rotational deformations $\emptyset_s$ occur in the springs. Hence, the flexural rotation of the plate at the column is $\emptyset_c - \emptyset_s$.

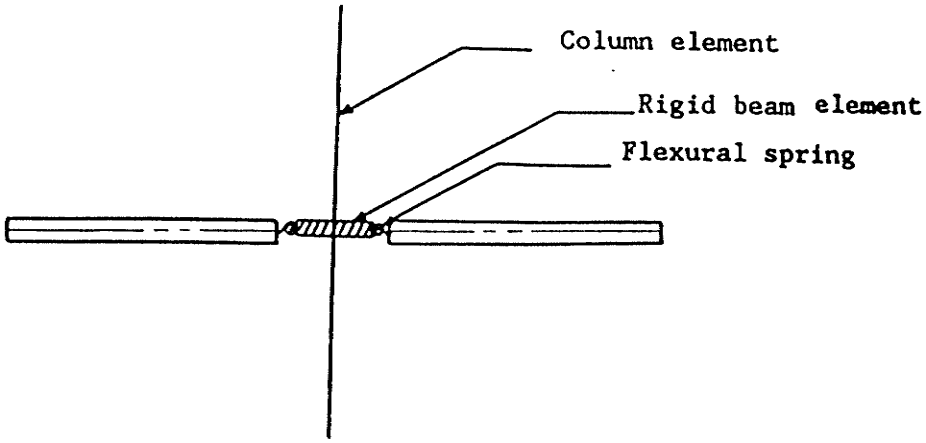

a) Connection before loading

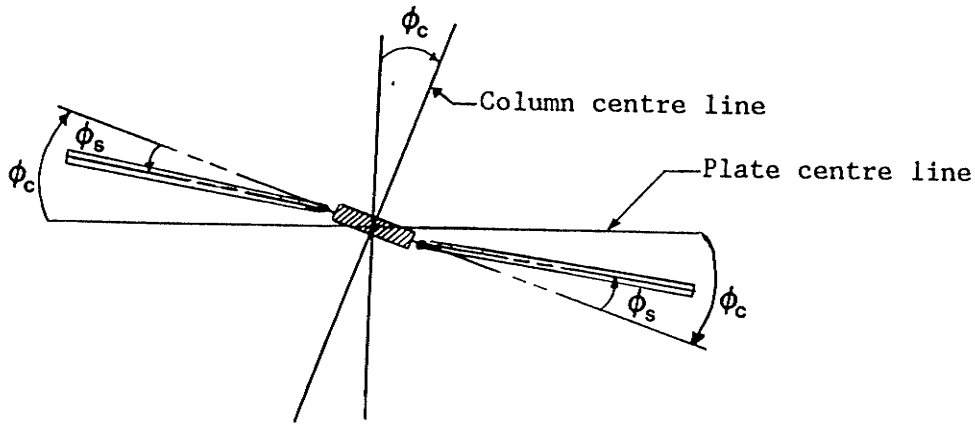

b) Connection after loading

Figure 3.11: Behaviour of plate-column connection model

Chapter IV

MODELLING OF THE FLAT PLATE STRUCTURE

4.1 MODELLING THE OVERALL STRUCTURE

In order to avoid the difficulties encountered when using the equivalent beam and equivalent frame models, the structure is modelled as a single rectangular three-dimensional frame. For analysis purposes, it is assumed to be built up from a series of flat-plate floor panels, columns and shear wall panels, as illustrated in Figure 4.1.

The computer program which performs the structural analysis accounts for the nonlinear moment-rotation behaviour at the plate-to-column connections by performing repeated cycles of linear analysis, each time modifying the connection stiffnesses. Alternatively, the program can be used to perform a single linear analysis.

For convenience, two coordinate systems are employed to describe the structure. They are the global and the local systems. The stuctural loads, displacements and geometry are expressed in the global coordinate system, which is illustrated in Figure 4.1. In this study, primed variables, such as force and displacement vectors, represent quantities expressed in the global coordinate system. For example, P_s'

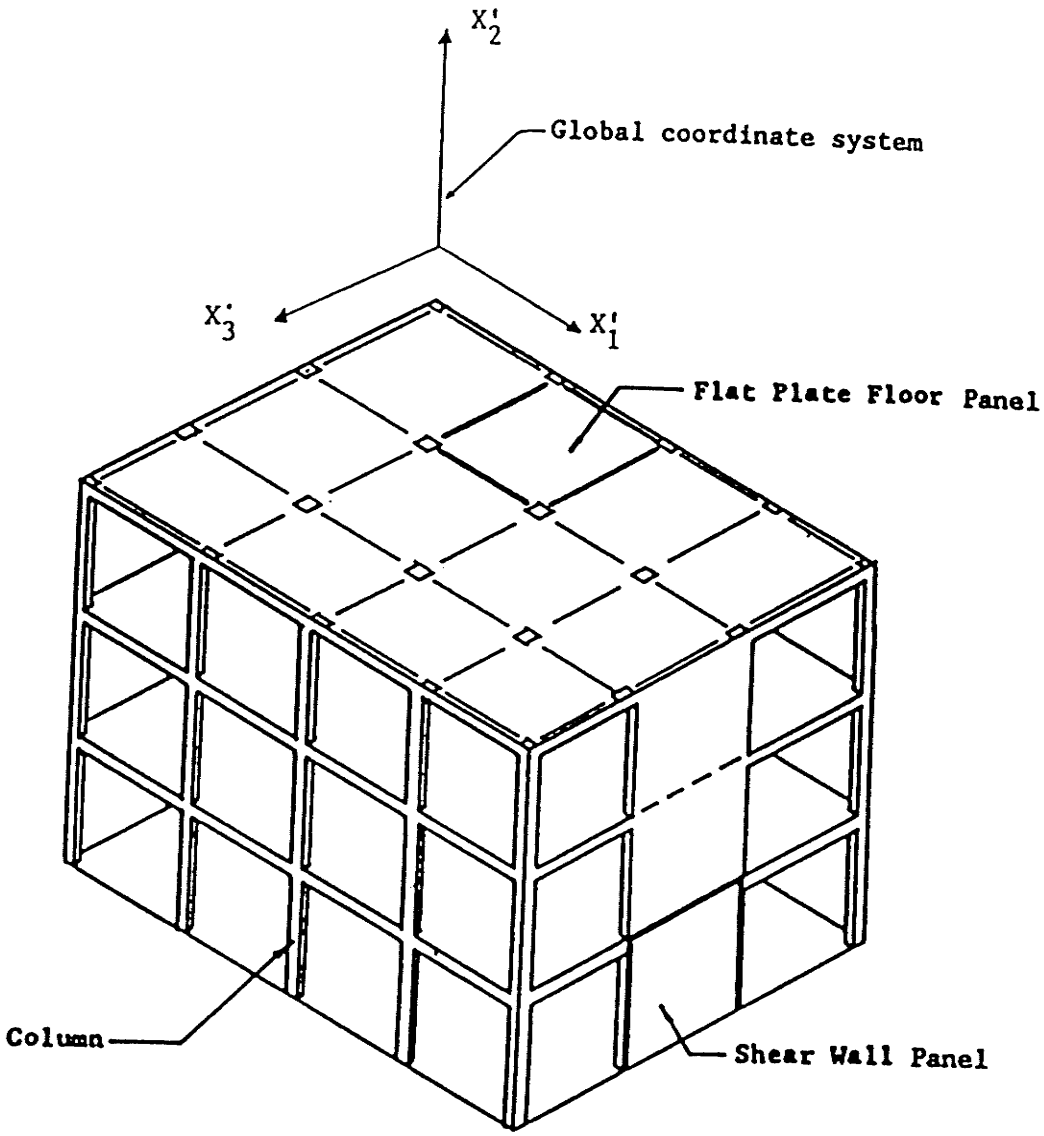

Figure 4.1: Structural Components of Flat-Plate Structure

is a force vector applied at s and expressed in the global coordinate system.

The force-deformation relationships for an individual element in the structure are expressed in a local coordinate system for that element, as illustrated in Figure 4.2. For each of the elements shown, the orientation of the coordinate axes for the local system is consistently that illustrated in the figure. Thus, for example, the local X_1 axis for the column element lies along the column axis, and axes X_2 and X_3 coincide with the principal axes of the column cross-section. In this study, variables such as force and displacement vectors are unprimed when they are expressed in a local coordinate system. Thus, for example, D_c represents a displacement vector at point c, expressed in the appropriate local coordinate system.

In general-purpose three-dimensional analysis programs, normally six degrees of freedom are assumed at each node in the structure, as shown in Figure 4.3. A node is assumed at each point where a column, or the corner of a shear wall, intersects a floor plate. For a typical node , three of the degrees of freedom, Δ'_1,Δ'_3 and θ'_2, are associated with in-plane displacements of the floor plate. The other three, Δ'_2,θ'_1 and θ'_3, are associated with out-of-plane displacements. For a frame with N nodes per floor, the total number of unknown displacements to be evaluated, and thus the number of equations to be solved, equals six times the number

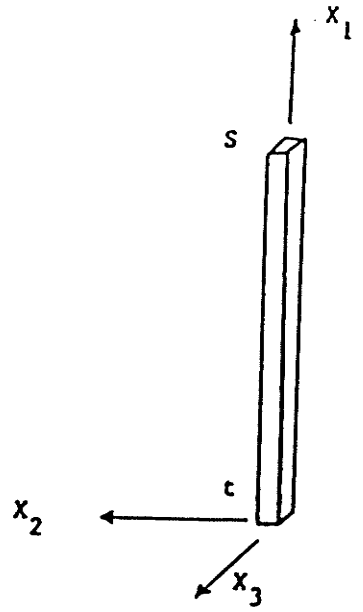

a) Column element

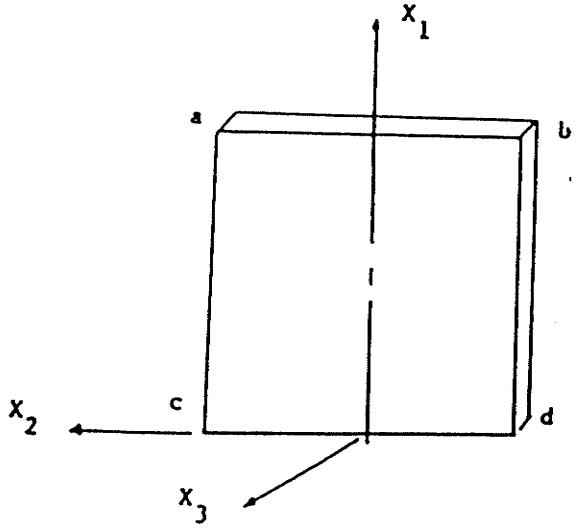

b) b) Shearwall element

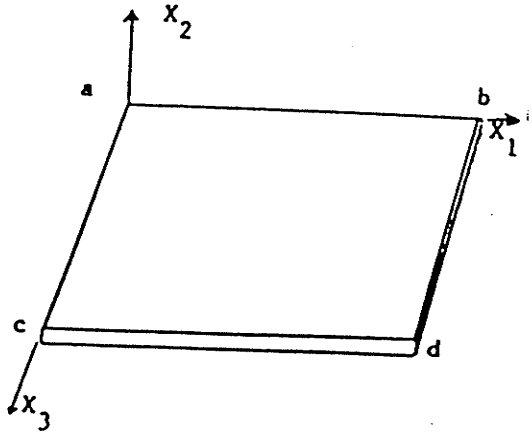

c) Plate element

Figure 4.2: Member Local Coordinate Systems

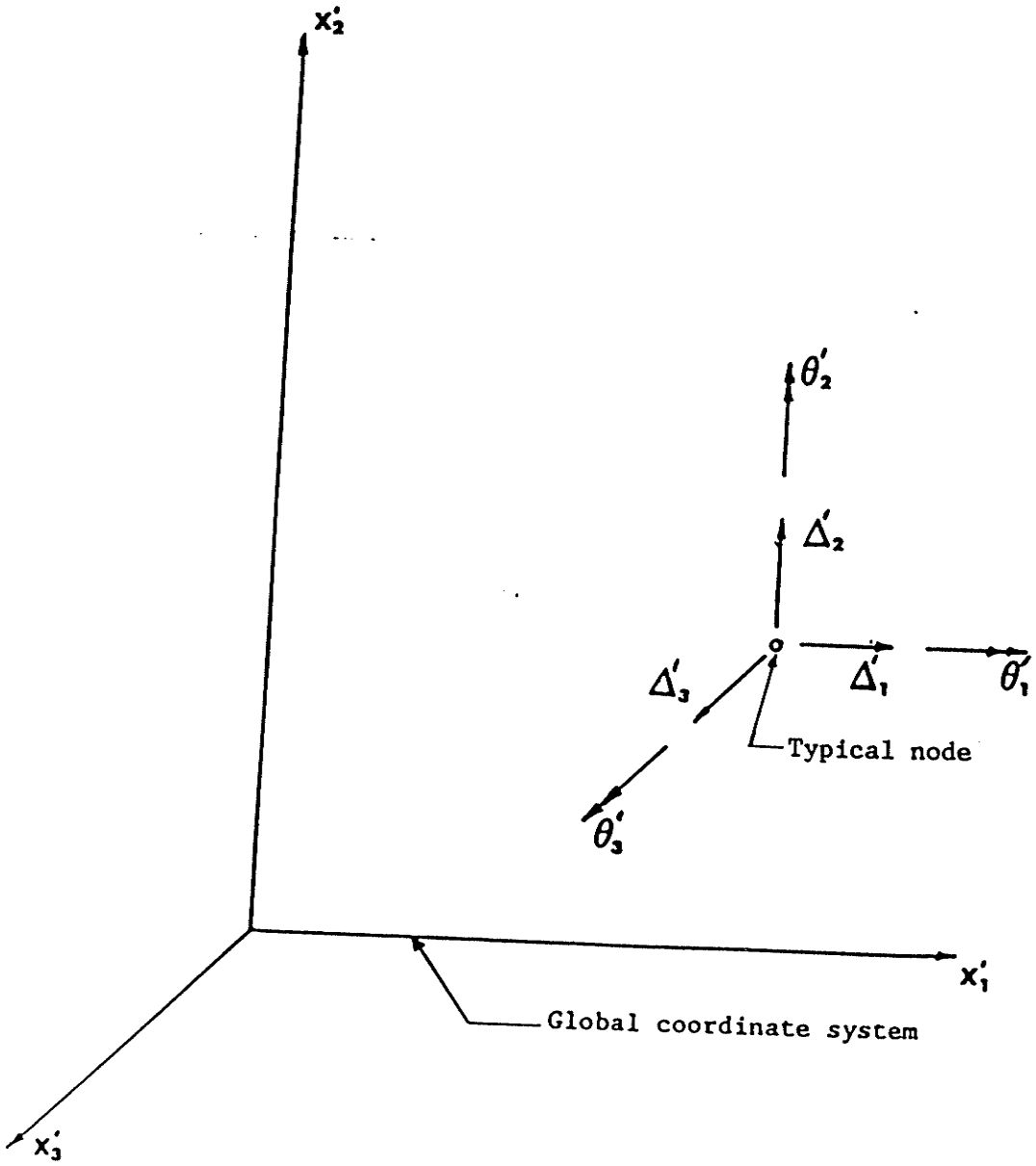

Figure 4.3: Global degrees of freedom

of nodes times the number of floors. Consequently, the large storage capacity required by general purpose three-dimensional analysis programs sometimes makes them prohibitively expensive for lateral load analysis of multi-storey flat-plate structures.

In flat-plate structures, resistance to lateral loading is provided by the flexural stiffness of the columns and the floor plate panels. Shear walls may be included to provide additional lateral stiffness. Typically, the in-plane stiffnesses of the floors are large compared to the stiffnesses of the elements which resist the lateral loading, and thus the floors are assumed to act as rigid diaphragms. The latter assumption is realistic, provided that there are no large openings in the floor and shear walls extend the full height of the building. As well, individual shear walls must be fairly uniform over the height of the building, (Poland, 1980).

For cross-wall buildings, where shear walls carry all gravity and lateral loads, the stiffness of the walls may be the same as or greater than the in-plane stiffnesses of the floors. Thus, the assumption that the floor acts as a rigid diaphragm may not be acceptable.

The term "rigid diaphragm" implies that the floors are assumed to be infinitely stiff in their own plane. No in-plane distortions can occur. The individual floor panels

experience rigid body displacements only. The in-plane displacements of all points in a given floor can be described by three degrees of freedom; linear displacements in the directions of the two horizontal axes and a rotation about the vertical axis. Thus the in-plane degrees of freedom at node j in Figure 4.4 can be related to those at node v. The nodes v and j are referred to as master and slave nodes, respectively. One master node is required for each floor. It may be located anywhere in the floor. Thus, the three in-plane degrees of freedom at each column node can be related to those at the master node. Consequently, for a structure with N frame nodes per floor, the number of degrees of freedom per floor is reduced from 6N to 3N+3. This procedure of slaving the column nodes to the master nodes permits a very significant saving in both storage requirements and execution time needed for equation solving.

In the structural analysis computer program, the lateral loads are applied as concentrated forces at the master nodes located in each of the floors only, as illustrated in Figure 4.5. These forces may vary from floor to floor in the structure. Thus, the program is capable of modelling any lateral load distribution.

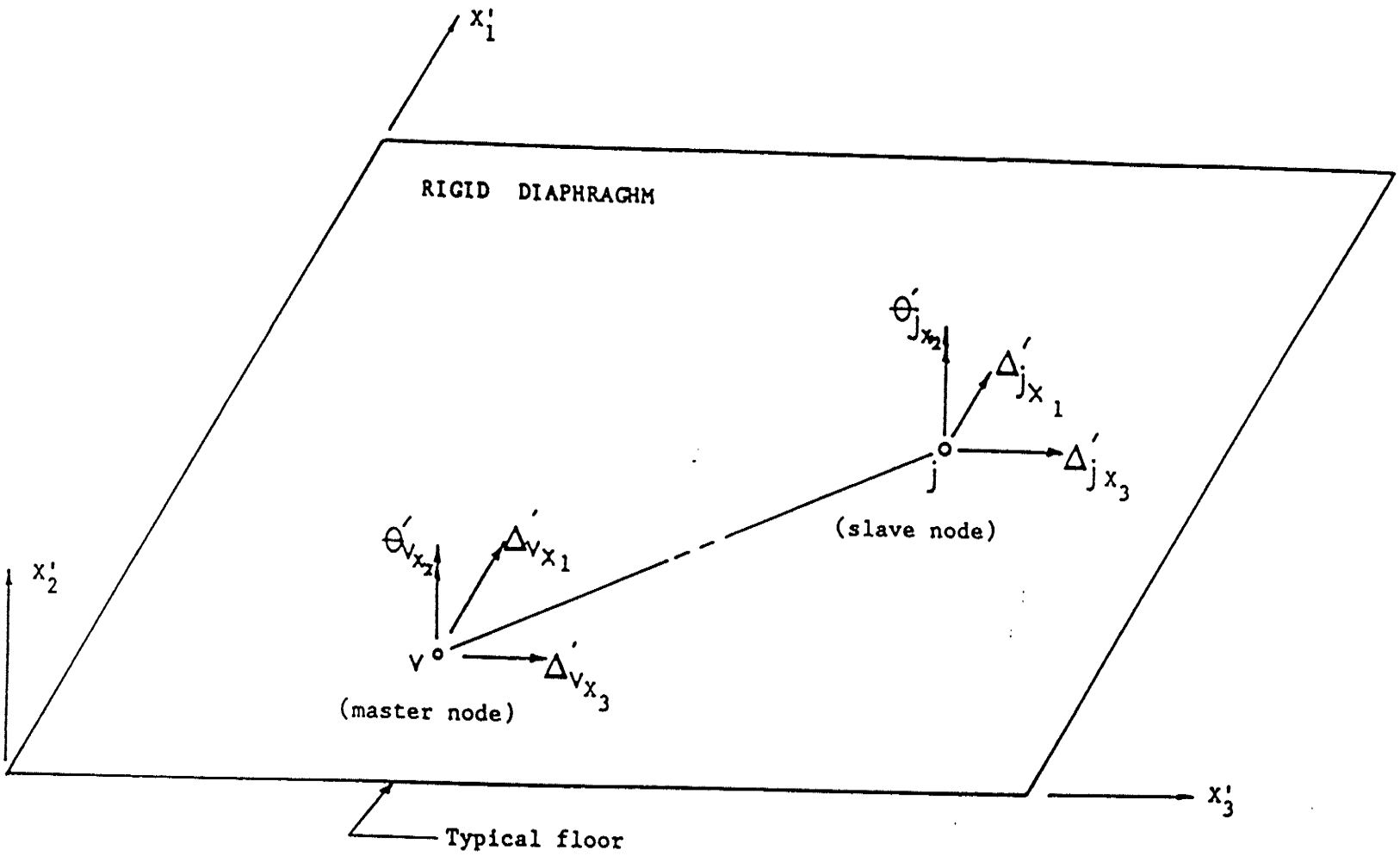

Figure 4.4: master and slave nodes

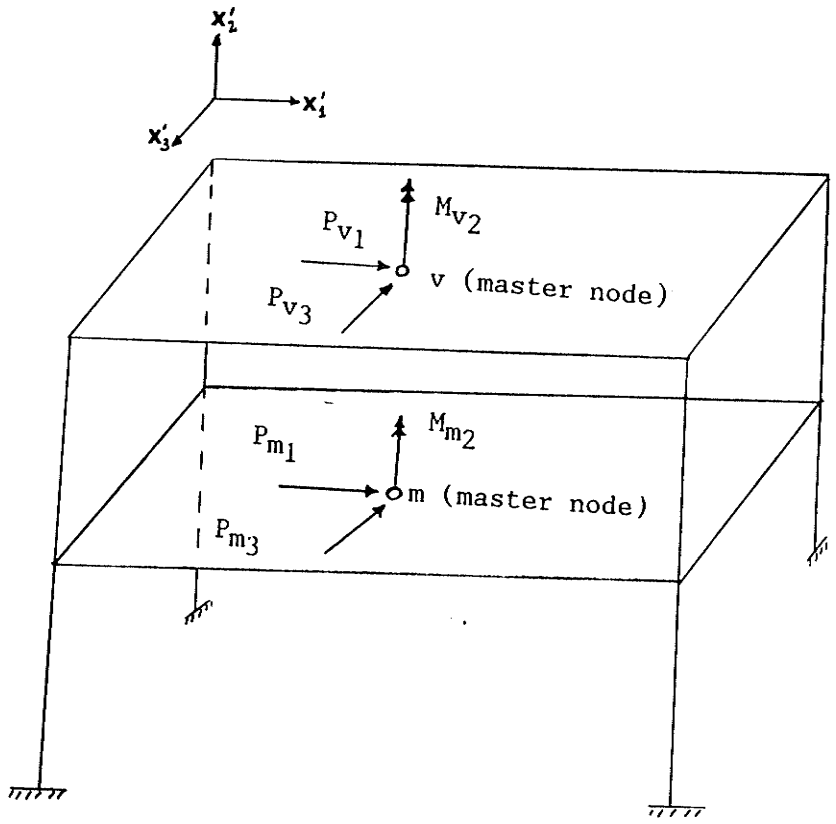

Figure 4.5: Lateral Load Applied to the Master Nodes

4.2 MODELLING OF THE COLUMN ELEMENT

The typical column is modelled using a one dimensional elastic element defined by its end nodes s and t as shown in Figure 4.6. Six degrees of freedom are assumed at each end of the column. The local stiffness matrix is defined by

$$P = K \quad D \tag{4.1}$$

where,

P = vector of local end force components

D = vector of local end displacement components

K = column local stiffness matrix.

The vectors and matrices in Equation (4.1) can be partitioned as follows, to distinguish between force and displacement vectors at nodes s and t.

$$\begin{Bmatrix} P_s \\ P_t \end{Bmatrix} = \begin{bmatrix} K_{ss} & K_{st} \\ K_{ts} & K_{tt} \end{bmatrix} \begin{Bmatrix} D_s \\ D_t \end{Bmatrix} \tag{4.2}$$

where,

$P_s = \{ P_{s1} \quad P_{s2} \quad P_{s3} \quad M_{s1} \quad M_{s2} \quad M_{s3} \}^T$
= local force vector for node s

$P_t = \{ P_{t1} \quad P_{t2} \quad P_{t3} \quad M_{t1} \quad M_{t2} \quad M_{t3} \}^T$
= local force vector for node t

$D_s = \{ \Delta_{s1} \quad \Delta_{s2} \quad \Delta_{s3} \quad \Theta_{s1} \quad \Theta_{s2} \quad \Theta_{s3} \}^T$
= local displacement vector for node s

$D_t = \{ \Delta_{t1} \quad \Delta_{t2} \quad \Delta_{t3} \quad \Theta_{t1} \quad \Theta_{t2} \quad \Theta_{t3} \}^T$
= local displacement vector for node t.

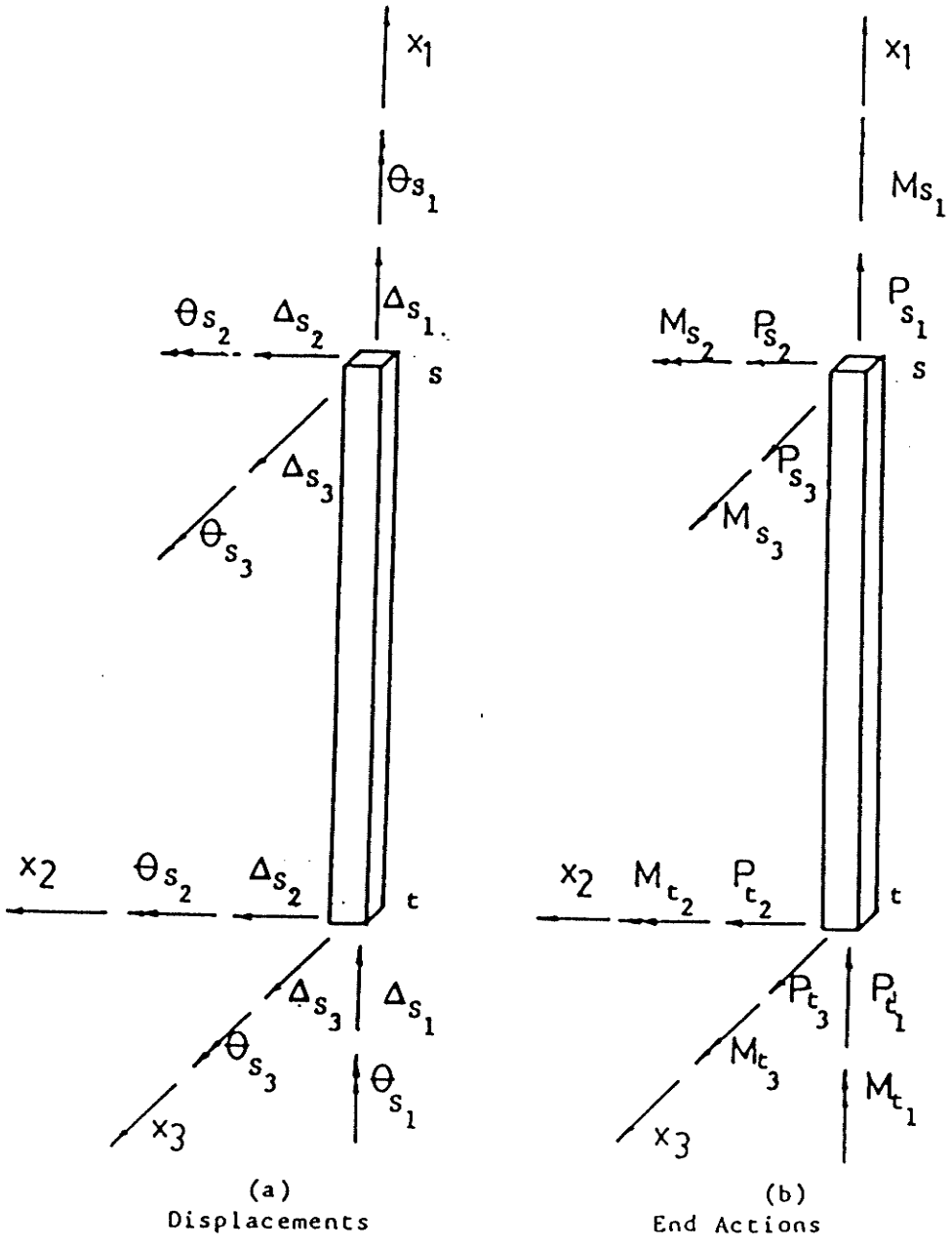

Figure 4.6: Column Element

The in-plane force and displacement components at a typical node in a given floor are related to those at the master node in that floor. Thus, as illustrated in Figure 4.7, the stiffness matrix for the column element can be partitioned further to express the relationships between the out-of-plane and the in-plane forces and displacements. Subscripts o and i denote the out-of-plane and in-plane force and displacement components, respectively. In partitioned form, the force and displacement components can be related by the following matrix equation

$$\begin{Bmatrix} P_{so} \\ P_{si} \\ P_{to} \\ P_{ti} \end{Bmatrix} = \begin{bmatrix} K_{ssoo} & K_{ssoi} & K_{stoo} & K_{stoi} \\ K_{ssio} & K_{ssii} & K_{stio} & K_{stii} \\ K_{tsoo} & K_{tsoi} & K_{ttoo} & K_{ttoi} \\ K_{tsio} & K_{tsii} & K_{ttio} & K_{ttii} \end{bmatrix} \begin{Bmatrix} D_{so} \\ D_{si} \\ D_{to} \\ D_{ti} \end{Bmatrix} \quad (4.3)$$

where,

$$P_{so} = \{ \; P_{s1} \quad M_{s2} \quad M_{s3} \; \}^T \quad (4.4)$$

is the out-of-plane force vector for node s

$$P_{si} = \{ \; P_{s2} \quad P_{s3} \quad M_{s1} \; \}^T \quad (4.5)$$

is the in-plane force vector for node s

$$P_{to} = \{ \; P_{t1} \quad M_{t2} \quad M_{t3} \; \}^T \quad (4.6)$$

is the out-of-plane force vector for node t

$$P_{ti} = \{ \; P_{t2} \quad P_{t3} \quad M_{t1} \; \}^T \quad (4.7)$$

is the in-plane force vector for node t

$$D_{so} = \{ \; \Delta_{s1} \quad \Theta_{s2} \quad \Theta_{s3} \; \}^T \quad (4.8)$$

is the out-of-plane displacement vector for node s

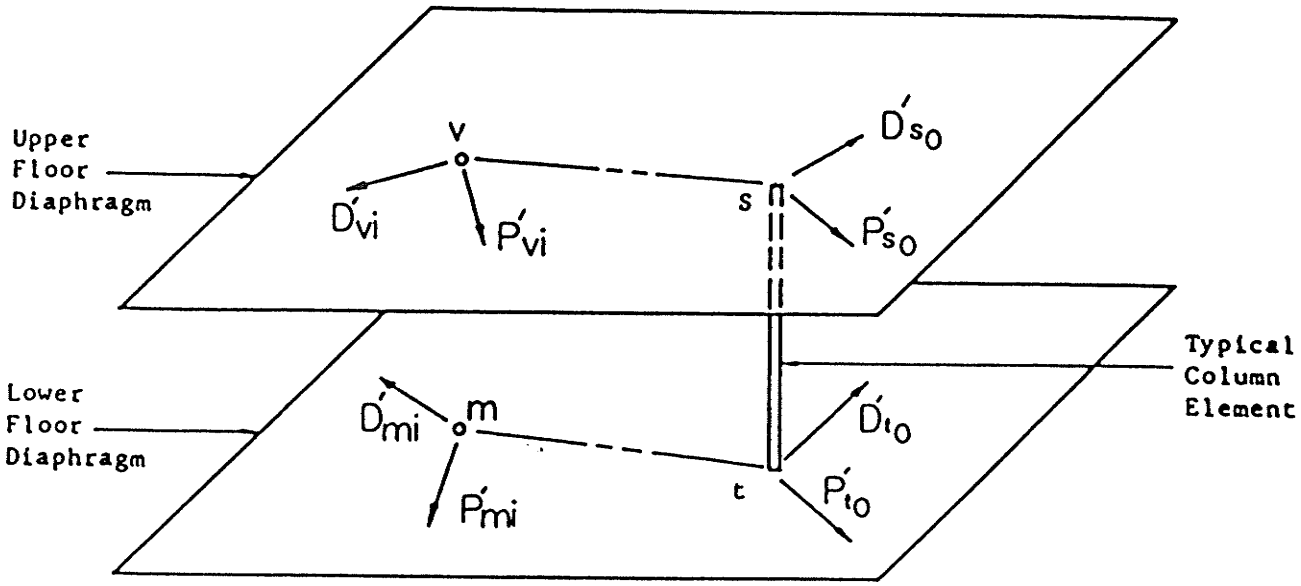

Figure 4.7: In-plane and Out-of-Plane Degrees of Freedom

$$D_{si} = \{ \quad \Delta_{s2} \quad \Delta_{s3} \quad \Theta_{s1} \quad \}^T \tag{4.9}$$

is the in-plane displacement vector for node s

$$D_{to} = \{ \quad \Delta_{t1} \quad \Theta_{t2} \quad \Theta_{t3} \quad \}^T \tag{4.10}$$

is the out-of-plane displacement vector for node t

$$D_{ti} = \{ \quad \Delta_{t2} \quad \Delta_{t3} \quad \Theta_{t1} \quad \}^T \tag{4.11}$$

is the in-plane displacement vector for node t

and

$$K_{ssoo} = \begin{bmatrix} S_1 & 0 & 0 \\ 0 & S_2 & 0 \\ 0 & 0 & S_3 \end{bmatrix} \tag{4.12}$$

$$K_{ssio} = \begin{bmatrix} 0 & 0 & -S_8 \\ 0 & S_7 & 0 \\ 0 & 0 & 0 \end{bmatrix} \tag{4.13}$$

$$K_{ssii} = \begin{bmatrix} S_4 & 0 & 0 \\ 0 & S_5 & 0 \\ 0 & 0 & S_6 \end{bmatrix} \tag{4.14}$$

$$K_{tsoo} = \begin{bmatrix} -S_1 & 0 & 0 \\ 0 & S_9 & 0 \\ 0 & 0 & S_{10} \end{bmatrix} \tag{4.15}$$

$$K_{tsoi} = \begin{bmatrix} 0 & 0 & 0 \\ 0 & S_7 & 0 \\ -S_8 & 0 & 0 \end{bmatrix} \qquad (4.16)$$

$$K_{tsio} = \begin{bmatrix} 0 & 0 & S_8 \\ 0 & -S_7 & 0 \\ 0 & 0 & 0 \end{bmatrix} \qquad (4.17)$$

$$K_{tsii} = \begin{bmatrix} -S_4 & 0 & 0 \\ 0 & -S_5 & 0 \\ 0 & 0 & -S_6 \end{bmatrix} \qquad (4.18)$$

$$K_{ttoo} = \begin{bmatrix} S_1 & 0 & 0 \\ 0 & S_2 & 0 \\ 0 & 0 & S_3 \end{bmatrix} \qquad (4.19)$$

$$K_{ttio} = \begin{bmatrix} 0 & 0 & S_8 \\ 0 & -S_7 & 0 \\ 0 & 0 & 0 \end{bmatrix} \qquad (4.20)$$

$$K_{ttii} = \begin{bmatrix} S_4 & 0 & 0 \\ 0 & S_5 & 0 \\ 0 & 0 & S_6 \end{bmatrix} \qquad (4.21)$$

$$K_{ssoi} = (K_{ssio})^T \qquad (4.22)$$

$$K_{stoo} = (K_{tsoo})^T \qquad (4.23)$$

$$K_{stoi} = (K_{stio})^T \qquad (4.24)$$

$$K_{stio} = (K_{tsio})^T \qquad (4.25)$$

$$K_{stii} = (K_{tsii})^T \qquad (4.26)$$

$$K_{ttoi} = (K_{ttio})^T \qquad (4.27)$$

In the above stiffness submatrices

$$S_1 = \frac{E\ A}{L_h}$$

$$S_2 = \frac{4\ E\ I_2}{L_h}$$

$$S_3 = \frac{4\ E\ I_3}{L_h}$$

$$S_4 = \frac{12\ E\ I_3}{L_h^3}$$

$$S_5 = \frac{12\ E\ I_2}{L_h^3} \qquad (4.28)$$

$$S_6 = \frac{G\ J}{L_h}$$

$$S_7 = \frac{6\ E\ I_2}{L_h^2}$$

$$S_8 = \frac{6\ E\ I_3}{L_h^2}$$

$$S_9 = \frac{2\ E\ I_2}{L_h}$$

$$S_{10} = \frac{2\ E\ I_3}{L_h}$$

and,

I_2 = second moment of area of the cross-section about the local X_2 axis

A = cross-sectional area

L_h = storey height

The partitioned local stiffness matrix for the column can be transformed to the global coordinate system using the following relationships between the local and global forces and displacements.

$$P_s' = R\ P_s \qquad (4.29)$$

$$P_t' = R\ P_t \qquad (4.30)$$

$$D_s = R^T D_s' \qquad (4.31)$$

$$D_t = R^T D_t' \qquad (4.32)$$

Where R = rotation transformation matrix.

Figure 4.8 shows the relationship between the global coordinate system and the column local coordinate system used consistently in this study. Thus, the rotation transformation matrix is

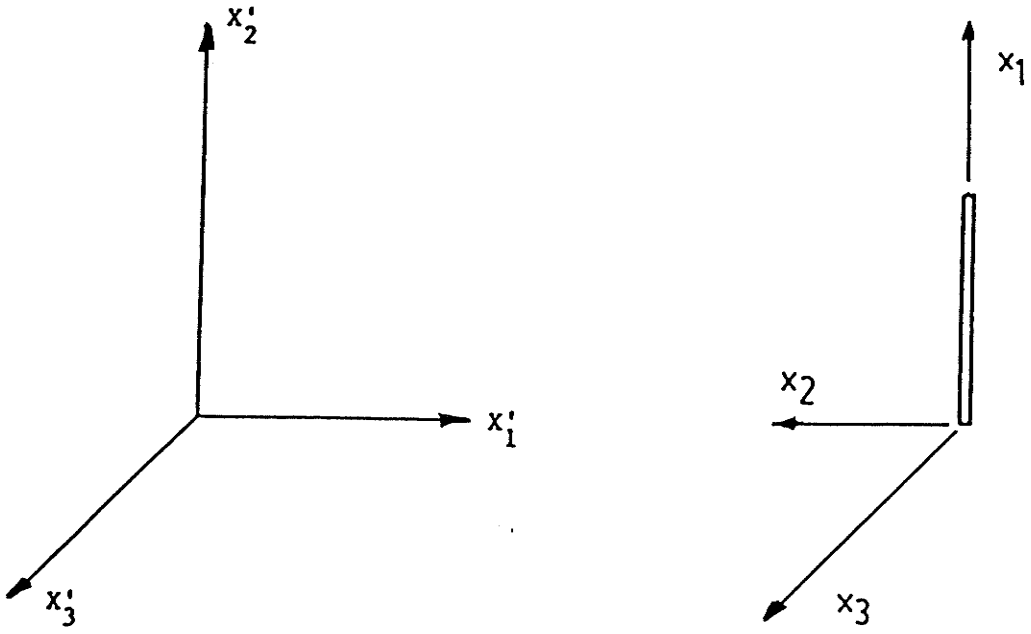

Figure 4.8: Column Local Coordinates and the Global Coordinates

$$R = \begin{bmatrix} R_{11} & 0 \\ 0 & R_{22} \end{bmatrix} = \left[\begin{array}{ccc|ccc} 1 & 0 & 0 & 0 & 0 & 0 \\ 0 & -1 & 0 & 0 & 0 & 0 \\ 0 & 0 & 1 & 0 & 0 & 0 \\ \hline 0 & 0 & 0 & -1 & 0 & 0 \\ 0 & 0 & 0 & 0 & 1 & 0 \\ 0 & 0 & 0 & 0 & 0 & 0 \end{array}\right] \quad (4.33)$$

where,

R_{11} = rotational transformation matrix to express local out-of-plane forces and displacements in the global coordinate system

R_{22} = rotational transformation matrix to express local in-plane forces and displacements in the global coordinate system

The global force-displacement relationship can thus be expressed as follows

$$\begin{Bmatrix} P'_{so} \\ P'_{si} \\ P'_{to} \\ P'_{ti} \end{Bmatrix} = \begin{bmatrix} K'_{ssoo} & K'_{ssoi} & K'_{stoo} & K'_{stoi} \\ K'_{ssio} & K'_{ssii} & K'_{stio} & K'_{stii} \\ K'_{tsoo} & K'_{tsoi} & K'_{ttoo} & K'_{ttoi} \\ K'_{tsio} & K'_{tsii} & K'_{ttio} & K'_{ttii} \end{bmatrix} \begin{Bmatrix} D'_{so} \\ D'_{si} \\ D'_{to} \\ D'_{ti} \end{Bmatrix} \quad (4.34)$$

Where,

$$\begin{aligned} K'_{ssoo} &= R_{11}\, K_{ssoo}\, R_{11} \\ K'_{ssoi} &= R_{11}\, K_{ssoi}\, R_{22} \\ K'_{stoo} &= R_{11}\, K_{stoo}\, R_{11} \\ K'_{stoi} &= R_{11}\, K_{stoi}\, R_{22} \\ K'_{ssio} &= R_{22}\, K_{ssio}\, R_{11} \\ K'_{ssii} &= R_{22}\, K_{ssii}\, R_{22} \\ K'_{stio} &= R_{22}\, K_{stio}\, R_{11} \\ K'_{stii} &= R_{22}\, K_{stii}\, R_{22} \\ K'_{tsoi} &= R_{11}\, K_{tsoi}\, R_{11} \end{aligned} \quad (4.35)$$

$$K'_{ttoo} = R_{11}\, K_{ttoo}\, R_{22}$$
$$K'_{ttoi} = R_{11}\, K_{ttoi}\, R_{11}$$
$$K'_{tsio} = R_{11}\, K_{tsio}\, R_{22}$$
$$K'_{tsii} = R_{22}\, K_{tsii}\, R_{11}$$
$$K'_{tsii} = R_{22}\, K_{tsii}\, R_{22}$$
$$K'_{ttio} = R_{22}\, K_{ttio}\, R_{11}$$
$$K'_{ttii} = R_{22}\, K_{ttii}\, R_{22}$$

The in-plane forces and displacements at nodes s and t can be related to those at the master nodes v and m respectively using the following translation transformations .

$$\begin{aligned} P'_v &= H'_{vs}\, P'_{si} \\ P'_m &= H'_{mt}\, P'_{ti} \\ D'_{si} &= (H'^{-1}_{vs})^T\, D'_v \\ D'_{ti} &= (H'^{-1}_{mt})^T\, D'_m \end{aligned} \qquad (4.36)$$

where H' is a translation transformation matrix. For example, H'_{vs} translates force vector P'_{si} from node s to node v. In equation (4.36)

$$H'_{vs} = \begin{bmatrix} 0 & 0 & 0 \\ 0 & 0 & 0 \\ (X'_{3_s} - X'_{3_v}) & (X'_{1_s} - X'_{1_v}) & 1 \end{bmatrix} \qquad (4.37)$$

$$H'_{mt} = \begin{bmatrix} 1 & 0 & 0 \\ 0 & 1 & 0 \\ (X'_{3_t} - X'_{3_m}) & (X'_{1_t} - X'_{1_m}) & 1 \end{bmatrix} \qquad (4.38)$$

In the translation transformation matrices, X'_{1_s} and X'_{3_s} are the global coordinates for node s, and the other coordinates are similarly expressed. Combining Equations (4.34) and (4.36), the transformed column force-displacement relationships become

$$\begin{Bmatrix} P'_s \\ P'_v \\ P'_t \\ P'_m \end{Bmatrix} = \begin{bmatrix} K'_{ss} & K'_{sv} & K'_{st} & K'_{sm} \\ K'_{vs} & K'_{vv} & K'_{vt} & K'_{vm} \\ K'_{ts} & K'_{tv} & K'_{tt} & K'_{tm} \\ K'_{ms} & K'_{mv} & K'_{mt} & K'_{mm} \end{bmatrix} \begin{Bmatrix} D'_s \\ D'_v \\ D'_t \\ D'_m \end{Bmatrix} \qquad (4.39)$$

where

$$\begin{aligned}
K'_{ss} &= K'_{ssoo} \\
K'_{sv} &= K'_{ssoi} \left(H'^{-1}_{vs}\right)^T \\
K'_{st} &= K'_{stoo} \\
K'_{sm} &= K'_{stoi} \left(H'^{-1}_{mt}\right)^T \\
K'_{vs} &= H'_{vs} K'_{ssoi} \\
K'_{vv} &= H'_{vs} K'_{ssii} \left(H'^{-1}_{vs}\right)^T \\
K'_{vt} &= H'_{vs} K'_{stio} \\
K'_{vm} &= H'_{vs} K'_{stii} \left(H'^{-1}_{mt}\right)^T \qquad (4.40) \\
K'_{ts} &= K'_{tsoo} \\
K'_{tv} &= K'_{tsoi} \left(H'^{-1}_{vs}\right)^T \\
K'_{tt} &= K'_{ttoo} \\
K'_{tm} &= K'_{ttoi} \left(H'^{-1}_{mt}\right)^T \\
K'_{ms} &= H'_{mt} K'_{tsio} \\
K'_{mv} &= H'_{mt} K'_{tsii} \left(H'^{-1}_{vs}\right)^T \\
K'_{mt} &= H'_{mt} K'_{tsio} \\
K'_{mm} &= H'_{mt} K'_{ttii} \left(H'^{-1}_{mt}\right)^T
\end{aligned}$$

Equation (4.39) relates out-of-plane force and displacement components at slave nodes s and t and in-plane components at master nodes v and m, as influenced by the column connecting nodes s and t. The stiffness submatrices in Equation (4.39) are inserted directly into the structure stiffness matrix.

4.3 MODELLING OF SHEAR WALLS

In this study, the portion of a shear wall between consecutive floors is modelled as a deep column. A typical shear wall element a-j-b-d-i-c is shown in Figure 4.9. The stiffness matrix for a deep column is identical to that of a regular column except for two modifications. Firstly, shearing deformations, as well as flexural deformations, are considered when computing the in-plane displacements of the wall. Secondly, for out-of-plane displacements, the shear wall is modelled as a wide beam.

When subjected to flexure, slender beams exhibit anticlastic behaviour, with cross-sectional deformations as illustrated in Figure 4.10 (a). Wide beams, on the other hand, experience anticlastic bending near their edges only, as illustrated in Figure 4.10 (b). It has been found experimentally that the consequent increase in the out-of-plane bending of wide beams can be accounted for by multiplying the modulus of elasticity by the factor $1/(1-\nu^2)$, (Timoshenko, 1941). Thus the out-of-plane modulus of elasticity can be expressed as

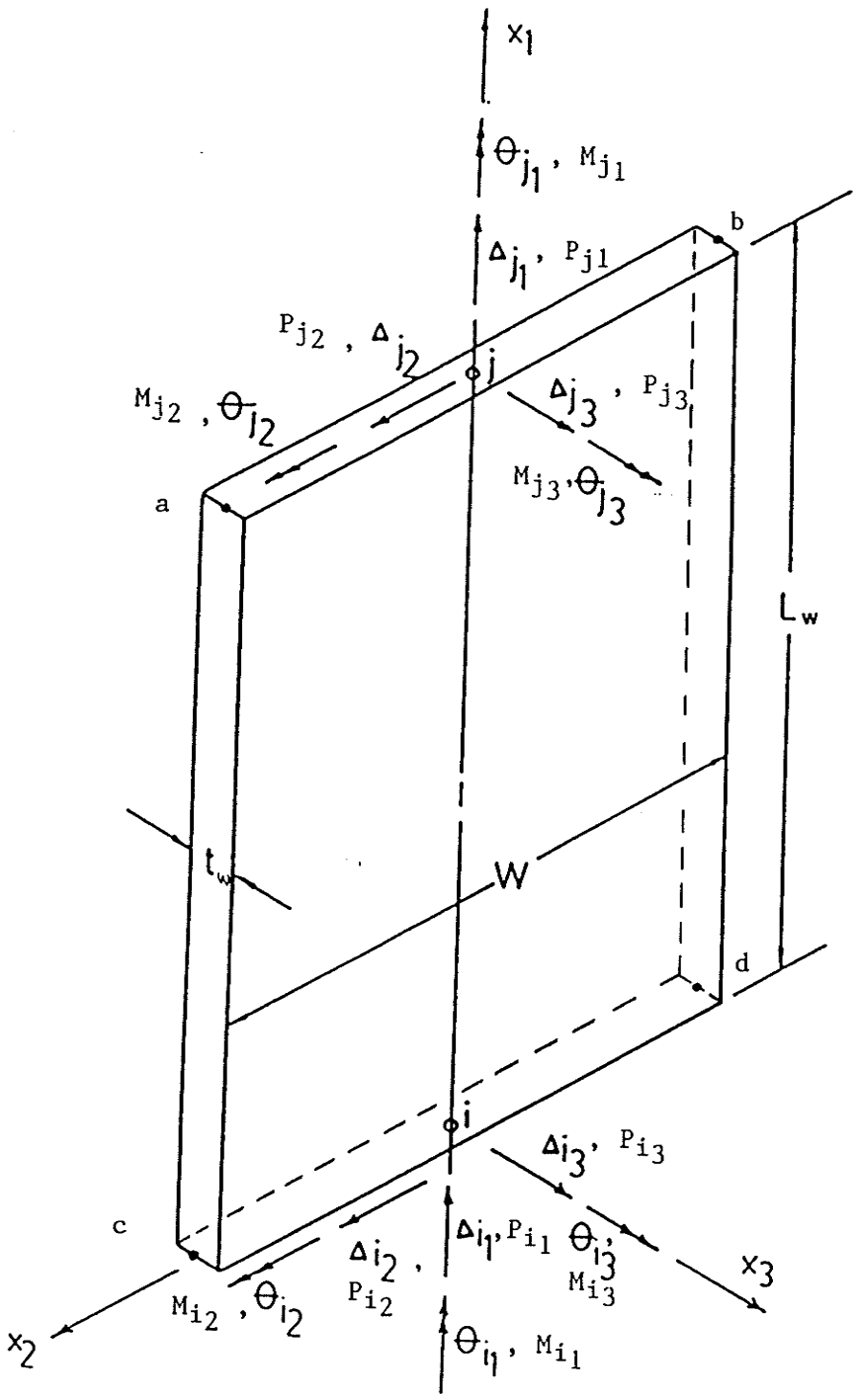

Figure 4.9 : Shear wall Element, Showing Force and Displacement Components at i and j

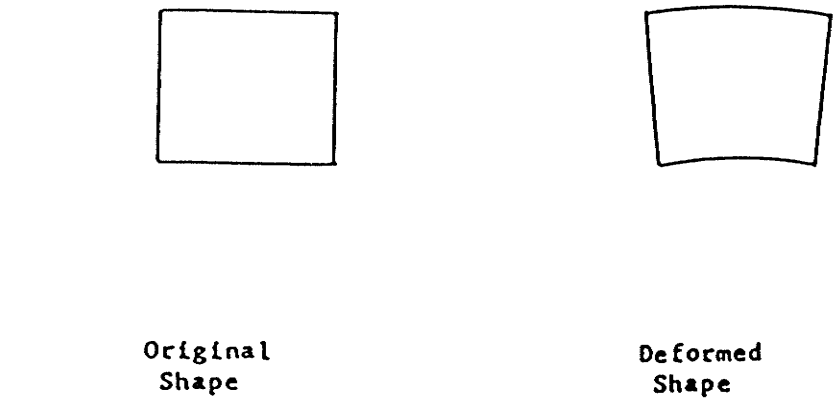

a) Slender beam cross-section

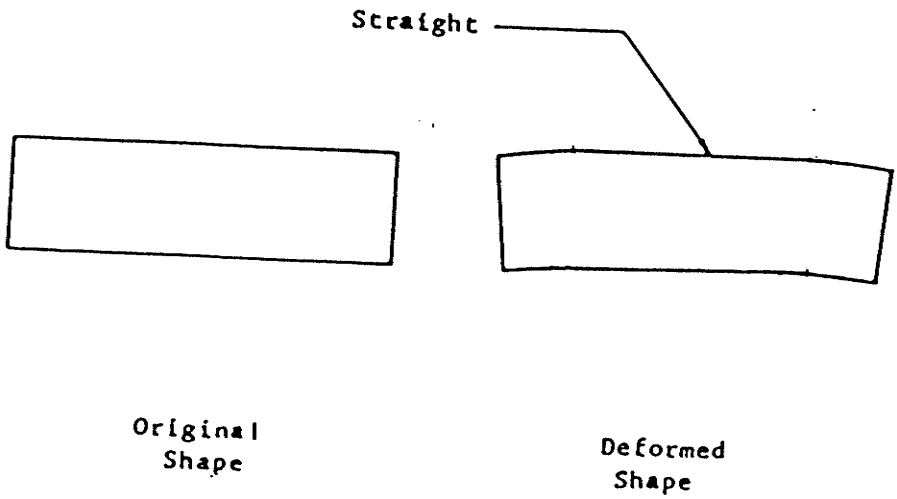

b) Wide beam cross-section

Figure 4.10: Beam Deformation Under Bending

$$E_w = \frac{E}{1-\nu^2} \qquad (4.41)$$

where,

E_w = effective out-of-plane modulus of elasticity for shear wall element

ν = Poisson ratio

As illustrated in Figure 4.11, the interaction between shear walls and the floor panels is provided by inserting rigid beams at floor levels in bays where shear walls are located. The rigid beams ensure that the cross-section of the wall remains plane after deformation, as is implied by the deep column model. They are assembled into the plate panel stiffness matrices. This constrains the panel edge node diplacements and provides shear wall-frame interaction. The rigid beams are automatically assembled into the floor stiffness matrix in the same manner as regular beams. They are made rigid by specifying suitably large beam properties.

The local force-deformation relationship for the shear wall element is :

$$\begin{Bmatrix} P_i \\ P_j \end{Bmatrix} = \begin{bmatrix} K_{ii} & K_{ij} \\ K_{ji} & K_{jj} \end{bmatrix} \begin{Bmatrix} D_i \\ D_j \end{Bmatrix} \qquad (4.42)$$

where

$$P_i = \{ P_{i1} \quad P_{i2} \quad P_{i3} \quad M_{i1} \quad M_{i2} \quad M_{i3} \}^T \qquad (4.43)$$

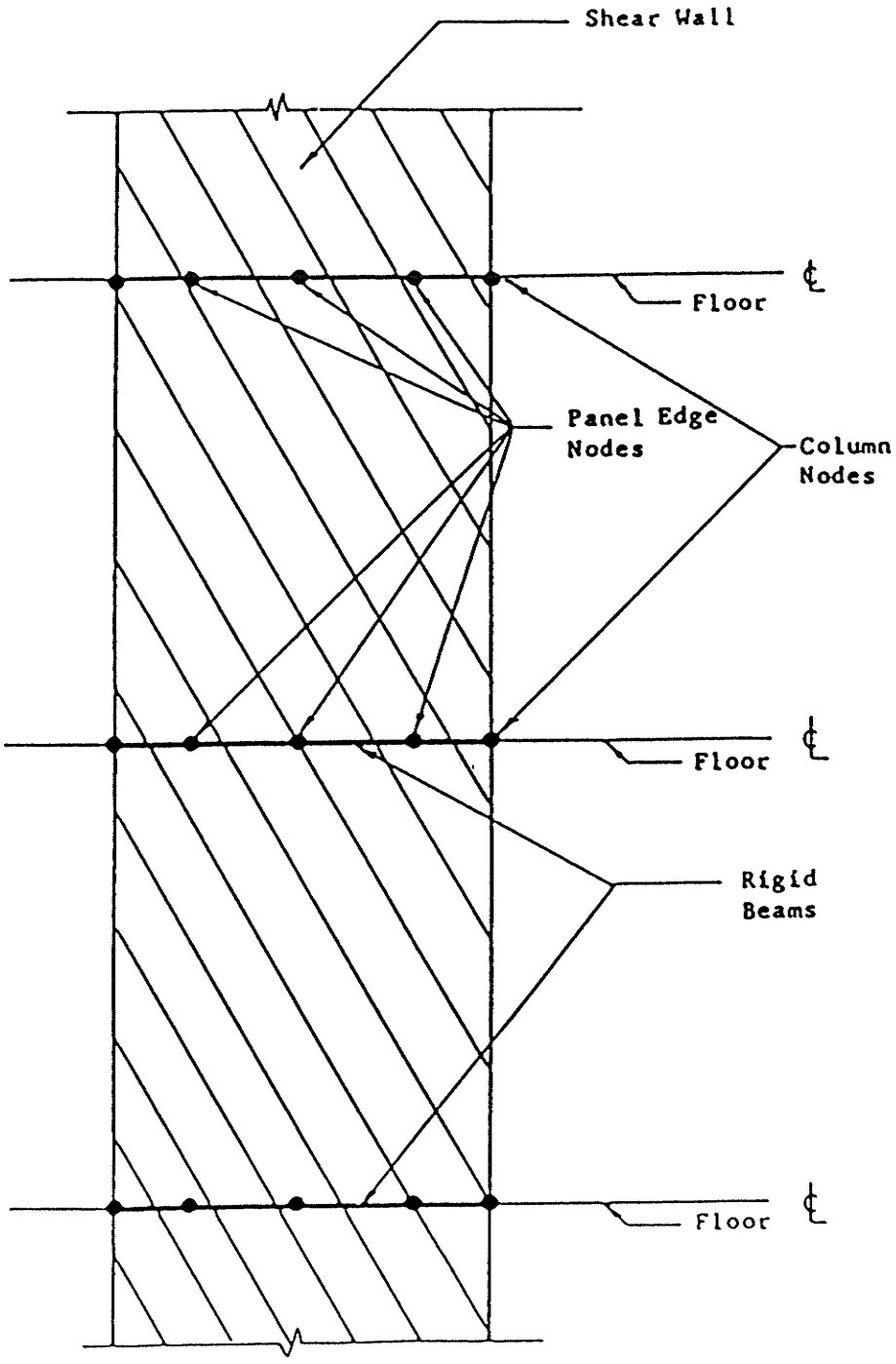

Figure 4.11: Shear Wall-Frame Interaction

is the local force vector for node i

$$P_j = \{ P_{j1} \quad P_{j2} \quad P_{j3} \quad M_{j1} \quad M_{j2} \quad M_{j3} \}^T \quad (4.44)$$

is the local force vector for node j

$$D_i = \{ \Delta_{i1} \quad \Delta_{i2} \quad \Delta_{i3} \quad \Theta_{i1} \quad \Theta_{i2} \quad \Theta_{i3} \}^T \quad (4.45)$$

is the local displacement vector for node i

$$D_j = \{ \Delta_{j1} \quad \Delta_{j2} \quad \Delta_{j3} \quad \Theta_{j1} \quad \Theta_{j2} \quad \Theta_{j3} \}^T \quad (4.46)$$

is the local displacement vector for node j

and

$$K_{ii} = \begin{bmatrix} S1 & 0 & 0 & 0 & 0 & 0 \\ 0 & S2 & 0 & 0 & 0 & 0 \\ 0 & 0 & S4 & 0 & -S5 & 0 \\ 0 & 0 & 0 & S6 & 0 & 0 \\ 0 & 0 & -S5 & 0 & S7 & 0 \\ 0 & S3 & 0 & 0 & 0 & S9 \end{bmatrix} \quad (4.47)$$

$$K_{ji} = \begin{bmatrix} -S1 & 0 & 0 & 0 & 0 & 0 \\ 0 & -S2 & 0 & 0 & 0 & -S3 \\ 0 & 0 & -S4 & 0 & 0 & S5 \\ 0 & 0 & 0 & -S6 & 0 & 0 \\ 0 & 0 & -S5 & 0 & S8 & 0 \\ 0 & S3 & 0 & 0 & 0 & S10 \end{bmatrix} \quad (4.48)$$

$$K_{ij} = (K_{ji})^T \quad (4.49)$$

$$K_{jj} = \begin{bmatrix} S1 & 0 & 0 & 0 & 0 & 0 \\ 0 & S2 & 0 & 0 & 0 & -S3 \\ 0 & 0 & S4 & 0 & S5 & 0 \\ 0 & 0 & 0 & S6 & 0 & 0 \\ 0 & 0 & S5 & 0 & S7 & 0 \\ 0 & -S3 & 0 & 0 & 0 & S9 \end{bmatrix} \qquad (4.50)$$

In the stiffness submatrices

$$S1 = \frac{A \ E}{L_h}$$

$$S2 = \frac{12 \ E \ I_3}{L_h^3 \ (1+\emptyset)}$$

$$S3 = \frac{6 \ E \ I_3}{L_h^2 \ (1+\emptyset)}$$

$$S4 = \frac{12 \ E_w I_2}{L_h^3}$$

$$S5 = \frac{6 \ E_w I_2}{L_h^2}$$

$$S6 = \frac{G \ J}{L_h}$$

$$S7 = \frac{4 \ E_w I_2}{L_h}$$

$$S8 = \frac{2 E_w I_2}{L_h}$$

$$S9 = \frac{(4+\emptyset) E I_3}{L_h (1+\emptyset)}$$

$$S10 = \frac{(2-\emptyset) E I_3}{L_h (1+\emptyset)}$$

$$\emptyset = \frac{12 E I_3}{G A_s L_h^2}$$

$$A_s = \frac{A}{1.2}$$

J = St. Venant torsion constant

$$= \frac{W t_w^3}{3}$$

I_2 = second moment of area of the shear wall cross-section about the local X_2 axis

$$= \frac{W t_w^3}{12}$$

I_3 = second moment of area of the shear wall cross-section about the local X_3 axis

$$= \frac{t_w W^3}{12}$$

W = shear wall width

t_w = shear wall thickness

A = cross-sectional area
= $t_w W$

Two transformations are required to transform the local system displacement components shown in Figure 4.9 to equivalent global system displacement components at a, b, c, and d, as illustrated in Figure 4.13. The displacement components at i and j, shown in Figure 4.9, are first expressed in terms of components d shown in Figure 4.12, using the following relationship

$$\begin{Bmatrix} \Delta_{i1} \\ \Delta_{i2} \\ \Delta_{i3} \\ \theta_{i1} \\ \theta_{i2} \\ \theta_{i3} \\ \Delta_{j1} \\ \Delta_{j2} \\ \Delta_{j3} \\ \theta_{j1} \\ \theta_{j2} \\ \theta_{j3} \end{Bmatrix} = \begin{bmatrix} 0 & 0 & 0 & 0 & 0 & 0 & \frac{1}{2} & 0 & \frac{L}{2} & 0 & 0 & 0 & 0 & 0 \\ 1 & 0 & 0 & 0 & 0 & 0 & 0 & 0 & 0 & 0 & 0 & 0 & 0 & 0 \\ 0 & 1 & 0 & 0 & 0 & 0 & 0 & 0 & 0 & 0 & 0 & 0 & 0 & 0 \\ 0 & 0 & 1 & 0 & 0 & 0 & 0 & 0 & 0 & 0 & 0 & 0 & 0 & 0 \\ 0 & 0 & 0 & 0 & 0 & 0 & 0 & \frac{1}{2} & 0 & \frac{1}{2} & 0 & 0 & 0 & 0 \\ 0 & 0 & 0 & 0 & 0 & 0 & \frac{-1}{W} & 0 & \frac{1}{W} & 0 & 0 & 0 & 0 & 0 \\ 0 & 0 & 0 & 0 & 0 & 0 & 0 & 0 & 0 & 0 & \frac{1}{2} & 0 & \frac{1}{2} & 0 \\ 0 & 0 & 0 & 1 & 0 & 0 & 0 & 0 & 0 & 0 & 0 & 0 & 0 & 0 \\ 0 & 0 & 0 & 0 & 1 & 0 & 0 & 0 & 0 & 0 & 0 & 0 & 0 & 0 \\ 0 & 0 & 0 & 0 & 0 & 1 & 0 & 0 & 0 & 0 & 0 & 0 & 0 & 0 \\ 0 & 0 & 0 & 0 & 0 & 0 & 0 & 0 & 0 & 0 & 0 & \frac{L}{2} & 0 & \frac{L}{2} \\ 0 & 0 & 0 & 0 & 0 & 0 & 0 & 0 & 0 & 0 & \frac{-1}{W} & 0 & \frac{1}{W} & 0 \end{bmatrix} \begin{Bmatrix} d_1 \\ d_2 \\ d_3 \\ d_4 \\ d_5 \\ d_6 \\ d_7 \\ d_8 \\ d_9 \\ d_{10} \\ d_{11} \\ d_{12} \\ d_{13} \\ d_{14} \end{Bmatrix} \tag{4.51}$$

or, $$D = C_L\, d \tag{4.52}$$

The displacements d are, in turn, expressed in terms of the global displacements D'_1 through D'_{18} shown in Figure 4.13. In the figure, the nodes m and v are the master nodes

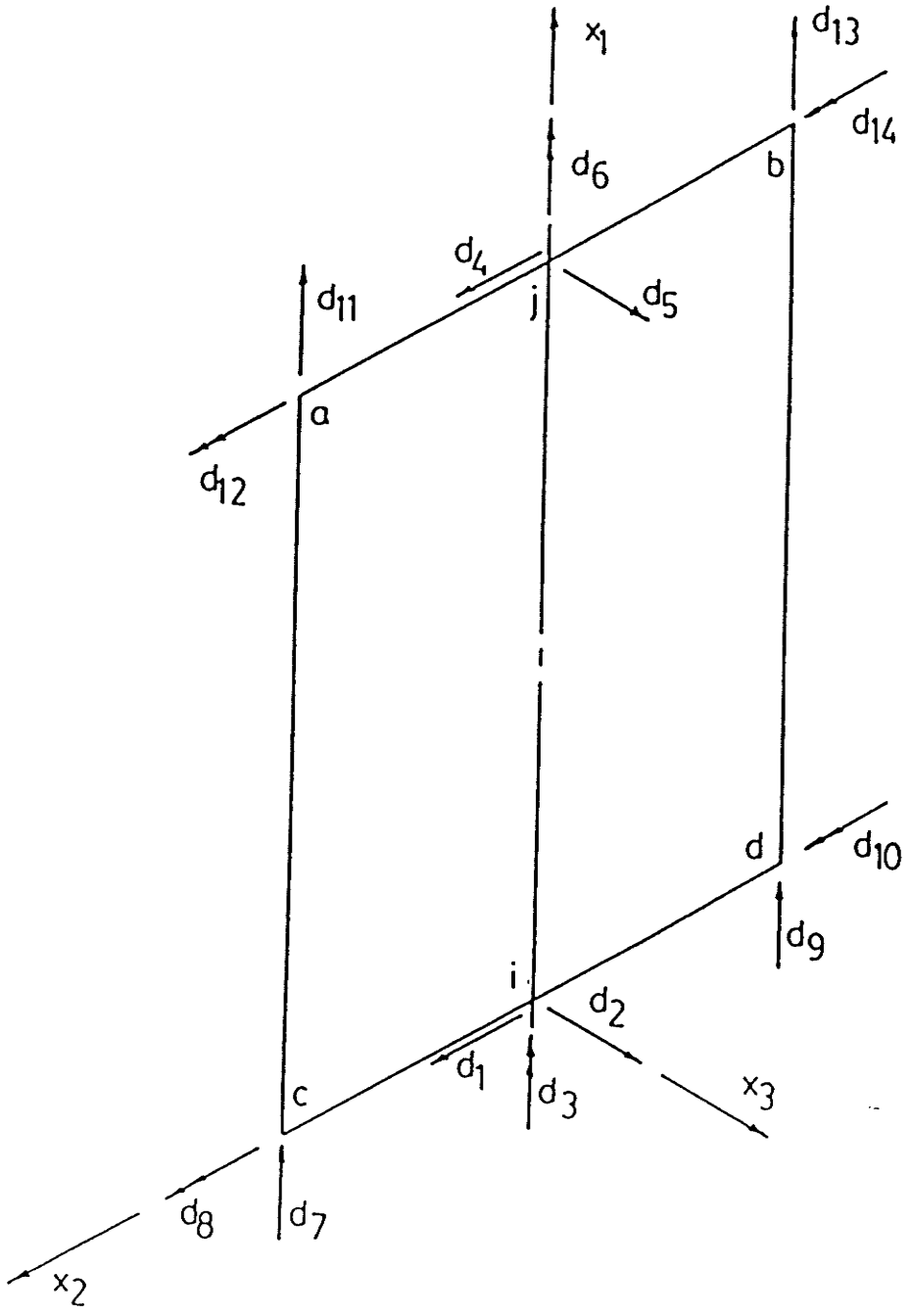

Figure 4.12: Local Wall Element Displacements

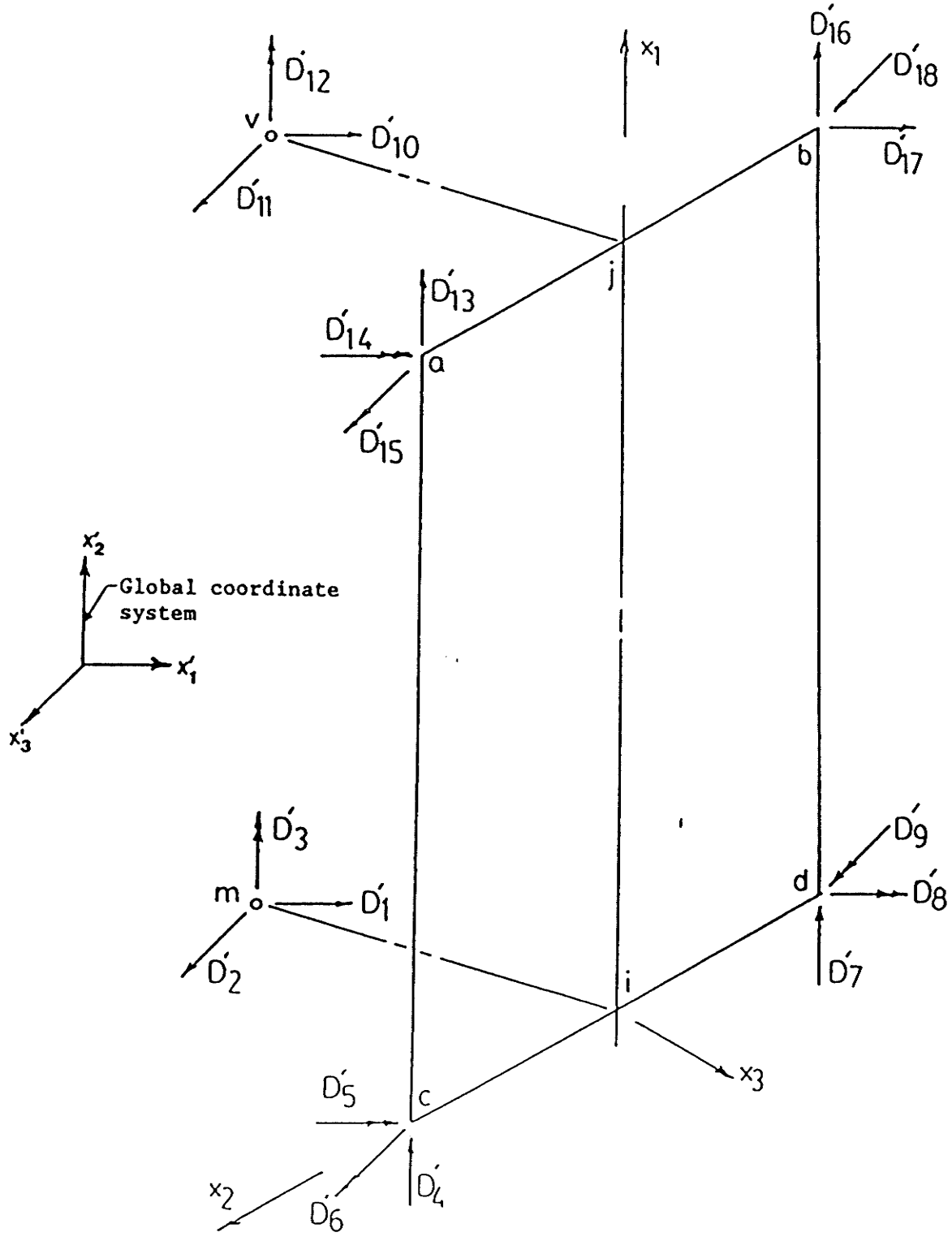

Figure 4.13: Shear Wall Global Displacements

for the upper and the lower floors, respectively. The required transformation is :

$$\begin{Bmatrix} d_1 \\ d_2 \\ d_3 \\ d_4 \\ d_5 \\ d_6 \\ d_7 \\ d_8 \\ d_9 \\ d_{10} \\ d_{11} \\ d_{12} \\ d_{13} \\ d_{14} \end{Bmatrix} = \begin{bmatrix} N & 0_1 & 0_1 & 0_1 & 0_1 & 0_1 \\ 0_1 & 0_1 & 0_1 & N & 0_1 & 0_1 \\ 0_2 & Q & 0_2 & 0_2 & 0_2 & 0_2 \\ 0_2 & 0_2 & Q & 0_2 & 0_2 & 0_2 \\ 0_2 & 0_2 & 0_2 & 0_2 & Q & 0_2 \\ 0_2 & 0_2 & 0_2 & 0_2 & 0_2 & Q \end{bmatrix} \begin{Bmatrix} D'_1 \\ D'_2 \\ D'_3 \\ D'_4 \\ D'_5 \\ D'_6 \\ D'_7 \\ D'_8 \\ D'_9 \\ D'_{10} \\ D'_{11} \\ D'_{12} \\ D'_{13} \\ D'_{14} \\ D'_{15} \\ D'_{16} \\ D'_{17} \\ D'_{18} \end{Bmatrix} \quad (4.53)$$

where

0_1 = null matrix (3x3)

0_2 = null matrix (2x3)

$$N = \begin{bmatrix} \cos\beta & \sin\beta & (Z\cos\beta - X\sin\beta) \\ \sin\beta & -\cos\beta & (Z\sin\beta - X\cos\beta) \\ 0 & 0 & 1 \end{bmatrix} \qquad (4.54)$$

$$Q = \begin{bmatrix} 1 & 0 & 0 \\ 0 & \cos\beta & \sin\beta \end{bmatrix} \qquad (4.55)$$

β = angle between local and global axes as shown in Figure 4.14.

X = distance from the master node to the centerline of the wall in the X_1' direction.

Z = distance from the master node to the centerline of the wall in the X_3' direction.

Equation (4.53) can be written as

$$d = C_G D' \qquad (4.56)$$

substituting Equation (4.56) into Equation 4.52

$$D = C_L C_G D' \qquad (4.57)$$

Because of the contragrediant nature of displacement and force transformations, it follows from Equation (4.57) that

$$P' = C_G^T C_L^T P \qquad (4.58)$$

The force-displacement relationship in terms of the global force and displacement vectors is thus

$$P' = K' D' \qquad (4.59)$$

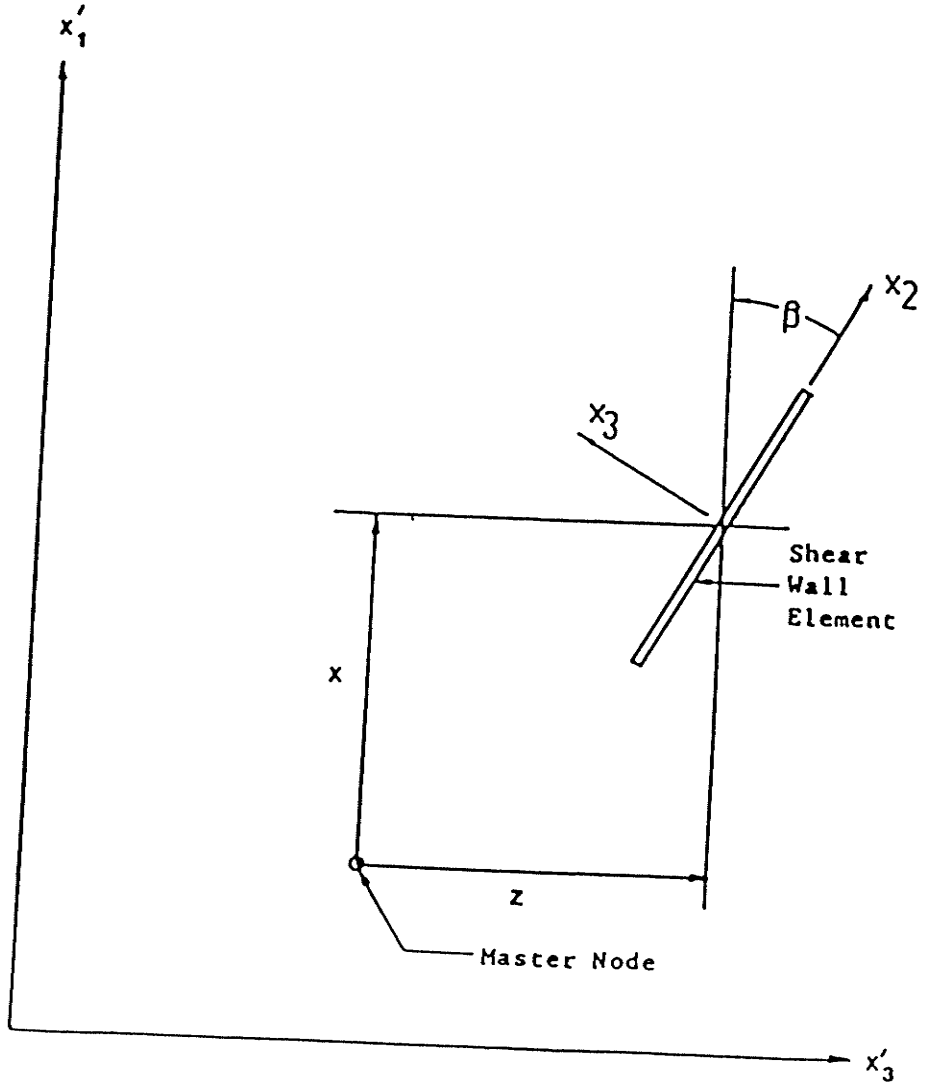

Figure 4.14: Plan View Showing Shear Wall Orientation

where

$$K' = C_G^T \; C_L^T \; K \; C_L \; C_G \qquad (4.60)$$

= shear wall stiffness matrix expressed in global system

In Equation (4.60)

K = shear wall local stiffness matrix

Equation (4.59) relates out-of-plane global force and displacement components at slave nodes a, b, c and d, and in-plane components at master nodes v and m, as influenced by shear wall panel a-b-c-d. The shear wall stiffness coefficients can be inserted directly into the structure stiffness matrix.

4.4 MODELLING OF PLATE PANELS

The typical flat-plate panel is assumed to comprise the portion of a flat-plate floor bounded by the center lines of the columns at its corners. As illustrated in Figure 4.15, the plate panel model includes also the cross-hatched regions at the panel corners, that are common to both the panel and the columns. The latter are outlined by rigid beam elements on the column center lines and along the plate-to-column boundaries. The beams on the column center lines are rigidly connected to columns, and are connected to the plate by means of nonlinear flexural springs designated FS_1 through FS_8 in the figure. The beams on the column-to-plate

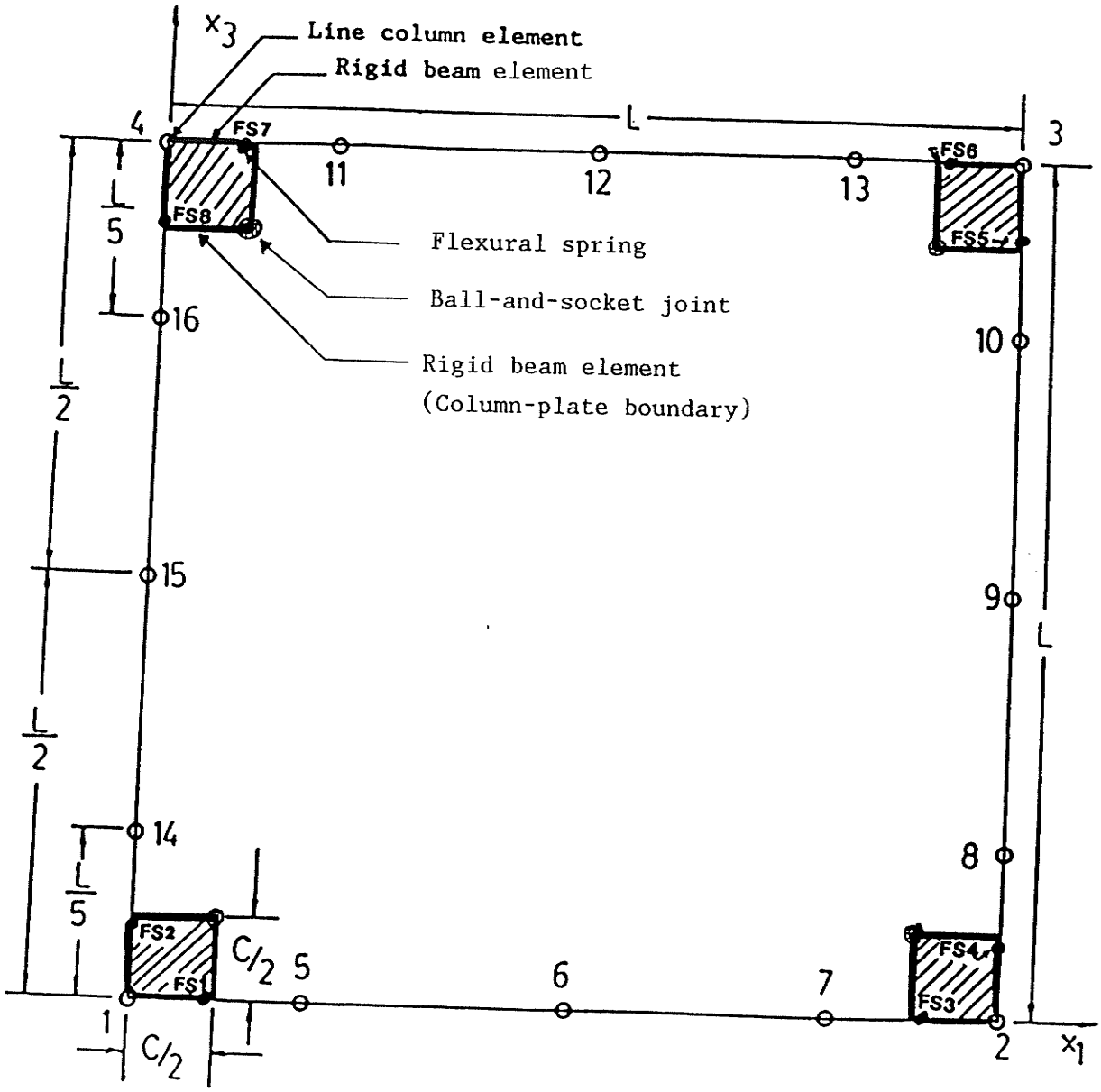

Figure 4.15: Model of Flat-Plate Panel

boundary are connected to the flexural spring and to the plate element. At the column corners the beams are connected to each other by ball-and-socket joints. The plate panel is assumed to be linearly elastic, except for the nonlinear flexural springs, homogeneous and isotropic.

Four corner nodes and twelve edge nodes are used in describing the force-displacement relationship for the panel. The edge nodes ensure that compatibility is enforced between adjacent plate panels. This is an improvement over the earlier work of French, Kabaila and Pulmano (1975) and that of French et al (1975), where compatibility was ensured at the panel corners only. As illustrated in Figure 4.16, three degrees of freedom are assumed at each node. This results in a total of 48 degrees of freedom for each flat-plate panel.

4.4.1 Derivation of Floor Panel Stiffness Matrix

The nonlinear stiffness matrix of the plate panel was derived numerically as a function of both the column-to-plate span ratio, C/L, and the flexibilities, SF_1 through SF_8, corresponding to flexural springs, FS_1 through FS_8, shown in Figure 4.15.

The finite element program HYBSLAB was used to model the flat-plate panel. The program was developed by Hrabok and Hrudey (1981) for the gravity load analysis of flat-plate

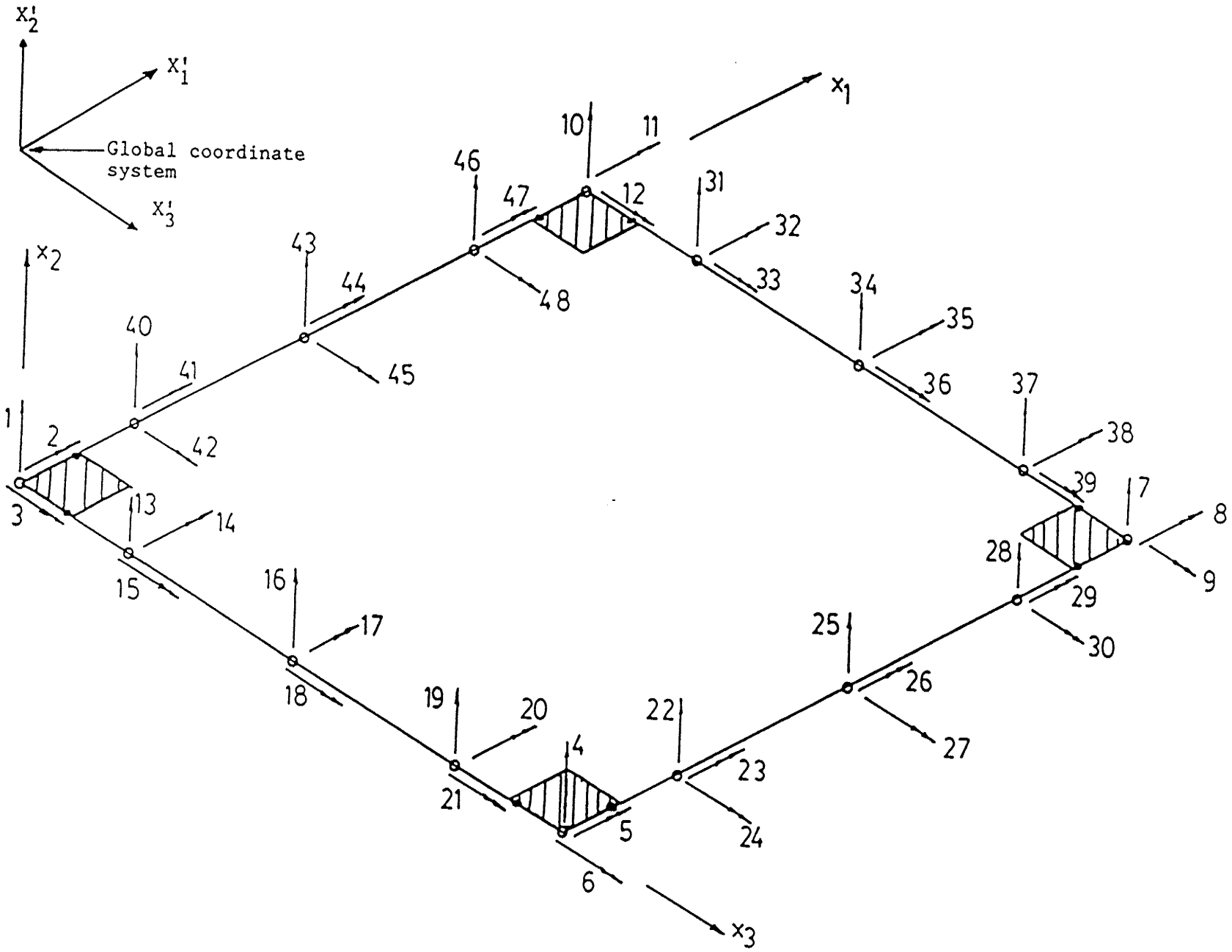

Figure 4.16: Plate Element Degrees of Freedom

floors. The plate bending elements used in the program were derived using the hybrid stress method, which is well suited to the analysis of flat-plate floor systems (Hrabok, 1981). The program has the capability of generating in-plane and plate bending stiffness matrices for a wide range of element shapes. The latter may vary from a 3-sided element (triangle) to a 6-sided irregular polygon. Some of the possible element configurations are shown in Figure 4.17. In order to model the plate panel, a subroutine was added to the finite element program to calculate and assemble the stiffness matrices of the beams connecting the column elements to the plate element.

A convergence test was performed to determine the appropriate mesh to be used in the analysis. As illustrated in Figures 4.18 through 4.22, five different meshes, ranging from 40 to 420 elements, were tested. Figure 4.23 illustrates the convergence of stiffness coefficient K_{11} for the different meshes considered. Similar convergence rates were observed for other panel stiffness coefficients. The 336 element mesh was chosen as the most appropriate for the analysis.

The stiffness matrix for the plate panel was derived by constructing the stiffness matrix for the entire finite element array and then condensing off all degrees of freedom except those for nodes 1 through 16 in Figure 4.21. This left the forty eight degrees of freedom shown in Figure 4.16

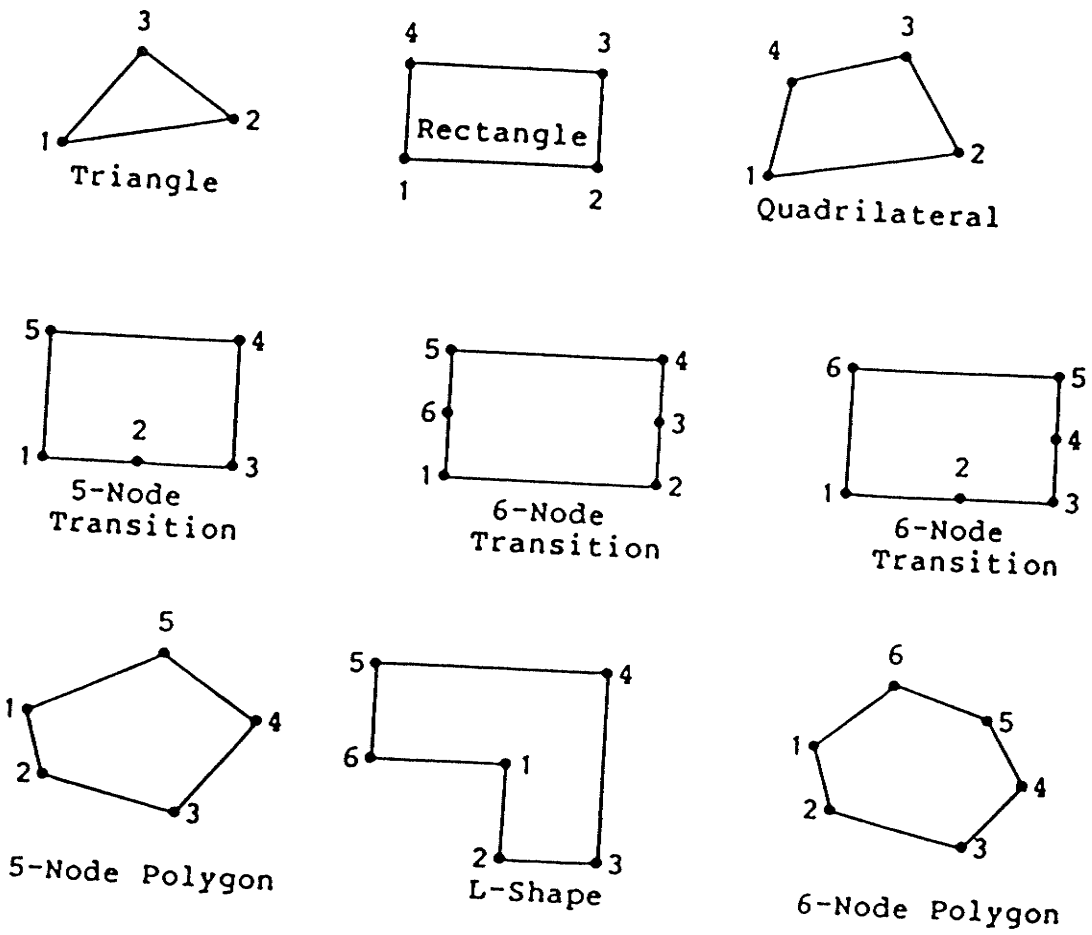

Figure 4.17: HYBSLAB Possible Element Configurations

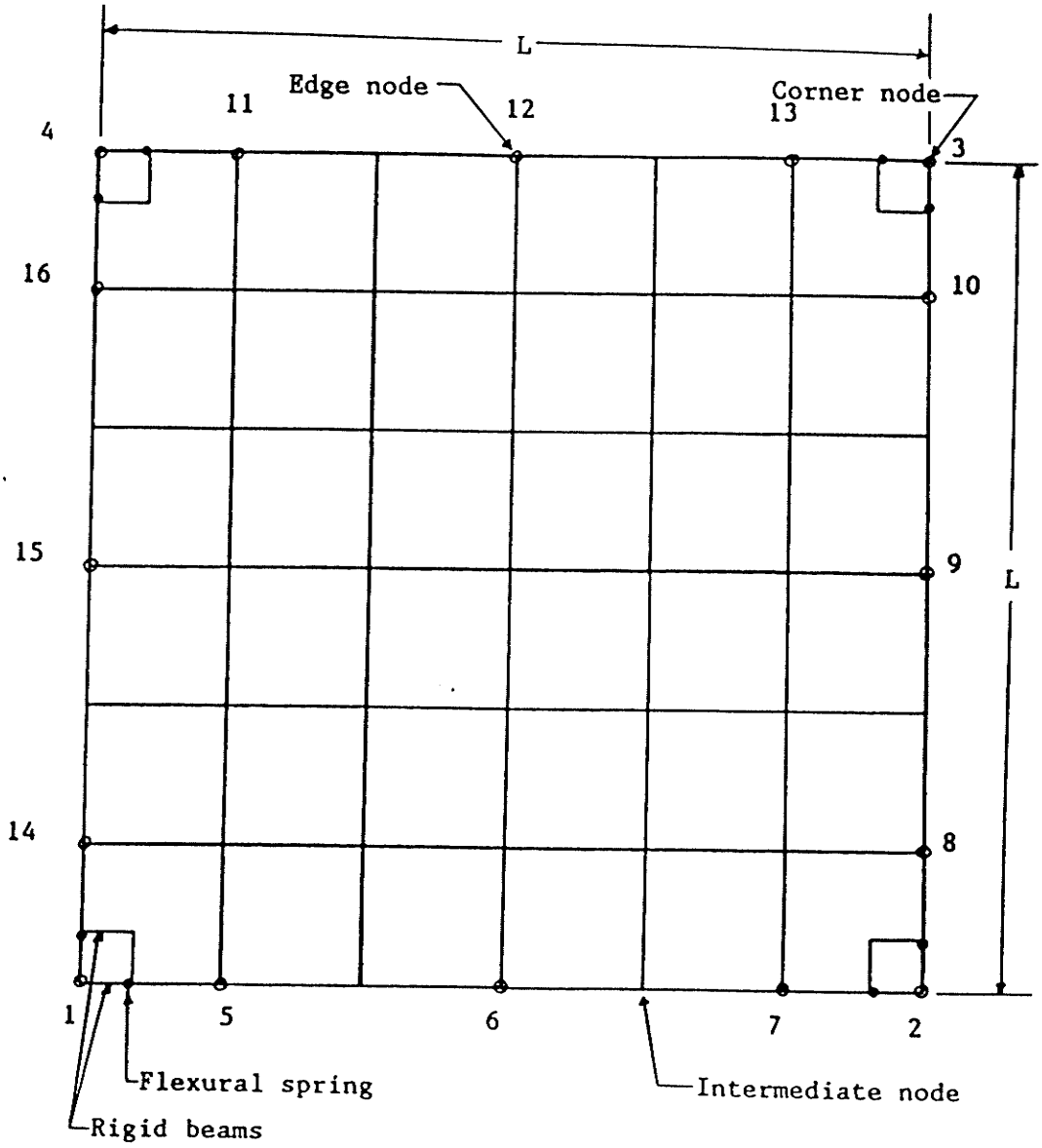

Plate panel

Figure 4.18: 36 Element Mesh

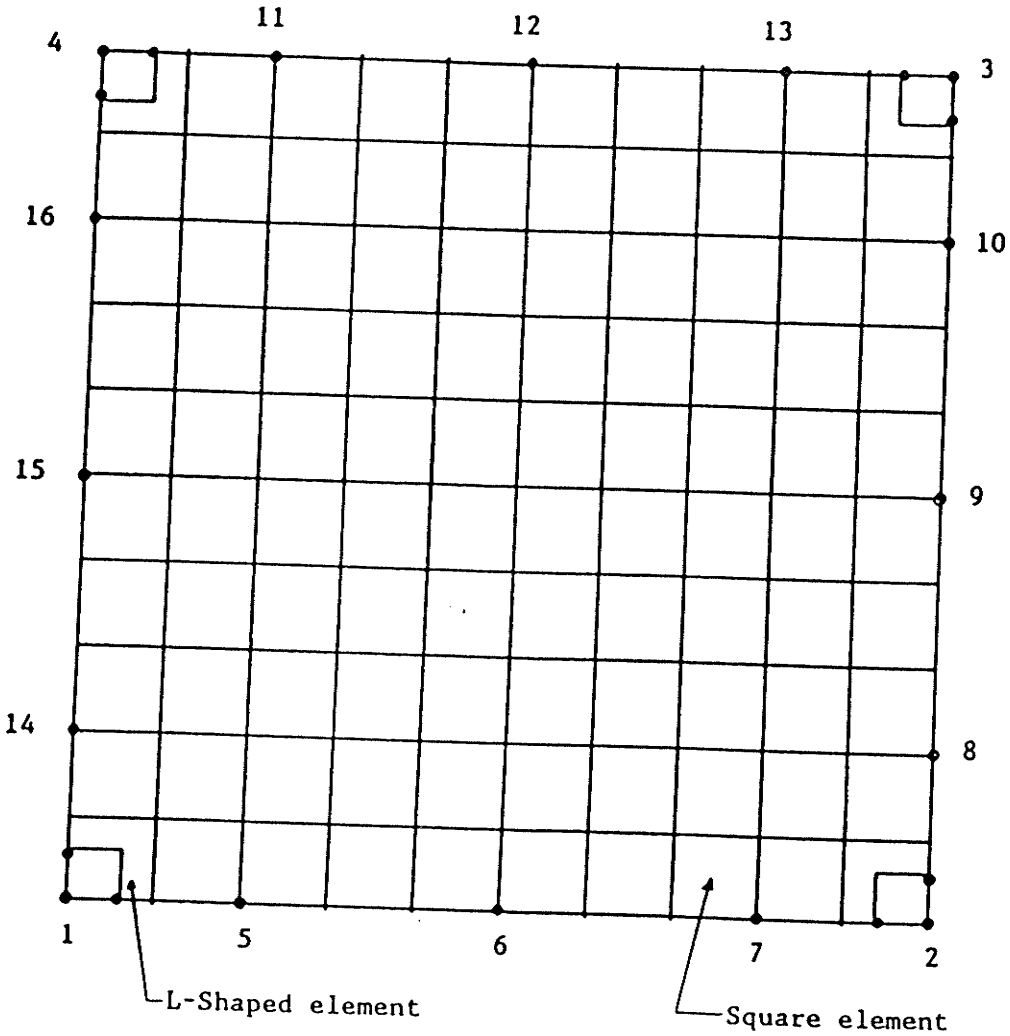

Figure 4.19: 100 Element Mesh

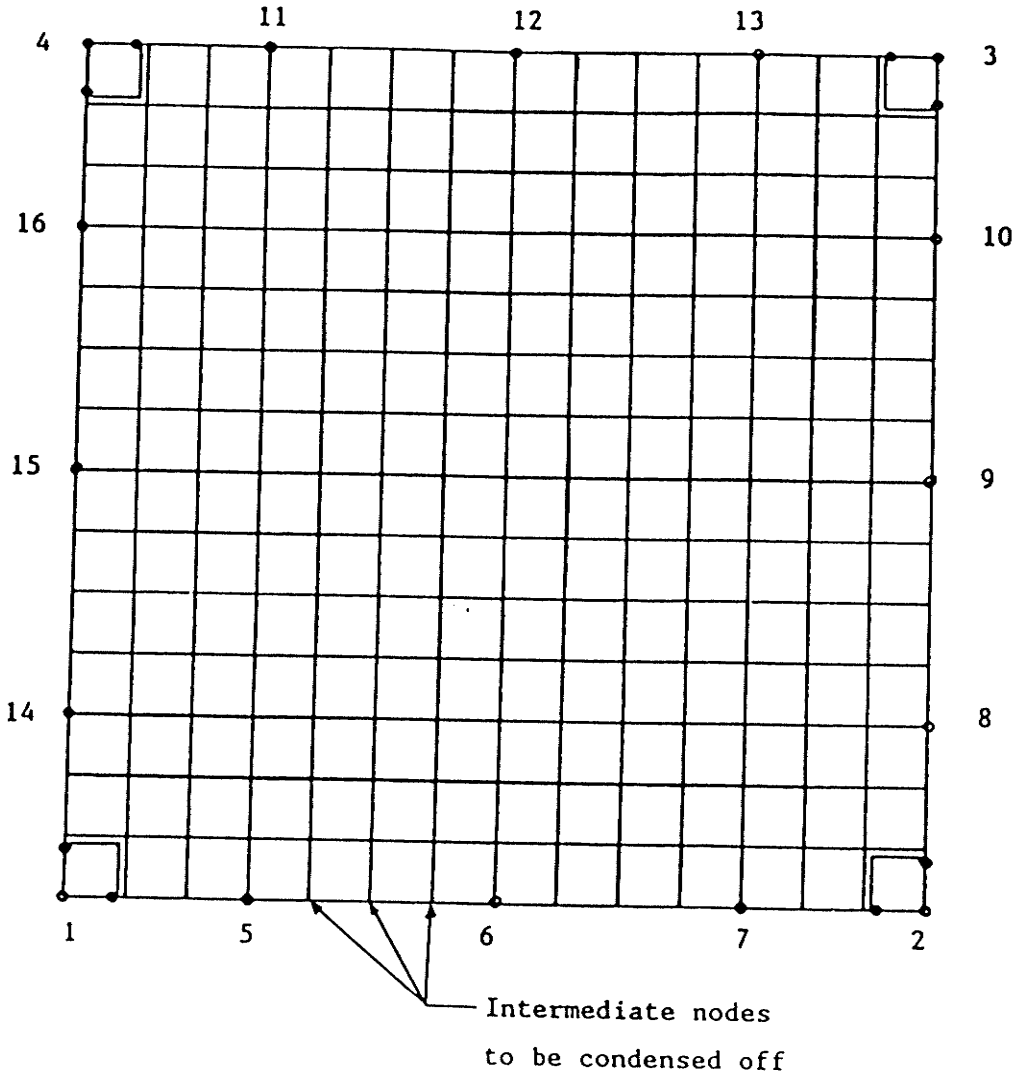

Figure 4.20: 196 Element Mesh

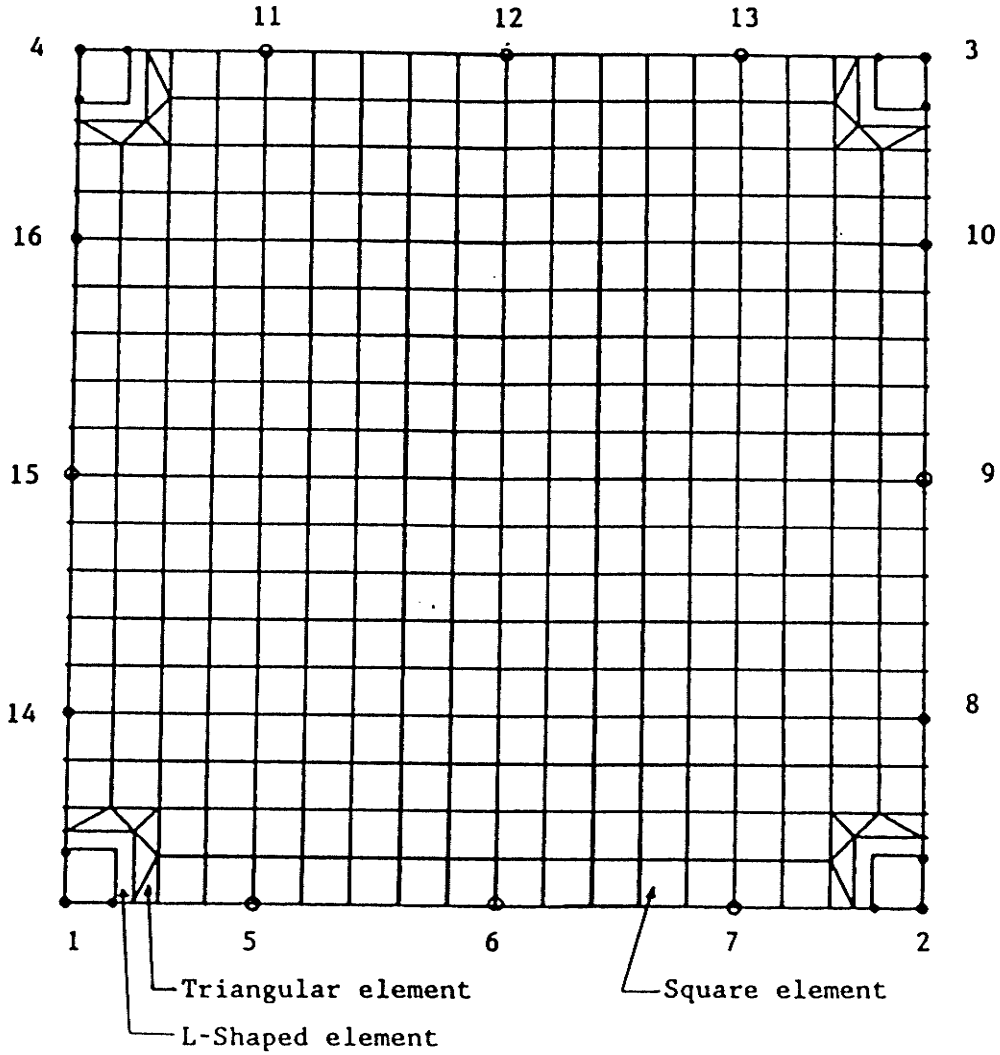

Figure 4.21: 336 Element Mesh

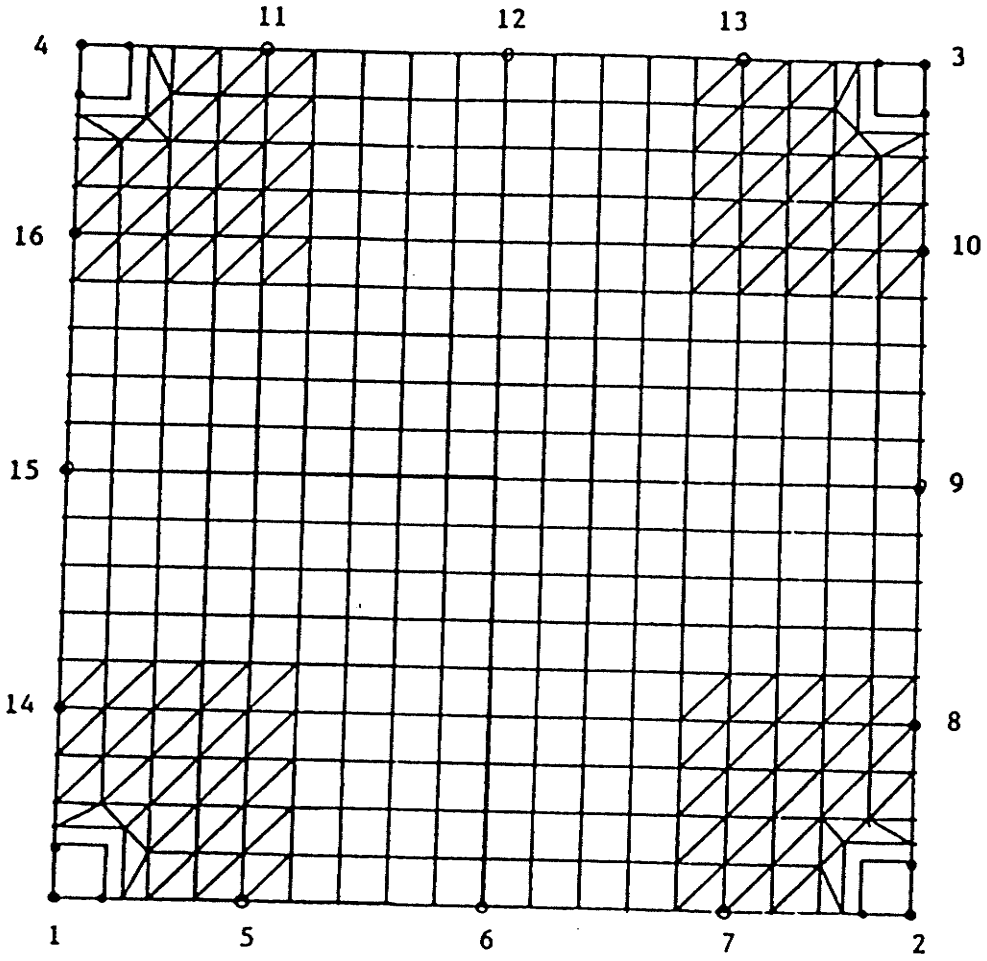

Figure 4.22: 420 Element Mesh

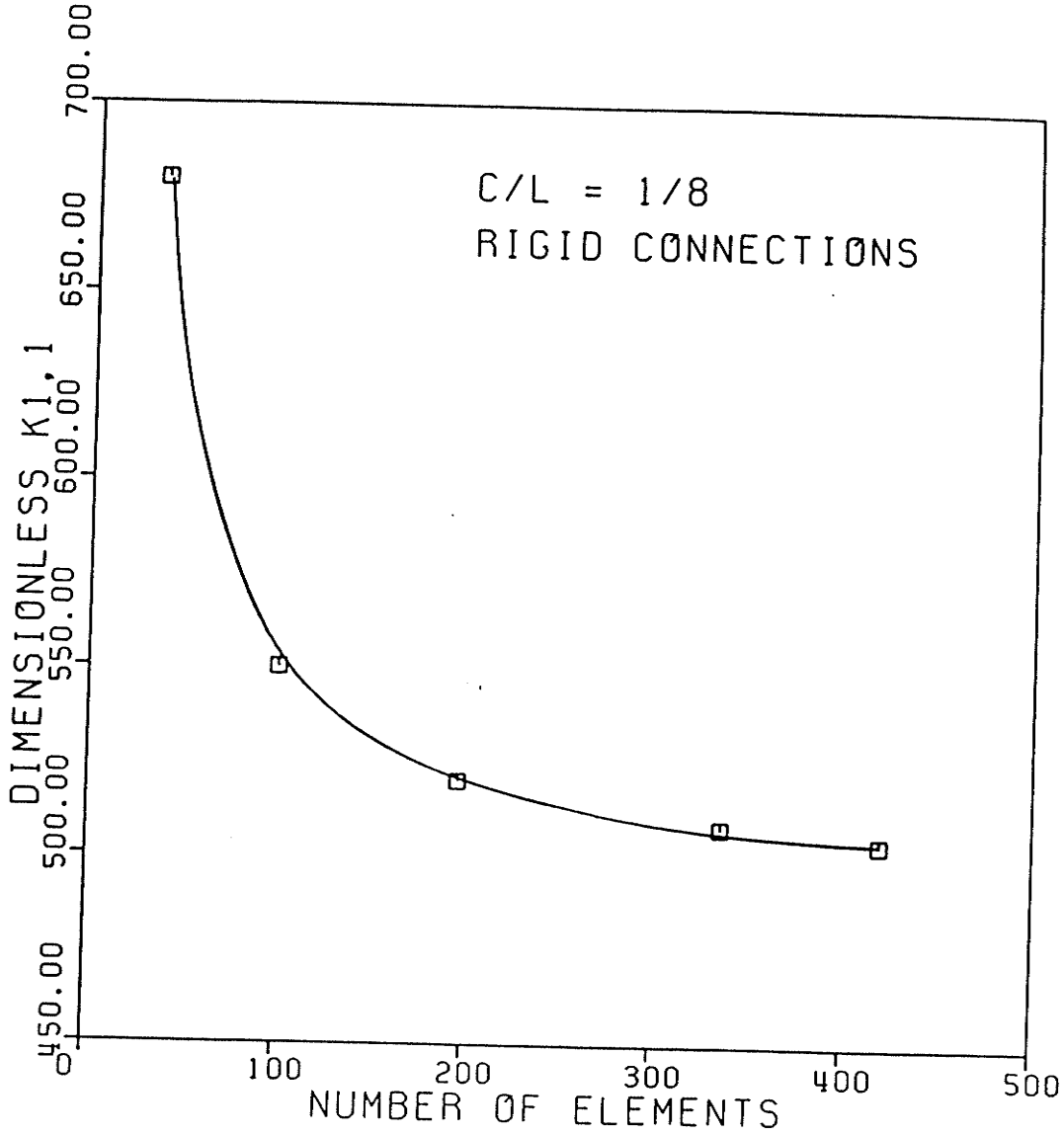

Figure 4.23: Convergence Test

to describe the force-displacement relationship for the panel. The force-displacement relationship for the 336-element mesh is described by the following matrix equation.

$$\begin{Bmatrix} P_e \\ P_c \end{Bmatrix} = \begin{bmatrix} K_{ee} & K_{ec} \\ K_{ce} & K_{cc} \end{bmatrix} \begin{Bmatrix} D_e \\ D_c \end{Bmatrix} \quad (4.61)$$

In Equation (4.61), subscript e denotes degrees of freedom to be condensed off, and subscript c denotes degrees of freedom associated with panel edge and corner nodes.

As no loads were applied at the nodes where degrees of freedom were to be condensed off, $P_e = 0$. Consequently, in Equation (4.61)

$$0 = K_{ee}\ D_e + K_{ec}\ D_c \quad (4.62)$$

and

$$P_c = K_{ce}\ D_e + K_{cc}\ D_c \quad (4.63)$$

From Equation (4.62)

$$D_e = -K_{ee}^{-1}\ K_{ec}\ D_c \quad (4.64)$$

Substituting Equation (4.64) into Equation (4.63)

$$P_c = (K_{cc} - K_{ce}\ K_{ee}^{-1}\ K_{ce})\ D_c \quad (4.65)$$

In Equation (4.65), the condensed stiffness matrix, K_p, which relates force and displacement components at the panel corner and edge nodes is defined as follows.

$$K_p = K_{cc} - K_{ce}\ K_{ee}^{-1}\ K_{ec} \quad (4.66)$$

Then, substituting Equation (4.66) into Equation (4.65)

$$P_c = K_p\ D_c$$

As illustrated in Figure 4.16 the plate local coordinate system coincides with the global system. Therefore, no transformation to the global system is required, and the elements of the plate panel condensed stiffness matrix, K_p, can be assembled directly into the structure stiffness matrix.

Because of the large number of degrees of freedom, the overall stiffness matrix for the plate panel is large. Consequently, conventional storage schemes accounting for the banded nature of the matrix would have required auxilliary storage. Therefore, taking advantage of the fact that the stiffness matrix is sparse, considerable reduction in the storage requirements was achieved by using a variable column height storage scheme.

In Equation (4.66), K_{ee} is large also. Therefore direct inversion would have been prohibitively expensive and as a consequence, row elimination methods were used. A Crout reduction procedure proposed by Mondkar and Powel (1974) was used. It has been shown to require a minimum number of unnecessary operations for sparse matrices, thus saving core space. The use of the Crout reduction procedure combined with the variable column height storage scheme permitted the stiffness matrix to be condensed in core, with no auxiliary storage requirement.

The HYBSLAB program was modified in order to take advantage of the storage and reduction procedures described above. The output of the modified program was the condensed 48 by 48 stiffness matrix for the plate panel, including the 8 rigid beam elements and the 8 flexural springs at the columns, as shown in Figure 4.16.

Using the modified HYBSLAB program, stiffness matrices for panel elements with column-to-plate span ratios of 1/8, 1/11, 1/16 and 1/25 were derived numerically as functions of the eight spring flexibilities, SF_1 through SF_8. The four column-to-plate-span ratios represent the practical range normally used in design.

The derived stiffness matrices were made dimensionless using the method suggested by French at al. (1975) and described here. Consider a typical 3x3 submatrix of the panel stiffness matrix which relates the forces at node i to the displacements at node j. The relationship between the dimensional and dimensionless submatrices is

$$\begin{bmatrix} k_{11} & k_{12} & k_{13} \\ k_{21} & k_{22} & k_{23} \\ k_{31} & k_{32} & k_{33} \end{bmatrix} = \frac{h}{L^2} \begin{bmatrix} k''_{11} & Lk''_{12} & Lk''_{13} \\ Lk''_{21} & L^2k''_{22} & L^2k''_{23} \\ Lk''_{31} & L^2k''_{32} & L^2k''_{33} \end{bmatrix} \quad (4.67)$$

where,

k_{ij} = Dimensional stiffness coefficient relating degrees of freedom i and j

k''_{ij} = Dimensionless stiffness coefficient relating degrees of freedom i and j

h = flexural rigidity of the flat-plate floor

$$= \frac{E\ t^3}{12(1-\nu^2)}$$

Once computed, the dimensionless stiffness coefficients were built into the structural analysis computer program. Thus, for any plate with a column-to-plate span ratio of 1/8, 1/11, 1/16 or 1/25, when values have been assigned to the plate span, L, and flexural rigidity, h, the program computes the dimensional stiffness matrix for the plate panel.

The stiffness matrix for a panel with a column-to-plate span ratio other than the ones mentioned above, is evaluated using Lagrange interpolation. The panel stiffness matrix for an arbitrary value of the column-to-plate span ratio of $1/\alpha$ is evaluated as follows.

$$[K_\alpha] = C_1\ [K_{25}] + C_2\ [K_{16}] + C_3\ [K_{11}] + C_4\ [K_8] \quad (4.68)$$

where,

$[K_\alpha]$ = interpolated panel stiffness matrix evaluated for column-plate span ratio $1/\alpha$

$[K_{25}]$, $[K_{16}]$, $[K_{11}]$ and $[K_8]$ = panel stiffness evaluated numerically for column-plate span ratios of 1/25, 1/16, 1/11, and 1/8 respectively. and

$$C_i = \prod_{\substack{j=1 \\ j\neq i}}^{4} \frac{(1/\alpha - 1/\alpha_j)}{(1/\alpha_i - 1/\alpha_j)} \qquad i=1,2,3,4$$

$\alpha_1 = 25$

$\alpha_2 = 16$

$\alpha_3 = 11$

$\alpha_4 = 8$

A study was conducted to determine the influence of the different spring flexibilities on the plate stiffness coefficients. This was done by considering different combinations of spring flexibilities SF_1 through SF_8. It was observed that the influence of the spring flexibilities is localized, the influence of a given spring being negligible beyond the quarter in which it is located. Thus, for example, the stiffness coefficients in quarter I of the plate shown in Figure 4.24 are influenced mainly by the flexibilities of springs FS_1 and FS_2. Consequently, instead of generating the stiffness matrix for the entire plate panel as a function of the eight spring flexibilities, the stiffness coefficients for only one quarter of the plate were evaluated as functions of the flexibilities of the two springs located in that quarter. Stiffness coefficients for the other three quarters were generated by symmetry. Furthermore, due to the symmetry of the plate panel with respect to its diagonals, only those stiffness coefficients relating degrees of freedom 1,3,13,14,15,16,17, and 18 to the 48 plate degrees of freedom had to be considered.

It was observed that most of the stiffness coefficients corresponding to the degrees of freedom in a particular plate quarter were influenced by the flexibility of only one of the adjacent springs, while a few were influenced by both

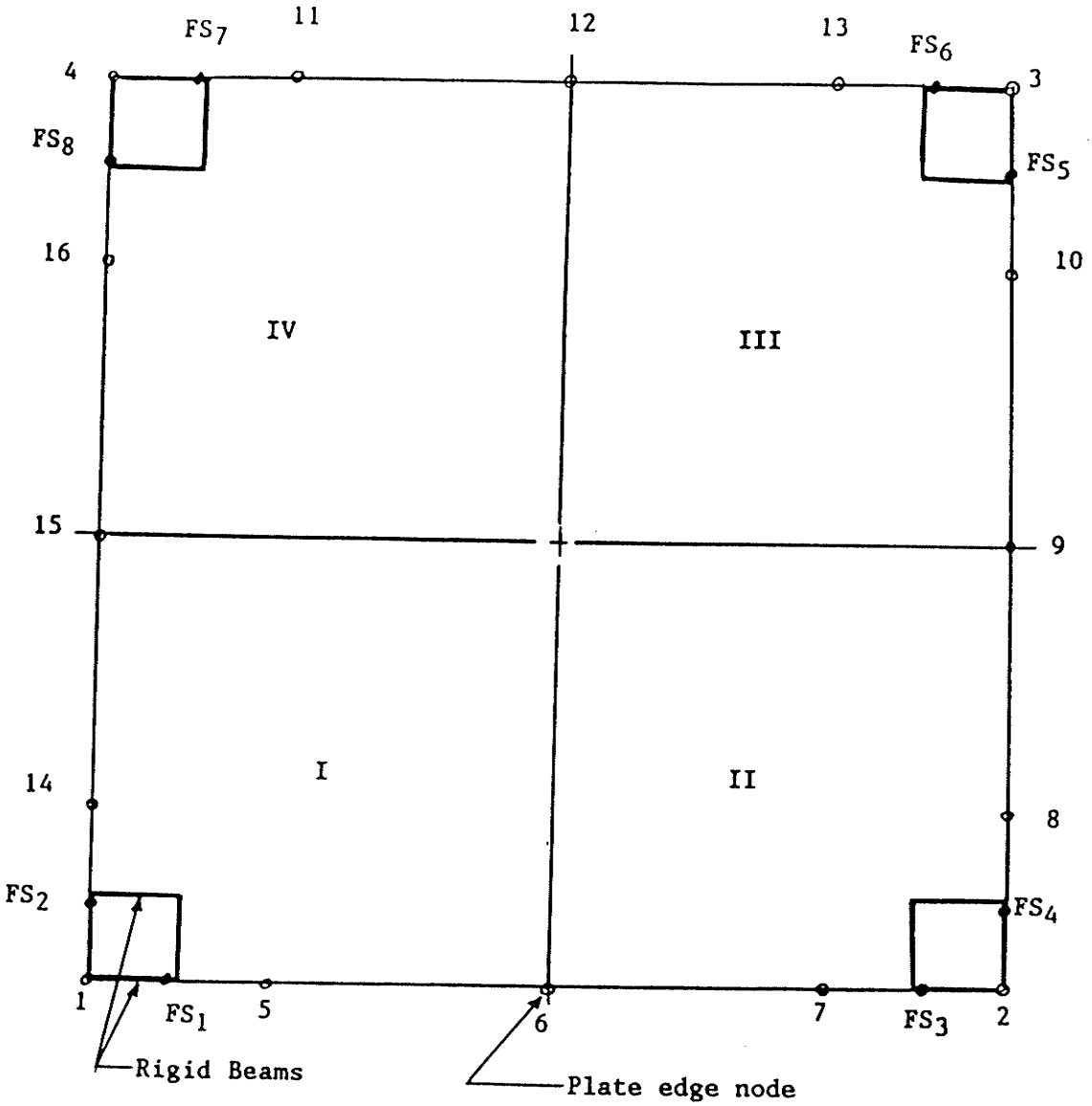

Figure 4.24: Influence of Spring Flexibilities on Plate Stiffnesses

of them. Thus, for example, for the plate panel shown in Figure 4.25, stiffness coefficients $k_{3,3}$, $k_{1,13}$ and $k_{3,14}$ were influenced by spring flexibility SF_1, while $k_{1,1}$, $k_{40,13}$ and $k_{14,41}$ were influenced by spring flexibilities SF_1 and SF_2.

The stiffness coefficients were found to vary exponentially with an increase in the spring flexibilities. Therefore, exponentially decaying functions were fitted to the stiffness coefficient values generated from the finite element analysis. The function used to fit stiffness coefficients dependent upon a single spring flexibility had the following form.

$$k_{ij} = F_2 + (F_1 - F_2)\ e^{-(a_1\ SF_1)} \qquad (4.69)$$

The function used to fit stiffness coefficients dependent upon two spring flexibilities had the form

$$k_{ij} = F_5 + (F_6 - F_5)\ e^{-(a_2\ SF_2)} \qquad (4.70)$$

In Equations (4.69) and (4.70),

k_{ij} = Stiffness coefficient relating degrees of freedom i and j

$$F_5 = F_4 + (F_3 - F_4)\ e^{-(a_1\ SF_1)}$$

$$F_6 = F_2 + (F_7 - F_2)\ e^{-(a_1\ SF_1)}$$

F_1 = value of k_{ij} when $SF_1 = 0$

F_2 = value of k_{ij} when $SF_1 = \infty$

F_3 = value of k_{ij} when $SF_2 = \infty$

F_4 = value of k_{ij} when $SF_2 = SF_1 = \infty$

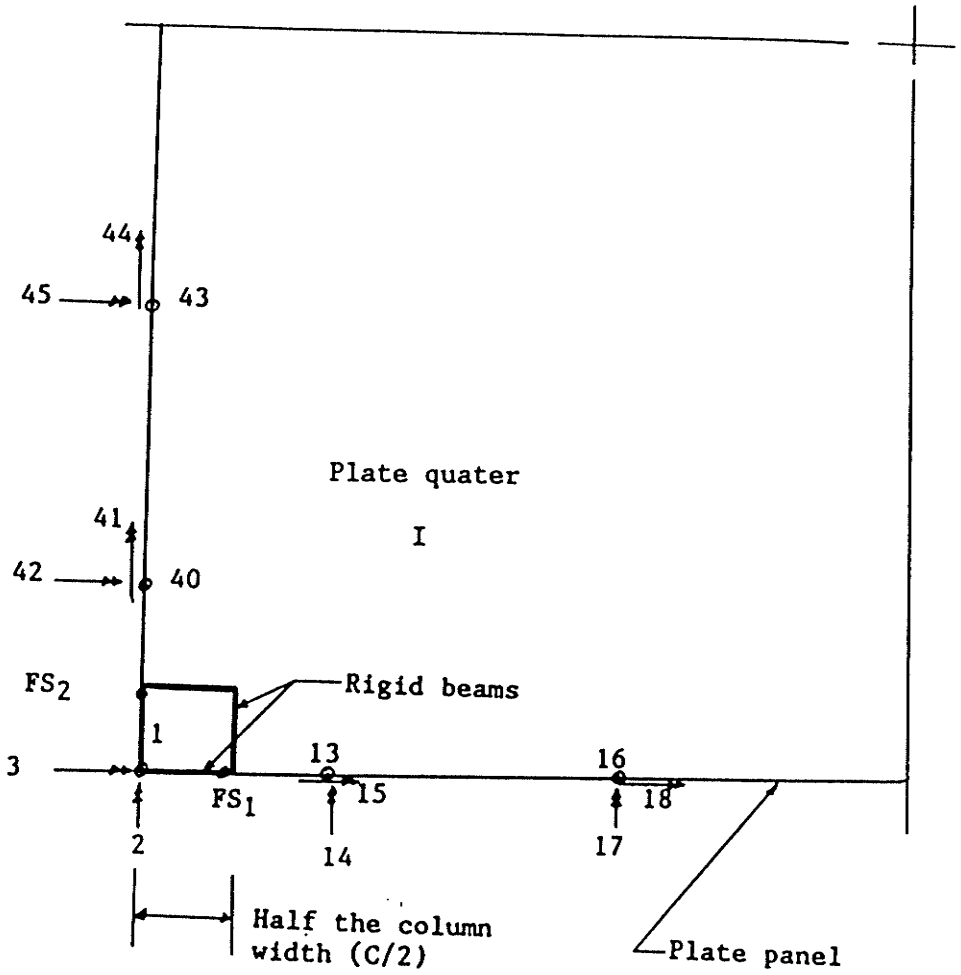

Figure 4.25: Plate Quarter I

F_7 = value of k_{ij} when $SF_2 = SF_1 = 0$

SF_1 and SF_2 = flexibilities of flexural springs FS_1 and FS_2 respectively

a_1 and a_2 = constants

The constant a_1 in Equation (4.69) was evaluated as follows.

$$a_1 = \frac{1}{SF_1} \ln \left[\frac{F_1 - F_2}{k_{ij} - F_2} \right] \qquad (4.71)$$

Equation (4.71) was evaluated for several spring flexibilities and the average value was used in Equation (4.69). Since it is difficult to solve analytically for constants a_1 and a_2 in Equation (4.70), and also since exponentially decaying functions were found not to be very sensitive to changes in these constants, they were evaluated using a trial and error procedure.

Typical plots of the variation of stiffness coefficients with the increase of spring flexibilities, and the functions used to fit these relationships, are shown in Figures 4.26 to 4.28.

4.5 ASSEMBLY OF FLOOR STIFFNESS MATRIX

In the structural analysis computer program, the out-of-plane stiffness of the flat-plate floor is modelled by assembling the various floor panel stiffness matrices into a single floor stiffness matrix. The degrees of freedom asso-

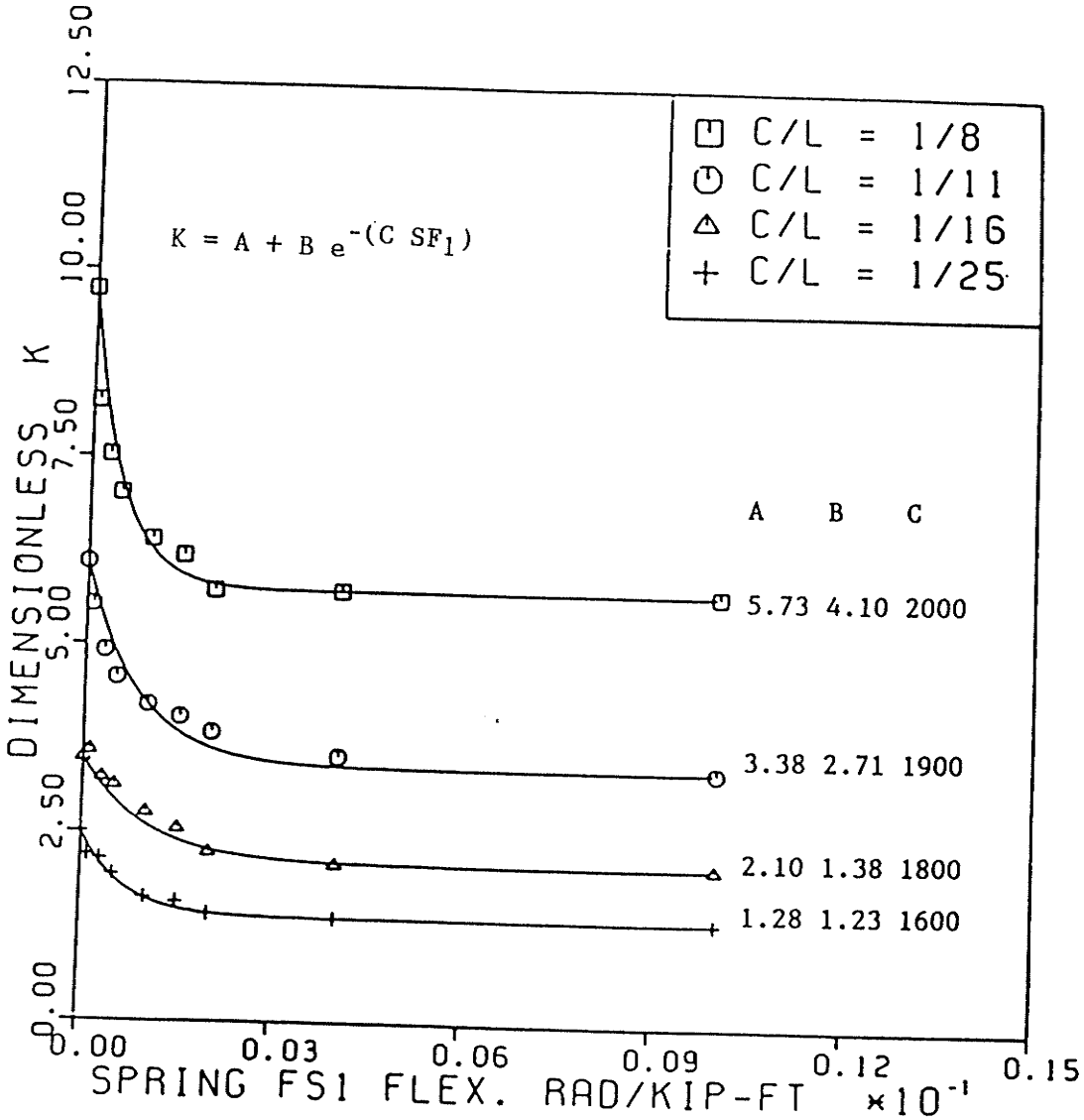

Figure 4.26: Stiffness Coefficient $K_{2,2}$

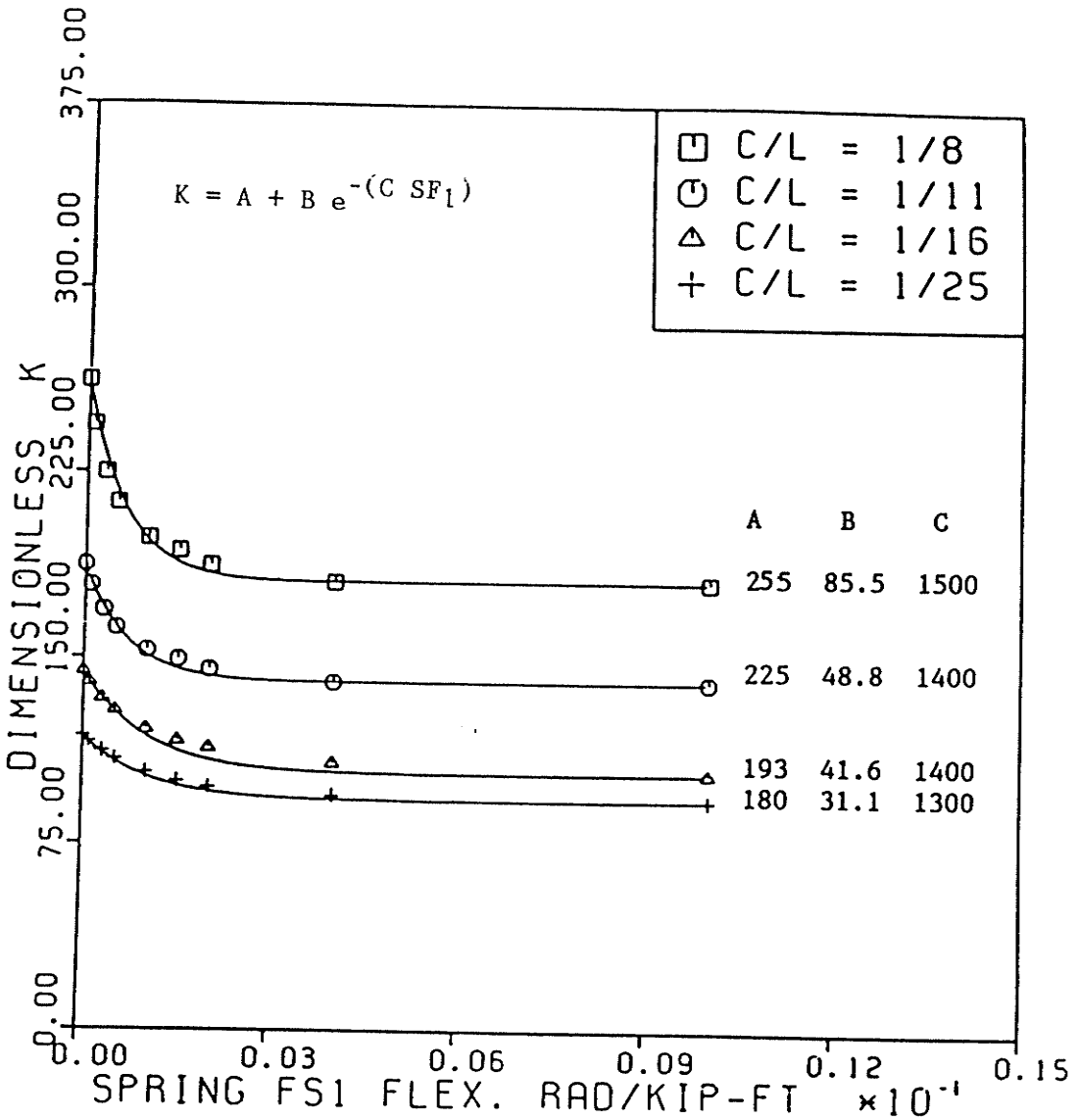

Figure 4.27: Stiffness Coefficient $K_{13,13}$

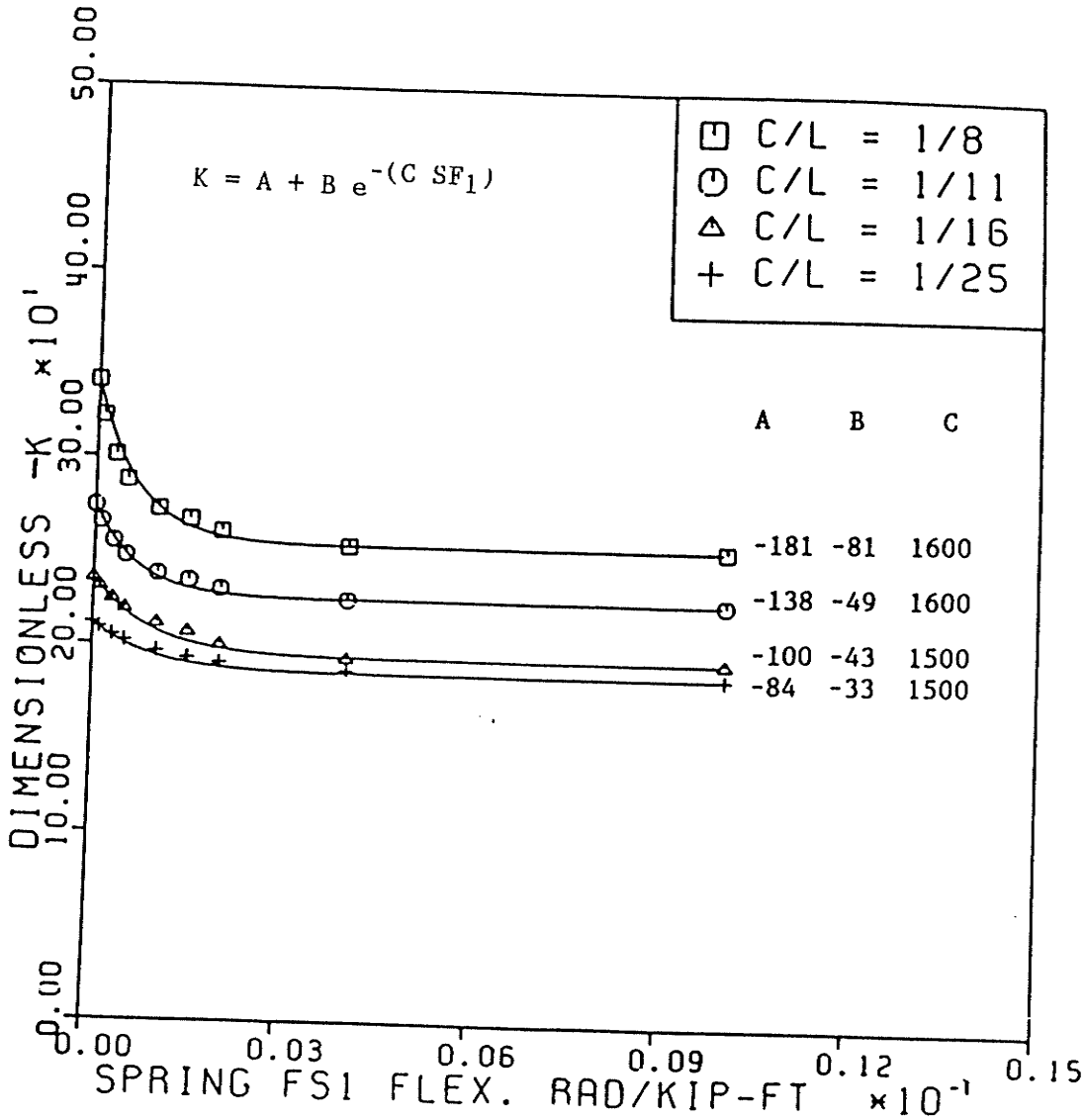

Figure 4.28: Stiffness Coefficient $K_{13,1}$

ciated with the panel edge nodes are then condensed off leaving a reduced stiffness matrix in terms of the column degrees of freedom only. This condensed floor stiffness matrix is then assembled into the structure stiffness matrix. The coordinate systems for all of the panel elements, the floors and the entire structure have identical orientations. Thus, no transformations are required.

For the nonlinear analysis, as discussed previously, the stiffness matrices of the plate panels are dependent upon the flexibility characteristics of their connections to the supporting columns. Since plate-to-column connection flexibilities vary from one connection to the next, plate panel stiffness matrices may vary from panel to panel within a given floor. Therefore, the stiffness matrix for each of the plate panels in the structure is evaluated before it is assembled into the structure stiffness matrix. This procedure is repeated for each cycle of iteration in the nonlinear analysis.

4.6 NONLINEAR ANALYSIS PROCEDURE

The basic premise of the iterative analysis procedure is that the correct deflections and internal forces for a structure with nonlinear connections can be obtained from a single linear analysis, provided the correct stiffness is assumed for each connection. The procedure thus involves repeated cycles of an iterative procedure whose purpose is

to determine appropriate flexibility characteristics for various connections in the structure. When these characteristics have been determined with sufficient accuracy, they are employed in a linear analysis to calculate the correct structural displacements and forces.

Consider a structure with plate-to-column connections having nonlinear moment-rotation functions, as illustrated in Figure 4.29, of the form

$$\emptyset = g(m) \qquad (4.72)$$

In Equation (4.72), g(m) is a nonlinear function of the moment acting on the connection. The function is replaced by a linear relationship of the form .

$$\emptyset = M / S_i \qquad (4.73)$$

where S_i is the slope of the initial tangent of the M-Ø curve. After calculating the initial stiffnesses for all of the connections in the structure, the stiffness matrices for all of the plate panels are generated and assembled into the floor stiffness matrix. Stiffness matrices for all of the other components of the structure are then generated and assembled into the overall structure stiffness matrix. A linear analysis is performed and the moments at all plate-to-column connections are computed. If the moment at the

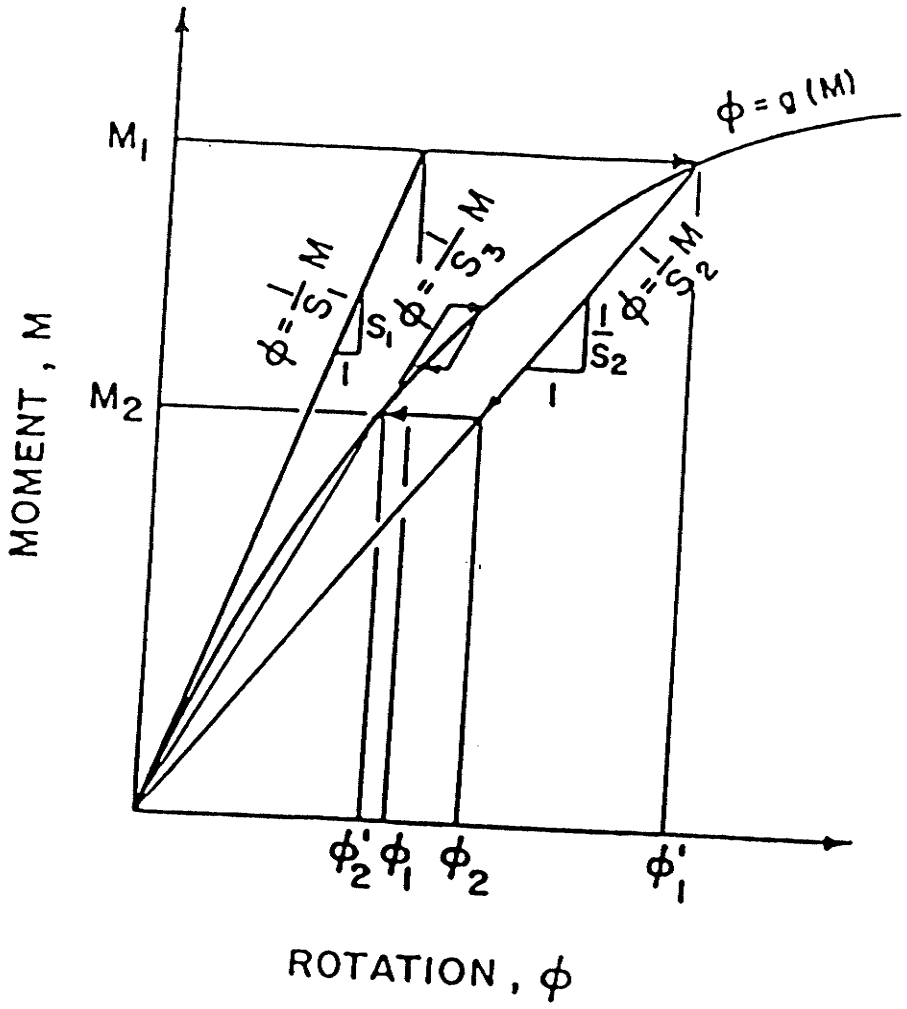

Figure 4.29: Modification of Connection Flexibility

connection originally considered is M_1, the corresponding rotational deformation is

$$\emptyset_1 = M_1 / S_1 \qquad (4.74)$$

However, the rotation calculated from the correct nonlinear relationship of Equation (4.72) is

$$\emptyset_1' = g(M_1) \qquad (4.75)$$

A better approximation to the moment-rotation functions is thus

$$\emptyset = M / S_2 \qquad (4.76)$$

where

$$S_2 = M_1 / \emptyset_1' \qquad (4.77)$$

as illustrated in Figure 4.29. Equation (4.77) and similar relationships for all other connections are then used to calculate the new member force-displacement relationships and a second linear analysis is performed. The procedure is repeated until the rotations at all connections, calculated from the linear relationships for the current cycle, are sufficiently close to those given by the appropriate nonlinear relationship of the form of Equation (4.72).

The convergence of the above procedure can be hastened by using only some fraction of the difference between $\emptyset'$ and $\emptyset$, rather than the total difference, when modifying the connection flexibility. A factor of one half was arbitrarily employed in this study.

4.7 DESCRIPTION OF PROGRAM

The computer analysis program is written in the FORTRAN H language. It has 5340 statements. In order to reduce the storage requirements, a storage pool is used. The program is implemented using the AMDAHL 470/V8 mainframe computer system at the University of Manitoba. With minor modifications, it can run using any compatible mainframe system. In its current version, it runs in the BATCH mode. Nonlinear analysis of a ten-storey structure with shear walls, such as the one described in Example 7 in chapter five, requires approximately 510 k-bytes of core storage and 59 seconds of CPU time to run.

The input can be divided into three blocks. The first describes the geometry of the structure. The second describes the properties of the structural components such as columns, plate panels, shear walls and plate-to-column connections. The third describes the loading. A detailed description of the required input is presented in Appendix B.

The program calculates and outputs the following information.

1. An echo of the input data.
2. The floor in-plane displacement components at the master nodes.
3. The out-of-plane displacements at all floor nodes.
4. The floor plate shears and moments at all nodes.
5. Column shears, moments and axial forces.
6. Shear wall shears, moments and axial forces.
7. Number of iterations required for the analysis to converge.

It is important to note here that floor shears and moments are calculated at plate panel corner nodes only.

Chapter V

APPLICATIONS AND DISCUSSION

5.1 INTRODUCTION

In this chapter, eight examples are presented to demonstrate the capabilities of the analysis procedure and the computer program. The results obtained using the program are compared with published results. The analysis program is capable of performing both linear and nonlinear analyses. Examples 1 and 2 illustrate the importance of considering the nonlinear behaviour of flat-plate structures when they are subjected to lateral loading. Examples 3 to 6 illustrate the influence of relevant physical parameters on the behaviour of a ten storey laterally-loaded flat-plate structure. The parameters include the plate reinforcement ratio in the vicinity of the column, the floor concrete strength, the column-depth-to-plate-span ratio and the plate thickness. In Example 7, a ten storey structure with shear walls is analyzed nonlinearly, and in Example 8 a six storey flat-plate structure with an unsymmetrical floor plan is analyzed nonlinearly.

5.2 EXAMPLE 1

The ten-storey flat-plate structure shown in Figure 5.1 was analyzed, first assuming rigid plate-to-column connections. Accordingly, the entire structure was assumed to behave linearly. Then the structure was reanalyzed assuming the plate-to-column connections to behave nonlinearly. The lateral loads were applied at the floor levels as shown in the figure, and it was assumed that no gravity load was acting. For the nonlinear analysis, the reinforcement ratio was 0.01 and the concrete strength was 30 MPa, values which would be common in engineering practice. The structure had been analyzed previously (Chislett, 1983) using methods recommended by several different researchers. They include the equivalent beam models proposed by Frazer (1983), Pecknold (1975) and Long and Kirk (1980), the equivalent frame method suggested by the American (ACI 318-83) and the Canadian (CSA A23.3 M83) specifications, the three dimensional linear analysis program developed by Chislett and Morris (1983), and the finite element model developed by Pulmano (1975). Equivalent beam section properties for the various equivalent beam models are presented in Table 5.1, and section properties for the equivalent columns are presented in Table 5.2.

The lateral drifts computed using the different models are summarized in Table 5.3 and plotted in Figure 5.2. As expected, the lateral drifts computed using the nonlinear

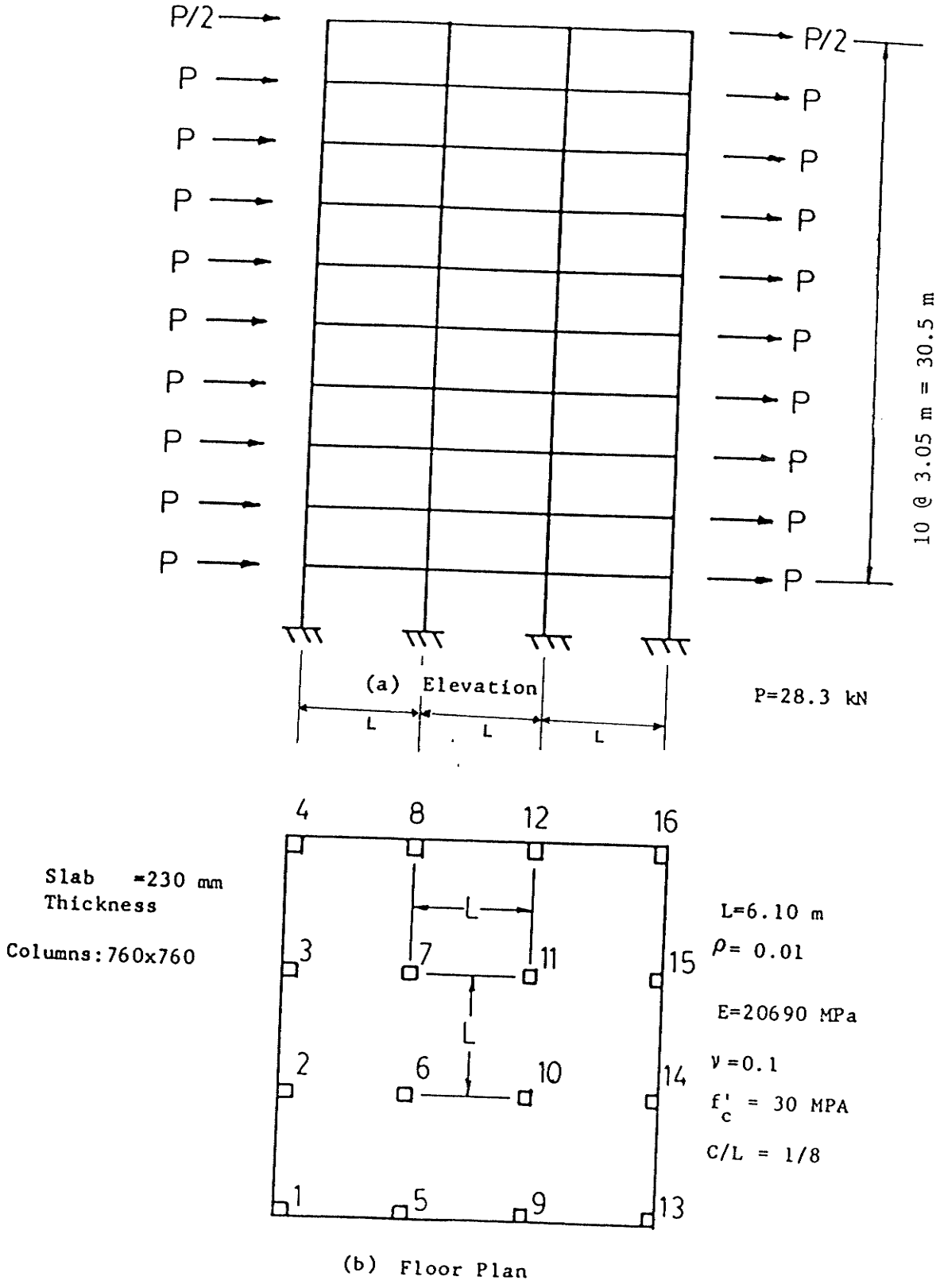

Figure 5.1: Ten storey example structure, Example 1

TABLE 5.1

Equivalent Beam Section Properties, Example 1

Author	Interior Beam			Edge Beam		
	Effective Width	J	I	Effective Width	J	I
	(mm)	(10^9 mm^4)	(10^9 mm^4)	(mm)	(10^9 mm^4)	(10^9 mm^4)
Long	1830	6.834	1.855	915	3.123	0.9277
Frazer	3553	13.82	3.602	2283	8.671	2.315
Pecknold	5612	22.17	5.690	2806	10.79	2.845

TABLE 5.2

Section Properties For Equivalent Columns , Example 1

Storey	Column Type	J (10^9 mm^4)	I_2 (10^9 mm^4)	I_3 (10^9 mm^4)	A (10^9 mm^2)
Top	Interior	47.04	11.21	11.21	577600
	Edge	47.04	11.21	6.72	577600
	Corner	47.04	6.72	6.72	577600
Other Storeys	Interior	47.04	13.43	13.43	577600
	Edge	47.04	13.43	7.46	577600
	Corner	47.04	7.46	7.46	577600

TABLE 5.3

Lateral Drifts Obtained from Different Analysis Models

Example 1 (mm)

STOREY	Model							
	1	2	3	4	5	6	7	8
10	10.6	10.7	11.5	12.3	12.3	14.3	16.6	25.9
9	10.3	10.3	11.2	11.9	11.9	13.7	15.9	24.5
8	9.8	9.8	10.8	11.3	11.2	13.0	15.0	22.7
7	9.0	9.1	10.1	10.4	10.4	11.9	13.7	20.5
6	8.0	8.1	9.1	9.2	9.2	10.6	12.1	17.9
5	6.8	6.9	7.9	7.8	7.8	8.9	10.1	14.7
4	5.4	5.4	6.5	6.1	6.1	7.0	7.9	11.2
3	3.8	3.8	4.8	4.3	4.3	4.8	5.4	7.5
2	2.1	2.2	2.9	2.4	2.4	2.7	2.9	4.0
1	0.7	0.7	1.0	0.7	0.7	0.8	0.9	1.2
0	0.0	0.0	0.0	0.0	0.0	0.0	0.0	0.0

1 - Pulmano
2 - Pecknold
3 - CAN 3-A23.3-M83
4 - Chislett and Morris
5 - Linear Frame Analysis (Author)
6 - Frazer
7 - Nonlinear Frame Analysis (Author)
8 - Long and Kirk

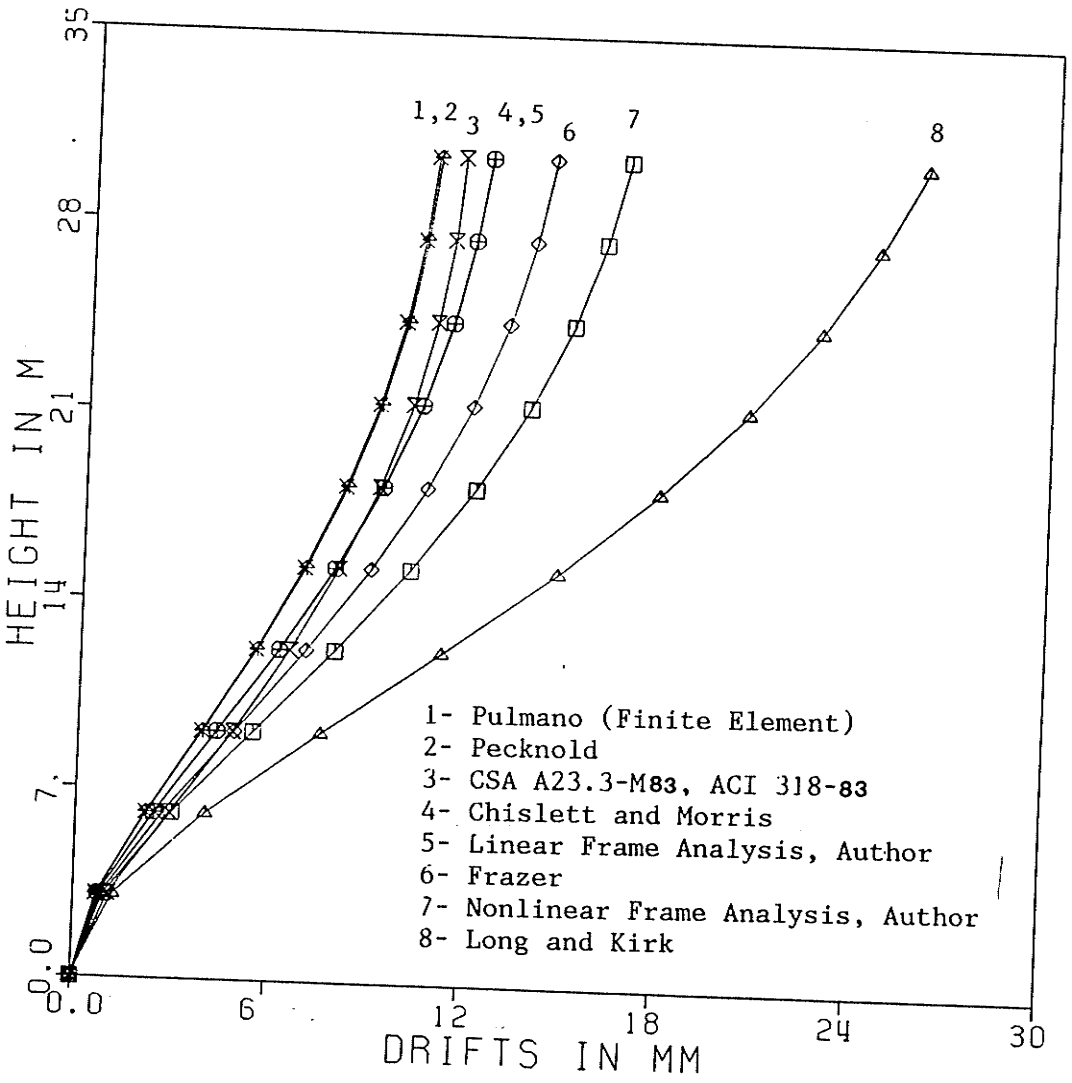

Figure 5.2: Comparison among different methods, Example 1

method were larger than these obtained using all of the linear methods except for that developed by Long and Kirk.

To account for the loss of stiffness resulting from the cracking of the concrete at the plate-to-column connections due to gravity loading, Long and Kirk recommended using a very small equivalent beam width of 0.3 times the plate width. This recommendation was based upon their experimental program using one third scale reinforced concrete models. The maximum difference between the drifts obtained from the nonlinear analysis and those obtained using Long and Kirk's method was found to be 56%. Long and Kirk suggested a conservative value for the equivalent beam width in order to emphasize the importance of the effects of concrete cracking at the plate-to-column boundaries. That probably explains the large difference between the drifts obtained by Long and Kirk and those obtained using the nonlinear analysis program.

Lateral drifts obtained using Frazer's equivalent beam width were as much as 14% smaller than those obtained using the nonlinear analysis program, while those obtained using Pecknold's equivalent beam width were as much as 36% smaller. Those drifts obtained using the CSA or ACI equivalent frame methods were as much as 31% smaller.

The lateral drifts obtained using the author's program assuming linear behaviour and Chislett and Morris' linear

analysis program were found to be virtually identical. The lateral drifts obtained using Pulmano's finite element analysis were found to be approximately 14% smaller than those obtained using the author's linear analysis. This is to be expected since Pulmano's finite element program uses compatible plate elements which normally result in an overestimation of the stiffness of the structure.

All of the equivalent beam methods have the same shortcoming; they assume a single value for the stiffness of the plate-to-column connections. In reality the stiffness depends upon several parameters, as discussed previously. Consequently, equivalent beam methods tend to overestimate the stiffness of some structures and to underestimate that of others.

Column shear forces for columns 1 and 6 obtained using the authors analysis program, the Chislett and Morris (1983) linear three-dimensional analysis program, and Pulmano's (1975) finite element program are presented in Table 5.4, and those for column 1 are plotted in Figure 5.3. Column moments for columns 1 and 6 obtained using the three methods of analysis described above, are presented in Table 5.5 and those for column 1 are plotted in Figure 5.4. It can be seen that these methods yield very similar column forces.

TABLE 5.4

Column Shear Forces (kN), Example 1

Storey	Column 1			Column 6		
	Linear	Chislett	Pulmano	Linear	Chislett	Pulmano
10	-2.20	-1.67	-0.99	7.66	6.69	5.48
9	1.72	1.99	2.52	10.65	10.09	9.08
8	3.27	3.58	4.38	16.99	16.34	14.80
7	5.19	5.46	6.46	22.83	22.21	20.26
6	7.00	7.23	8.45	28.81	28.22	25.83
5	8.90	9.18	10.57	34.52	33.98	31.15
4	11.35	11.49	12.95	39.69	39.23	36.26
3	14.60	14.87	16.07	43.59	43.23	40.33
2	19.34	19.39	20.45	45.32	45.09	42.72
1	28.76	28.77	29.19	40.47	40.38	39.39

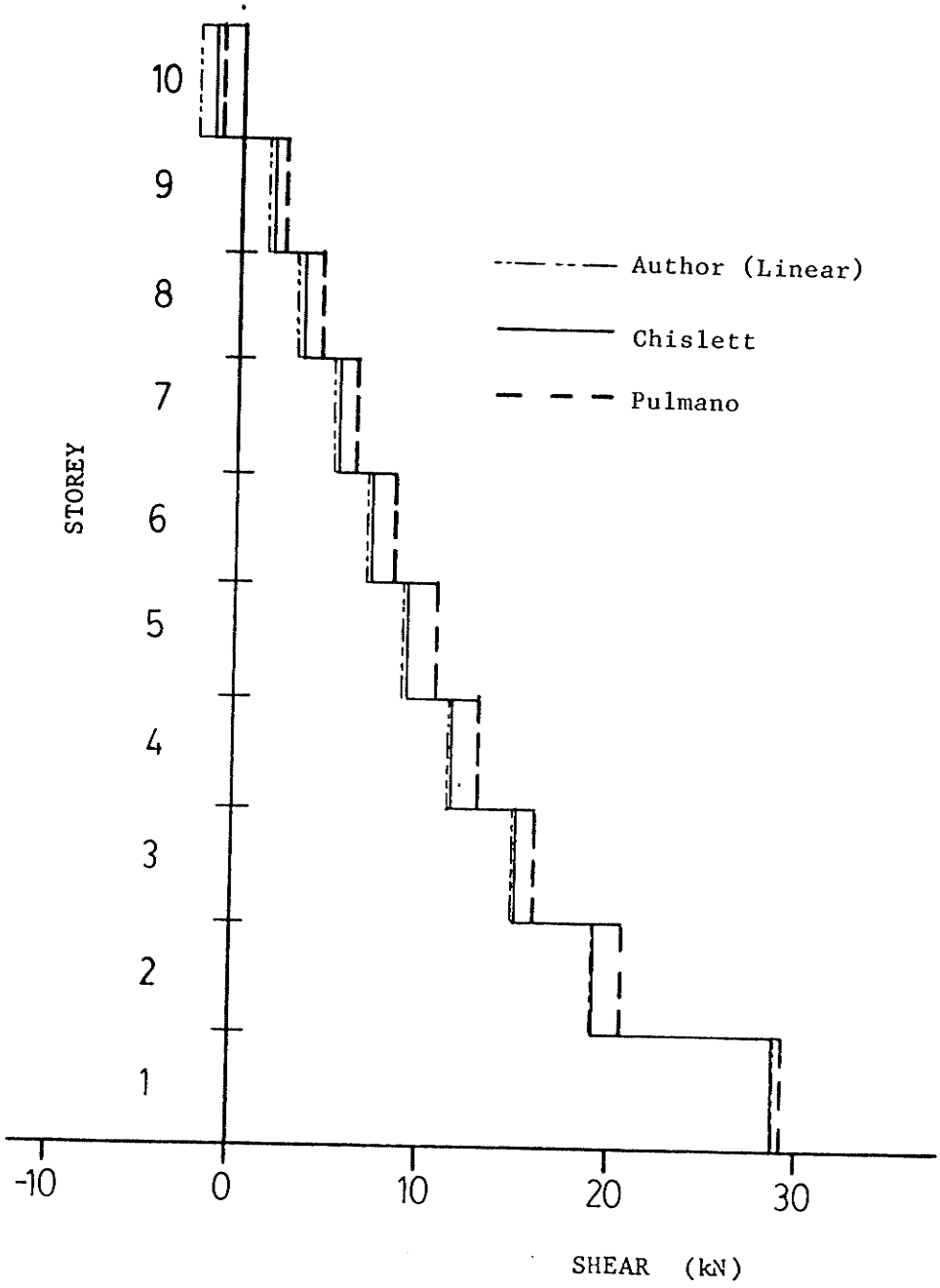

Figure 5.3: Column Shear Forces For Column 1, Example 1

TABLE 5.5

Column Bending Moments (kN-m), Example 1

Storey	Column 1			Column 6		
	Linear	Chislett	Pulmano	Linear	Chislett	Pulmano
10 top	4.05	5.11	5.37	21.13	19.45	16.38
bottom	-10.77	-10.21	-8.40	2.23	0.96	0.34
9 top	16.76	17.26	16.27	28.85	28.16	25.08
bottom	-11.52	-11.18	-8.59	3.63	2.63	2.61
8 top	21.03	21.68	20.75	41.11	40.23	35.87
bottom	-11.07	-10.76	-7.40	10.70	18.10	17.19
7 top	24.63	25.22	24.50	50.44	49.65	44.60
bottom	-8.79	-8.57	-4.80	19.17	18.10	17.19
6 top	26.59	27.15	27.00	58.87	58.12	52.60
bottom	-5.24	-5.09	-1.24	29.00	27.96	26.17
5 top	27.13	27.62	28.40	65.21	64.54	59.00
bottom	0.31	0.38	3.84	40.07	39.10	36.02
4 top	25.12	25.50	27.64	67.80	67.21	62.60
bottom	9.50	9.54	11.87	53.26	52.44	48.00
3 top	18.15	18.34	22.43	62.58	62.06	59.50
bottom	26.38	26.46	26.58	70.36	69.79	63.50
2 top	0.58	0.50	7.16	41.46	40.94	42.10
bottom	58.41	58.64	55.20	96.76	96.57	88.20
1 top	-38.28	-38.69	-29.68	-14.55	-15.07	-8.95
bottom	125.99	126.43	118.70	137.97	138.24	129.10

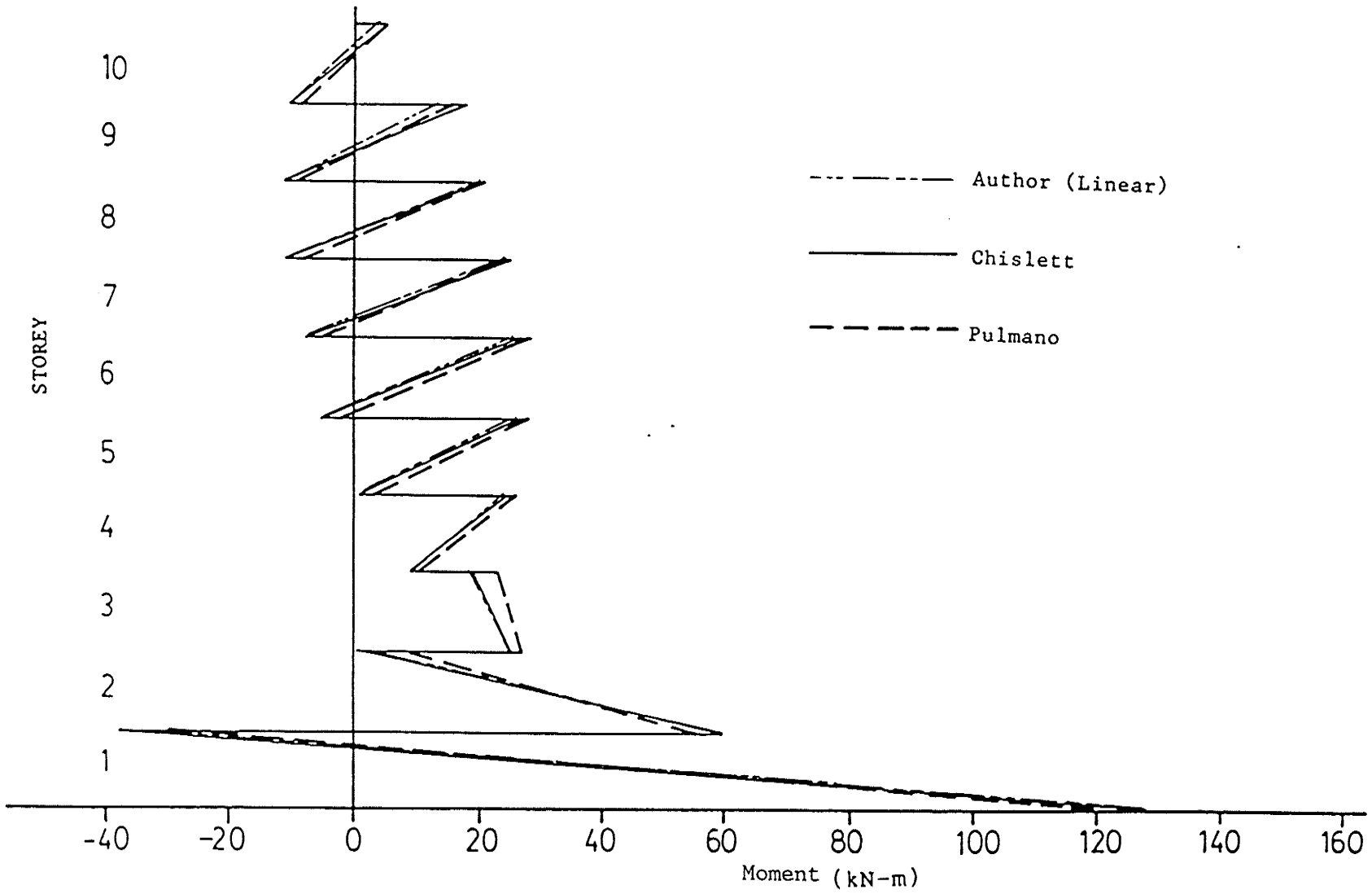

Figure 5.4: Column Moments For Column 1, Example 1

5.3 EXAMPLE 2

The ten-storey structure considered in Example 1 was analyzed nonlinearly under four different lateral loads and three gravity load levels. The lateral loads,P, considered were 20 kN, 40 kN, 80 kN and 100 kN. Low, moderate and high gravity load levels were considered. The structure was also analyzed assuming rigid connections between the columns and the plates under the four lateral loading conditions. For the nonlinear analysis, The steel ratio was assumed to be 0.02, the floor concrete strength was 30 MPa, the plate thickness was 230 mm and the column-depth-to-plate-span ratio was 1/8.

The roof lateral drifts for the different loading cases considered are shown in Figure 5.5 and listed in Table 5.6. It can be seen from the figure that the lateral drifts obtained from the nonlinear analysis deviate considerably from those obtained from the linear analysis. The deviation increases as the lateral load increases. Thus, the ratio of the roof drifts for the high-gravity-load and the linear analysis cases is 1.24 at a transverse load of 20 kN. At a transverse load of 100 kN, the ratio has increased to 1.65. In practice this could mean the difference between considering the structure to meet the code serviceability requirements or not.

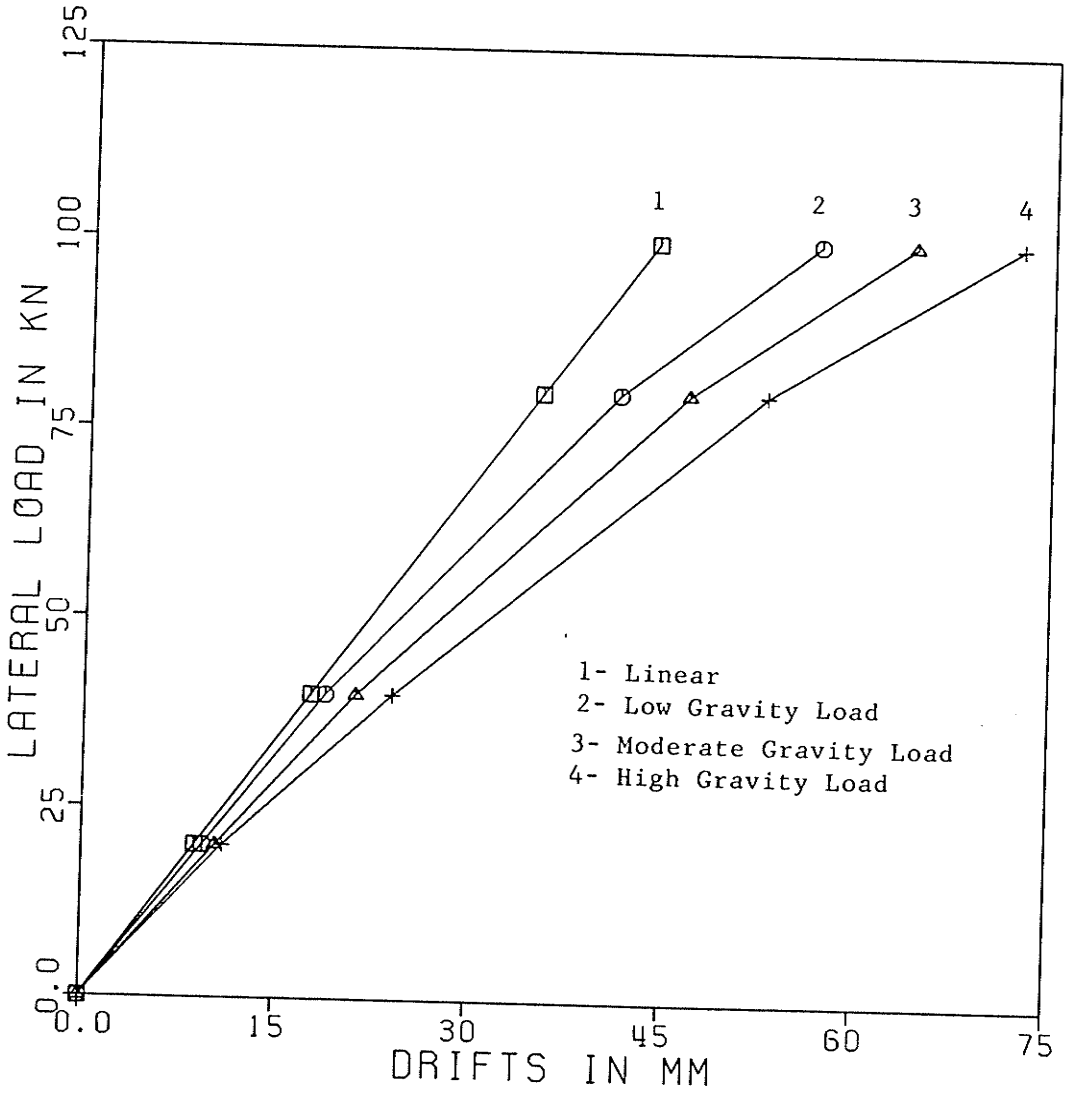

Figure 5.5: Lateral Drifts For Various Loading Conditions, Example 2

TABLE 5.6

Structure Drifts Under Various Loading Conditions,

Example 2 (mm)

Lateral load (kN)	Linear	Low Gravity Load	Moderate Gravity Load	High Gravity Load
20.0	8	9	10	10
40.0	17	18	21	23
80.0	35	41	46	52
100.0	44	56	61	72

The level of gravity loading applied to the structure influences its behaviour under lateral load also. Thus, for example, in Figure 5.5 it can be seen that as the gravity load level is increased from "low" to "high", while holding the lateral load constant at 100 kN, the lateral drift increases by 28 percent. This is due mainly to the cracking of the concrete at the column face caused by gravity loading. That cracking results in a loss of stiffness at the connections between the plates and the columns. A variation in gravity load level has virtually no influence on column end shears and moments due to lateral load. It is important to recall that in this study, the influence of the gravity loading was considered for interior plate-to-column connections only. The influence of the gravity loading on the stiffness of the overall structure would increase if it were accounted for in the derivation of the standardized functions for corner and edge connection types.

5.4 EXAMPLE 3

In this example, the influence of the plate steel ratio in the vicinity of the column is demonstrated. The ten-storey structure shown in Figure 5.1 was analyzed assuming steel ratios at the connections of 0.04, 0.03, 0.02 and 0.01. They represent the practical range used in design. The structure was assumed to be subjected to lateral loads, P, of 50 kN, and moderate gravity loading. The concrete strength was assumed to be 30 MPa, while the plate thickness was 230 mm and the column-depth-to-plate-span ratio was 1/8.

The lateral drifts for the structure are listed in Table 5.7 and plotted in Figure 5.6. Figure 5.7 shows a plot of various storey drifts as a function of the floor reinforcement ratio. It can be seen from the figures that the lateral response of the structure is influenced significantly by the total amount of reinforcement present at the plate-to-column connections. It can be seen in Figure 5.6 that there is an increase in the stiffness of the structure with the increase of the connection reinforcement ratio until the latter exceeds about 3 percent, after which little stiffness is gained by increasing the reinforcement ratio. Thus, an increase in the total steel ratio in the column region from 0.01 to 0.02 resulted in a 19% reduction in the lateral drift, while an increase from 0.03 to 0.04 resulted in only a 4% reduction in the lateral drift. This phenomenon has been observed by Akiyama (1984).

TABLE 5.7

Lateral Drifts For Different Steel Ratios, Example 3

(mm)

Storey	$\rho_{total} = \rho_{top} + \rho_{bottom}$			
	0.040	0.030	0.020	0.010
10	22	23	26	31
9	21	22	25	30
8	20	21	23	28
7	19	19	22	26
6	16	17	19	23
5	14	14	16	19
4	11	11	12	15
3	7	8	8	10
2	4	4	4	5
1	1	1	1	1

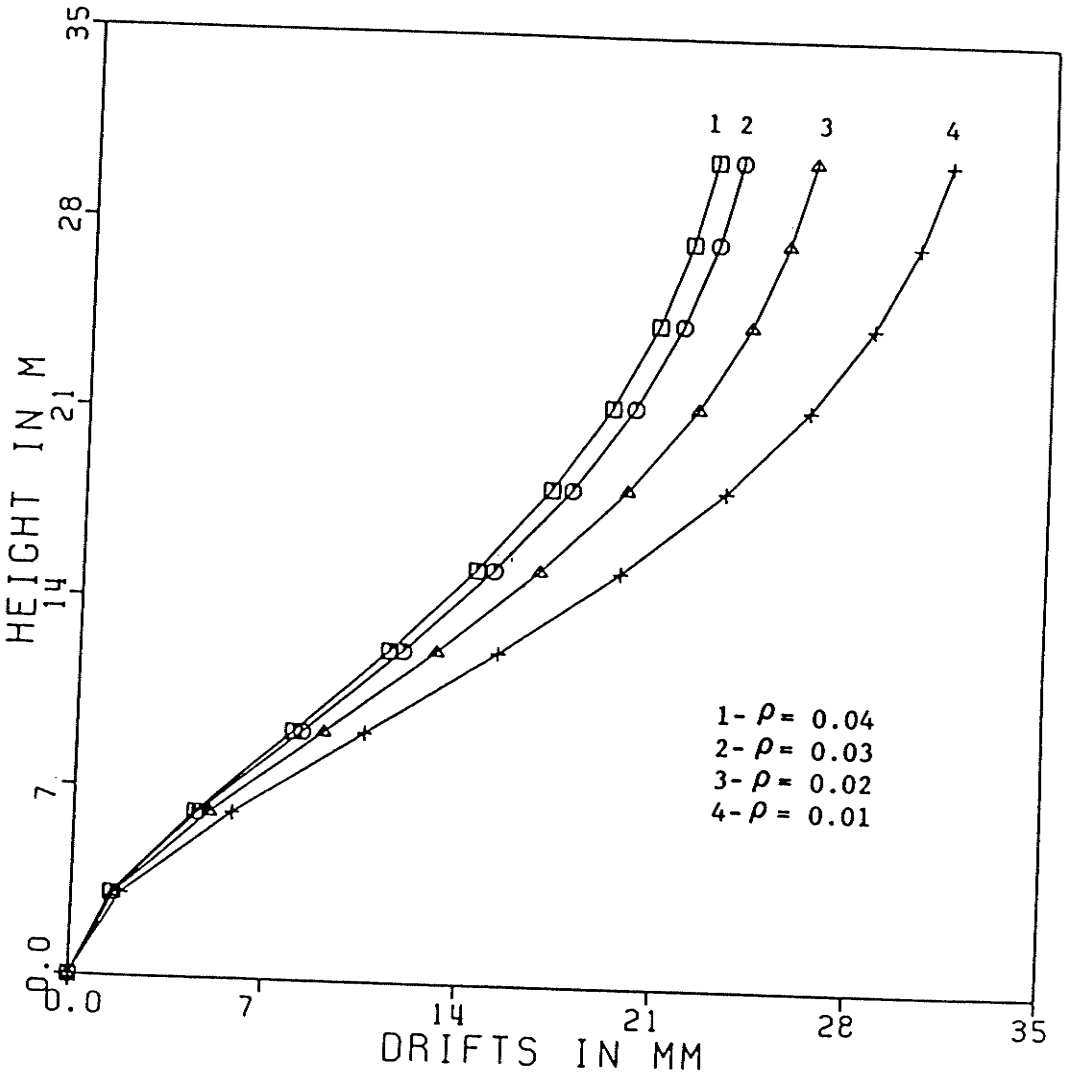

Figure 5.6: **Lateral Drifts For Different Reinforcement Ratios**, Example 3

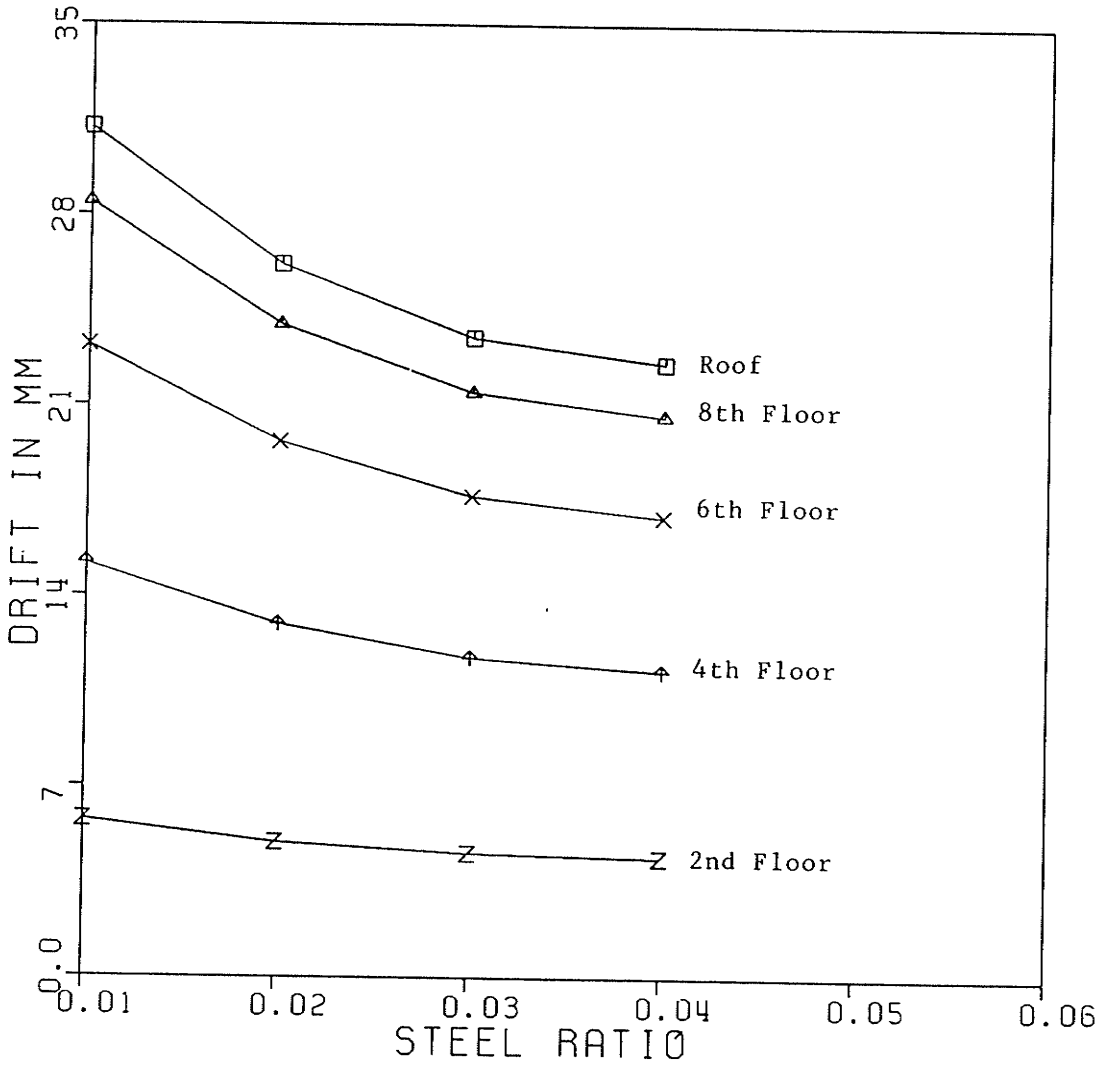

Figure 5.7: Steel Ratio vs Lateral Drifts,
Example 3

Column moments for column 6 are plotted in Figure 5.8 for steel ratios of 0.01 and 0.04. It can be seen from the figure that the column moments are not very sensitive to variations in the floor reinforcement ratio.

The program assumes all connections of the same type in a given floor to have the same steel ratio. This assumption is considered to be reasonable for practical design applications.

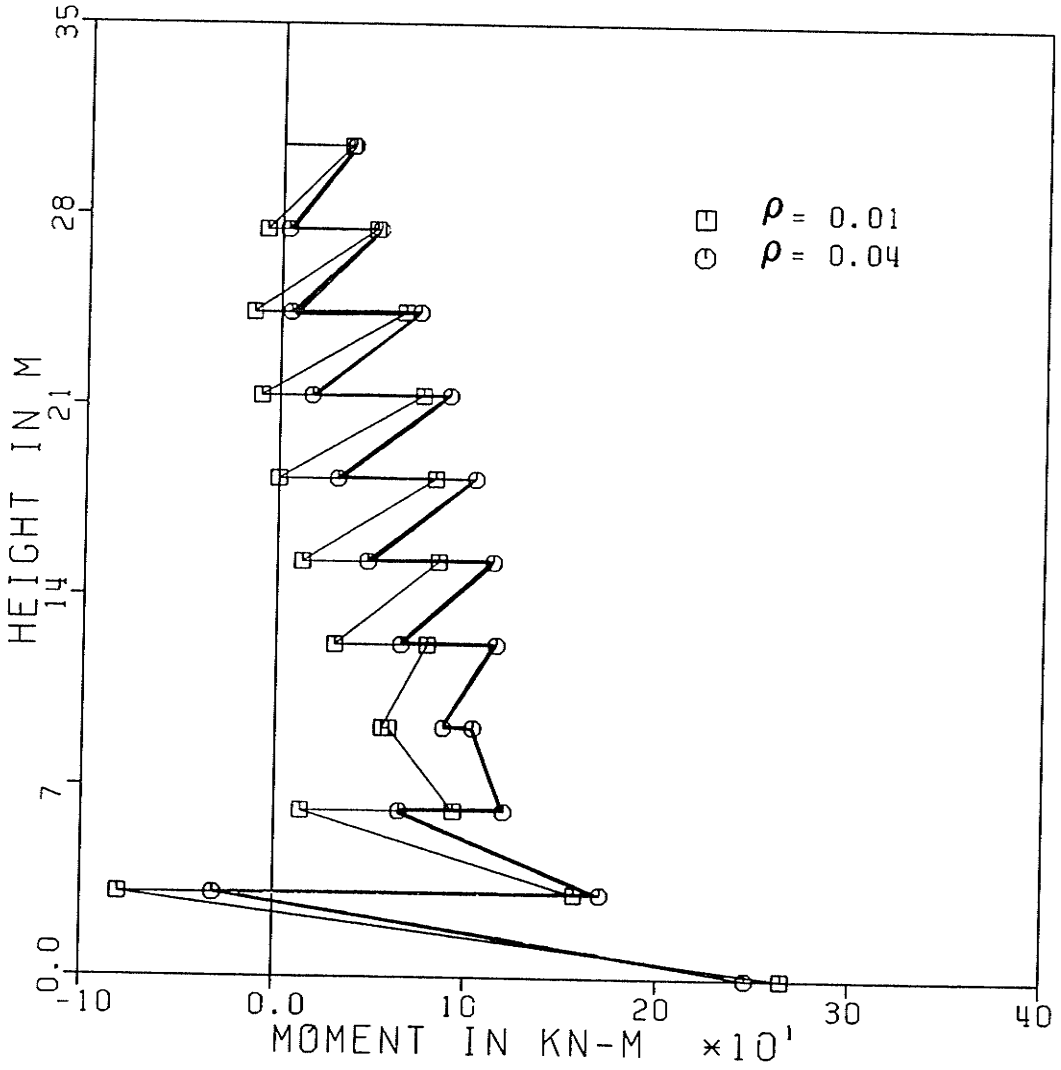

Figure 5.8: Column Moments for Column 6, Example 3

5.5 EXAMPLE 4

This example illustrates the influence of the column-depth-to-plate-span ratio on the behaviour of a structure. The structure shown in Figure 5.1 was analyzed assuming square column dimensions of 760, 555, 381, and 244 mm, corresponding to column-depth-to-plate-span ratios of 1/8, 1/11, 1/16, 1/25, respectively. These ratios cover the range normally used in design. The steel ratio was assumed to be 0.02, the floor concrete strength was 30 MPa, and the plate thickness was 230 mm. The lateral loads, P, were 50 kN, and moderate gravity loading was assumed.

The lateral drifts are listed in Table 5.8 and plotted in Figure 5.9. Figure 5.10 shows a plot of various storey drifts as a function of the column-depth-to-plate-span ratio. It can be seen that the lateral behaviour of the structure was strongly influenced by that parameter. In this study, the influence of the column-to-plate span ratio was accounted for in deriving the standardized functions for the different types of connections, and also in the derivation of the plate-element stiffness matrix. Therefore, an increase in the column-depth-to-plate-span ratio increases the stiffnesses of the plate-to-column connections and also the stiffness of the floor plate panels. Thus, for example, an increase in the column-depth-to-plate-span ratio from 1/25 to 1/8 results in a decrease of the roof lateral drift by a factor of 7.

TABLE 5.8

Lateral Drifts For Different Column/Plate Span Ratios, Example 4

(mm)

Storey	Column / Plate Span Ratio C/L			
	1/8	1/11	1/16	1/25
10	26	29	63	180
9	25	29	62	178
8	23	28	60	172
7	22	26	57	163
6	19	24	52	150
5	16	21	46	134
4	12	17	38	113
3	8	12	29	89
2	4	7	18	60
1	1	2	7	28
Supports	0.0	0.0	0.0	0.0

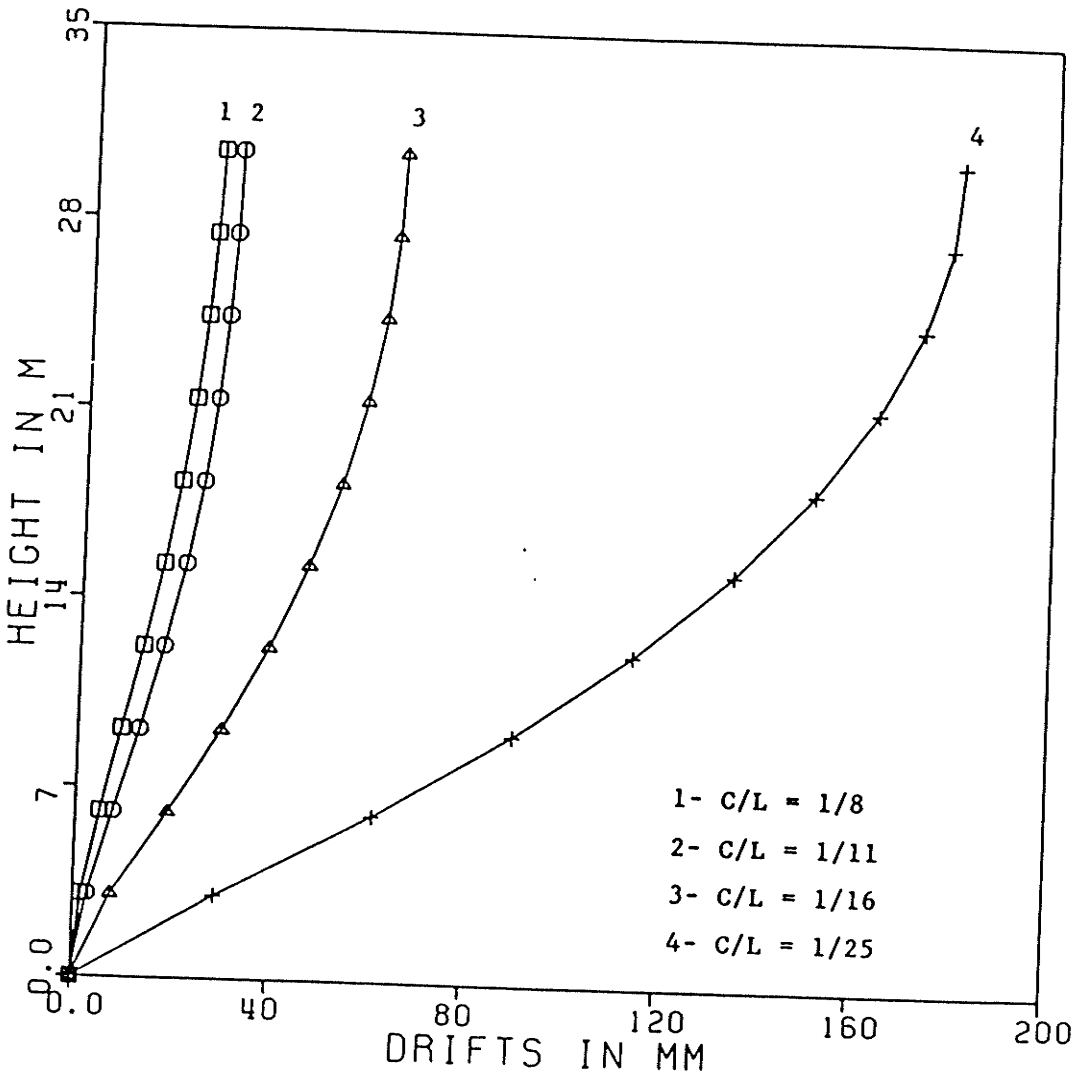

Figure 5.9: Lateral Drifts For Different Column/Plate Span Ratios, Example 4

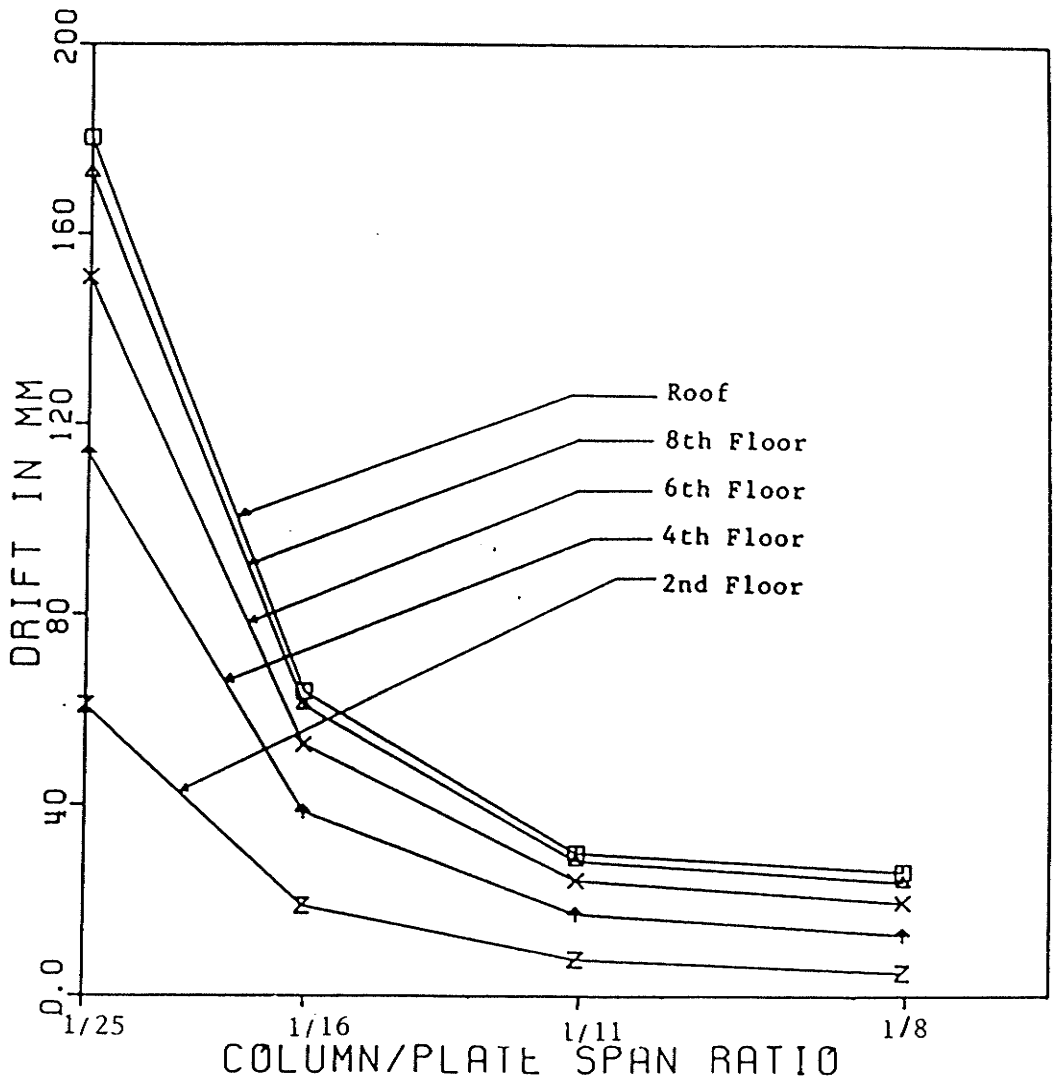

Figure 5.10: Column/Plate span ratio vs Lateral Drifts
Example 4

It is evident from Figure 5.9 that the lateral stiffness of the structure is very sensitive to changes in the column-depth-to-plate-span ratio when the floors are relatively flexible. However, when the floors are stiff, a further increase in the plate-to-column-ratio produces only a small increase in lateral stiffness. For example, increasing the column-depth-to-plate-span ratio from 1/25 to 1/16 resulted in a reduction of the roof drift of 65 percent, while increasing the ratio from 1/11 to 1/8 produced only a 13 percent reduction.

Column moments for columns 1 and 6 are plotted in Figure 5.11 for column-depth-to-plate-span ratios of 1/8 and 1/25. It can be seen that the column moments are extremely sensitive to changes in the ratio.

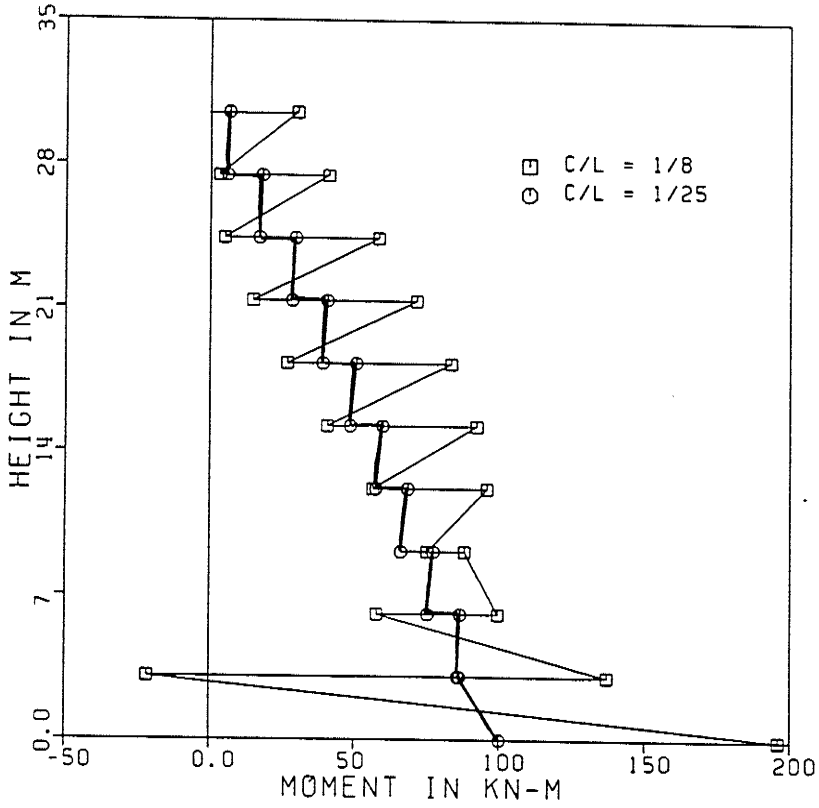

Column 6

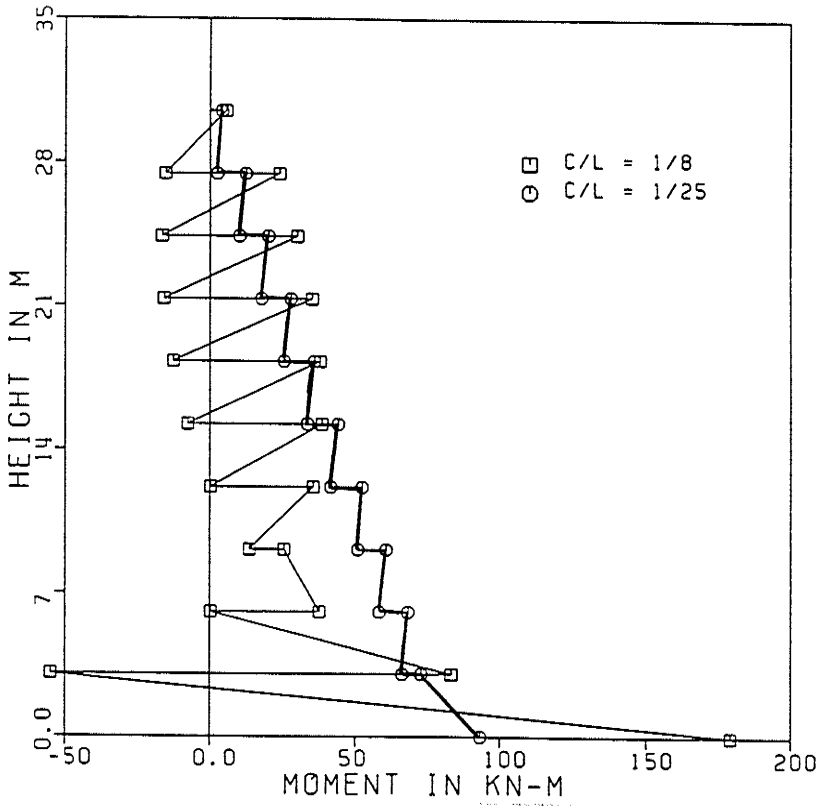

Column 1

Figure 5.11: Column Moments for Columns 1 and 6, Example 4

5.6 EXAMPLE 5

The influence of floor concrete strength on the behaviour of the overall structure is demonstrated in this example. The structure shown in Figure 5.1 was analyzed assuming different floor concrete strengths. The concrete strengths considered were 20, 25, 30, 35 and 40 MPa, which represent the practical range of values normally used in design. The reinforcement ratio was 0.02, the plate thickness was 230 mm and the column-to-plate-span ratio was 1/8. The structure was subjected to a lateral loads, P, of 50 kN and it supported moderate gravity loads.

The computed lateral drifts are listed in Table 5.9 and plotted in Figure 5.12. In Figure 5.13, the various storey drifts are plotted as a function of the floor concrete strength. The results shown in Figure 5.12 and 5.13 demonstrate that the concrete strength has less influence on the behaviour of the structure than does the steel ratio. The concrete strength influences the extent and propagation of the cracks in the column region. Therefore, as it increases, although only moderately, the stiffness of the connections and that of the overall structure increases. It was found, for example, that increasing the floor concrete strength from 20 to 40 MPa resulted in a 15% reduction in the lateral drift at the roof level.

TABLE 5.9

Lateral Drifts For Different Floor Concrete Strengths, Example 5

(mm)

Storey	Floor Concrete Strength f_c'				
	20.00	25.00	30.00	35.00	40.00
10	28	27	26	25	24
9	27	16	25	24	23
8	25	24	23	23	22
7	23	22	22	21	20
6	20	20	19	19	18
5	17	17	16	16	15
4	13	13	12	12	12
3	9	9	8	8	8
2	5	5	4	4	4
1	1	1	1	1	1

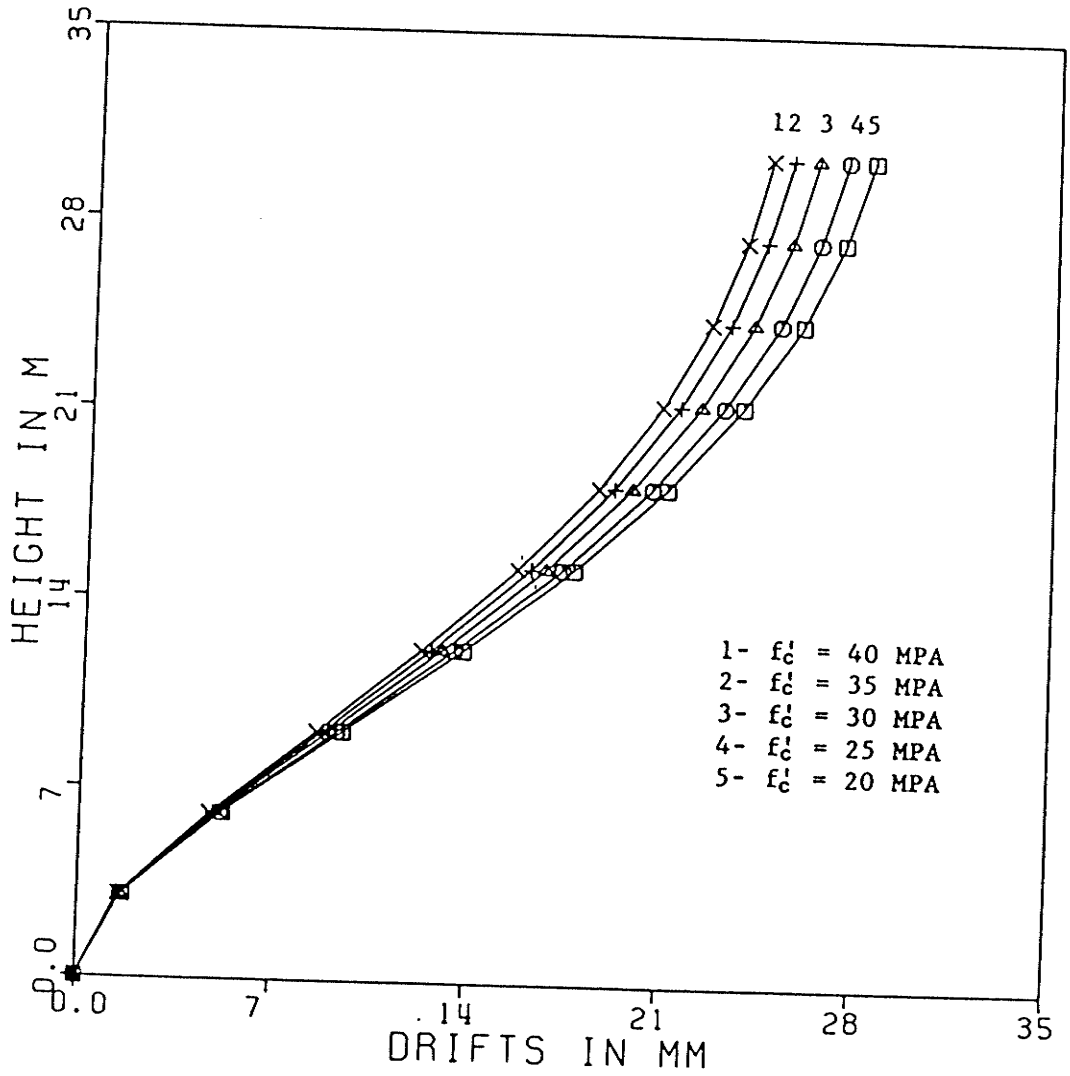

Figure 5.12: Storey Drifts For Different Floor Concrete Strengths , Example 5

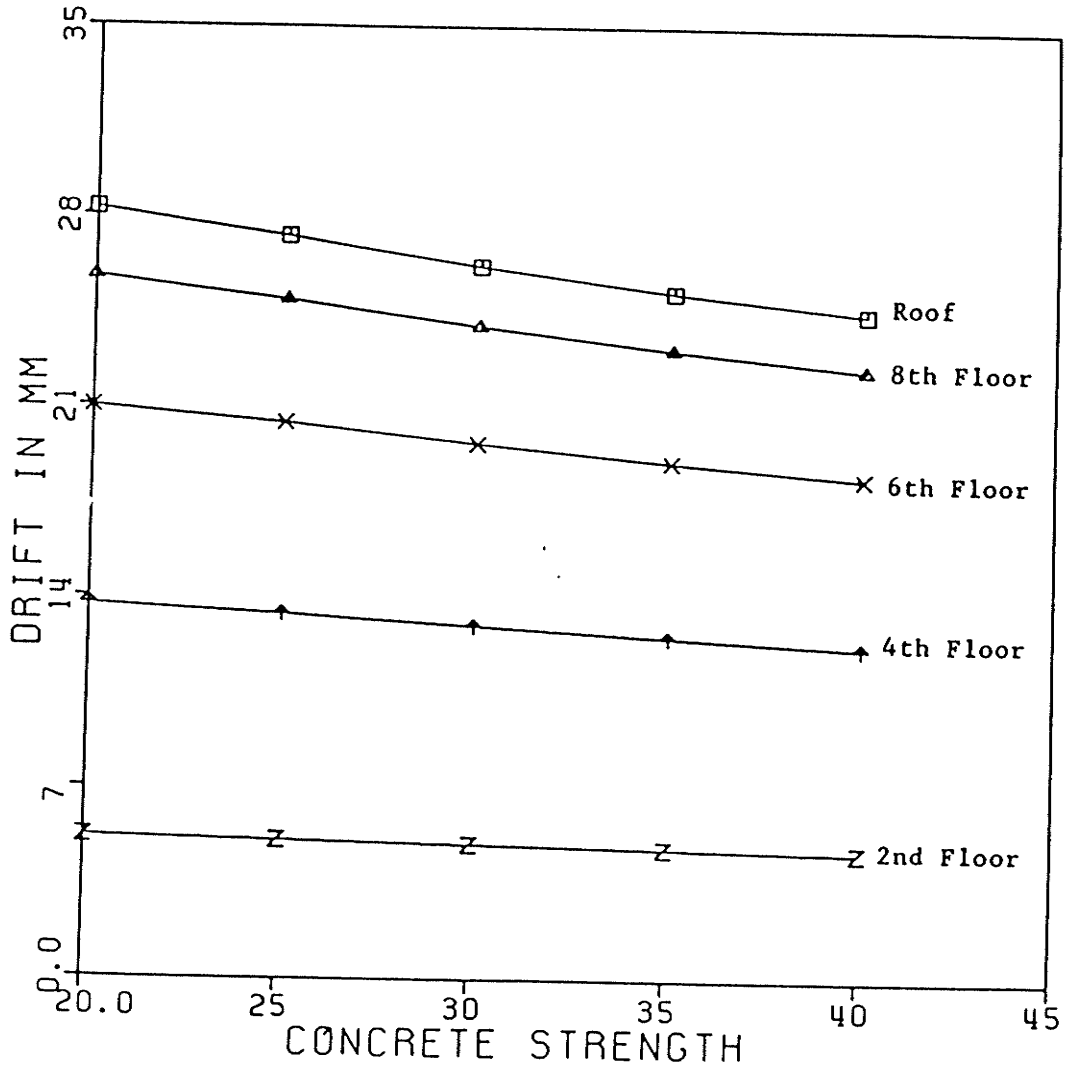

Figure 5.13: Concrete Strength vs Lateral Drifts,
Example 5

Column moments for column 6 are plotted in Figure 5.14 for concrete strengths 20 and 40 MPa. It can be seen that the floor concrete strength has little effect on the column moments.

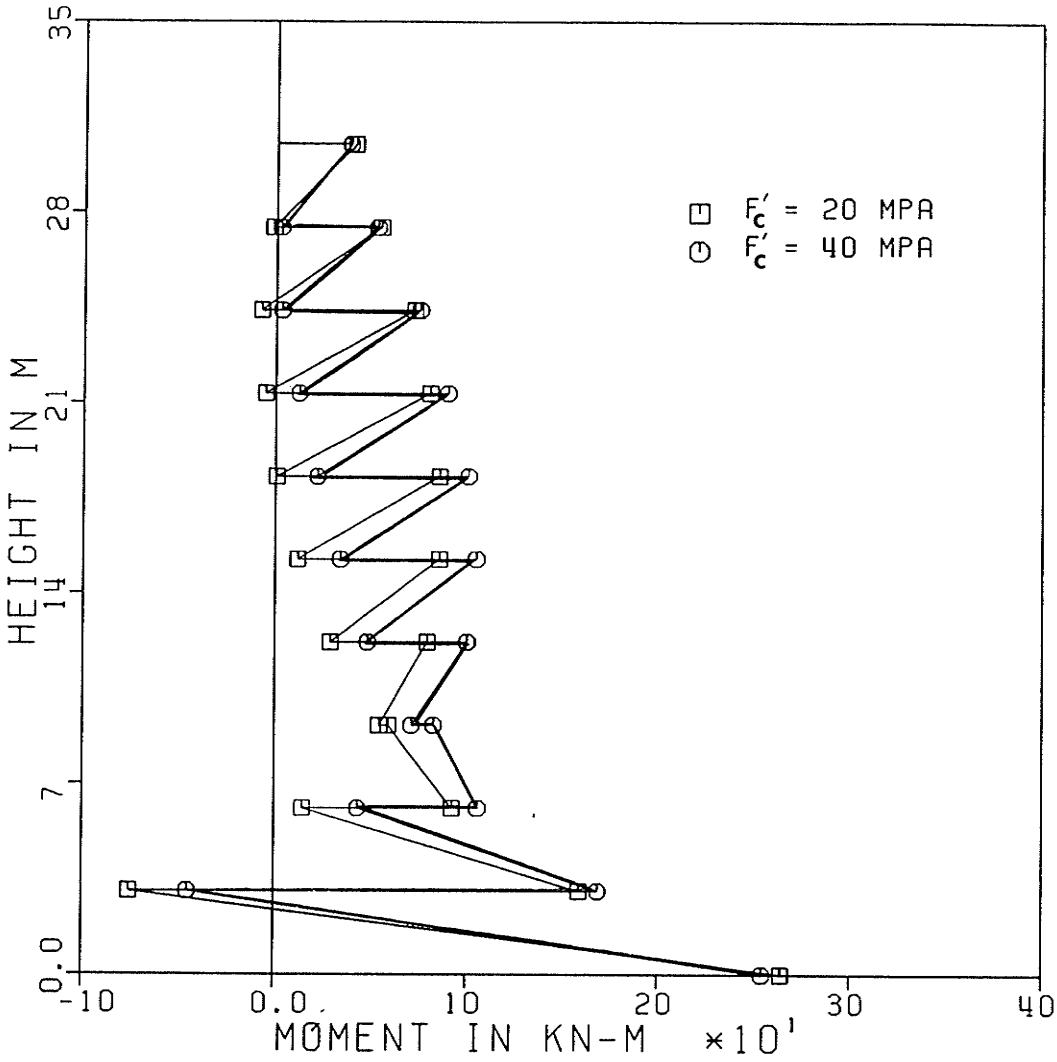

Figure 5.14: Column Moments for Column 6, Example 5

5.7 EXAMPLE 6

The influence of the thickness of the floor plate on the behaviour of the structure is illustrated in this example. The ten-storey structure shown in Figure 5.1 was analyzed assuming floor plate thicknesses of 150, 190, 230, 270, 310 and 350 mm. The plate reinforcement ratio in the vicinity of the column was 0.02, the floor concrete strength was 30 MPa, and the column-to-plate-span ratio was 1/8. The structure was assumed to support lateral loads, P, of 50 kN, and moderate gravity load.

The lateral drifts are listed in Table 5.10 and plotted in Figure 5.15. Figure 5.16 shows a plot of various storey drifts as a function of the floor plate thickness. It is demonstrated in Figures 5.15 and 5.16 that the plate thickness strongly influences the response of flat-plate structures to lateral loads. As would be expected, an increase in the plate thickness causes an increase in its stiffness, thus a decrease in the lateral drift. The figures illustrate as well however, that the thicker the floor plate, the less sensitive to plate thickness is the lateral drift. Thus, for the structure considered in this example, increasing the plate thickness from 150 to 190 mm resulted in a 43% reduction in the roof lateral drift, while increasing the thickness from 310 to 350 mm resulted in only a 27% reduction in the drift.

TABLE 5.10

Lateral Drifts For Different Plate Thicknesses, Example 6

(mm)

Storey	Plate Thickness t (mm)					
	150	190	230	270	310	350
10	76	43	26	16	11	8
9	71	41	25	16	11	8
8	64	38	23	15	10	7
7	57	35	22	14	10	7
6	48	30	19	13	9	6
5	39	25	16	11	7	5
4	28	19	12	8	6	4
3	18	12	8	6	4	3
2	9	6	4	3	2	2
1	2	2	1	1	0.9	0.7
Supports	0.0	0.0	0.0	0.0	0.0	0.0

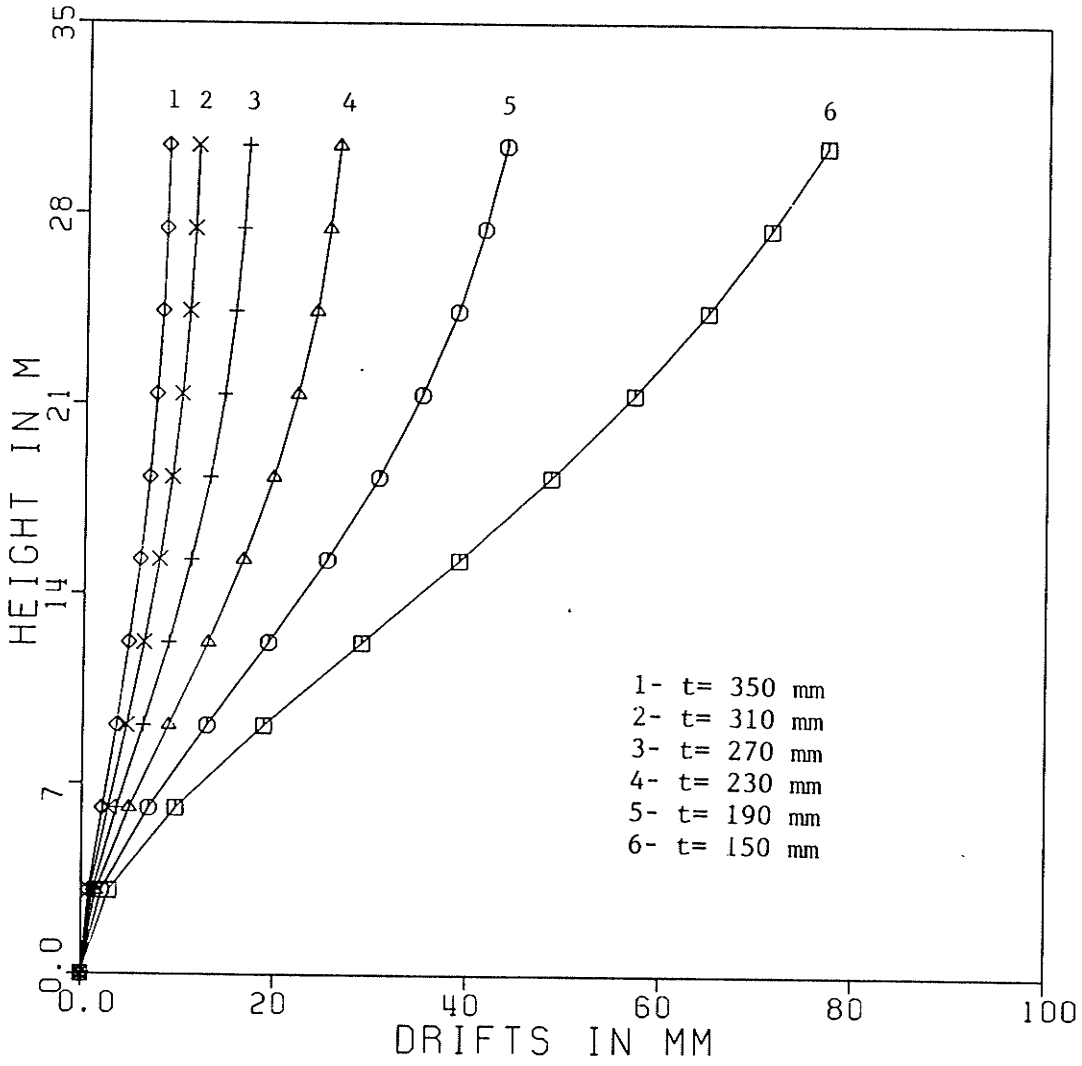

Figure 5.15: Storey Drifts For Different Plate Thicknesses, Example 6

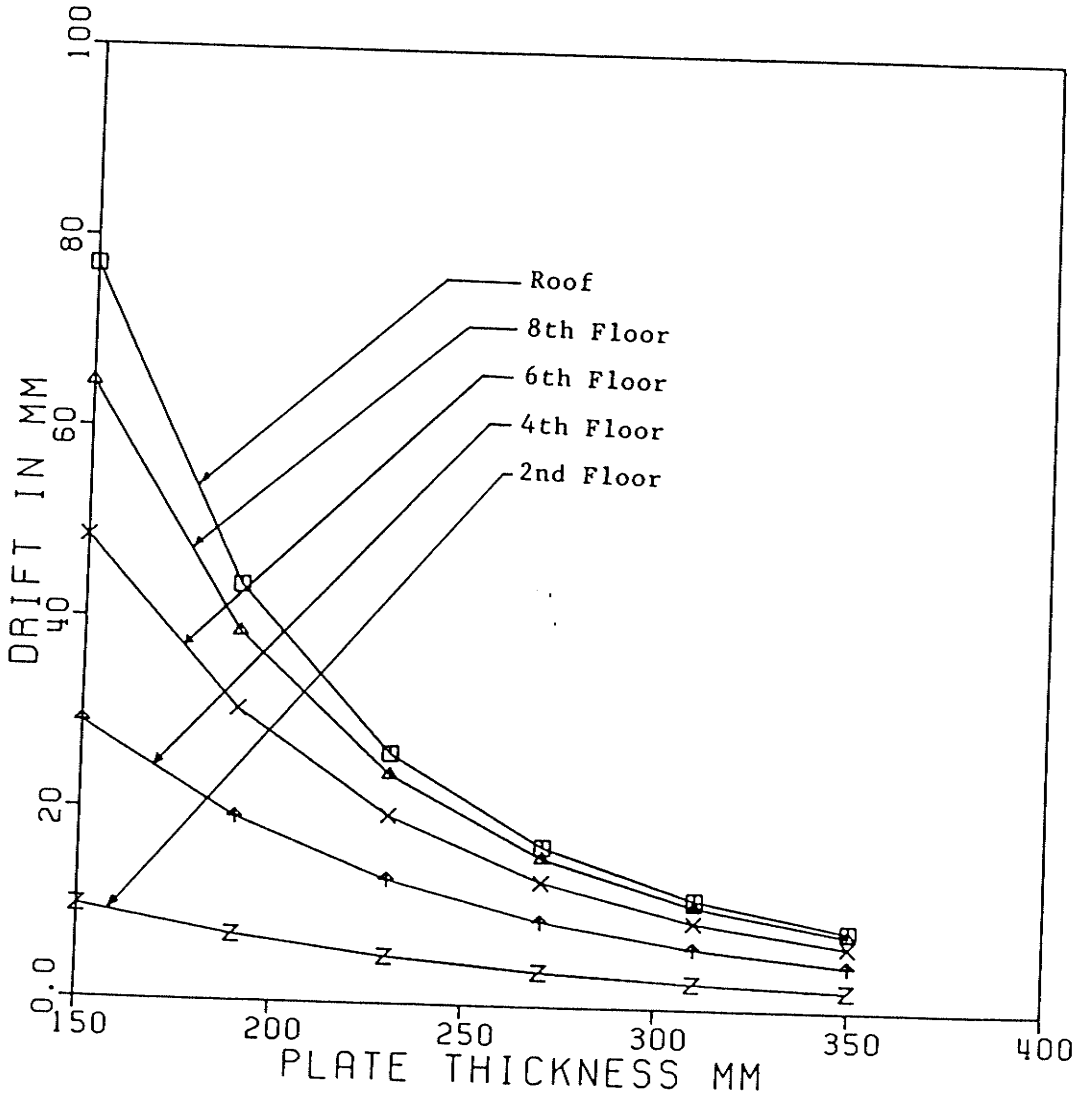

Figure 5.16: Plate Thickness vs Lateral Drifts, Example 6

Column moments for columns 1 and 6 are plotted in Figure 5.17 for plate thicknesses of 150 and 350 mm. It can be seen from the figure that column moments are sensitive to variations in the floor plate thickness. Comparison of figures 5.13 and 5.17 illustrates that the influence of column-depth-to-plate-span ratio on column moments is smaller than that of plate thickness.

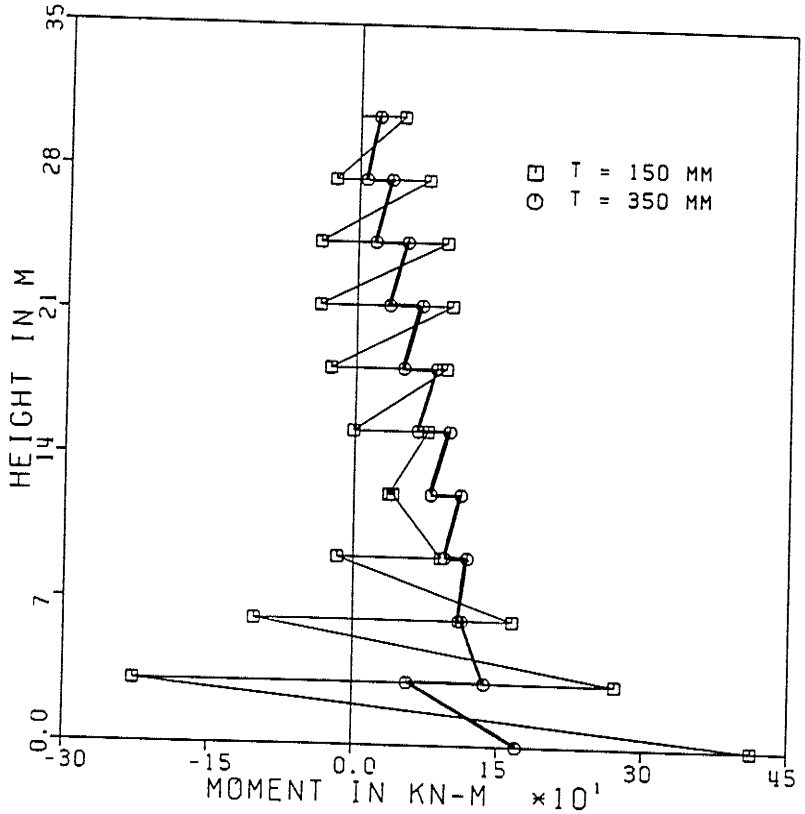

Column 6

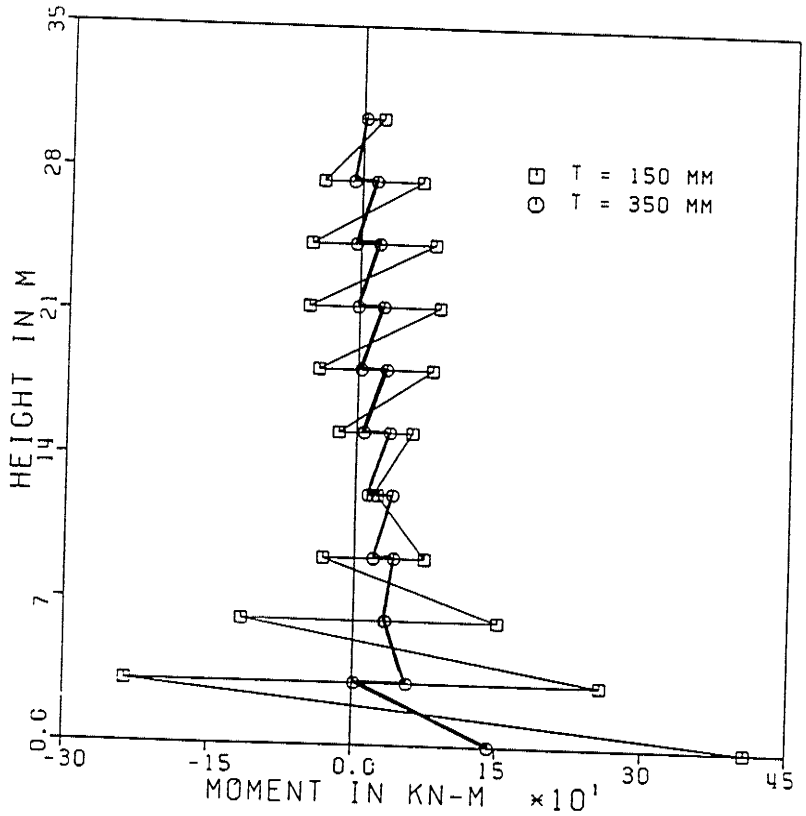

Column 1

Figure 5.17: Column Moments for Columns 1 and 6, Example 6

5.8 EXAMPLE 7

The structure shown in Figure 5.18 was analyzed nonlinearly. The lateral loads, P, were applied as shown in the figure. The steel ratio was 0.02, the column-depth-to-plate-span ratio was 1/16, the floor concrete strength was 30 MPa, and the floor thickness was 230 mm. The thickness of the shear walls was 200 mm and their Poisson's ratio was 0.20.

The lateral drifts obtained for the ten storey structure with and without shear walls are plotted in Figure 5.19. It can be seen from the figure that the presence of shear walls reduced the roof lateral drift by 80%.

The total shears in the structure are normally resisted by both the frame, which comprises the floor plate panels and the columns, and the shear walls. Shear forces resisted by the frame and those resisted by the shear walls at different floor levels are plotted in Figure 5.20. It can be seen from the figure that the shear wall resisted 82 percent of the total shear forces in the structure. As well, a sudden increase in the roof shear forces was observed. This is a result of the tendency of the frame to restrict the free deflection of the wall. Similar behaviour has been observed by Khan and Sbarounis (1964) for multistorey structures with shear walls.

Numerical comparisons between influence curves proposed by Khan and Sbarounis and shear forces obtained from the

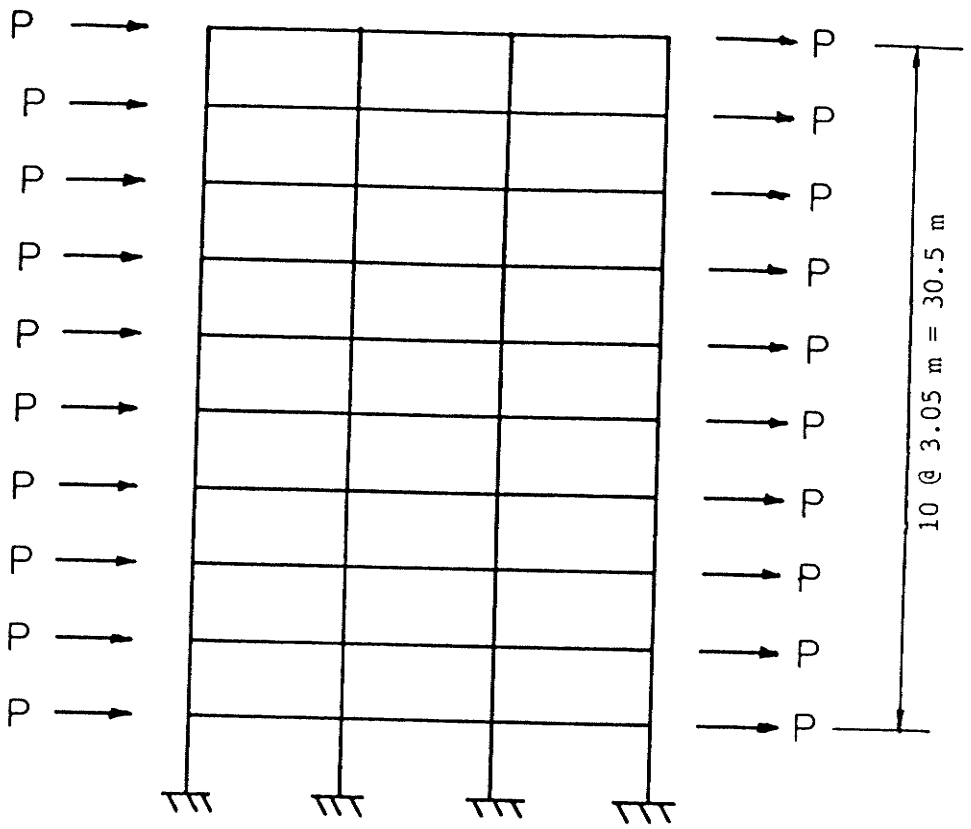

(a) Elevation

P= 40.0 kN

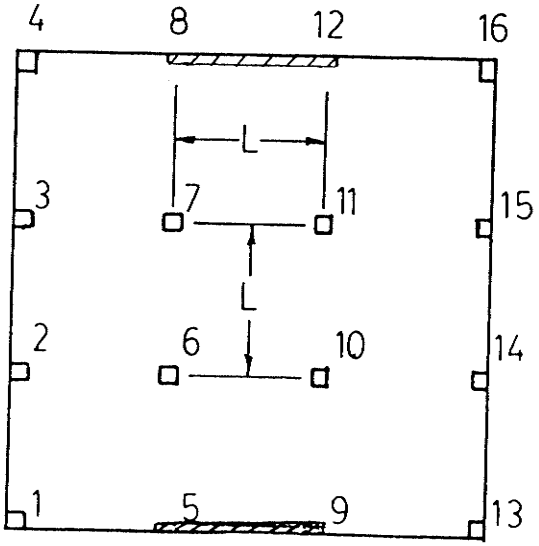

Slab Thickness =230 mm

Columns : 555x555 mm

Shear wall thickness = 200 mm

Shear wall poisson ratio = 0.2

L=6.10 m

ρ = 0.02

E=20690 MPa

ν = 0.1

f'_c = 30 MPA

C/L = 1/11

(b) Floor Plan

Figure 5.18: Ten Storey Structure With Shear Walls

Example 7

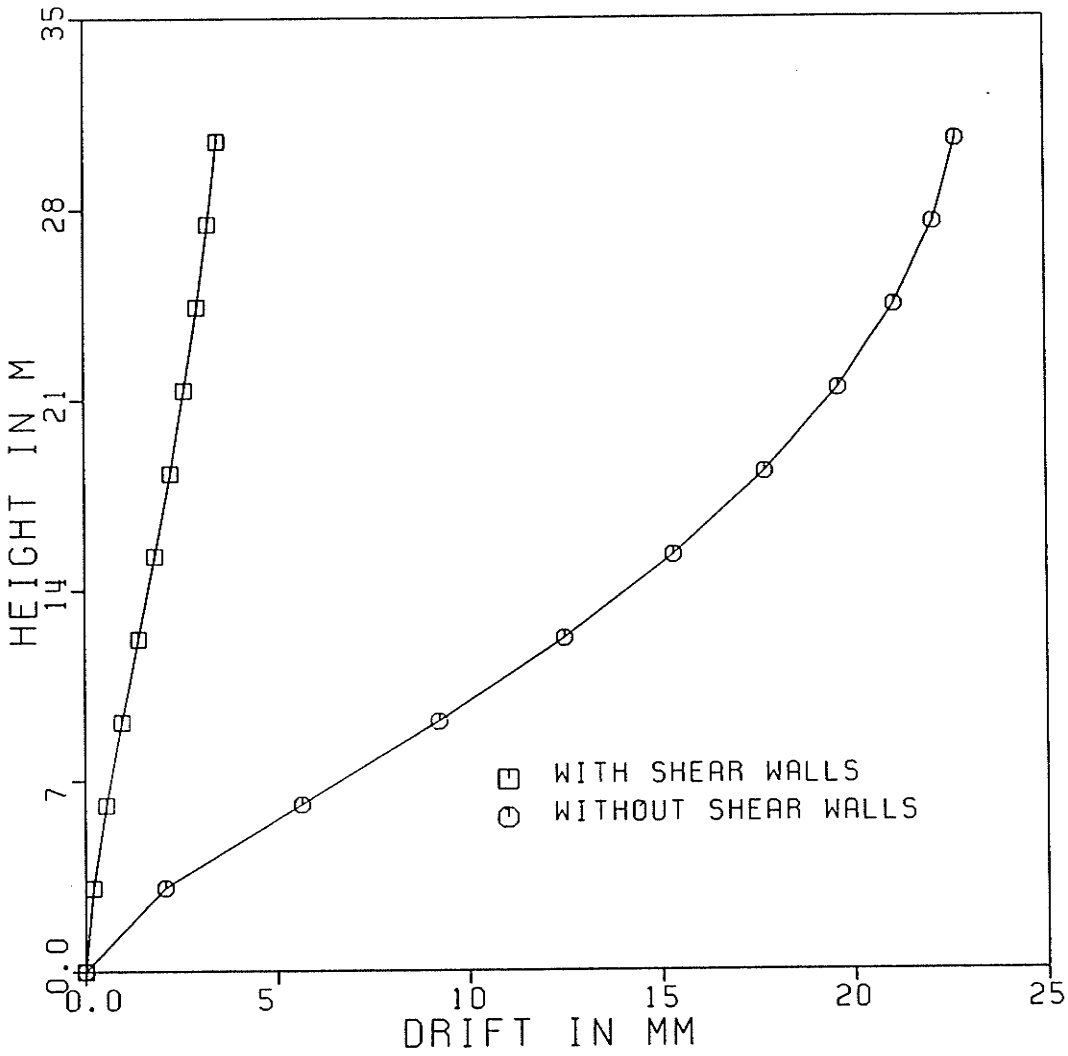

Figure 5.19: Lateral Drifts for the Structure With and Without Shear Walls, Example 7

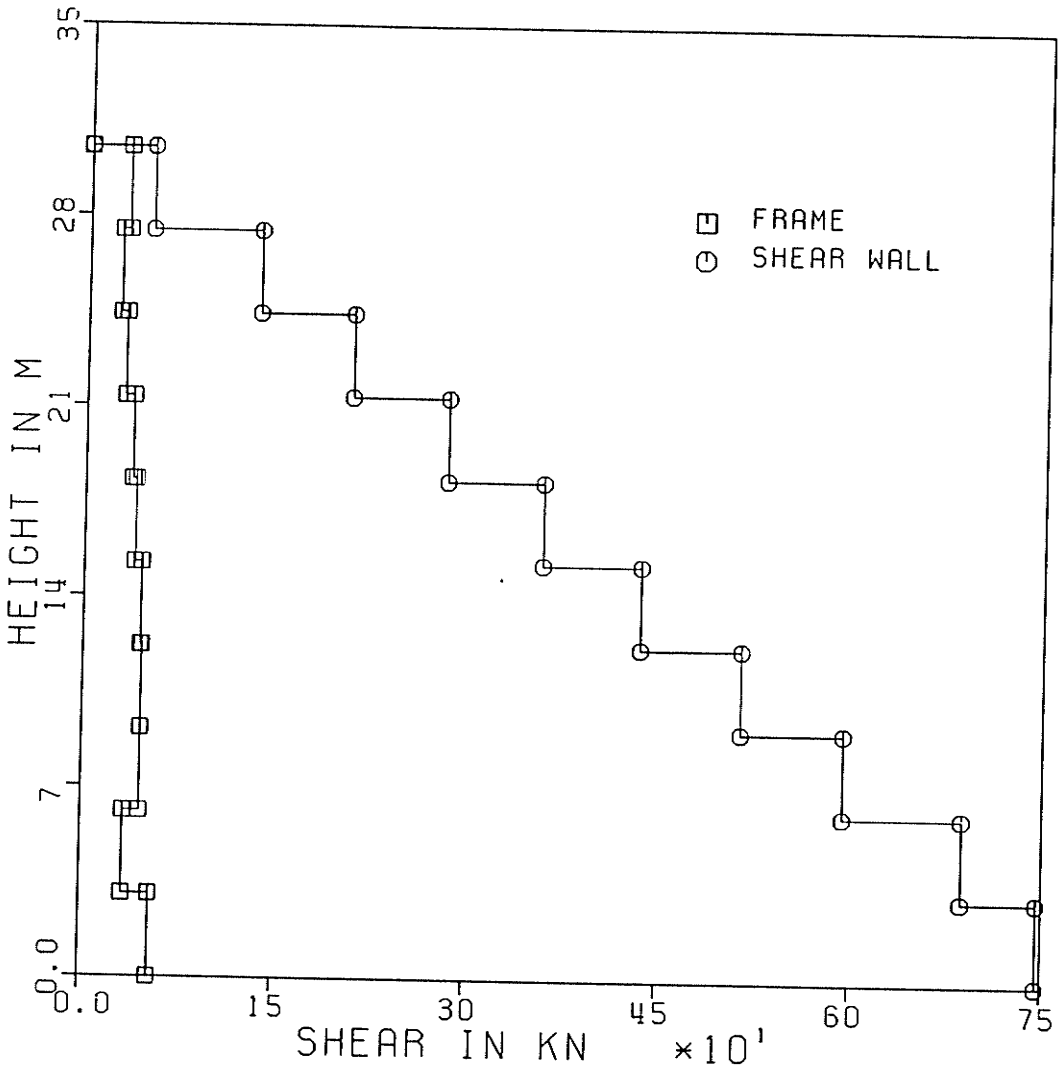

Figure 5.20: Shear Forces Resisted by the Frame and the Shear Walls, Example 7

author's nonlinear analysis program are difficult to make for the following reasons. Firstly, the influence curves proposed by Khan and Sbarounis are for two dimensional frames, while the author's analysis program assumes a three-dimensional frame. Secondly, the stiffness parameters for the structure considered in this example were beyond the ranges considered in the influence curves proposed.

5.9 EXAMPLE 8

The six storey structure with an unsymmetrical floor plan shown in Figure 5.21 was analyzed nonlinearly. The lateral load distribution is shown in the figure. The loads were applied as concentrated loads at the master nodes on the various floors. The steel ratio was 0.015 for interior connections, 0.010 for corner connections, and 0.020 for edge connections. The column-depth-to-plate-span ratio was 0.08, the floor concrete strength was 30 MPa and the floor thickness was 200 mm. The square column dimension was 500 mm for the upper three storeys and 600 mm for the lower three, as shown in the figure. The master nodes are located at coordinates X'_1 = 10.5 m and X'_3 = 14.0 m as shown.

Figure 5.22 shows the data input required to describe the structure. Because of the data generation provisions that were built into the program, only a relatively small number of statements were required to describe the structure and loading.

The lateral drifts in the direction of the lateral load at the master nodes at the various floor levels are plotted in Figure 5.23. Figure 5.24 shows the magnitudes of the rotations of the various floors about a vertical axis. The original and displaced positions of the roof are illustrated in Figure 5.25.

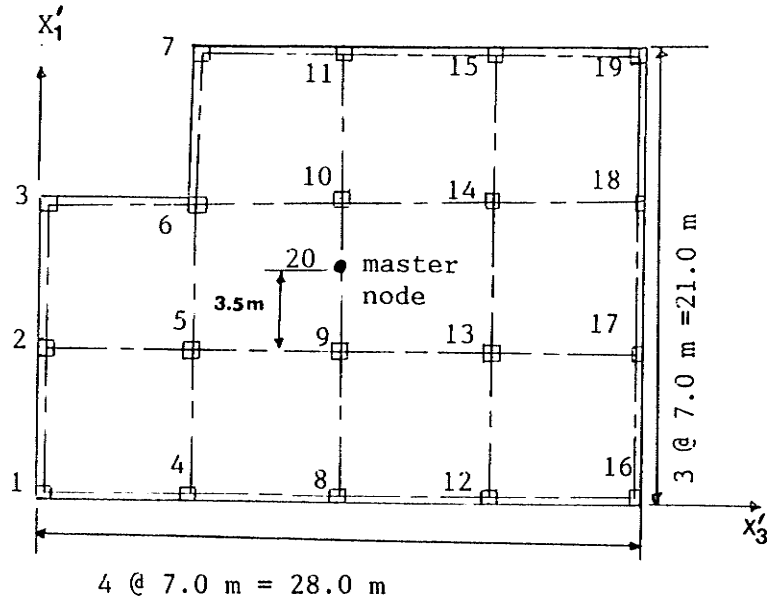

(a) Plan

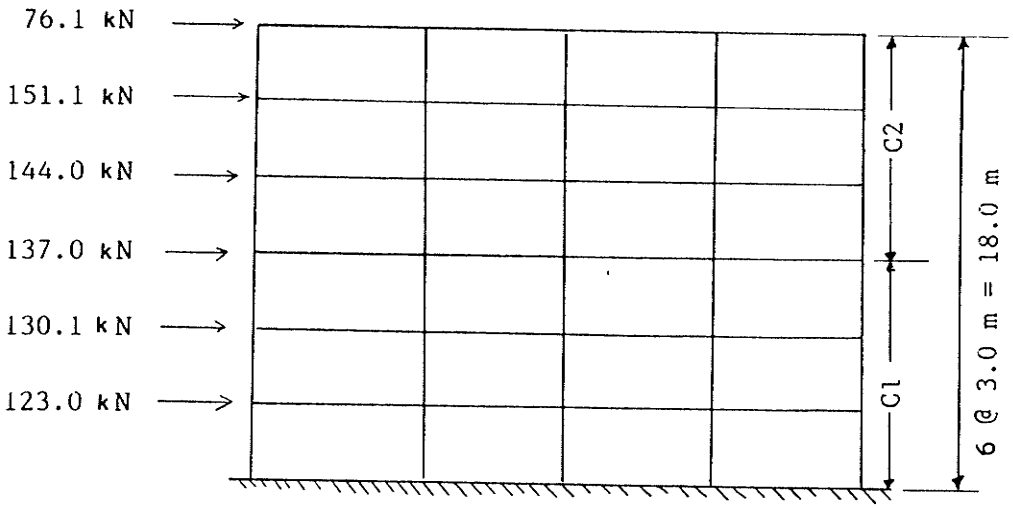

Columns : C1 ; 600mm x 600mm
C2 ; 500mm x 500mm

(b) Elevation

Figure 5.21: Six Storey Structure, Example 8

```
EXAMPLE STRUCTURE NO SHEARWALLS
19          6           28          11.667
19          11          0           10.5        14                  NONLINEAR
1           0           0           2           0           7
4           0           7           3           3           7           7
3           6
COLUMNS     2
8.813E9     5.208E9     5.208E9     2.5E5       500         300
1.827E10    1.080E10    1.080E10    3.6E5       600         200
1           1           57          1
58          2           57          1
FLOORS      1           1
200         20          0.3         20
1           1           4           5           2           2
3           4           8           9           5           3
6           8           12          13          9           3
9           12          16          17          13          3
LOADS
20
76.1
40
151.1
60
144.0
80
137.0
100
130.1
120
123.0
CONNECTION
6           0.015       0.020       0.010
2
SOLVE
/*
```

Figure 5.22: Input Data Required to Describe the Structure and Loading, Example 8

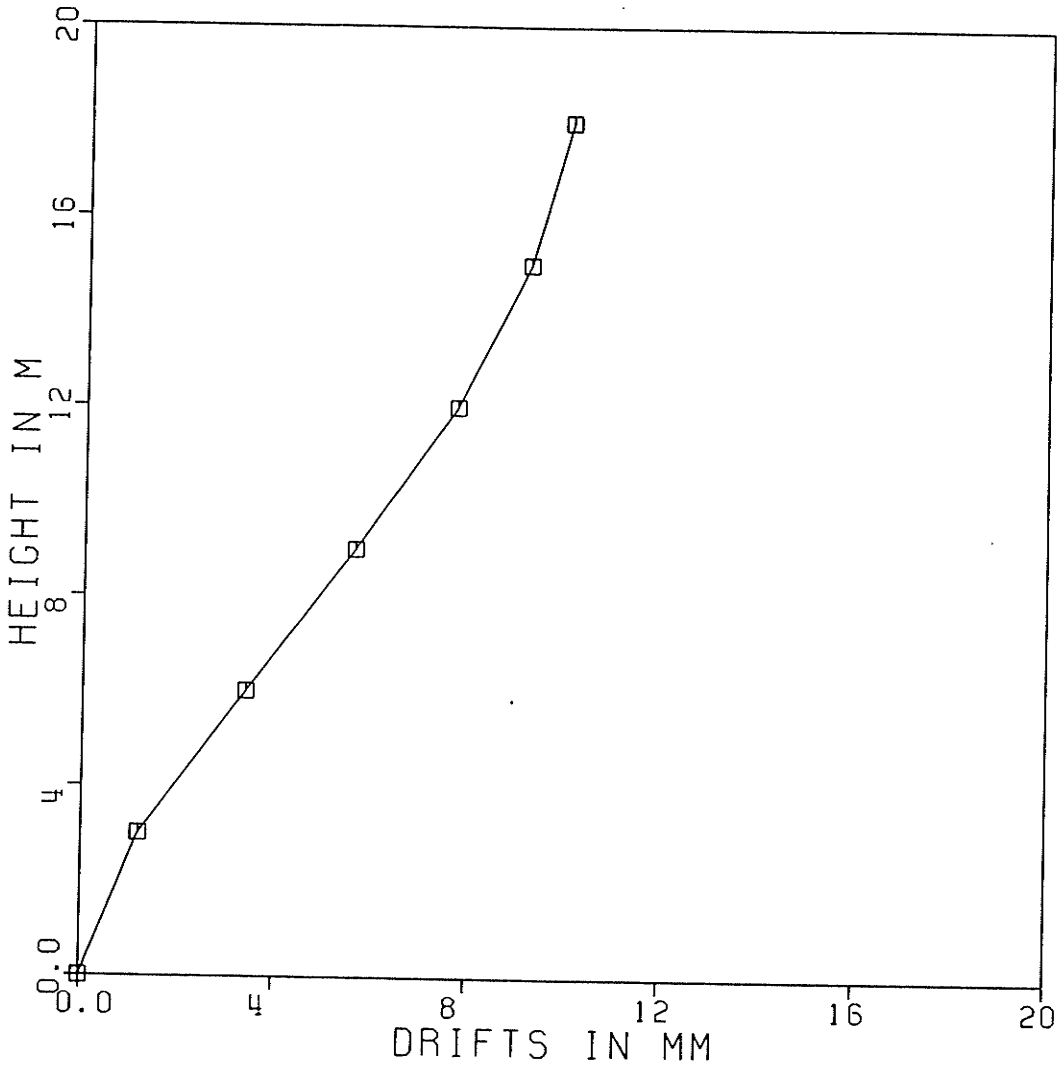

Figure 5.23 : Lateral Drifts at Floor Master Nodes,
Example 8

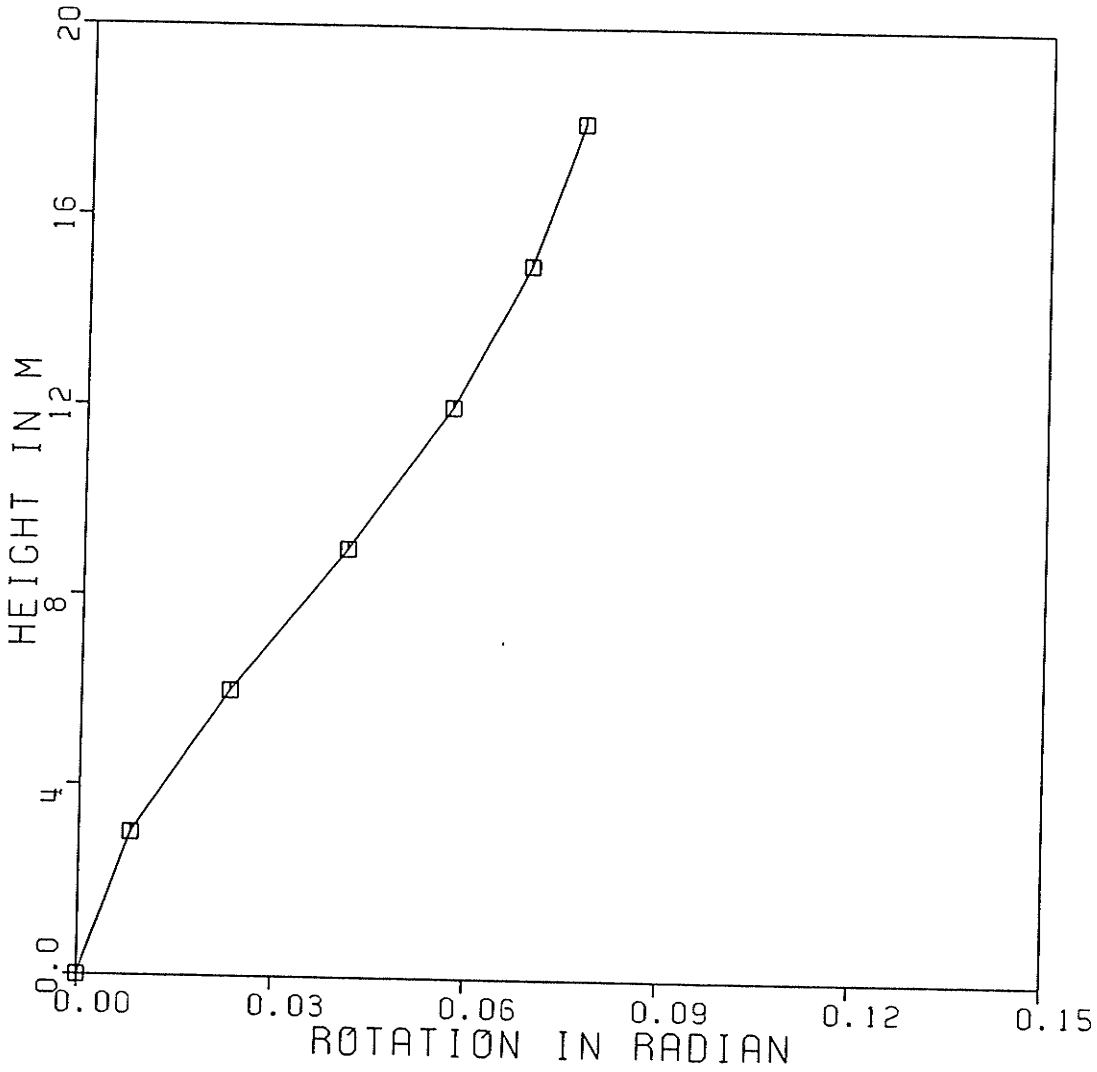

Figure 5.24 : Rotations of Floors About a Vertical Axis, Example 8

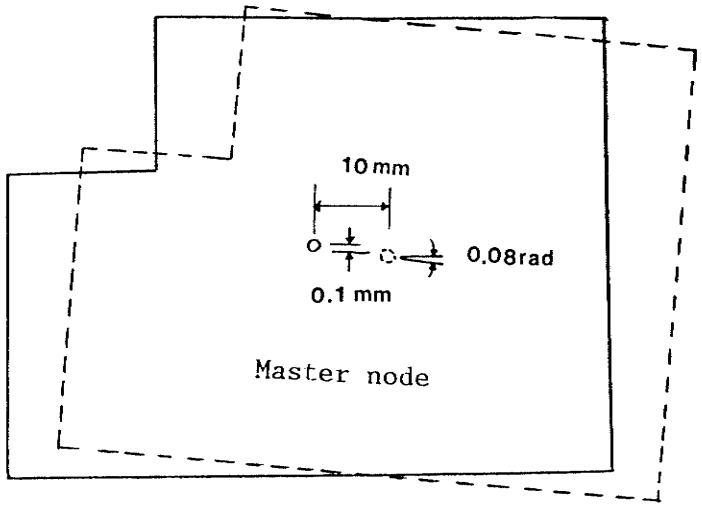

——— Original Position

— — — Displaced Position

Figure 5.25 : Roof Displacement , Example 8

As the lateral loads are applied at the master nodes (X'_1 = 10.5 m) and as the center of resistance for the columns in a given floor is at X'_1 less than 10.5 m, it is to be expected that the rotation of the roof would be clockwise, as illustrated in Figure 5.24.

Chapter VI

SUMMARY, CONCLUSIONS AND RECOMMENDATIONS

6.1 SUMMARY AND CONCLUSIONS

1. A computer program has been developed for the lateral load analysis of flat-plate building frames with or without shear walls. The program is capable of performing both linear and nonlinear analyses.
2. For the nonlinear analysis, all of the structural components are assumed to be linearly elastic, except for the connections between the plates and the columns.
3. Using all available experimental data, standardized functions have been derived to model the moment-rotation behaviour of floor-plate-to-column connections. The functions are expressed in terms of the geometric and material parameters that influence most strongly the behaviour of the connections. Once the standardized functions had been derived, the parameters for each of the test specimens on which they were based were back substituted to check the acccuracy of the standardization procedure. For most of the test specimens there was good agreement between the experimental data and the "reconstructed" moment-rotation

data. The maximum percentage difference between predicted and experimental values was smaller than 20% for all of the connections considered. Even though this might be considered only a crude estimation of the actual connection behaviour, it is asserted that it provides a more realistic approximation than the commonly used assumption of rigid connections.

4. Nonlinear stiffness matrices have been determined numerically to model the out-of-plane stiffnesses of flat-plate floors. The stiffness coefficients were derived as functions of both the flexibilities of the plate-to-column connections and the column-depth-to-plate-span ratio.

5. Examples have been presented to illustrate the influence of several parameters on the behaviour of reinforced concrete flat plate structures. The parameters included the gravity load level, the column-depth-to-plate-span ratio, the total floor steel ratio in the vicinity of the column, the floor concrete strength, and the floor plate thickness.

6. An example has been presented in which several models were compared with the author's procedure. The lateral drifts obtained using the author's nonlinear analysis were found to be about 28% larger than those drifts obtained using most of the linear methods of analysis. Lateral drifts obtained using Long and Kirk's recommendations were found to be 56% larger

than those obtained using the nonlinear analysis. The latter authors "calibrated" their linear analysis procedure to account approximately for the effects of cracking at the plate-to-column connections.

7. Using the CSA A23.3-M84 equivalent frame method to analyze flat plate structures subjected to lateral load can result in gross overestimation of the stiffness of the structure. Therefore, it is strongly recommended that this method not be used for lateral load analyses. This confirms observations made by Allen and Darvall (1977) and Elias and Geogiadis (1978).

6.2 RECOMMENDATIONS FOR FURTHER STUDIES

1. The primary purpose of the present study was to develop the methodology for accounting for the nonlinear connection behaviour in the lateral load analysis of flat-plate structures. The accuracy of the analysis procedure depends primarily upon the experimental data used in deriving the standardized moment-rotation functions. As experimental data at present are limited, more experimental research is needed to determine the influence of the various geometric and material parameters on the moment-rotation behaviour. In particular more research is needed on edge and corner connections.

2. In this study, only square flat-plate floor panels and columns of square cross-section were considered. The program should be extended to model rectangular panels and columns.
3. The program considers only static lateral loads. Provisions should be added to allow for dynamic loading.
4. At present, the computer program calculates shears and moments in the floor plates at the column nodes only. A procedure to determine the actions in the flat plate floors at other points should be incorporated.
5. The effect of gravity loading has not been adequately accounted for. No provision has been made to account for loading on one side of the column, and unloading on the other side when transverse loading is superimposed on gravity loading. It is recommended that more experimental research be carried out to study this behaviour, and provisions to account for this behaviour should be added to the computer analysis program, in order to correctly account for the gravity loading effects on the analysis.

REFERENCES

American Concrete Institute Committee 318, "Building Code Requirements for Reinforced Concrete", ACI, Detroit, Michigan, 1983.

Akiyama, Karuki, "Response of Flat-Plate Concrete Structures to Lateral Loading", Ph.D. Thesis, Dept. of Civil Engineering, University of Washington, Seattle, WA, 1984.

Allen, F., and Darvall, P.L., "Lateral Load Equivalent Frame", ACI Journal, Vol. 74, pp. 229-294, 1977.

Ang, K.M., "Behaviour of Three Dimensional Flexibly Connected Steel Frames", M.Sc. Thesis, Civil Engineering Department, University of Manitoba, Winnipeg, Manitoba, 1983.

Canadian Standards Association, "Code for the Design of Concrete Structures for Buildings", CSA Standards CAN3-A23.3-M83, CSA, Rexdale, Ontario, 1984.

Chaichanavong, T., "Slab-Edge Column Connections Transferring High Intensity Reversing Moments Parallel to the Edge of the Slab", MSCE Thesis, Dept. of Civil Engineering, University of Washington, Seattle, WA, 1979.

Chislett, M., and Morris, G., "Lateral Load Analysis of Three-Dimensional Flat-Plate Structures", Canadian Journal of Civil Engineering, Vol 12, No. 2, pp. 351-361, 1985.

Elias, Z.M. and Georgiadis, C., "Stiffness Coefficients and Fixed End Moments for Structural Analysis of Flat Plate Frames", Structures and Mechanics Report SM 78-2, Department of Civil Engineering, University of Washington, Seattle, WA., August 1978.

Frazer, D.J., "Elastic Analysis of Laterally Loaded Frames", Journal of the Structural Division, ASCE, 109 (ST9), pp. 1479-1489, 1983.

French, S., et al., "Panel Method for Multistorey Flat Plate Structures", Memoires, International Association for Bridge and Structural Engineering, V. 35-II, pp. 65-82, Zurich, 1975.

French, S., Kabaila, A.P., and Pulmano, V.A., "Single Element Panel for Flat-Plate Structures", Journal of Structural Division, ASCE, 101 (ST9), pp. 1801-1811, 1975.

Hanna, S.N., Mitchell, D., and Hawkins, N.M., "Slab-Column Connections Containing Shear Reinforcement and Transferring High Intensity Reversed Moments", Progress Report on NSF Project GI-38717, SM 75-1, Dept. of Civil Engineering, University of Washington, Seattle, WA, August 1975.

Hawkins, N.M., Mitchell, D., and Sheu, M.S., "Cyclic Behaviour of Six Reinforced Concrete Slab-Column Specimens Transferring Moment and Shear", Progress Report 1973-74 on NSF Project GI-38717, Section II, Dept. of Civil Engineering, University of Washington, Seattle, WA, 1974.

Hawkins, N.M., "Lateral Load Design Considerations for Flat Plate Structures", Study No. 14, Non-Linear Design of Concrete Structures, Solid Mechanics Division, University of Waterloo, Waterloo, Canada, 1980.

Hawkins, N.M., Mitchell, D., and Sheu, M.S., "Reversed Cyclic Load Behaviour of Reinforced Concrete Slab-Column Connections", Proceedings, U.S. National Conference on Earthquake Engineering, Ann Arbor, Michigan, June, 1975.

Hrabok, M.M., and Hrudy, T.M., "Stiffened Plate Analysis By The Hybrid Stress Finite Element Method", Structural Engineering Report No. 100, Department of Civil Engineering, University of Alberta, Edmonton, Alberta, October 1981.

Jamieson, P.D., Johnson, C.D., "Second-Order Analysis of Steel Structures With Semi-Rigid Joints", BSCE Thesis, School of Engineering, Lakehead University, Thunder Bay, Ontario, May 1984.

Khan, F.R., and Sbarounis, J.A., "Interaction of Shear Walls and Frames", Journal of the Structural Division, ASCE, 90 (ST3), pp. 285-335, 1964.

Long, A.E., and Kirk, D.W., "Lateral Load Stiffness of Slab-Column Structures", Reinforced Concrete Structures Subjected to Wind and Earthquake Forces, SP-63, ACI, Detroit, Michigan, pp. 197-220, 1980.

Ma, K.H., "Analysis of Three Dimensional Frames with Flat Plate Floors", M.Sc. Thesis, Civil Engineering Department, University of Manitoba, Winnipeg, Manitoba, Canada, 1976.

Mondkar, D.P. and Powell, G.H., "Towards Optimal In-Core Equation Solving", Computers and Structures, V. 4, pp. 531-548, 1974.

Morrison, G., Hirasawa, I., and Sozen, M.A., "Lateral Load Tests of R/C Slab-Column Connections", Journal of Structural Engineering, ASCE, Vol. 109, No. 11, pp. 2698-2714, 1983.

Mulcahy, J.F., and Rotter, J.M., "Moment Rotation Characteristics of Flat Plate and Column Systems", ACI Journal, March/April, pp. 85-92, 1983.

Pavlovic, M.N. and Poulton, S.M., "On The Computation of Slab-Effective Widths", Journal of Structural Engineering, ASCE, Vol. 111, No. 2, pp. 363-377, 1985.

Pecknold, D.A., "Slab Effective Width for Equivalent Frame Analysis", ACI Journal, Vol. 72, No. 4, pp. 135-137, 1975.

Poland, C.D., "Practical Application of Computer Analysis to the Design of Reinforced Concrete Structures for Earthquake Forces", Reinforced Concrete Structures Subjected to Wind and Earthquake Forces, SP-63, American Concrete Institute, pp. 409-436, 1980.

Pulmano, V.A., Black, D.C., and Kabaila, A.P., "Substructure Analysis of Multi-Storey Flat-Slab Buildings", Proceedings of the ASCE-IABSE Regional Conference on Tall Buildings, Bangkok, Thailand, pp. 447-460, 1974.

Ramberg, W., and Osgood, W.R., "Description of Stress-Strain Curves by Three Parameters", NACA Technical Report No. 902, 1943.

Sheu, M.S. and Hawkins, N.M., "Grid Model for Predicting the Monotonic and Hysteretic Behaviour of Slab-Column Connections Transferring Moments", Reinforced Concrete Structures Subjected to Wind and Earthquake Forces, SP-63, ACI, Detroit, MI, pp. 79-111, 1980.

Simpson, E.G., Symmonds, D.G., and Hawkins, N.M., "The effect of Column Properties on the Behaviour of Slab-Column Connections Transferring Reversed Moments", Report SM 76-4, Dept. of Civil Engineering, University of Washington, Seattle, WA, Oct. 1976.

Symmonds, D.W., Mitchell, D., and Hawkins, N.M., "Slab-Column Connections Subjected to High Intensity Shears and Transferring Reversed Moments", Progress Report on NSF Project GI-38717, Dept. of Civil Engineering, University of Washington, Seattle, WA, October 1976.

Timoshenko, S., "Strength of Materials Part II: Advanced Theory and Problems", 2nd Edition, D. Van Nonstrand Co.,Inc., pp. 119-120, 1941.

Wilson, E.L., Hollings, J.P. and Dovey H.H., "Three Dimensional Analysis of Building Systems (Extended Version)", Report No. EERC 75-13, University of California, Berkley, California, 1975.

Wong, Y.C., and Coull, A., "Effective Slab Stiffness in Flat-Plate Structures", Proceedings-The Institution of Civil Engineering, 69, Part 2, pp. 721-735, 1980.

Wong, C.F., Yang, C.H. and Hawkins, N.M., "Slab-Edge Column Connections Transferring High Intensity Reversing Moments Normal to the Edge of the Slab", Progress Report on NSF Project ENV 72-03585, SM 78-1, Dept. of Civil Engineering, University of Washington, Seattle, WA, May 1978.

Yamazaki, J. and Hawkins, N.M., "Finite Element Predictions of the Behaviour of Slab-Column Connections Transferring Moment", Reinforced Concrete Structures Subjected to Wind and Earthquake Forces, SP-63, ACI, Detroit, MI, pp. 49-78, 1980.

Yu, S.W., "Reinforced Concrete Slab-Corner Column Connections Transferring High Intensity Cyclic Moments", MSCE Thesis, University of Washington, Seattle, WA, 1979.

Appendix A

PLATE-TO-COLUMN CONNECTION MOMENT-ROTATION CURVES

In this appendix, moment-rotation curves are presented for the plate-column connection specimens used in the derivation of the standardized functions. The experimental curves were obtained directly from curves provided by the original authors. The applied moments were then normalized as follows

$$M' = \frac{M}{f_c' \quad L \quad t^2}$$

Where,

M' = normalized applied moment

f_c' = concrete 28 day compressive strength

L = plate panel breadth

t = plate thickness

The predicted moment-rotation curve for a particular connection is obtained by substituting the connection parameters into the appropriate standardized moment-rotation function.

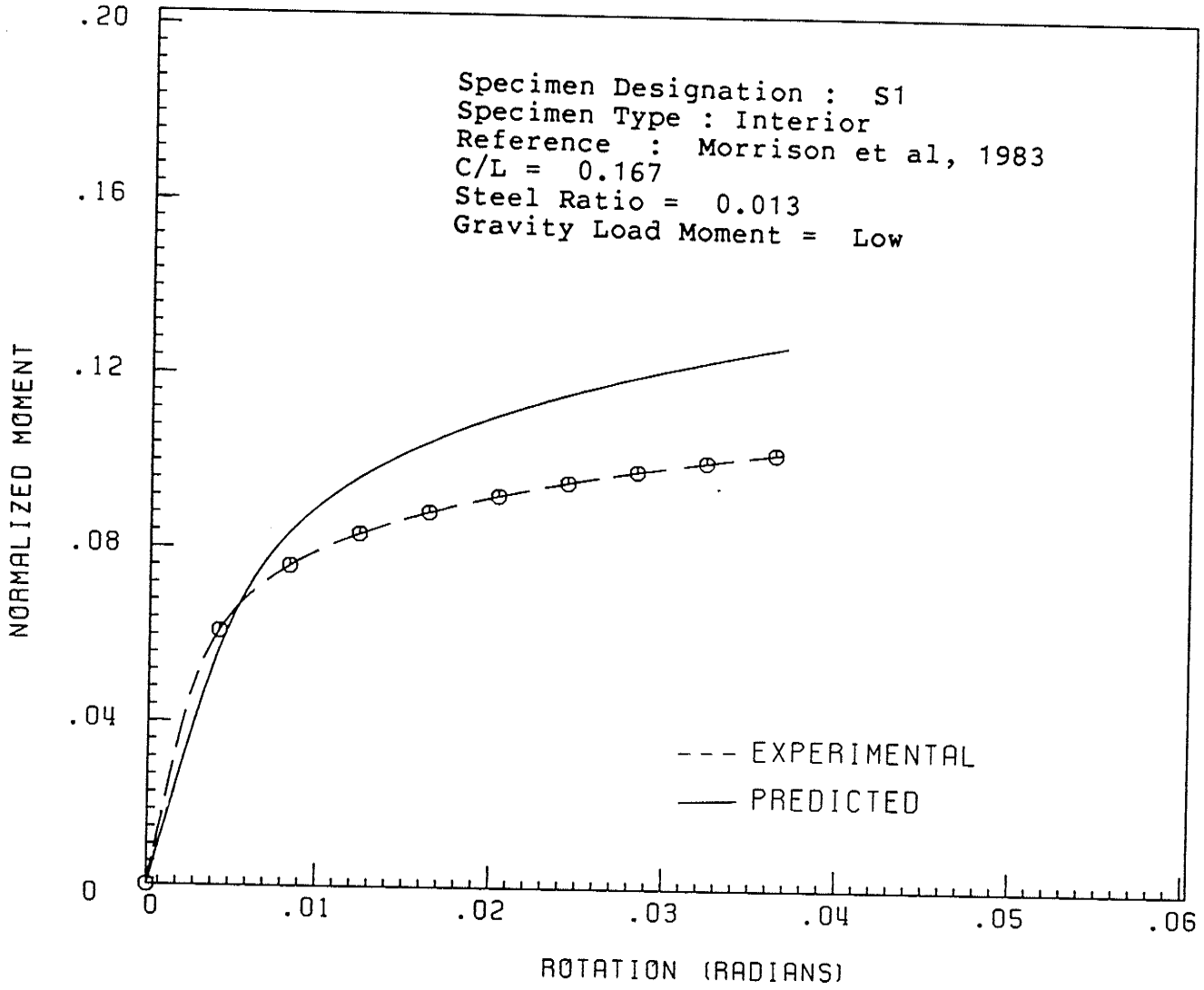
Specimen Designation : S1
Specimen Type : Interior
Reference : Morrison et al, 1983
C/L = 0.167
Steel Ratio = 0.013
Gravity Load Moment = Low
--- EXPERIMENTAL
—— PREDICTED
NORMALIZED MOMENT
ROTATION (RADIANS)
0
.04
.08
.12
.16
.20
0
.01
.02
.03
.04
.05
.06

Figure A.1

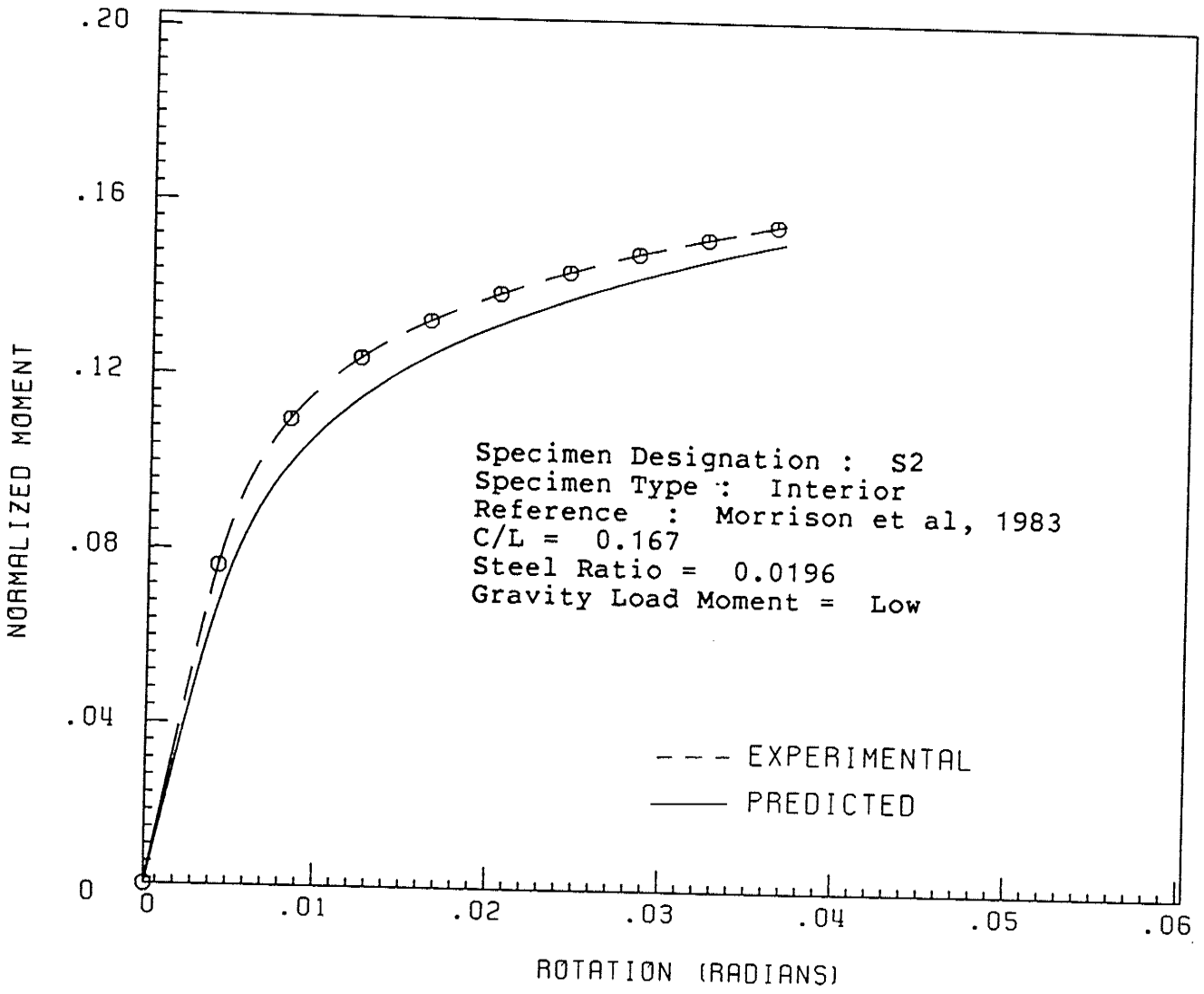
.20
.16
.12
.08
.04
0
NORMALIZED MOMENT
0
.01
.02
.03
.04
.05
.06
ROTATION (RADIANS)
Specimen Designation : S2
Specimen Type : Interior
Reference : Morrison et al, 1983
C/L = 0.167
Steel Ratio = 0.0196
Gravity Load Moment = Low
EXPERIMENTAL
PREDICTED

Figure A.2

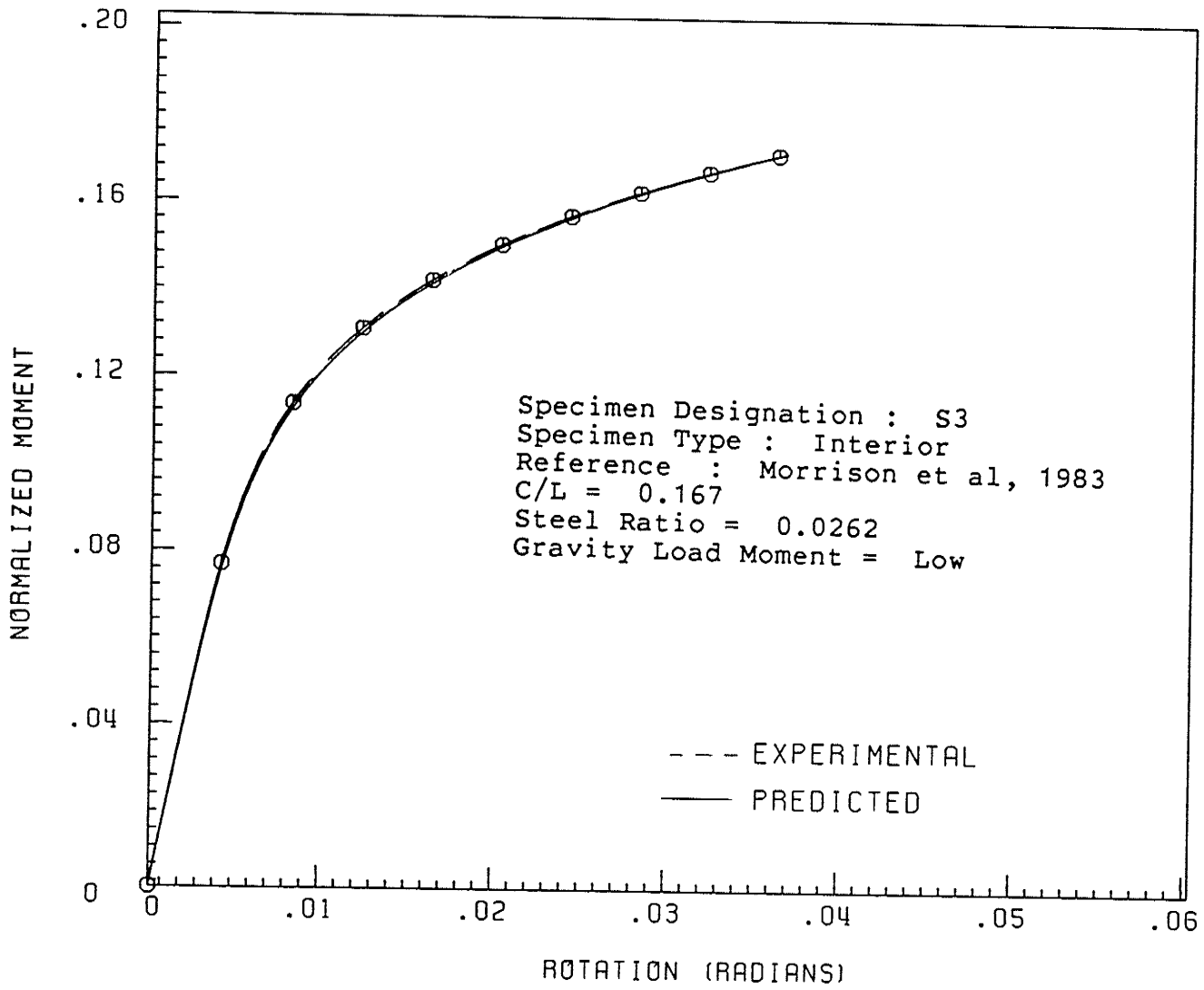
.20
.16
.12
.08
.04
0
NORMALIZED MOMENT
0
.01
.02
.03
.04
.05
.06
ROTATION (RADIANS)
Specimen Designation : S3
Specimen Type : Interior
Reference : Morrison et al, 1983
C/L = 0.167
Steel Ratio = 0.0262
Gravity Load Moment = Low
EXPERIMENTAL
PREDICTED

Figure A.3

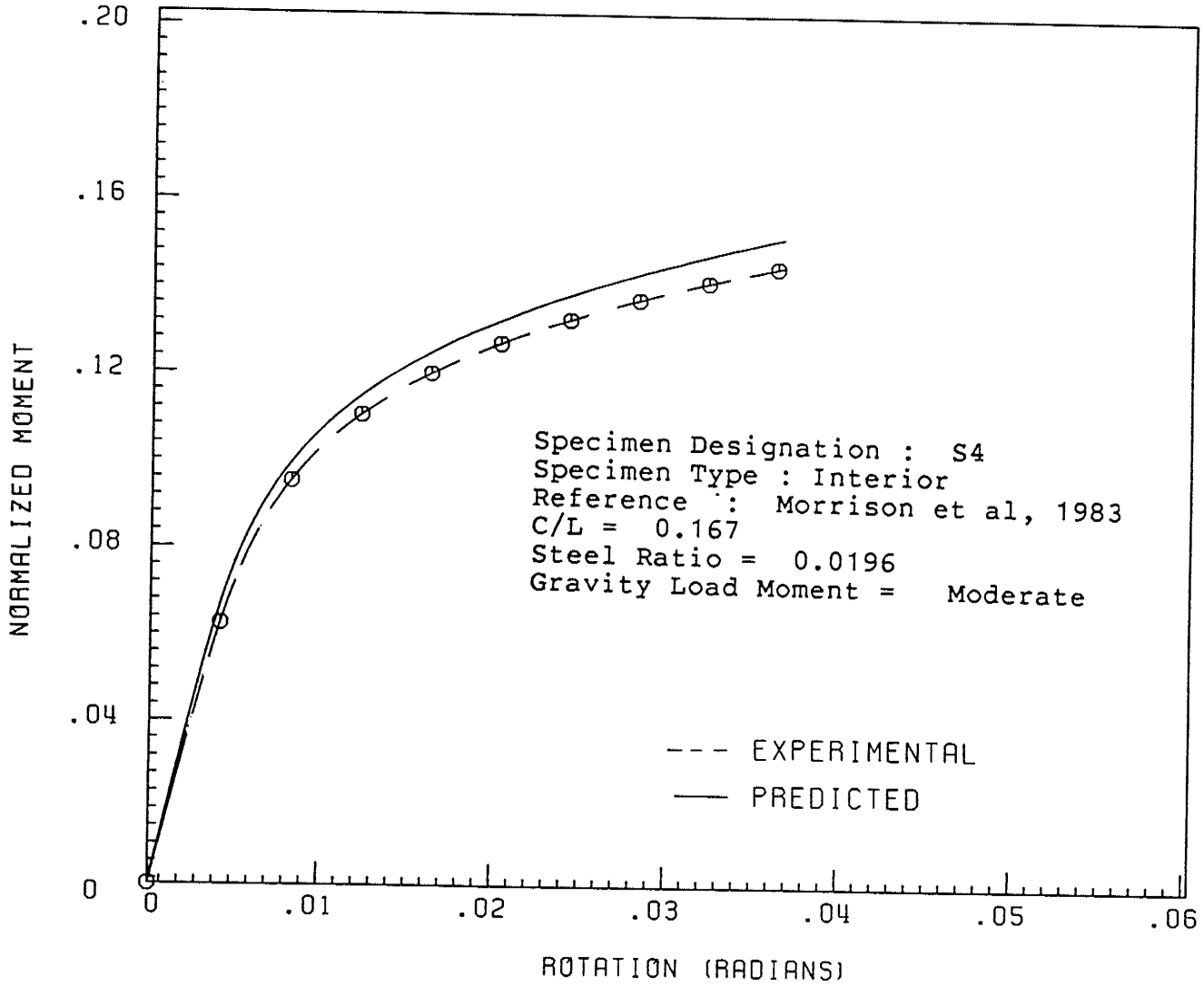
.20
.16
.12
.08
.04
0
NORMALIZED MOMENT
0
.01
.02
.03
.04
.05
.06
ROTATION (RADIANS)
Specimen Designation : S4
Specimen Type : Interior
Reference : Morrison et al, 1983
C/L = 0.167
Steel Ratio = 0.0196
Gravity Load Moment = Moderate
--- EXPERIMENTAL
—— PREDICTED

Figure A.4

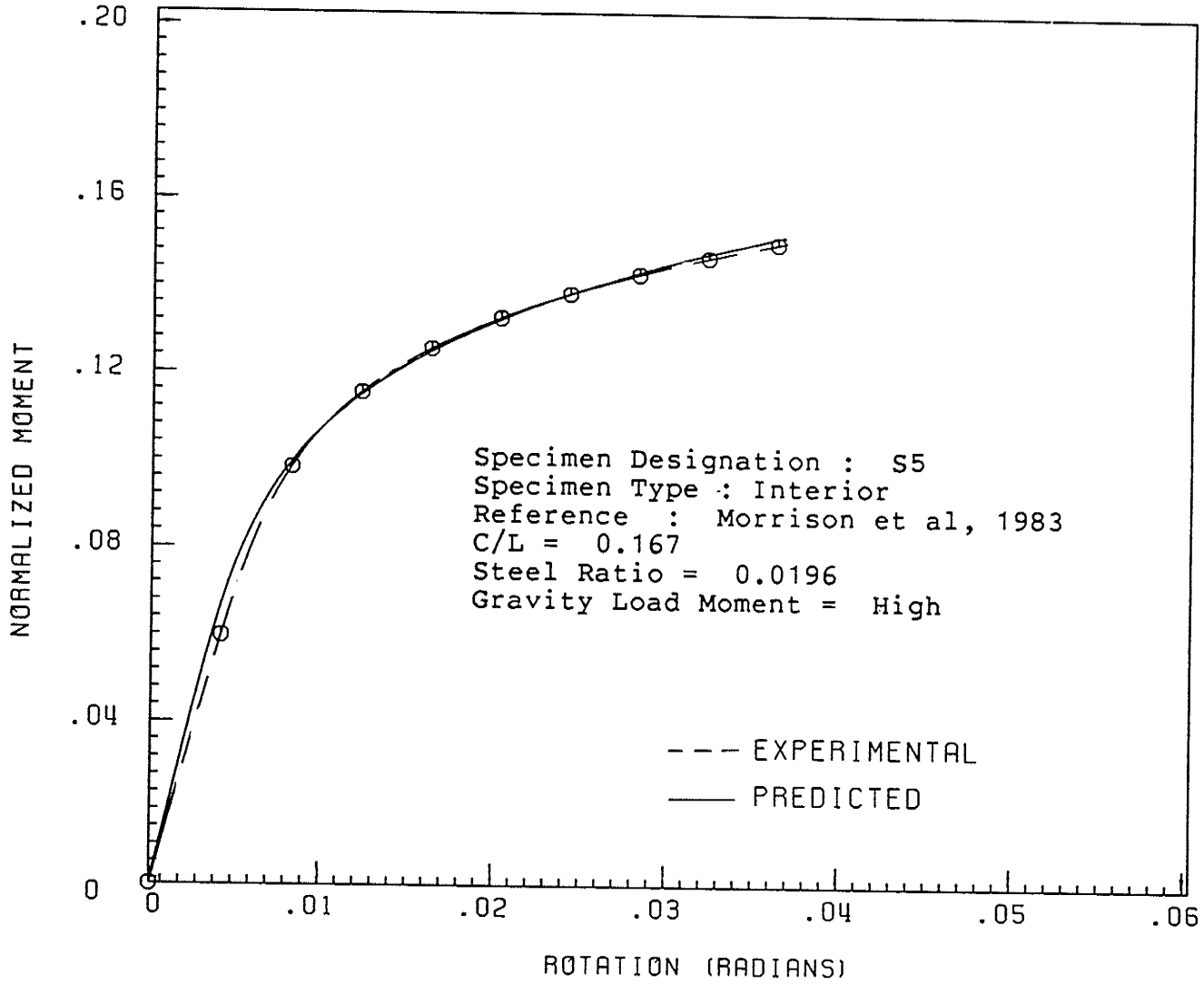
.20
.16
.12
.08
.04
0
NORMALIZED MOMENT
0
.01
.02
.03
.04
.05
.06
ROTATION (RADIANS)
Specimen Designation : S5
Specimen Type : Interior
Reference : Morrison et al, 1983
C/L = 0.167
Steel Ratio = 0.0196
Gravity Load Moment = High
EXPERIMENTAL
PREDICTED

Figure A.5

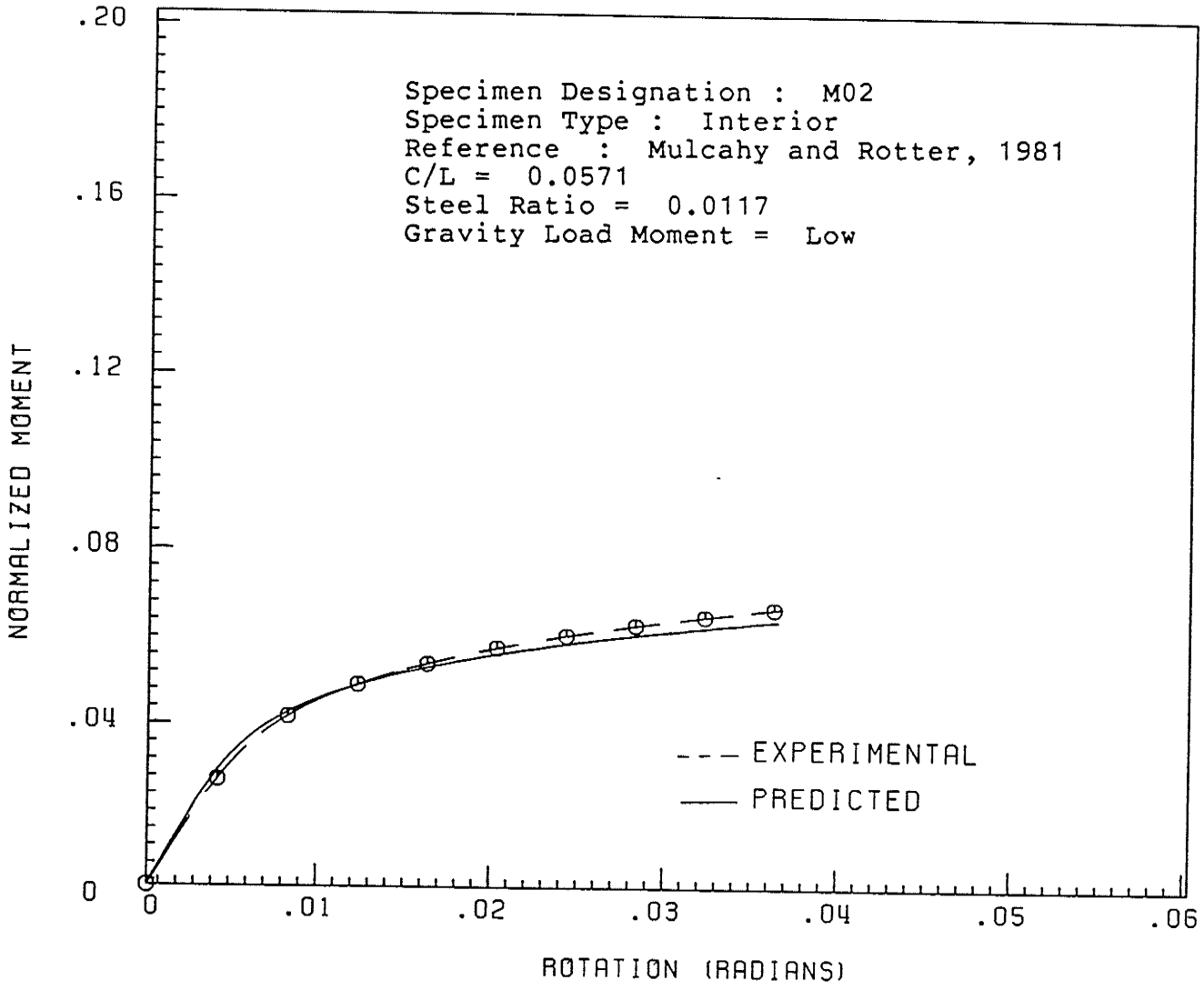
Specimen Designation : M02
Specimen Type : Interior
Reference : Mulcahy and Rotter, 1981
C/L = 0.0571
Steel Ratio = 0.0117
Gravity Load Moment = Low
NORMALIZED MOMENT
.20
.16
.12
.08
.04
0
0
.01
.02
.03
.04
.05
.06
ROTATION (RADIANS)
--- EXPERIMENTAL
—— PREDICTED

Figure A.6

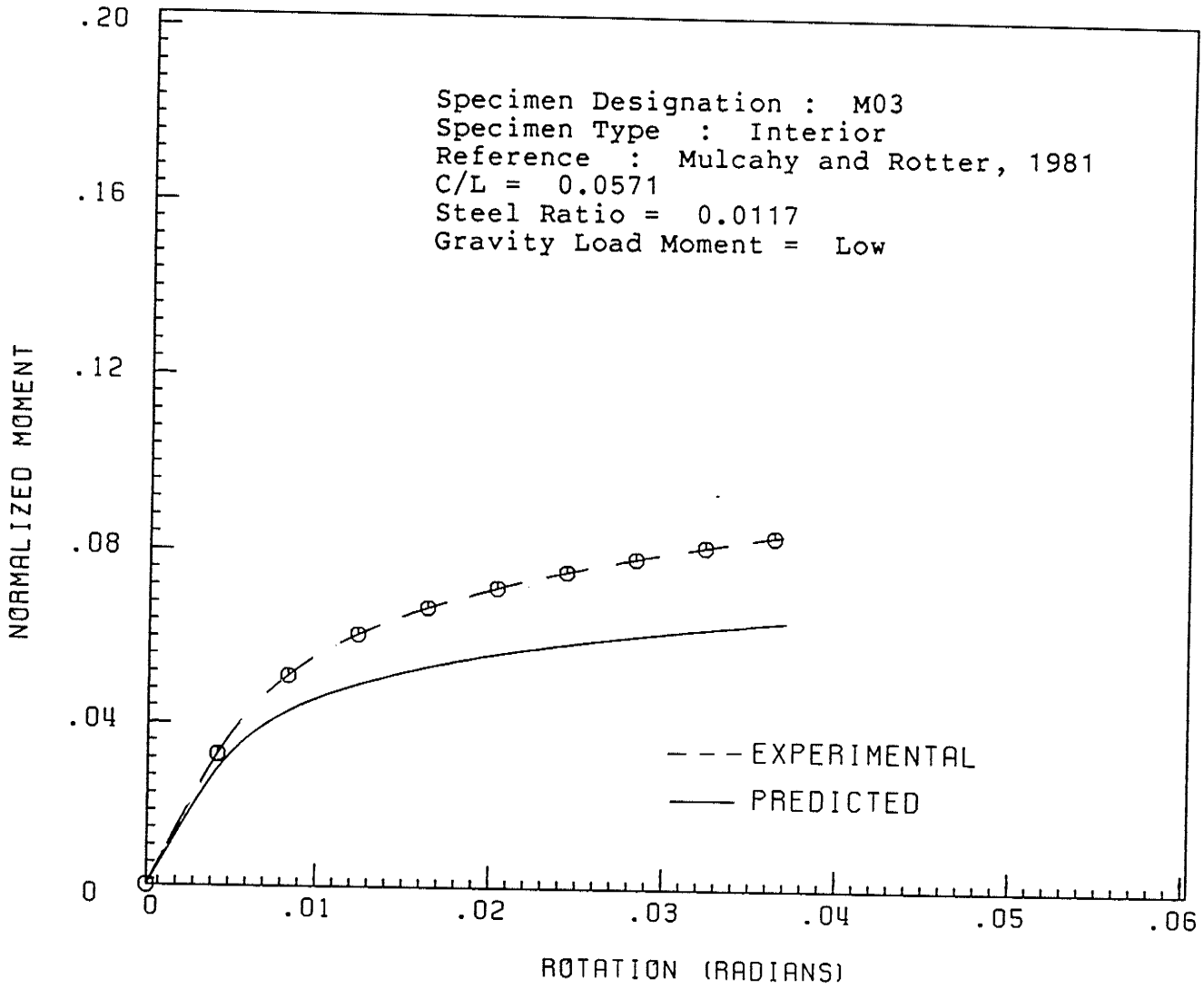
Specimen Designation : M03
Specimen Type : Interior
Reference : Mulcahy and Rotter, 1981
C/L = 0.0571
Steel Ratio = 0.0117
Gravity Load Moment = Low
EXPERIMENTAL
PREDICTED
NORMALIZED MOMENT
ROTATION (RADIANS)
0
.04
.08
.12
.16
.20
.01
.02
.03
.05
.06

Figure A.7

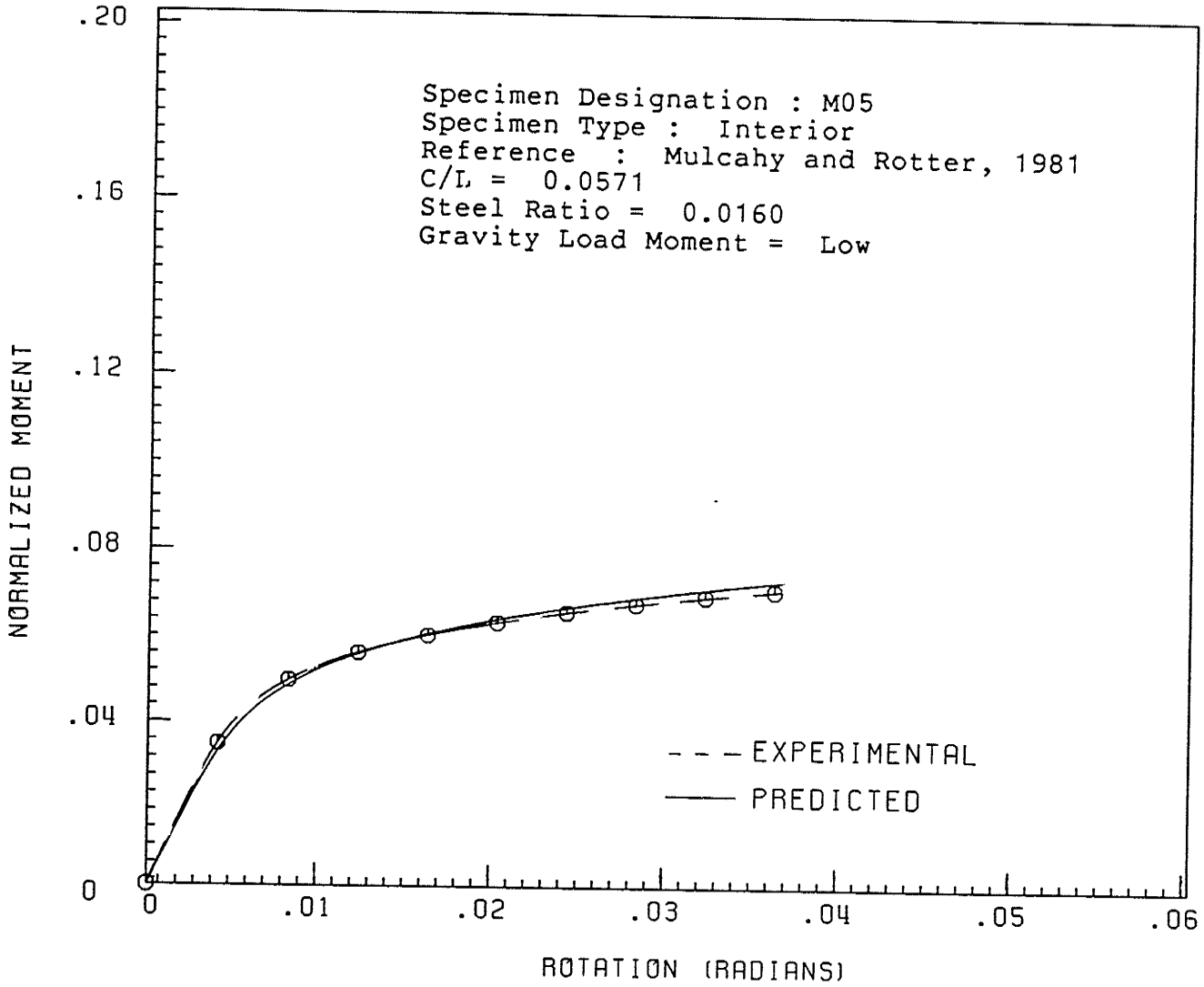
Specimen Designation : M05
Specimen Type : Interior
Reference : Mulcahy and Rotter, 1981
C/L = 0.0571
Steel Ratio = 0.0160
Gravity Load Moment = Low
NORMALIZED MOMENT
.20
.16
.12
.08
.04
0
0
.01
.02
.03
.04
.05
.06
ROTATION (RADIANS)
EXPERIMENTAL
PREDICTED

Figure A.8

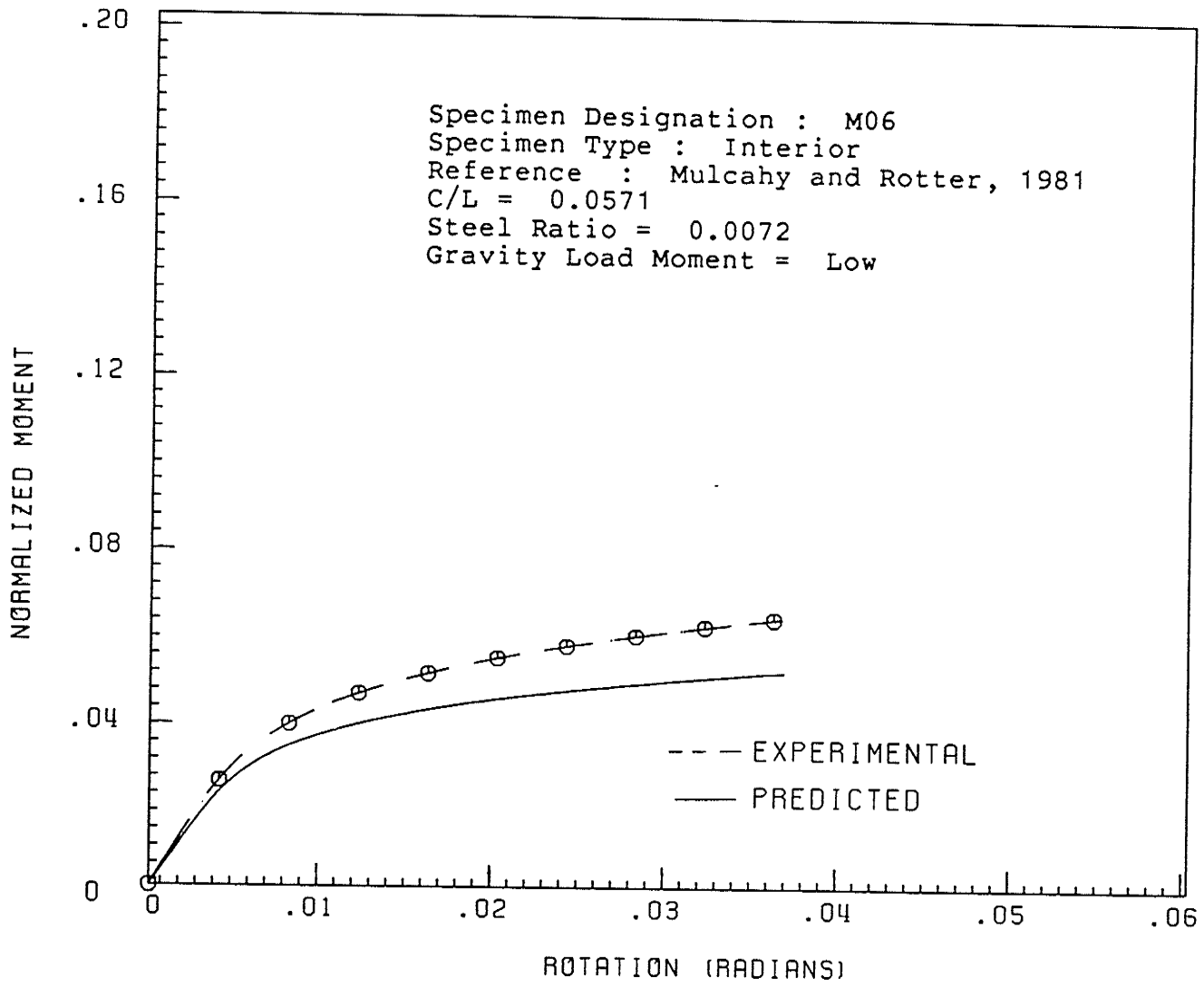
Specimen Designation : M06
Specimen Type : Interior
Reference : Mulcahy and Rotter, 1981
C/L = 0.0571
Steel Ratio = 0.0072
Gravity Load Moment = Low
EXPERIMENTAL
PREDICTED
NORMALIZED MOMENT
ROTATION (RADIANS)
.20
.16
.12
.08
.04
0
0
.01
.02
.03
.04
.05
.06

Figure A.9

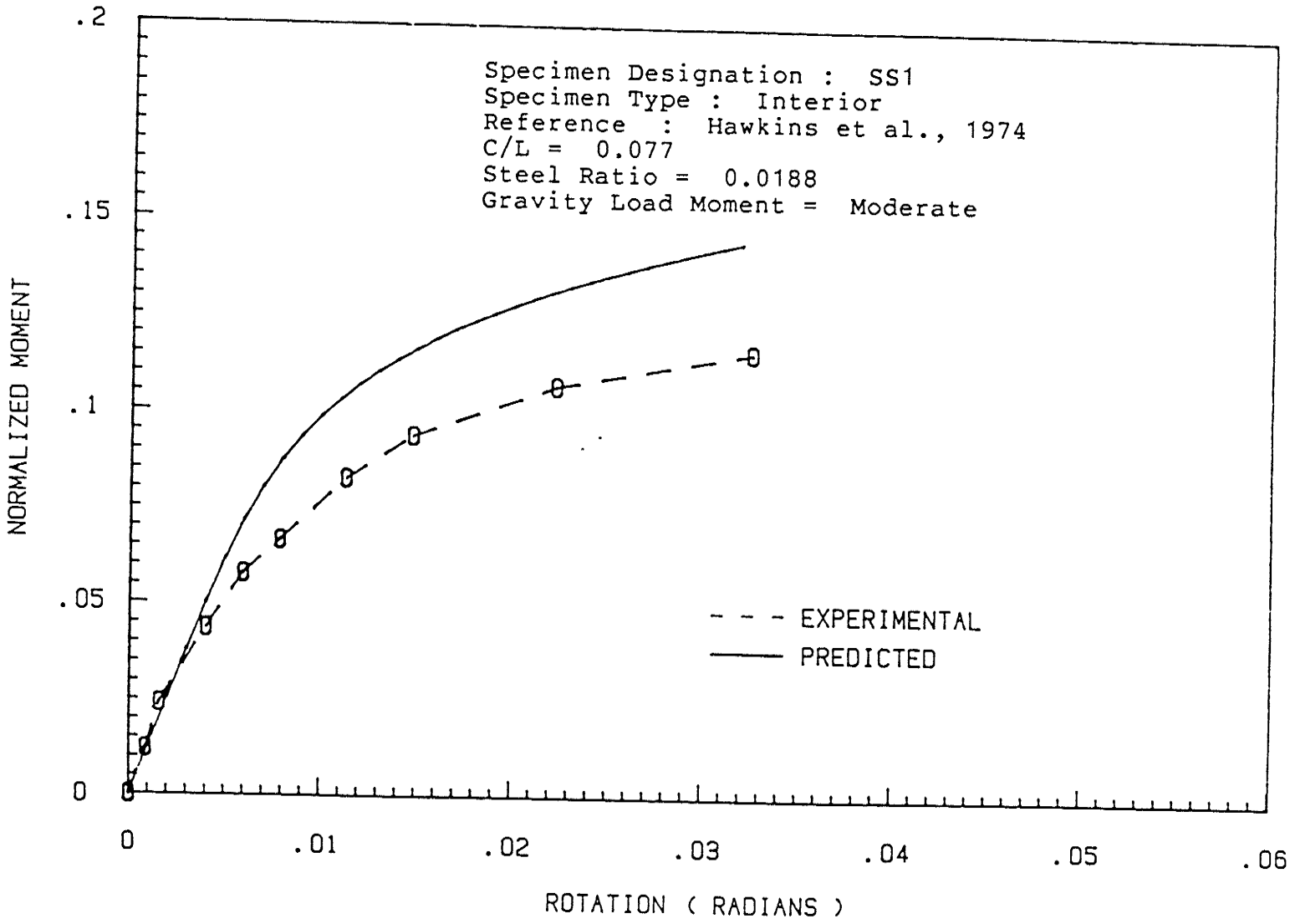
Specimen Designation : SS1
Specimen Type : Interior
Reference : Hawkins et al., 1974
C/L = 0.077
Steel Ratio = 0.0188
Gravity Load Moment = Moderate
EXPERIMENTAL
PREDICTED
NORMALIZED MOMENT
ROTATION (RADIANS)
0
.05
.1
.15
.2
.01
.02
.03
.04
.06

Figure A.10

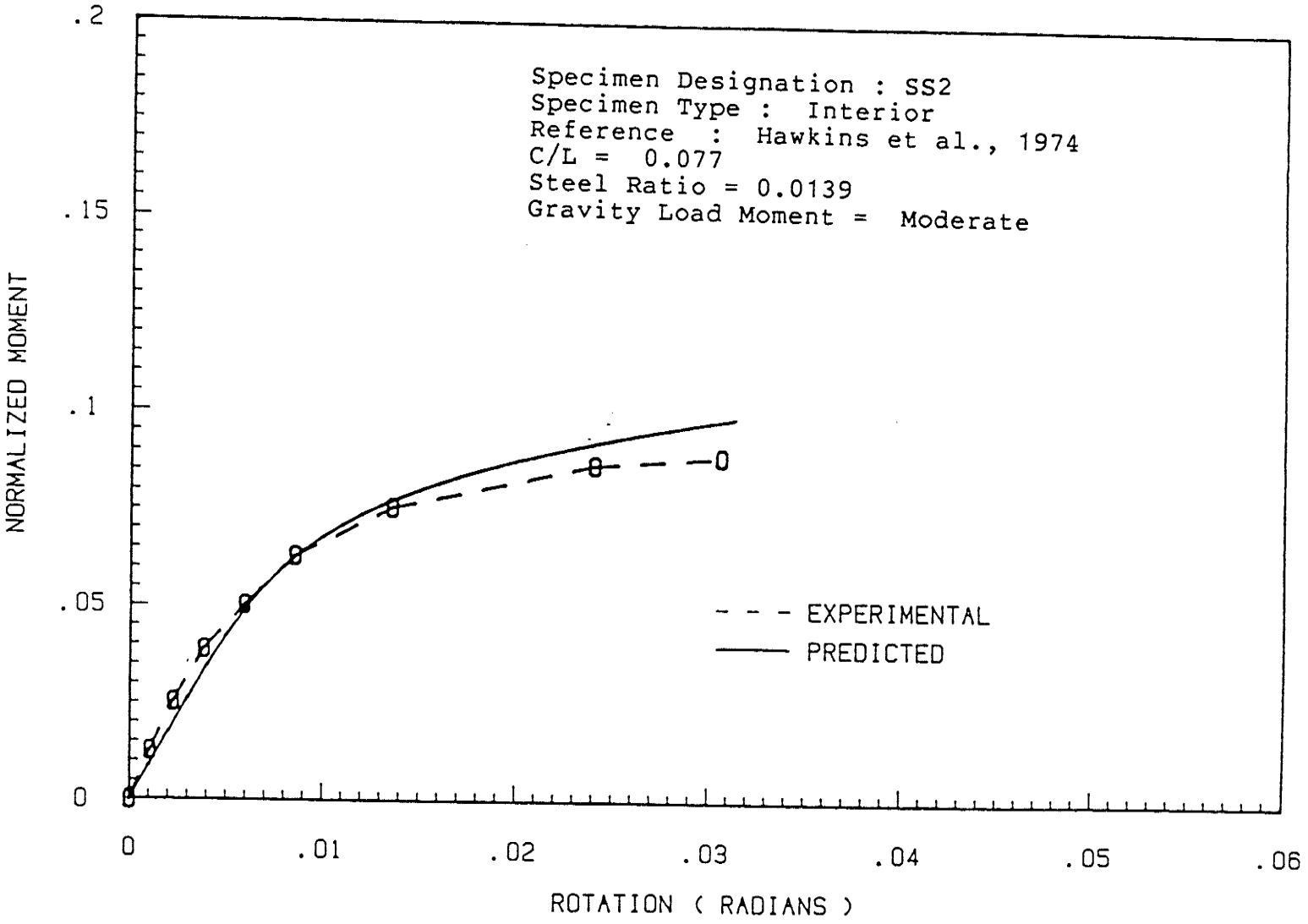
Specimen Designation : SS2
Specimen Type : Interior
Reference : Hawkins et al., 1974
C/L = 0.077
Steel Ratio = 0.0139
Gravity Load Moment = Moderate
EXPERIMENTAL
PREDICTED
NORMALIZED MOMENT
ROTATION (RADIANS)
0
.05
.1
.15
.2
.01
.02
.03
.04
.05
.06

Figure A.11

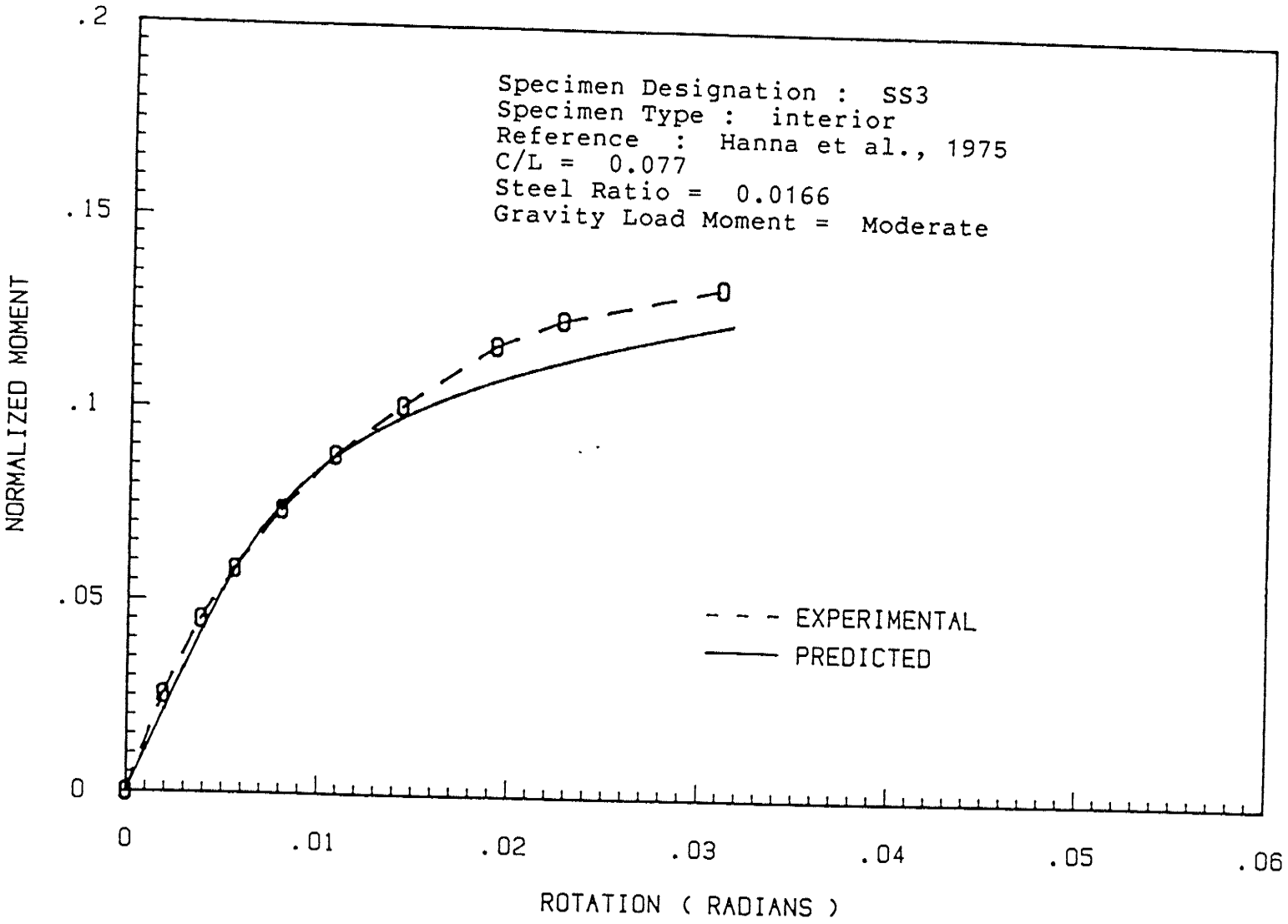
Specimen Designation : SS3
Specimen Type : interior
Reference : Hanna et al., 1975
C/L = 0.077
Steel Ratio = 0.0166
Gravity Load Moment = Moderate
EXPERIMENTAL
PREDICTED
NORMALIZED MOMENT
.2
.15
.1
.05
0
0
.01
.02
.03
.04
.05
.06
ROTATION (RADIANS)

Figure A.12

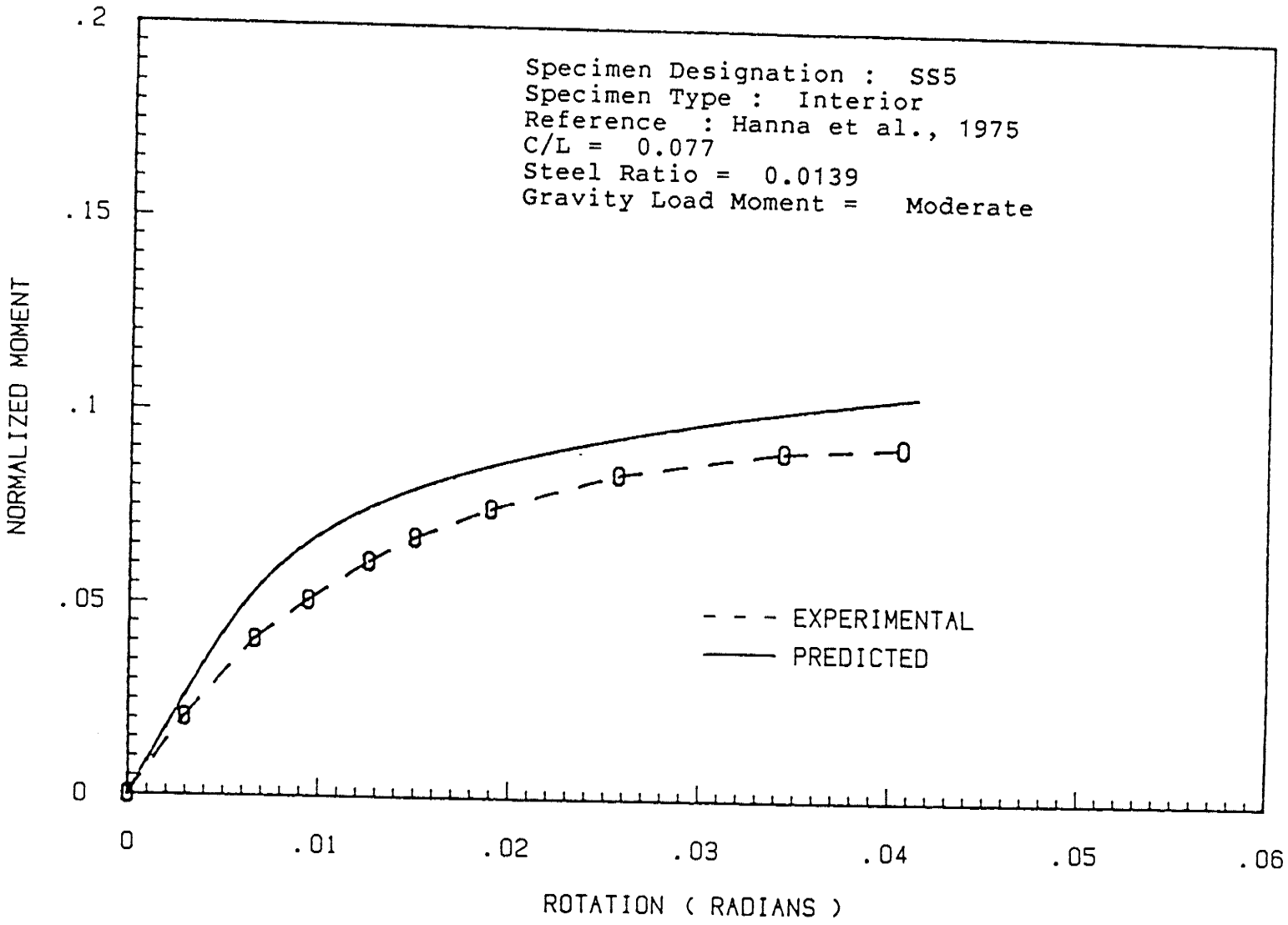
Specimen Designation : SS5
Specimen Type : Interior
Reference : Hanna et al., 1975
C/L = 0.077
Steel Ratio = 0.0139
Gravity Load Moment = Moderate
NORMALIZED MOMENT
.2
.15
.1
.05
0
0
.01
.02
.03
.04
.05
.06
ROTATION (RADIANS)
EXPERIMENTAL
PREDICTED

Figure A.13

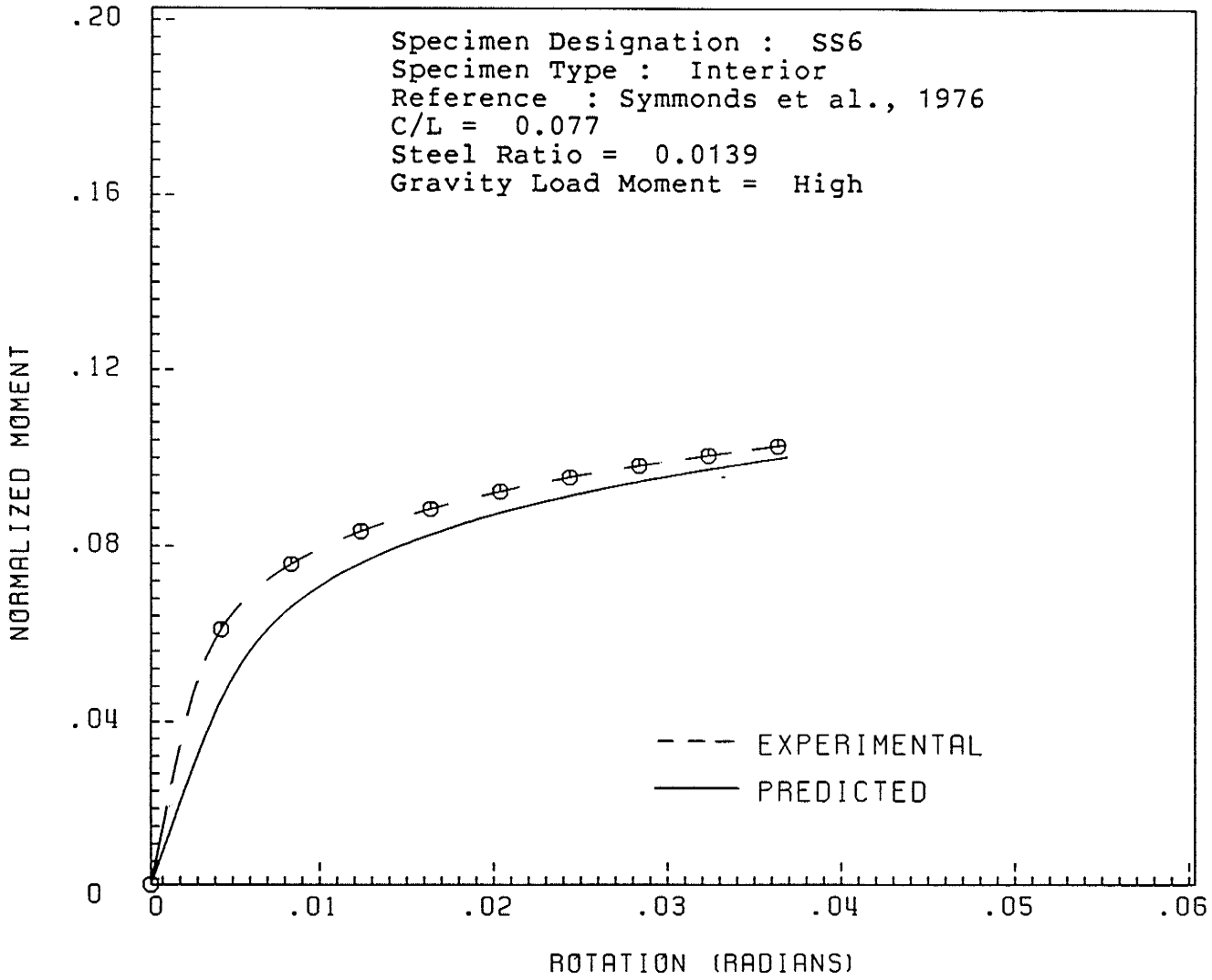
Specimen Designation : SS6
Specimen Type : Interior
Reference : Symmonds et al., 1976
C/L = 0.077
Steel Ratio = 0.0139
Gravity Load Moment = High
NORMALIZED MOMENT
.20
.16
.12
.08
.04
0
0
.01
.02
.03
.04
.05
.06
ROTATION (RADIANS)
EXPERIMENTAL
PREDICTED

Figure A.14

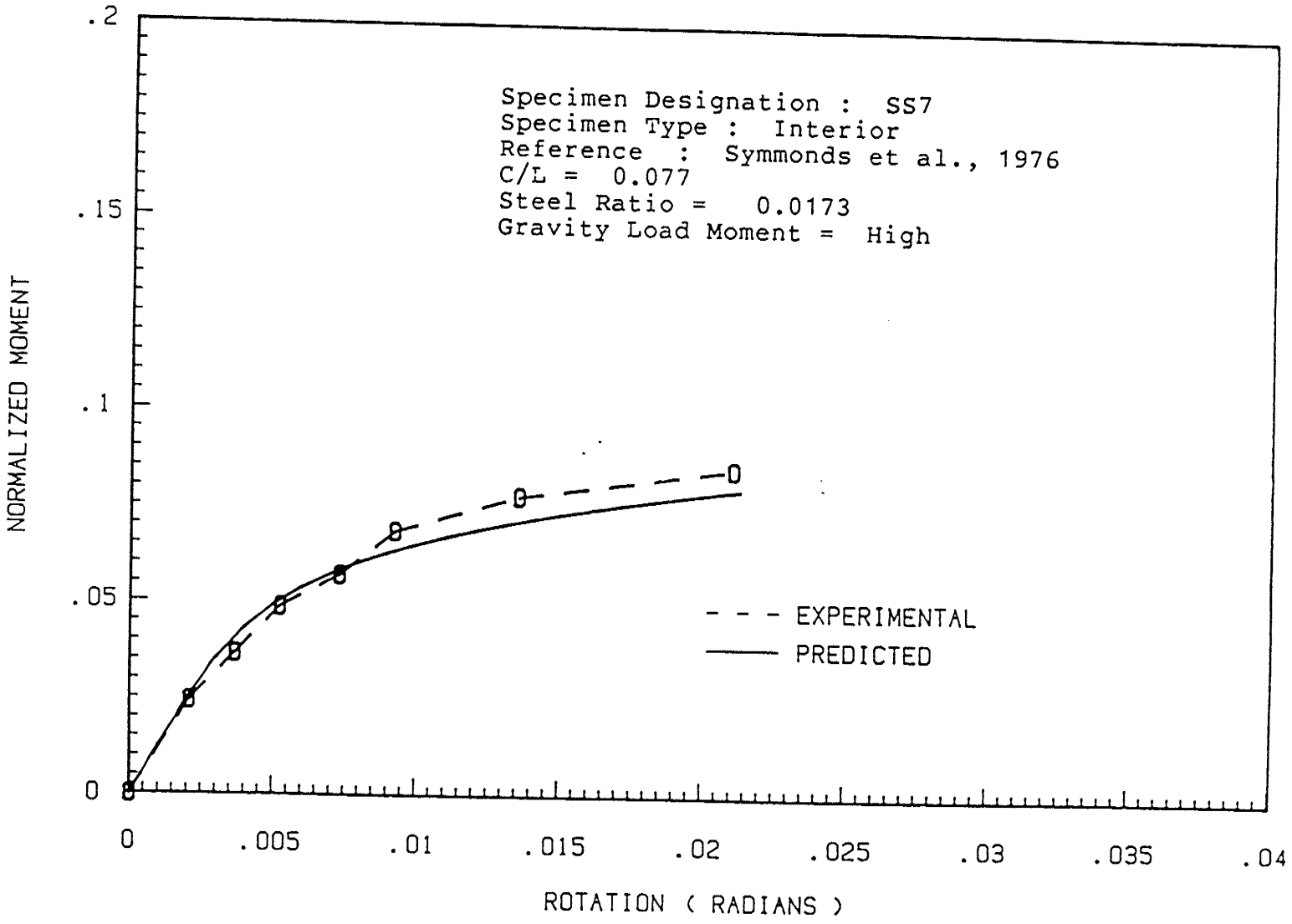
Specimen Designation : SS7
Specimen Type : Interior
Reference : Symmonds et al., 1976
C/L = 0.077
Steel Ratio = 0.0173
Gravity Load Moment = High
EXPERIMENTAL
PREDICTED
NORMALIZED MOMENT
ROTATION (RADIANS)
0
.05
.1
.15
.2
0
.005
.01
.015
.02
.025
.03
.035
.04

Figure A.15

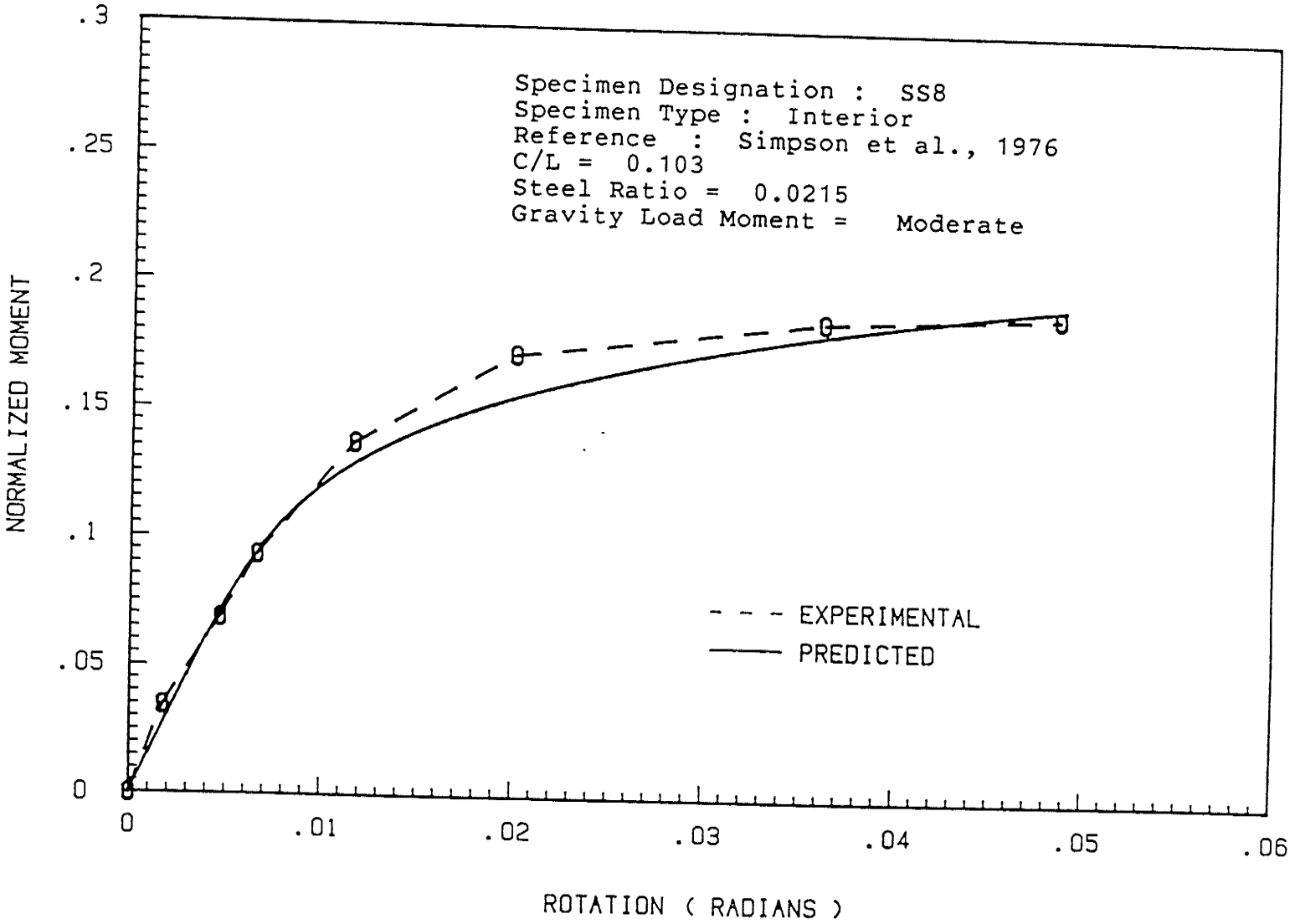
Specimen Designation : SS8
Specimen Type : Interior
Reference : Simpson et al., 1976
C/L = 0.103
Steel Ratio = 0.0215
Gravity Load Moment = Moderate
EXPERIMENTAL
PREDICTED
NORMALIZED MOMENT
ROTATION (RADIANS)
0
.05
.1
.15
.2
.25
.3
0
.01
.02
.03
.04
.05
.06

Figure A.16

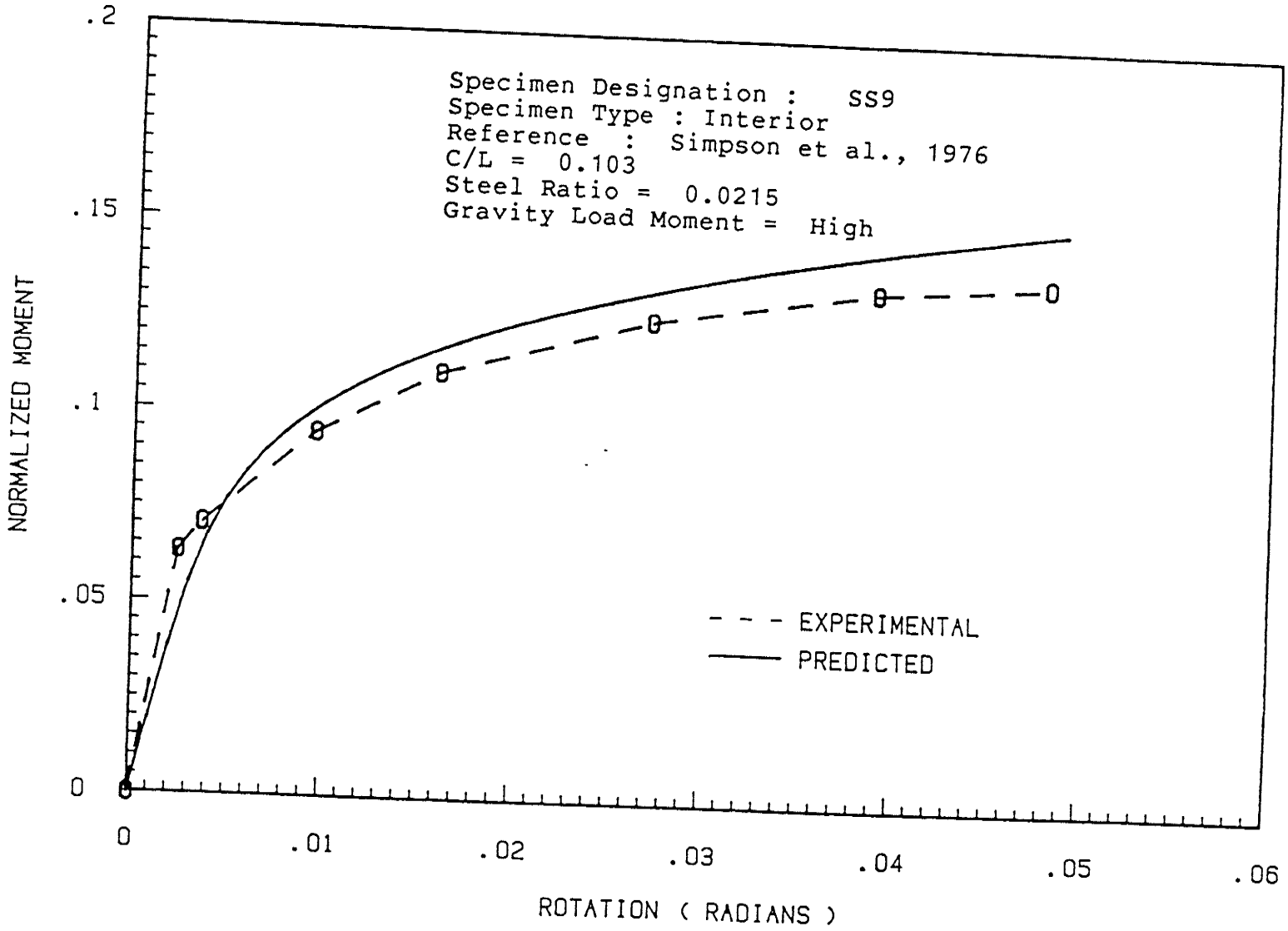
Specimen Designation : SS9
Specimen Type : Interior
Reference : Simpson et al., 1976
C/L = 0.103
Steel Ratio = 0.0215
Gravity Load Moment = High
EXPERIMENTAL
PREDICTED
NORMALIZED MOMENT
ROTATION (RADIANS)
0
.05
.1
.15
.2
.01
.02
.03
.04
.05
.06

Figure A.17

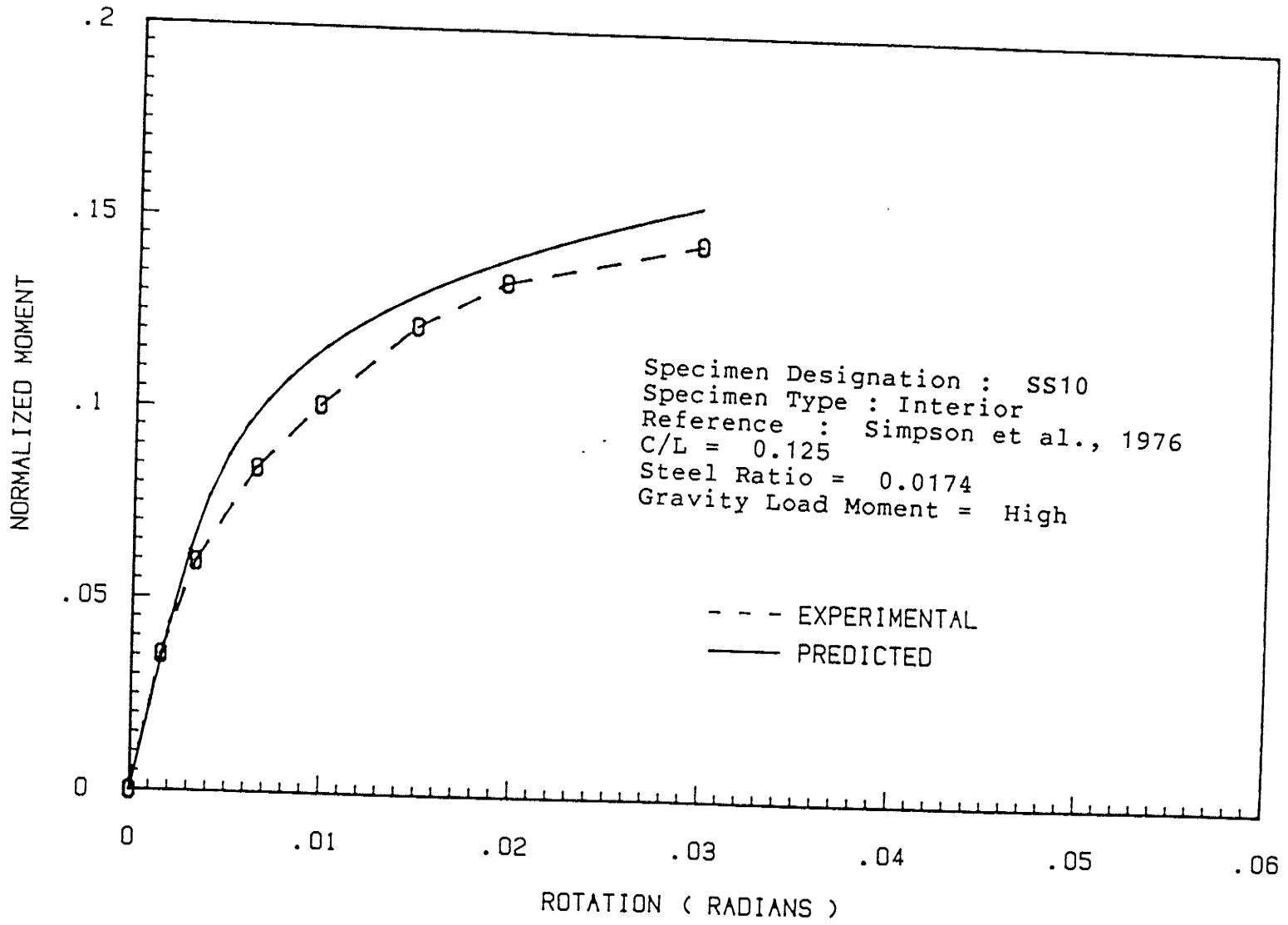
.2
.15
.1
.05
0
NORMALIZED MOMENT
0
.01
.02
.03
.04
.05
.06
ROTATION (RADIANS)
Specimen Designation : SS10
Specimen Type : Interior
Reference : Simpson et al., 1976
C/L = 0.125
Steel Ratio = 0.0174
Gravity Load Moment = High
- - - EXPERIMENTAL
—— PREDICTED

Figure A.18

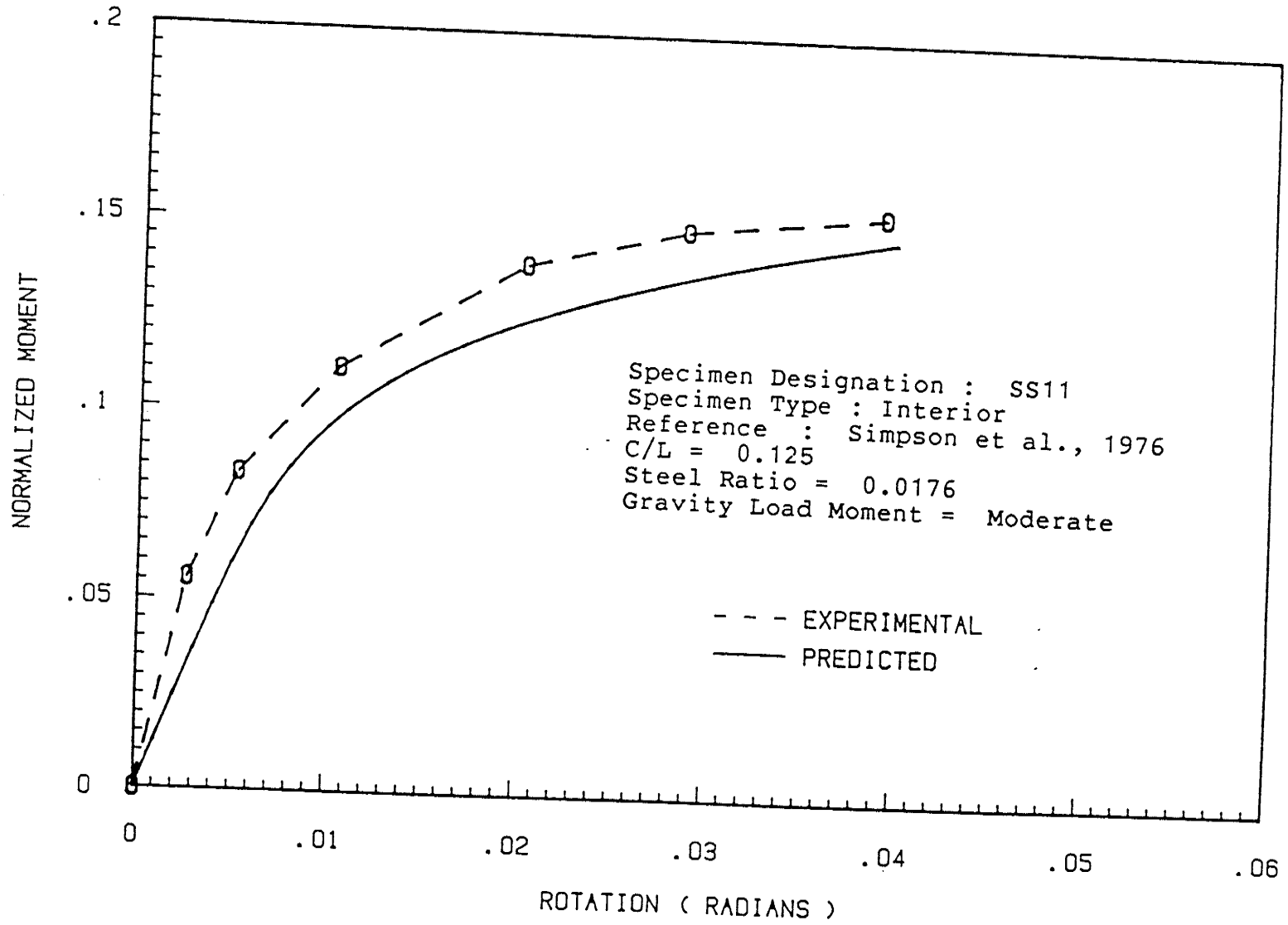
.2
.15
.1
.05
0
NORMALIZED MOMENT
0
.01
.02
.03
.04
.05
.06
ROTATION (RADIANS)
Specimen Designation : SS11
Specimen Type : Interior
Reference : Simpson et al., 1976
C/L = 0.125
Steel Ratio = 0.0176
Gravity Load Moment = Moderate
EXPERIMENTAL
PREDICTED

Figure A.19

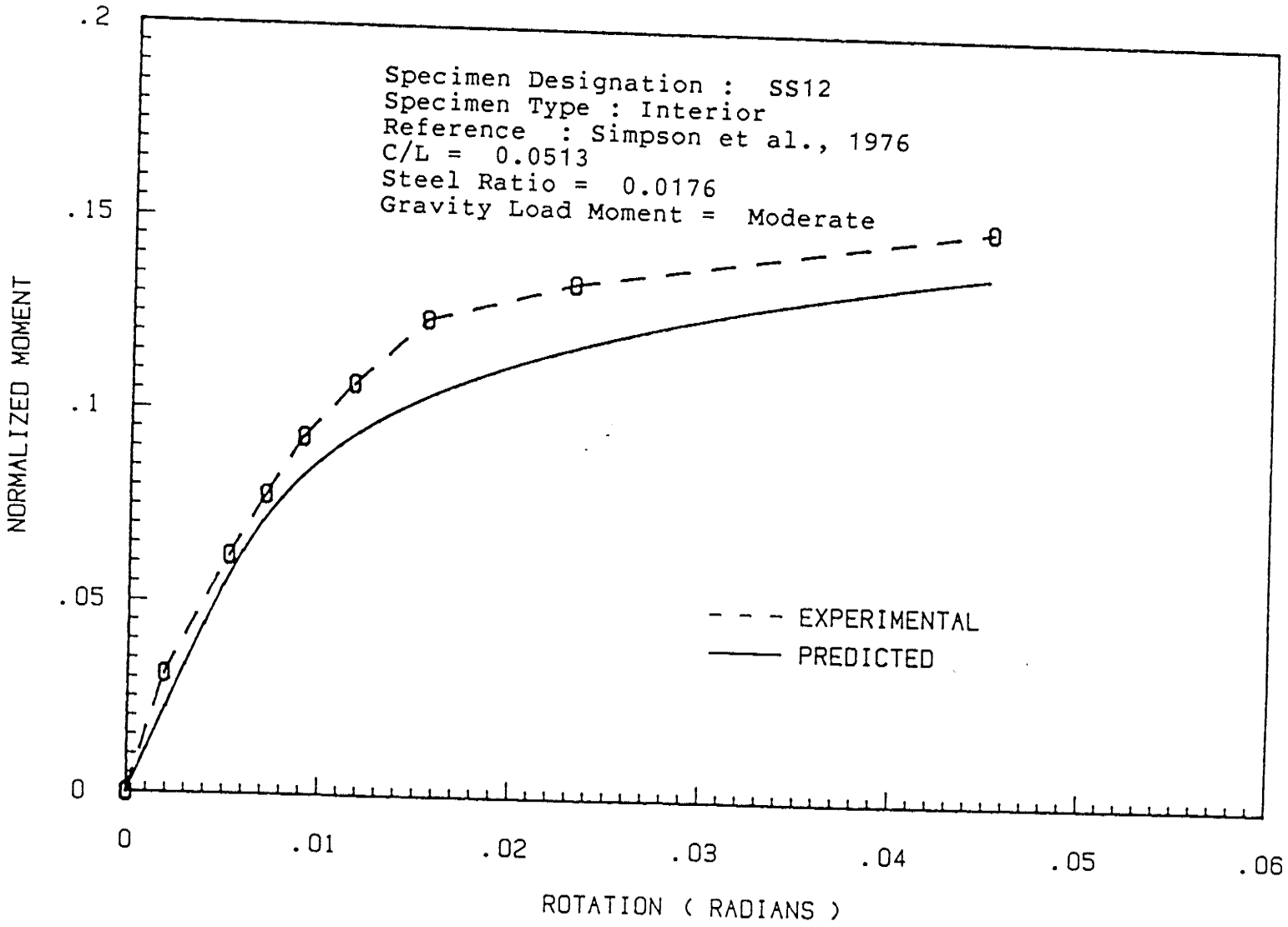
Specimen Designation : SS12
Specimen Type : Interior
Reference : Simpson et al., 1976
C/L = 0.0513
Steel Ratio = 0.0176
Gravity Load Moment = Moderate
EXPERIMENTAL
PREDICTED
NORMALIZED MOMENT
ROTATION (RADIANS)
0
.05
.1
.15
.2
0
.01
.02
.03
.04
.05
.06

Figure A.20

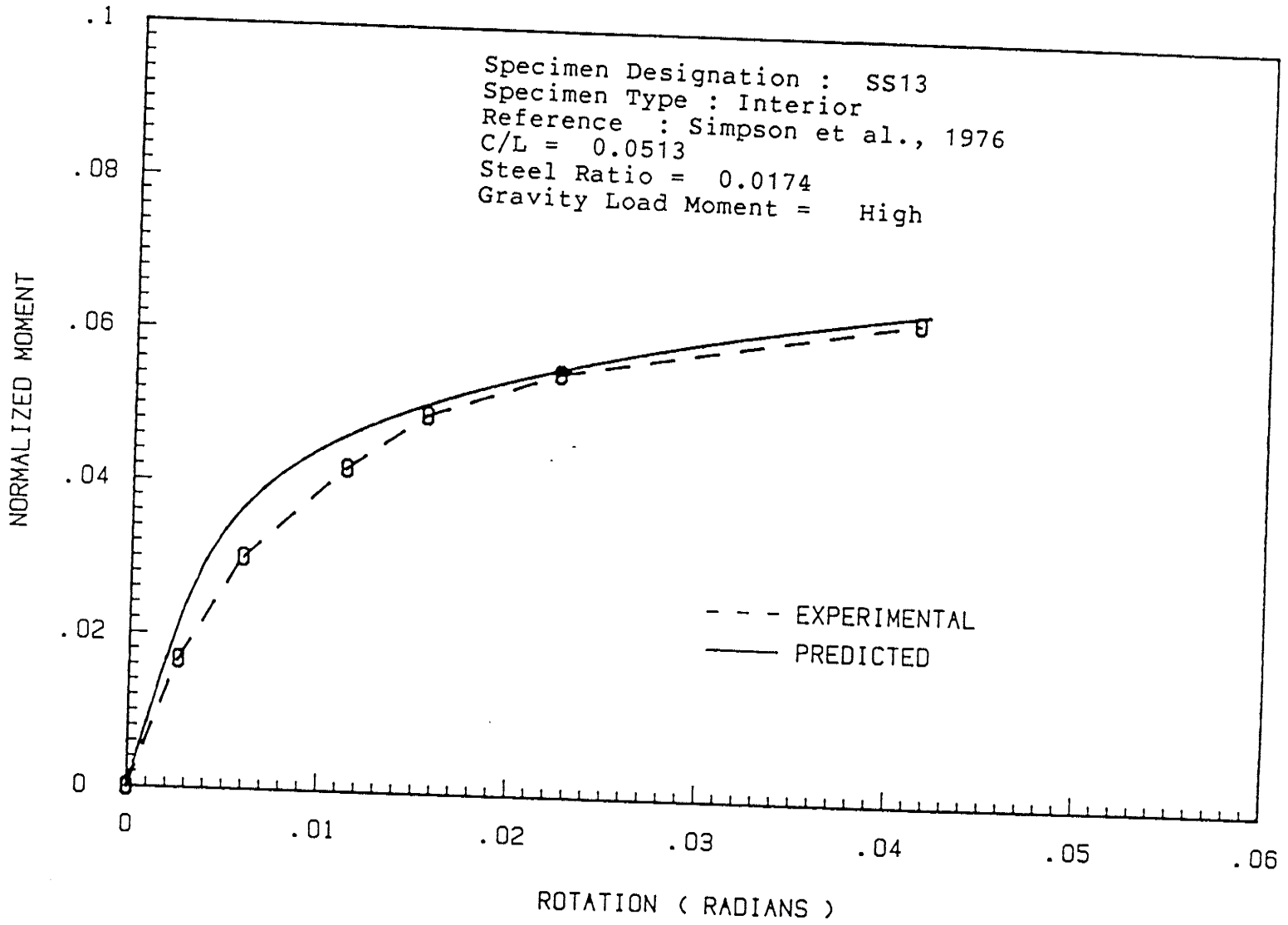
Specimen Designation : SS13
Specimen Type : Interior
Reference : Simpson et al., 1976
C/L = 0.0513
Steel Ratio = 0.0174
Gravity Load Moment = High
EXPERIMENTAL
PREDICTED
NORMALIZED MOMENT
ROTATION (RADIANS)
0
.02
.04
.06
.08
.1
0
.01
.02
.03
.04
.05
.06

Figure A.21

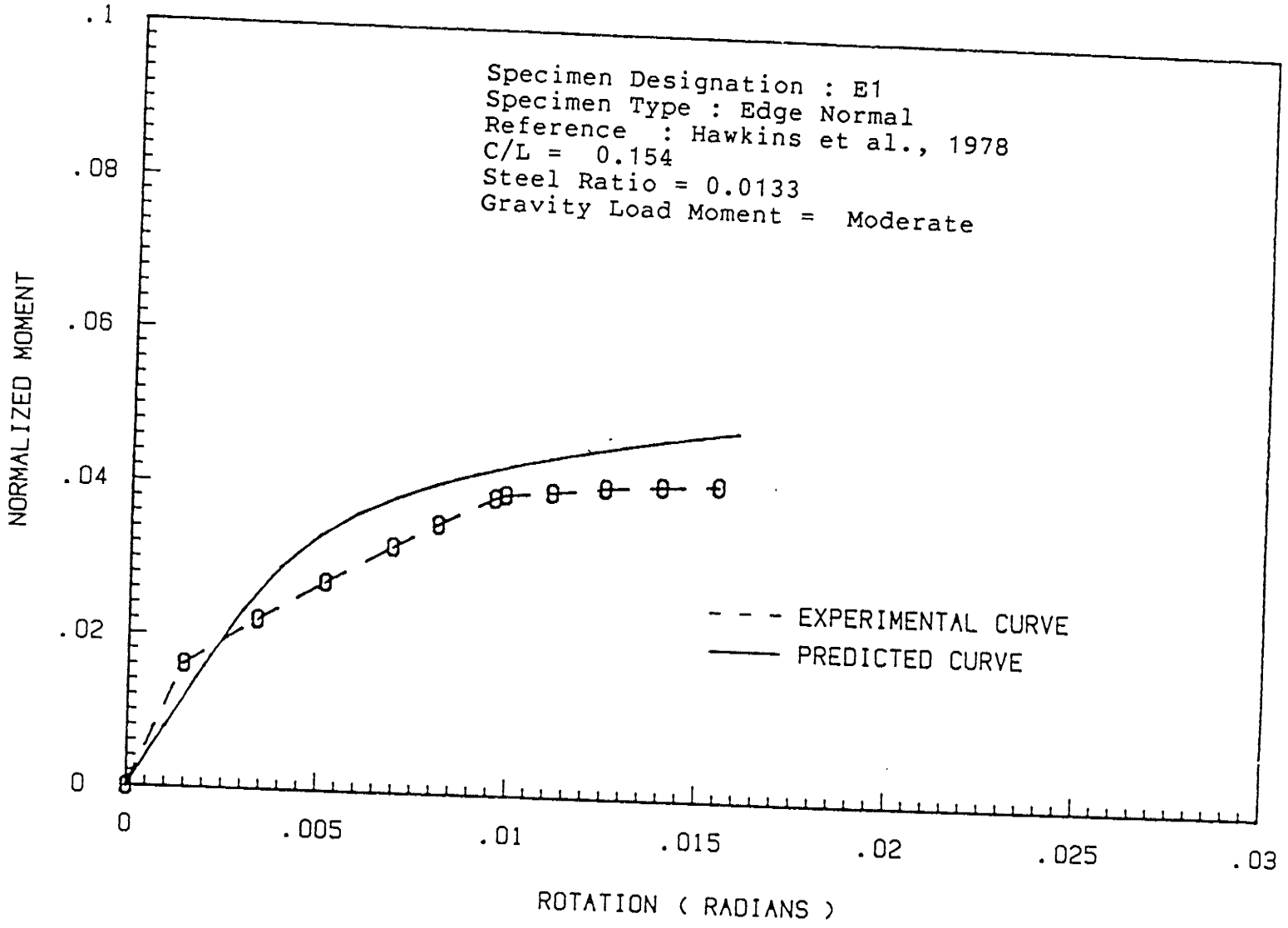
Specimen Designation : E1
Specimen Type : Edge Normal
Reference : Hawkins et al., 1978
C/L = 0.154
Steel Ratio = 0.0133
Gravity Load Moment = Moderate
EXPERIMENTAL CURVE
PREDICTED CURVE
NORMALIZED MOMENT
ROTATION (RADIANS)
0
.02
.04
.06
.08
.1
.005
.01
.015
.02
.025
.03

Figure A.22

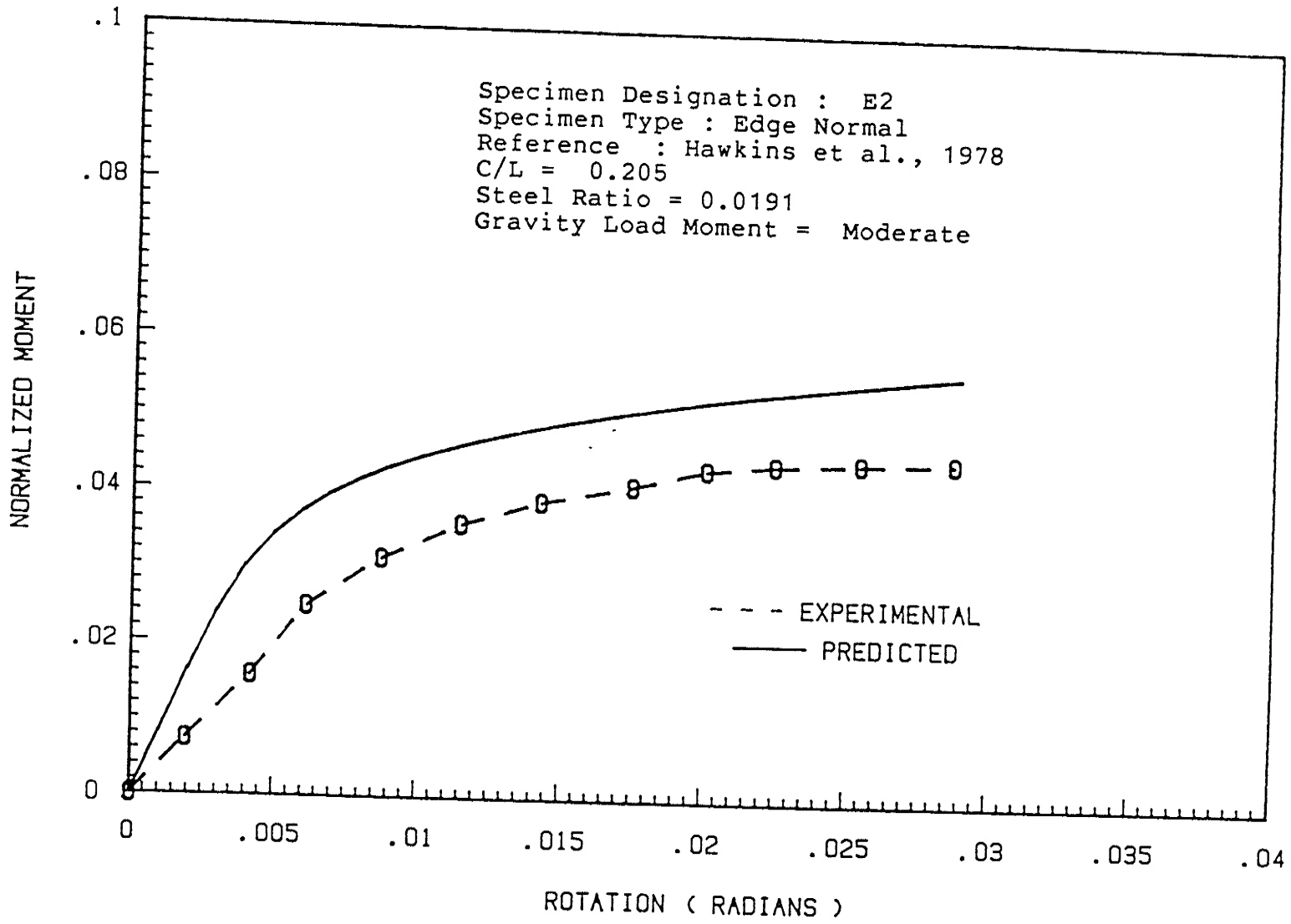
Specimen Designation : E2
Specimen Type : Edge Normal
Reference : Hawkins et al., 1978
C/L = 0.205
Steel Ratio = 0.0191
Gravity Load Moment = Moderate
EXPERIMENTAL
PREDICTED
NORMALIZED MOMENT
ROTATION (RADIANS)
0
.02
.04
.06
.08
.1
0
.005
.01
.015
.02
.025
.03
.035
.04

Figure A.23

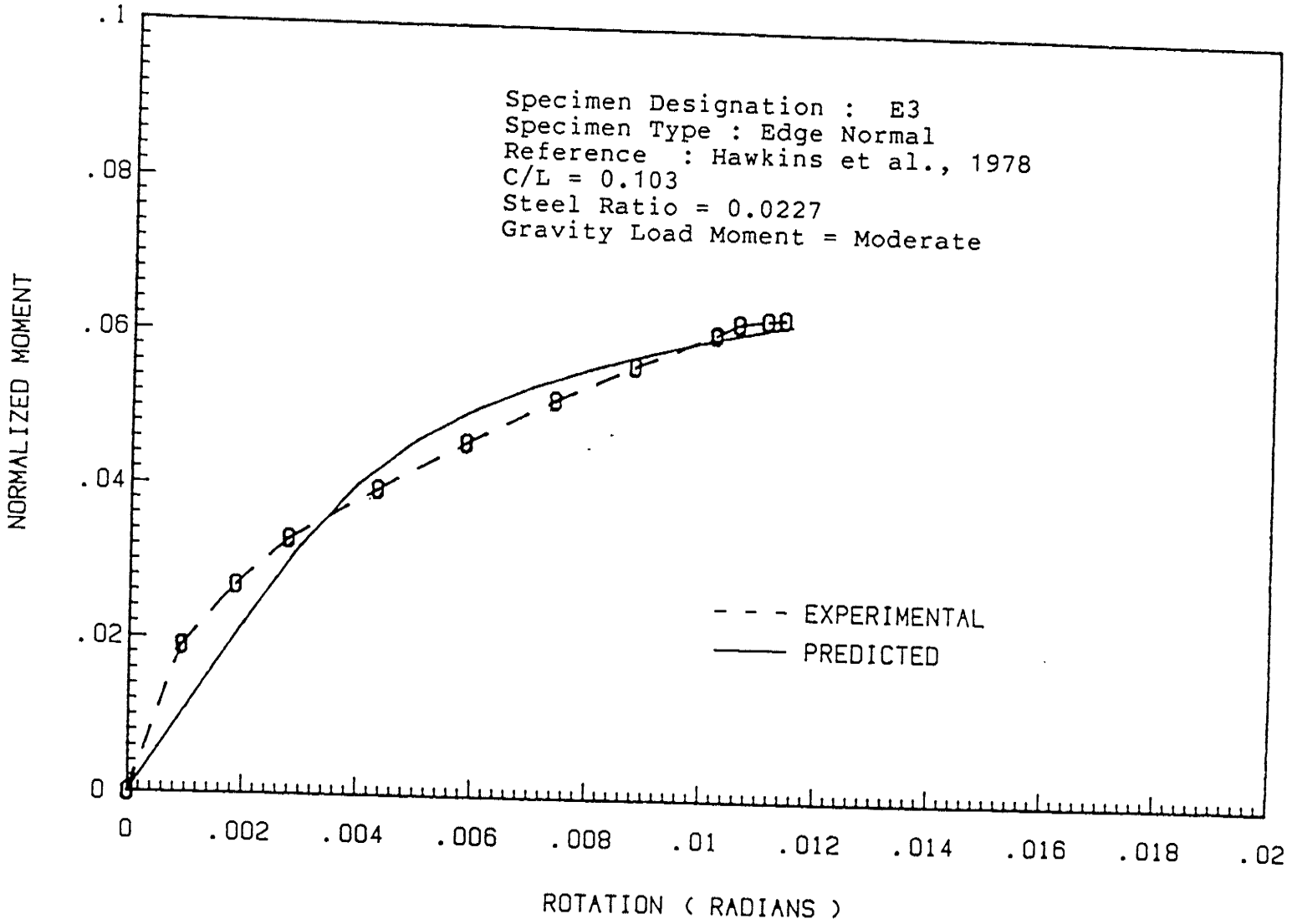
Specimen Designation : E3
Specimen Type : Edge Normal
Reference : Hawkins et al., 1978
C/L = 0.103
Steel Ratio = 0.0227
Gravity Load Moment = Moderate
- - - EXPERIMENTAL
—— PREDICTED
NORMALIZED MOMENT
.1
.08
.06
.04
.02
0
0
.002
.004
.006
.008
.01
.012
.014
.016
.018
.02
ROTATION (RADIANS)

Figure A.24

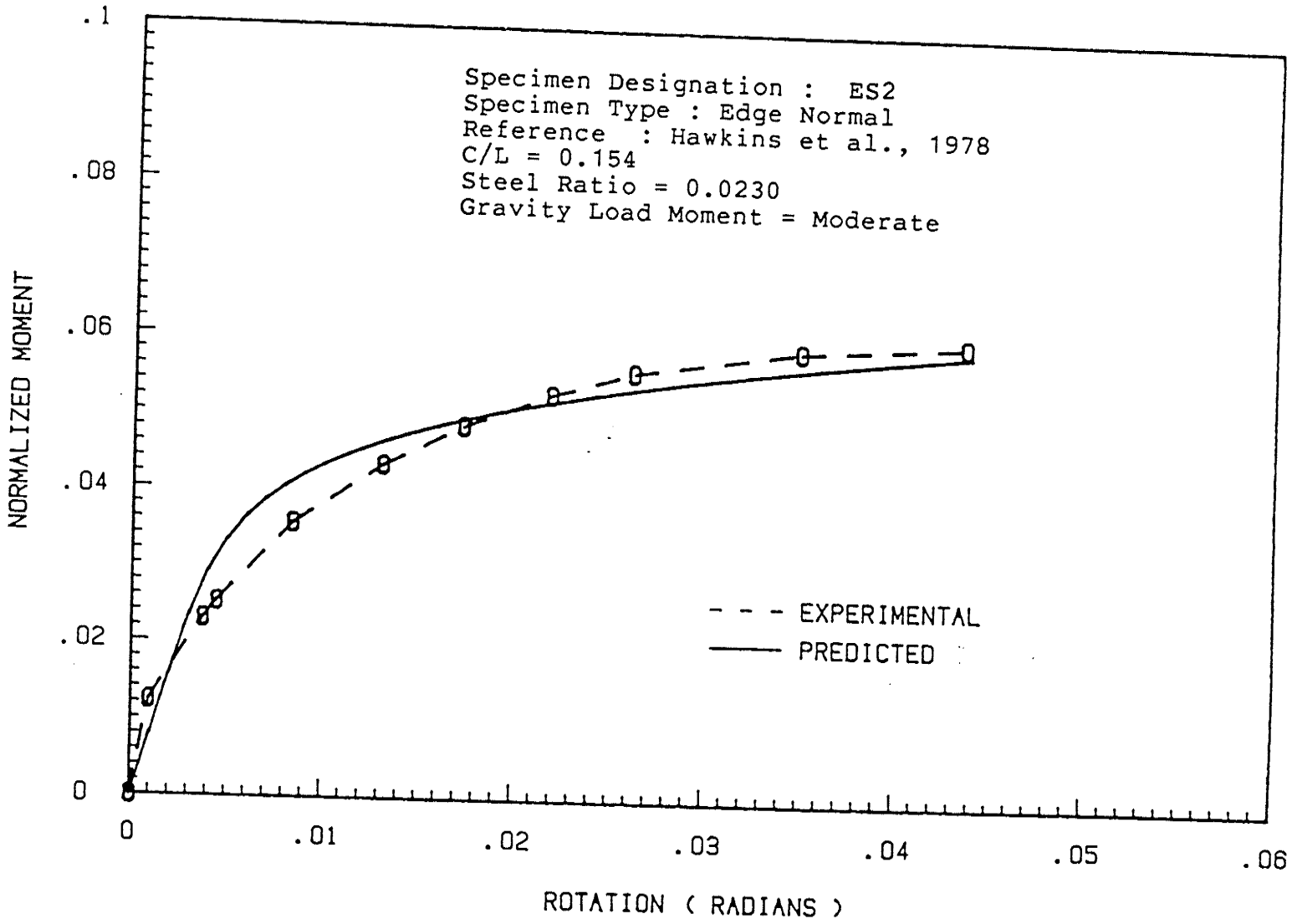
Specimen Designation : ES2
Specimen Type : Edge Normal
Reference : Hawkins et al., 1978
C/L = 0.154
Steel Ratio = 0.0230
Gravity Load Moment = Moderate
EXPERIMENTAL
PREDICTED
NORMALIZED MOMENT
.1
.08
.06
.04
.02
0
0
.01
.02
.03
.04
.05
.06
ROTATION (RADIANS)

Figure A.25

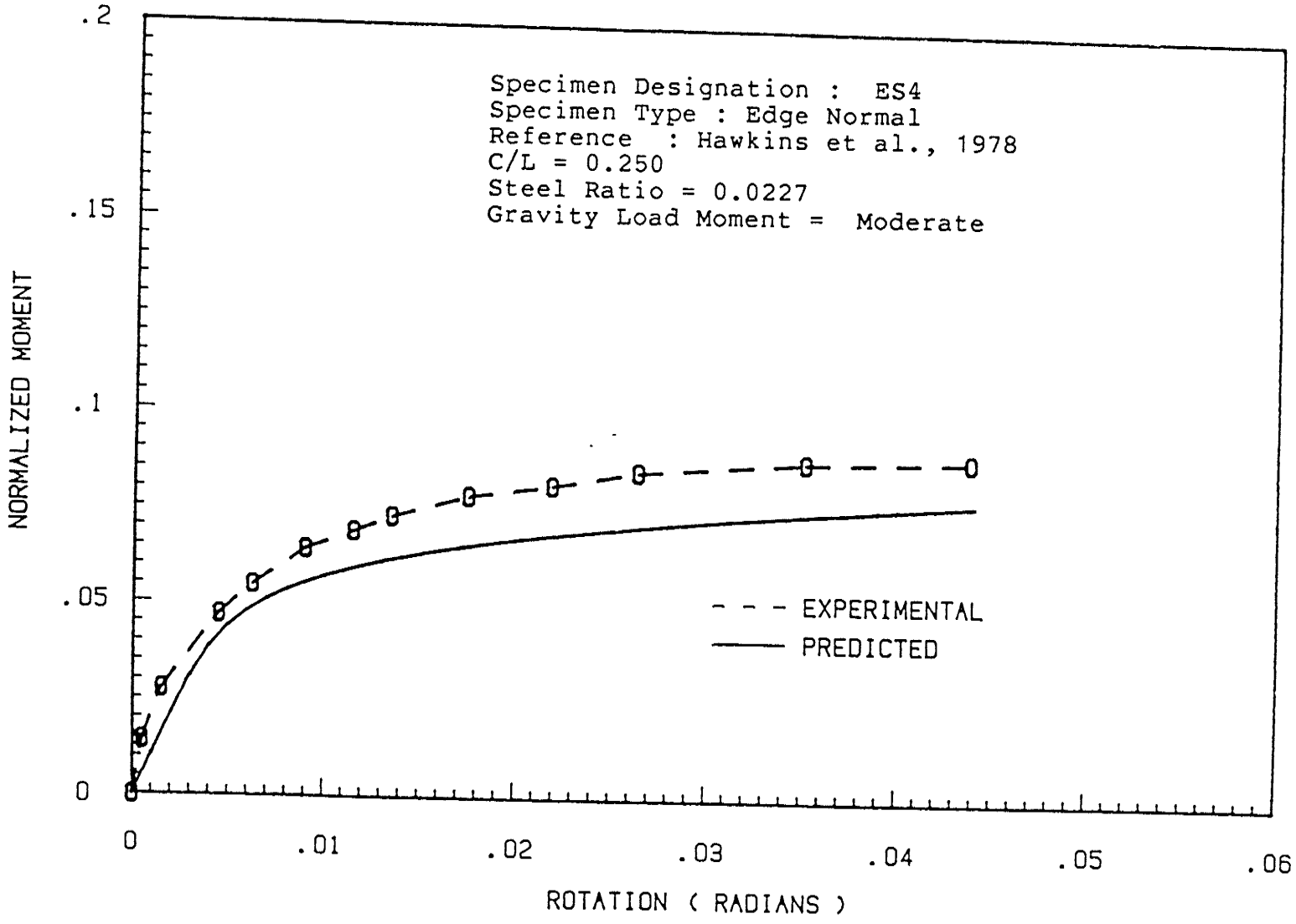
Specimen Designation : ES4
Specimen Type : Edge Normal
Reference : Hawkins et al., 1978
C/L = 0.250
Steel Ratio = 0.0227
Gravity Load Moment = Moderate
EXPERIMENTAL
PREDICTED
NORMALIZED MOMENT
ROTATION (RADIANS)
0
.05
.1
.15
.2
.01
.02
.03
.04
.05
.06

Figure A.26

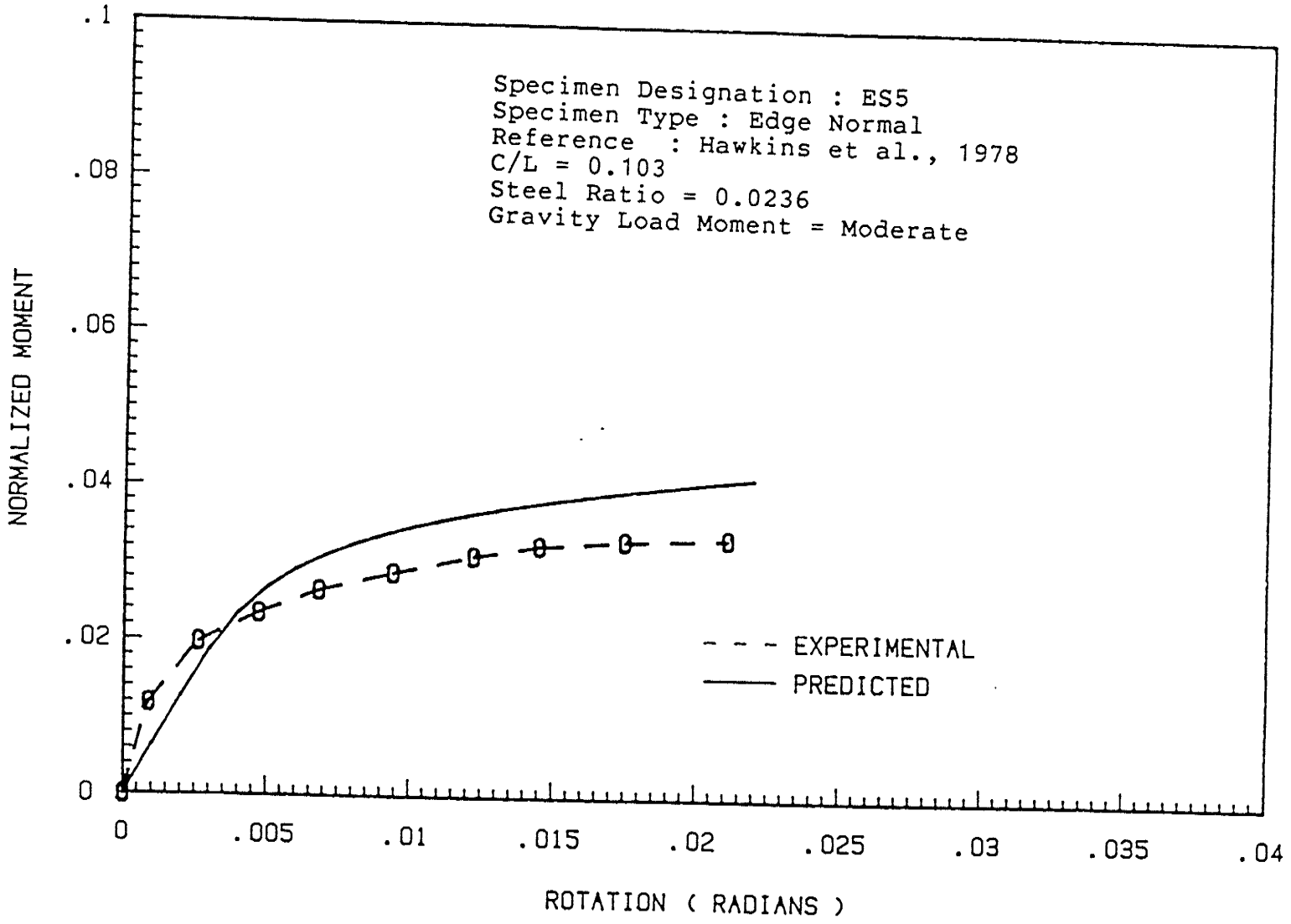
Specimen Designation : ES5
Specimen Type : Edge Normal
Reference : Hawkins et al., 1978
C/L = 0.103
Steel Ratio = 0.0236
Gravity Load Moment = Moderate
NORMALIZED MOMENT
.1
.08
.06
.04
.02
0
0
.005
.01
.015
.02
.025
.03
.035
.04
ROTATION (RADIANS)
EXPERIMENTAL
PREDICTED

Figure A.27

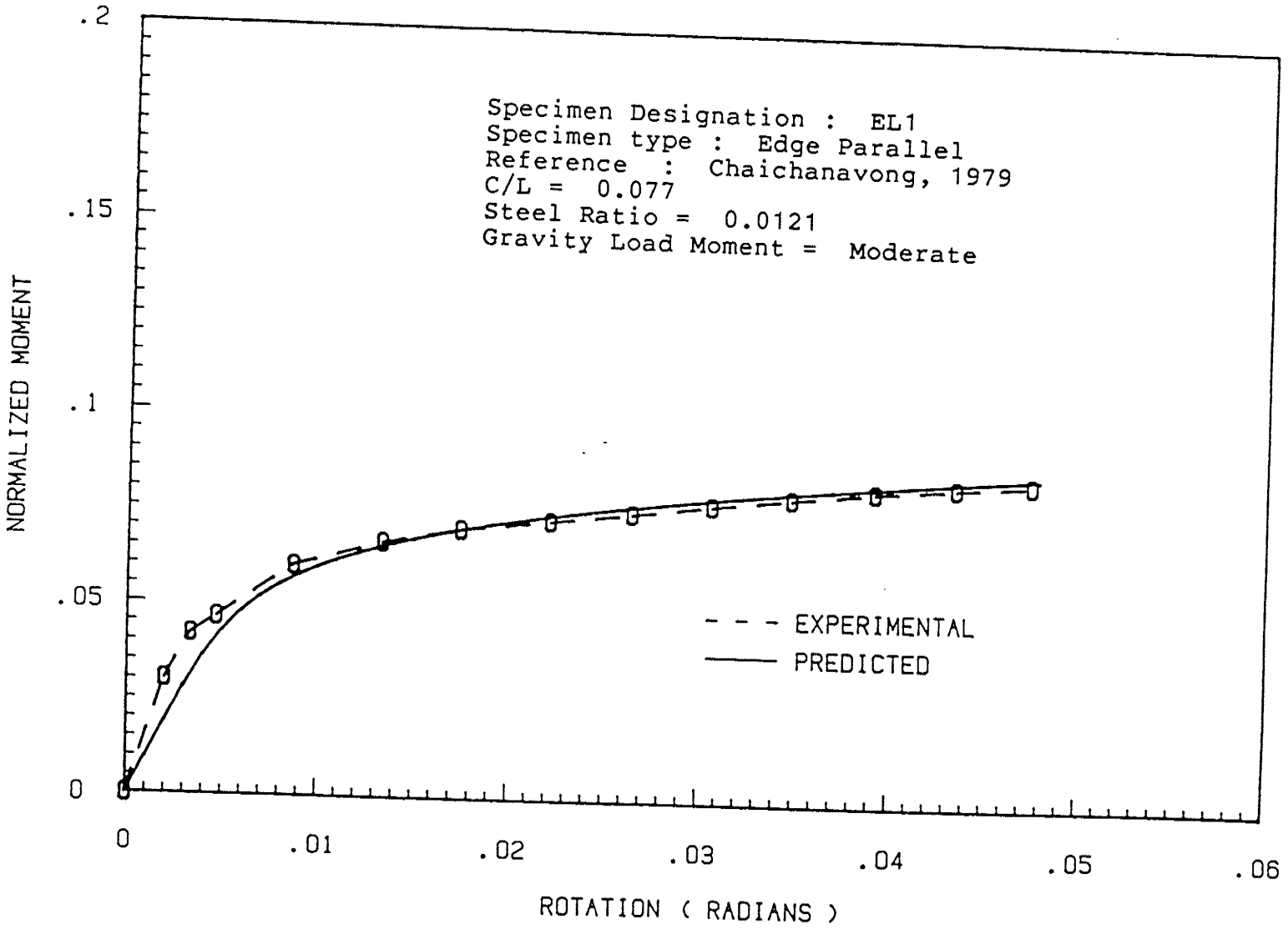
Specimen Designation : EL1
Specimen type : Edge Parallel
Reference : Chaichanavong, 1979
C/L = 0.077
Steel Ratio = 0.0121
Gravity Load Moment = Moderate
EXPERIMENTAL
PREDICTED
NORMALIZED MOMENT
.2
.15
.1
.05
0
0
.01
.02
.03
.04
.05
.06
ROTATION (RADIANS)

Figure A.28

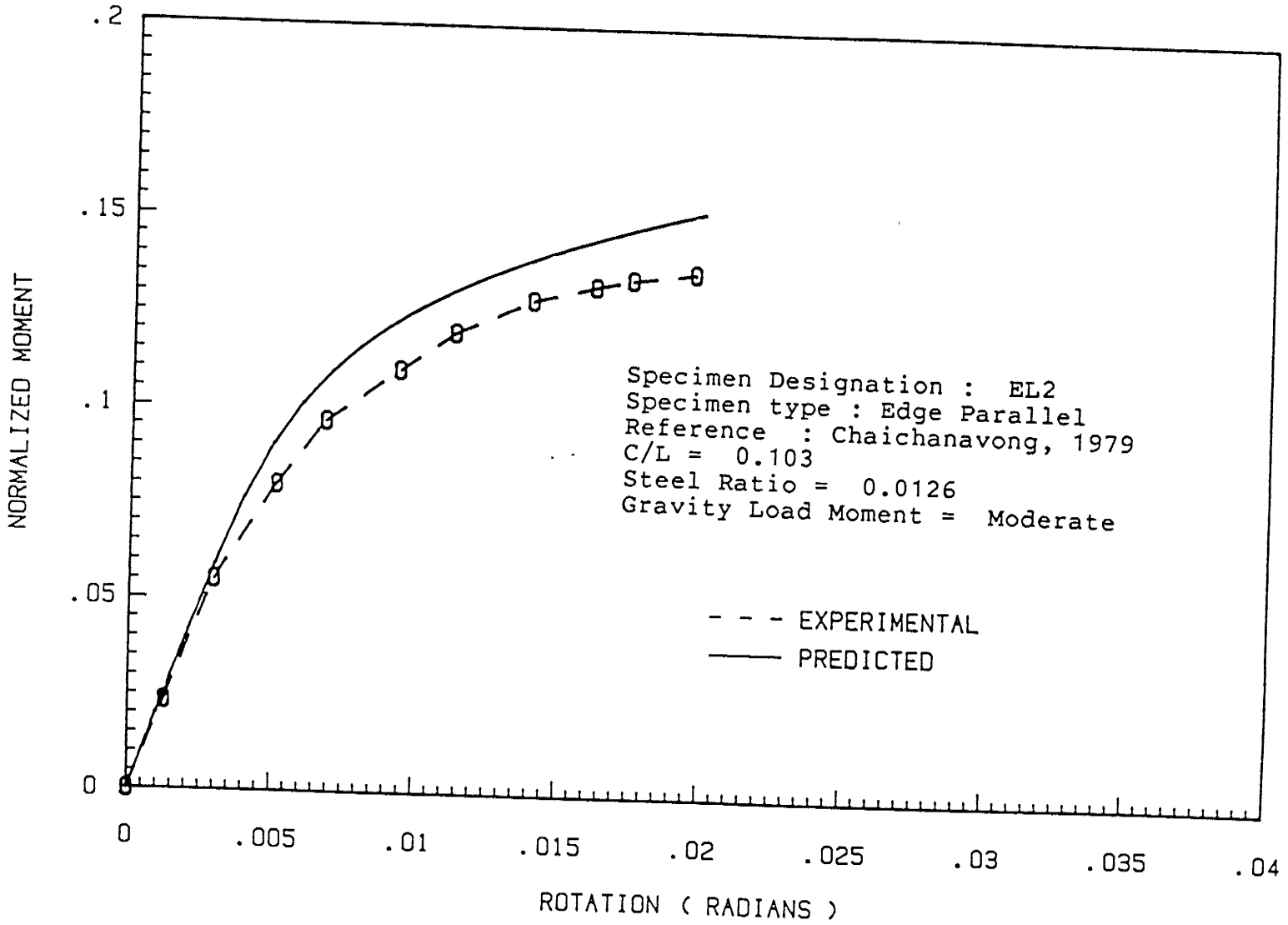
.2
.15
.1
.05
0
NORMALIZED MOMENT
0
.005
.01
.015
.02
.025
.03
.035
.04
ROTATION (RADIANS)
Specimen Designation : EL2
Specimen type : Edge Parallel
Reference : Chaichanavong, 1979
C/L = 0.103
Steel Ratio = 0.0126
Gravity Load Moment = Moderate
EXPERIMENTAL
PREDICTED

Figure A.29

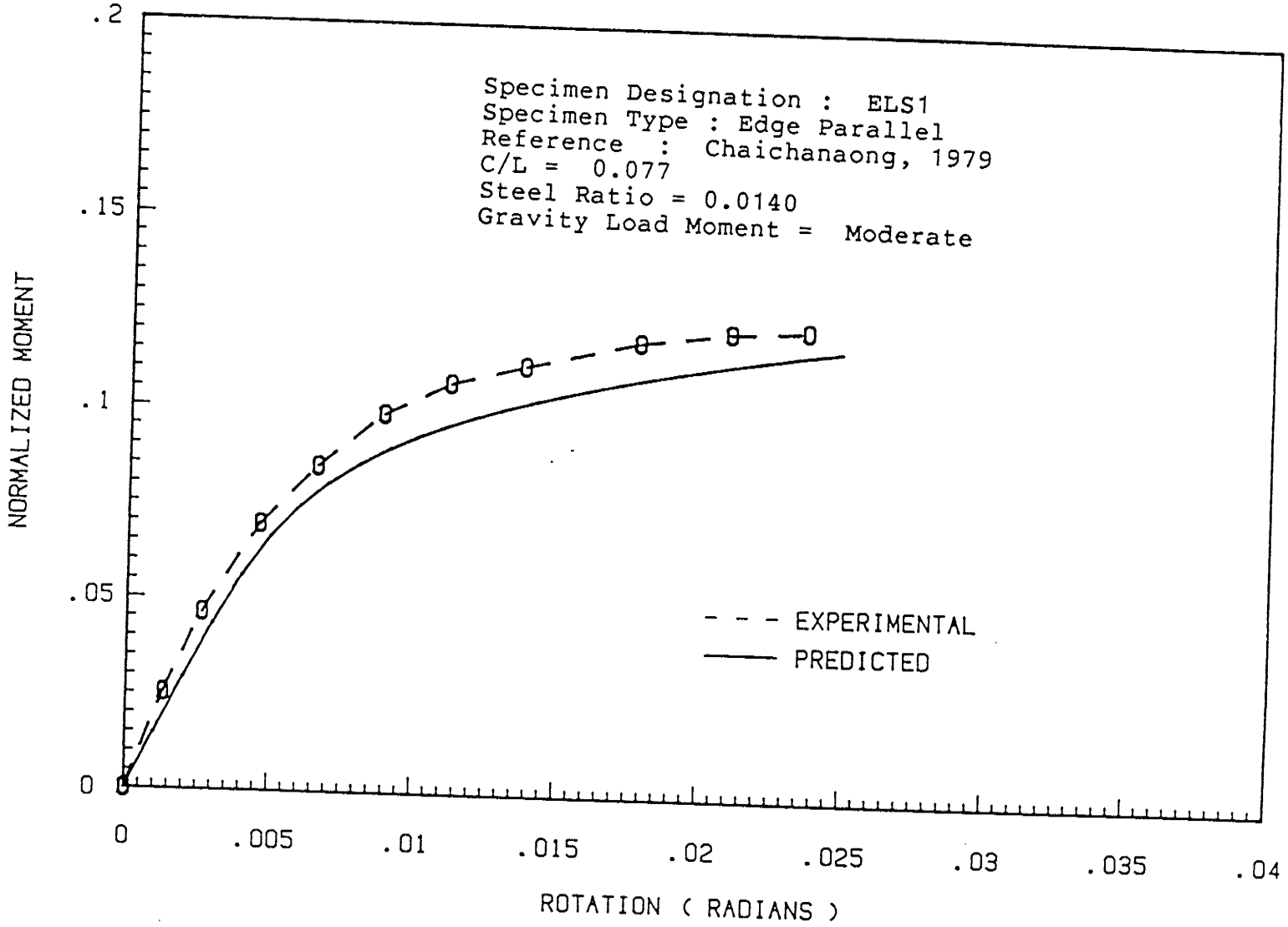
Specimen Designation : ELS1
Specimen Type : Edge Parallel
Reference : Chaichanaong, 1979
C/L = 0.077
Steel Ratio = 0.0140
Gravity Load Moment = Moderate
EXPERIMENTAL
PREDICTED
NORMALIZED MOMENT
.2
.15
.1
.05
0
0
.005
.01
.015
.02
.025
.03
.035
.04
ROTATION (RADIANS)

Figure A.30

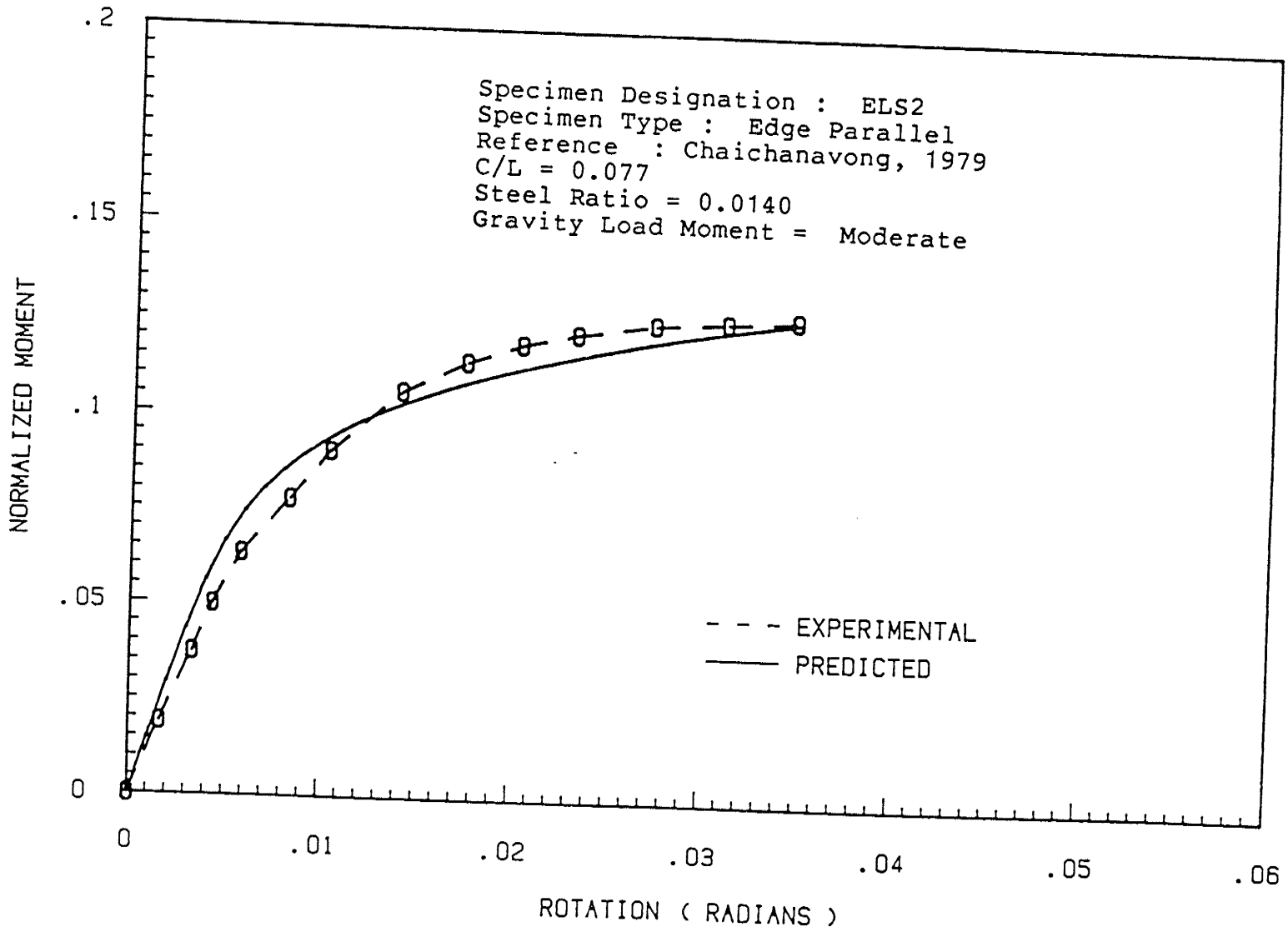
Specimen Designation : ELS2
Specimen Type : Edge Parallel
Reference : Chaichanavong, 1979
C/L = 0.077
Steel Ratio = 0.0140
Gravity Load Moment = Moderate
EXPERIMENTAL
PREDICTED
NORMALIZED MOMENT
.2
.15
.1
.05
0
0
.01
.02
.03
.04
.05
.06
ROTATION (RADIANS)

Figure A.31

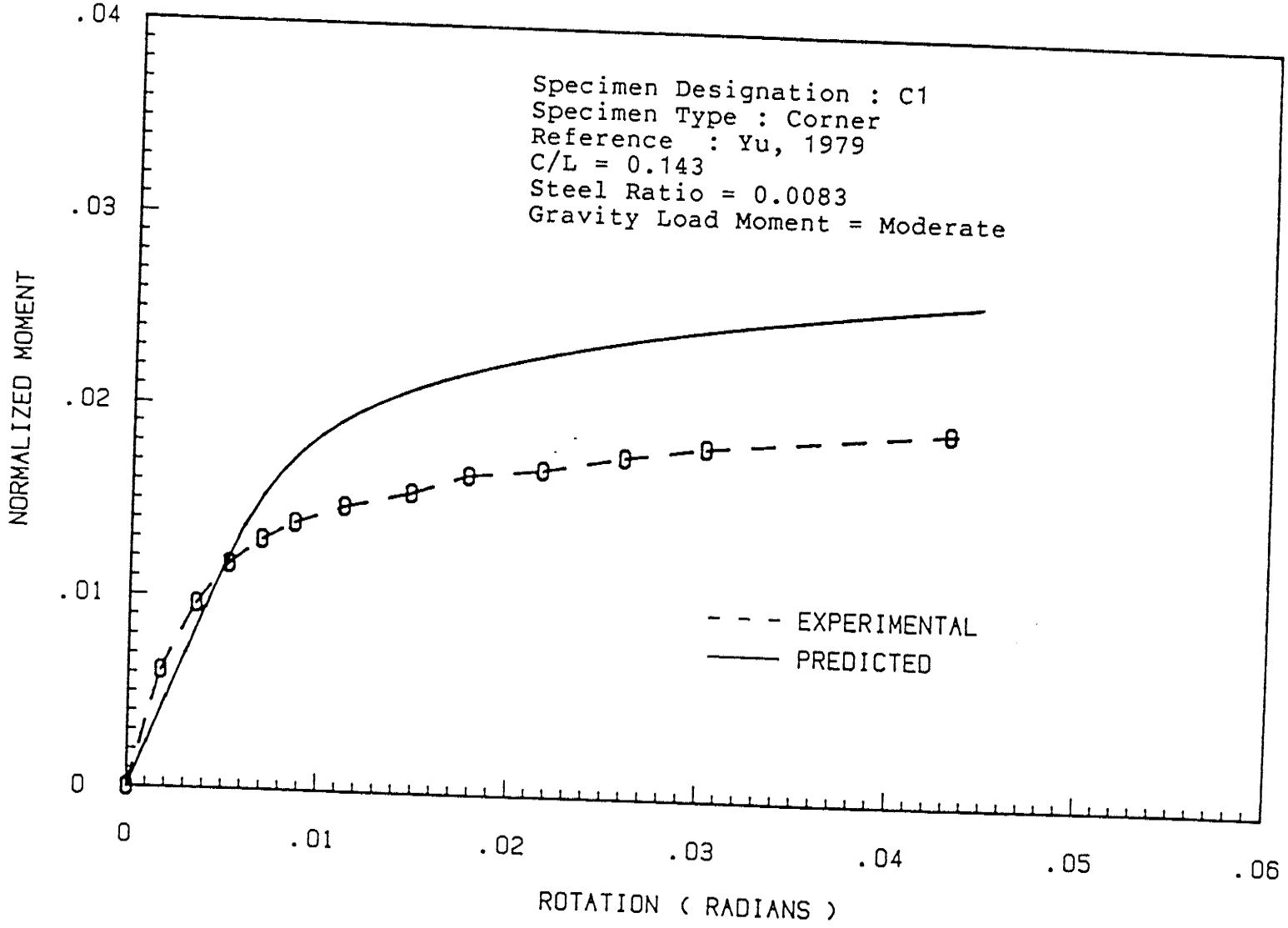
Specimen Designation : C1
Specimen Type : Corner
Reference : Yu, 1979
C/L = 0.143
Steel Ratio = 0.0083
Gravity Load Moment = Moderate
EXPERIMENTAL
PREDICTED
NORMALIZED MOMENT
ROTATION (RADIANS)
0
.01
.02
.03
.04
.05
.06

Figure A.32

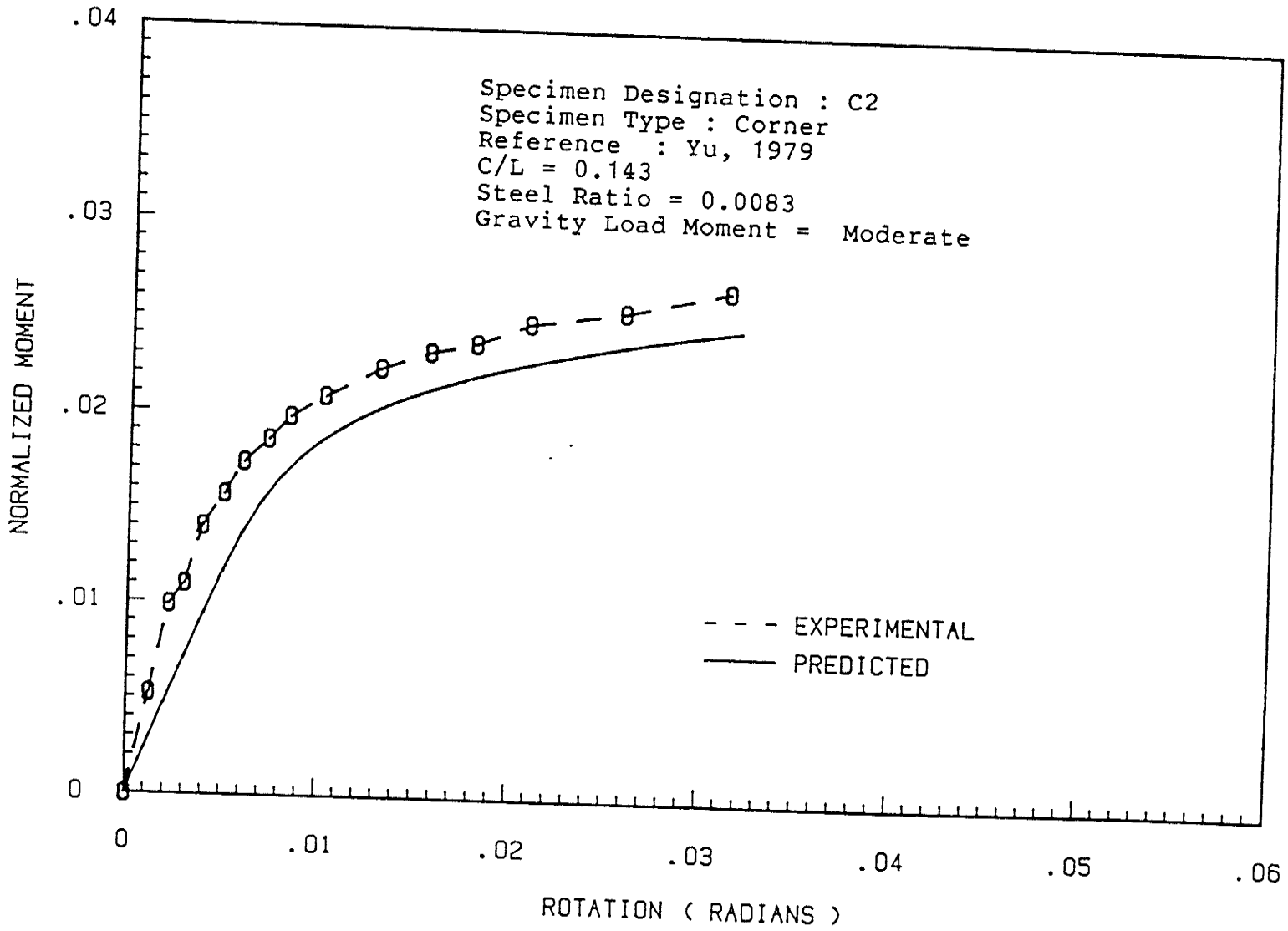
Specimen Designation : C2
Specimen Type : Corner
Reference : Yu, 1979
C/L = 0.143
Steel Ratio = 0.0083
Gravity Load Moment = Moderate
EXPERIMENTAL
PREDICTED
NORMALIZED MOMENT
ROTATION (RADIANS)
0
.01
.02
.03
.04
.05
.06

Figure A.33

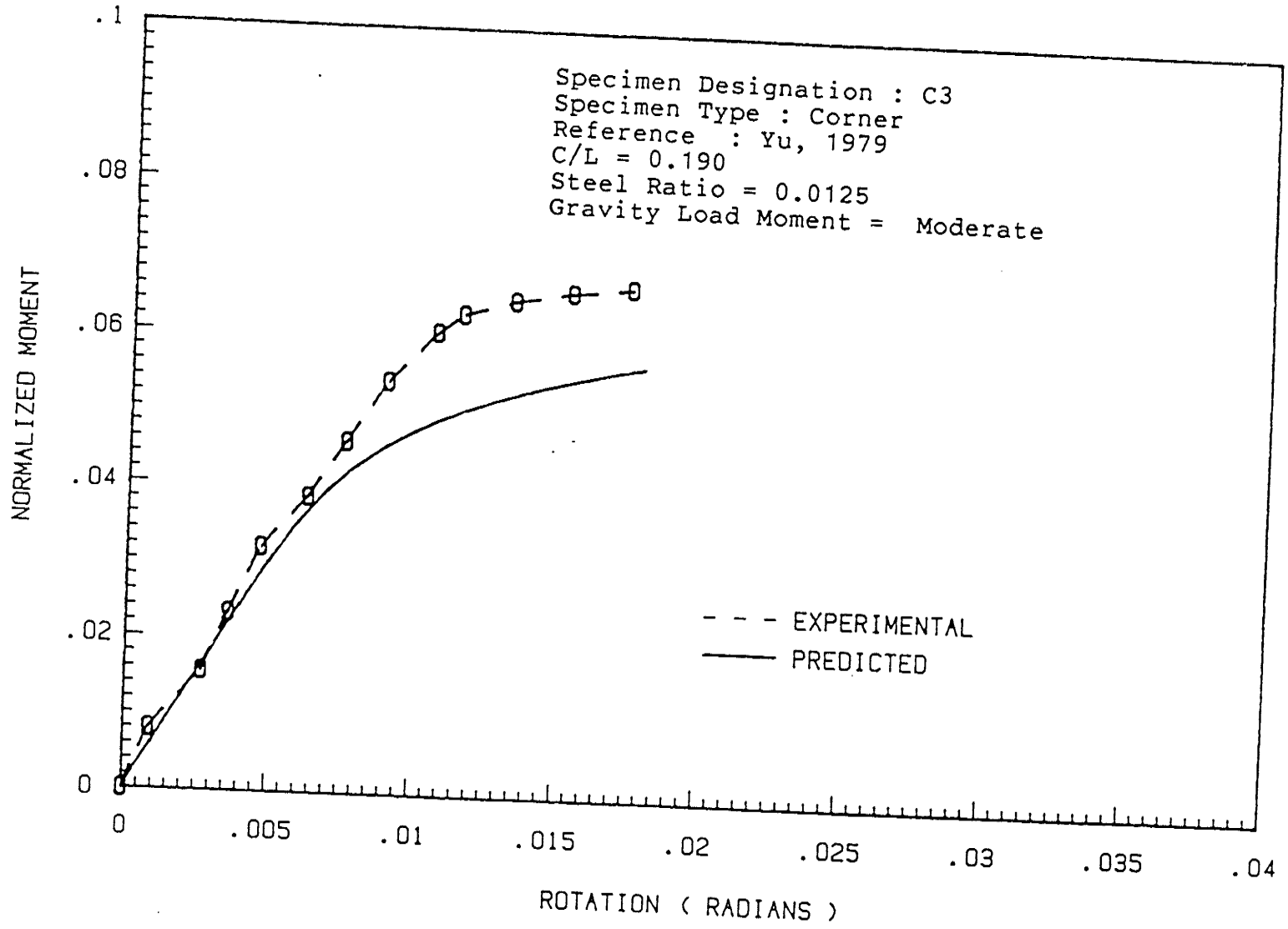
Specimen Designation : C3
Specimen Type : Corner
Reference : Yu, 1979
C/L = 0.190
Steel Ratio = 0.0125
Gravity Load Moment = Moderate
EXPERIMENTAL
PREDICTED
NORMALIZED MOMENT
ROTATION (RADIANS)
0
.02
.04
.06
.08
.1
0
.005
.01
.015
.02
.025
.03
.035
.04

Figure A.34

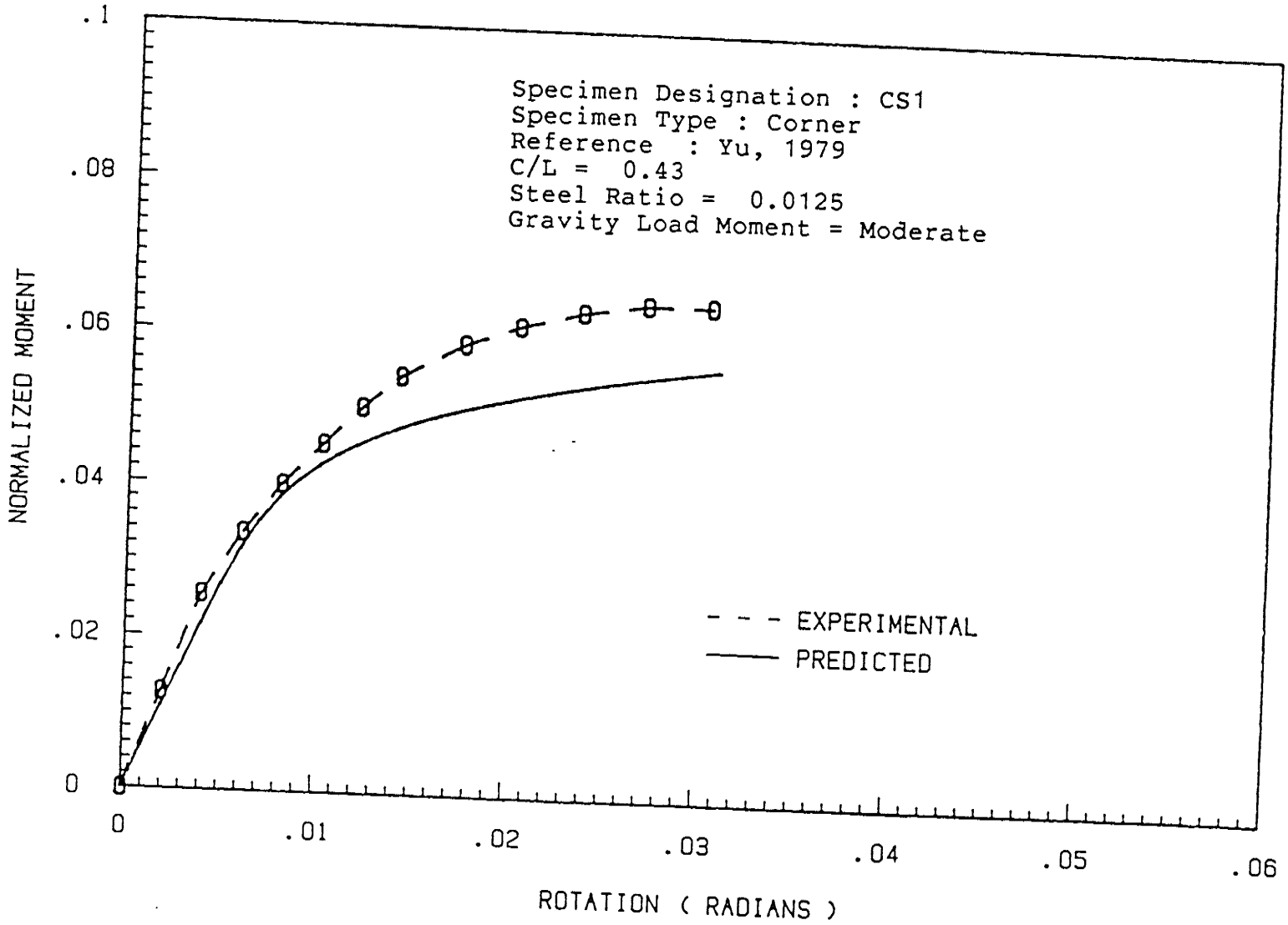
Specimen Designation : CS1
Specimen Type : Corner
Reference : Yu, 1979
C/L = 0.43
Steel Ratio = 0.0125
Gravity Load Moment = Moderate
EXPERIMENTAL
PREDICTED
NORMALIZED MOMENT
ROTATION (RADIANS)
0
.02
.04
.06
.08
.1
0
.01
.02
.03
.04
.05
.06

Figure A.35

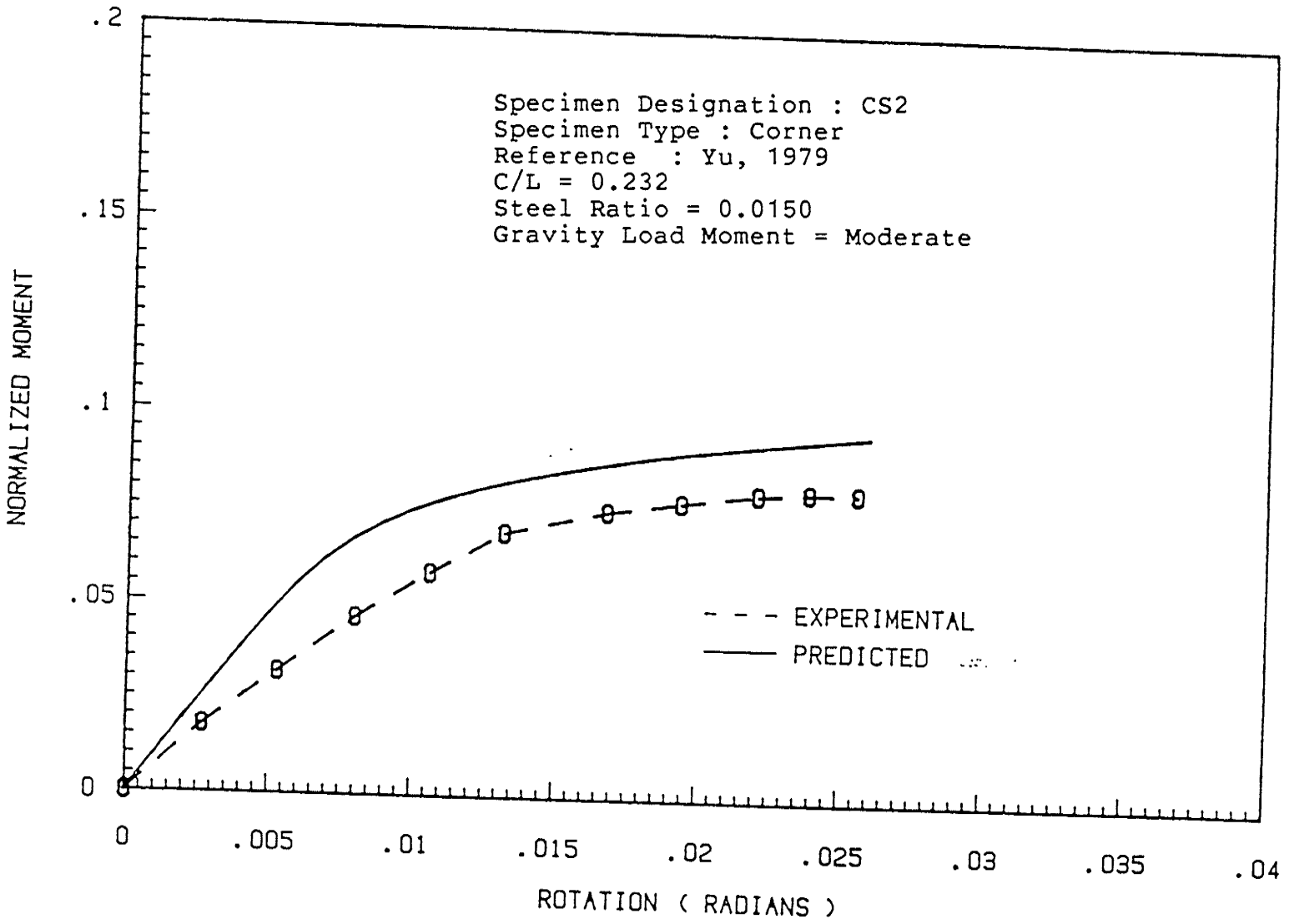
Specimen Designation : CS2
Specimen Type : Corner
Reference : Yu, 1979
C/L = 0.232
Steel Ratio = 0.0150
Gravity Load Moment = Moderate
NORMALIZED MOMENT
.2
.15
.1
.05
0
0
.005
.01
.015
.02
.025
.03
.035
.04
ROTATION (RADIANS)
EXPERIMENTAL
PREDICTED

Figure A.36

Appendix B

COMPUTER PROGRAM USER'S MANUAL

B.1 DESCRIPTION OF PROGRAM

The computer analysis program presented here is capable of performing nonlinear or linearly elastic analysis of laterally loaded flat-plate structures. Column, floor panel and shear wall elements are used to model the structure. To reduce the task of preparing input, simplified formatting is used. Data generation is incorporated wherever possible.

B.2 FORMAT FOR INPUT

With the exception of the title record, all data are entered in ten-column fields. No distinction between real and integer numbers is required. Data may appear anywhere within the field. When SI units are used, member section properties tend to be large. To accommodate these large numbers, the FORTRAN 'E' format may be used. For example, if a column has a St. Venant torsion constant of $700.\times10^{6}$ mm^{4}, this may be entered as 700 E6. The 'E' format can be used for inputing section properties only.

In the text below, defaults indicate the values which the program assigns to the variables if they are not specified in the input data.

B.3 DESCRIPTION OF THE STRUCTURE

The geometry of the structure is described by the global coordinate system X'_1, X'_2, X'_3. The X'_2 axis is vertical; the X'_1-X'_3 plane (X'_2=0.0) is horizontal and contains the structure supports.

The storeys, floors and all the structural elements are numbered from the roof down. Nodes, floor panels and shear walls are input for the roof only. The program generates the nodes and element incidences for all floors below the roof. The program also generates all column incidences from the node data. Figure B.1 shows a typical structure and floor plan.

B.4 INPUT DATA

I) Title Record

80 alpha-numeric characters to be printed as a title over the program output

II) Frame Data

Field	Variable
1	NCL
2	NST
3	EE
4	GG
5	UNITS
6	ANALT

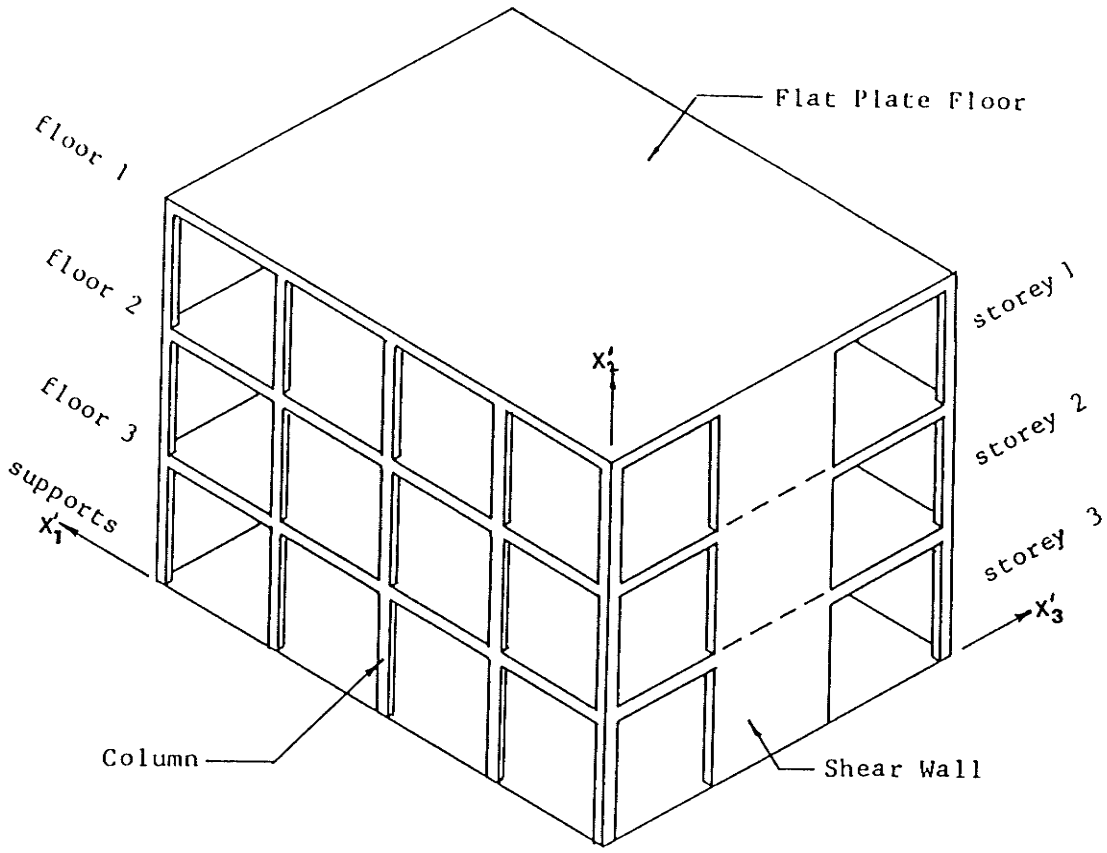

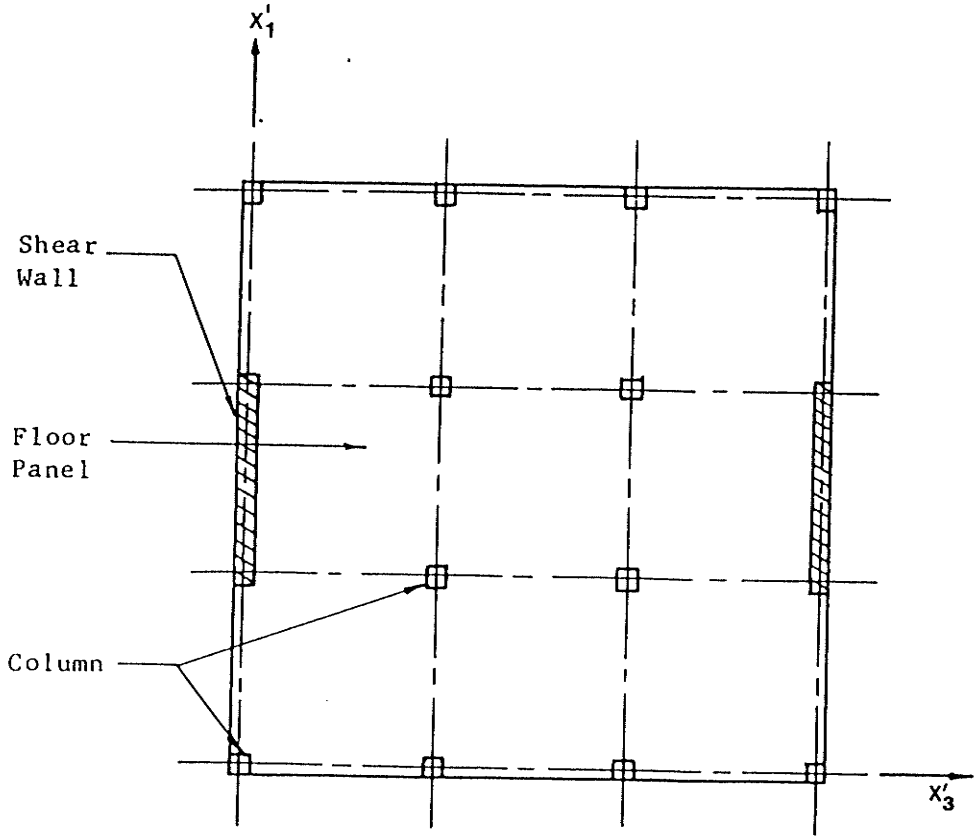

Figure B.1: Typical Flat-Plate Structure

NCL = number of columns per storey

NST = number of storeys

EE = modulus of elasticity for columns (GPa or ksi)

GG = shear modulus for columns (GPa or ksi)

UNITS = system of measurement. If 'BR' appears in field 5, then British units are used. Otherwise the international system of units is used (SI)

ANALT = type of analysis used. If 'NONLINEAR' appears in field 6, then nonlinear analysis is performed. Otherwise linear analysis is performed.

Defaults

EE = 200,000 GPa or 29,000 ksi

GG = 80,000 GPa or 12,000 ksi

ANALT = LINEAR

III) Storey Data

1)

Field	Variable
1	NSCPF
2	NPPF
3	NSWPS
4	MNODE1
5	MNODE2

NSCPF = number of plate-to-column connections per floor

NPPF = number of floor panel elements per floor

NSWPS = number of shear wall elements per storey

MNODE1 = global X'_1 coordinate of master nodes (m or feet)

MNODE2 = global X'_3 coordinate of master nodes (m or feet)

NOTES

1) The master nodes are usually located near the center of the floor plan.

IV) Nodal Data

1)

Field	Variable
1	J
2	X
3	Z
4	KX
5	KZ
6	SX
7	SZ

J = node number

X = global X'_1 coordinate of node J (m or feet)

Z = global X'_3 coordinate of node J (m or feet)

KX = number of bays generated in global X'_1 direction

KZ = number of bays generated in global X'_3 direction

SX = bay span length in global X'_1 direction (m or feet)

SZ = bay span length in global X'_3 direction (m or feet)

DEFAULTS

KX = 0

KZ = 0

i.e., only node j is input

NOTES

1) Only the roof nodes are input. Floors below the roof are generated by the program.

2) Nodes are numbered from the roof down. All nodes in a given floor are numbered consecutively. The number of nodes at each floor level is equal to the number of columns per floor plus one master node.

3) By specifying KX, KZ, SX, and SZ, a grid of nodes may be generated as follows. The first node created is node 'J' and is located at the point (X'_1,X'_3). Additional nodes are generated along a line parallel to the global X'_1 axis until 'KX' bays are formed, each with a span of 'SX'. If 'KZ' is greater than zero, a new line of nodes is created, parallel to the global X'_3 axis and spaced 'SX' from the first line. This continues until 'KZ' bays are formed in the X'_3 direction.

EXAMPLE

Suppose the structure being analyzed has the floor plan shown in Figure B.2. The grid is generated by the following records:

1	0	0	4	3	7.5	7.5
21	15	30	2	1	7.5	7.5

The program numbers the nodes as shown. Nodes 1 through 20 are generated by the first record; the rest by the second record. In this case there are 27 nodes per floor (26 nodes + 1 master node). Note that the master node location has already been specified and is not to be input here.

V) Storey Heights

Field	Variable
1	DHE
2	KS

DHE = storey heights (m or feet)

KS = number of storeys to be generated

DEFAULTS

KS = 1

NOTES

1) Values are entered in order from the roof down.

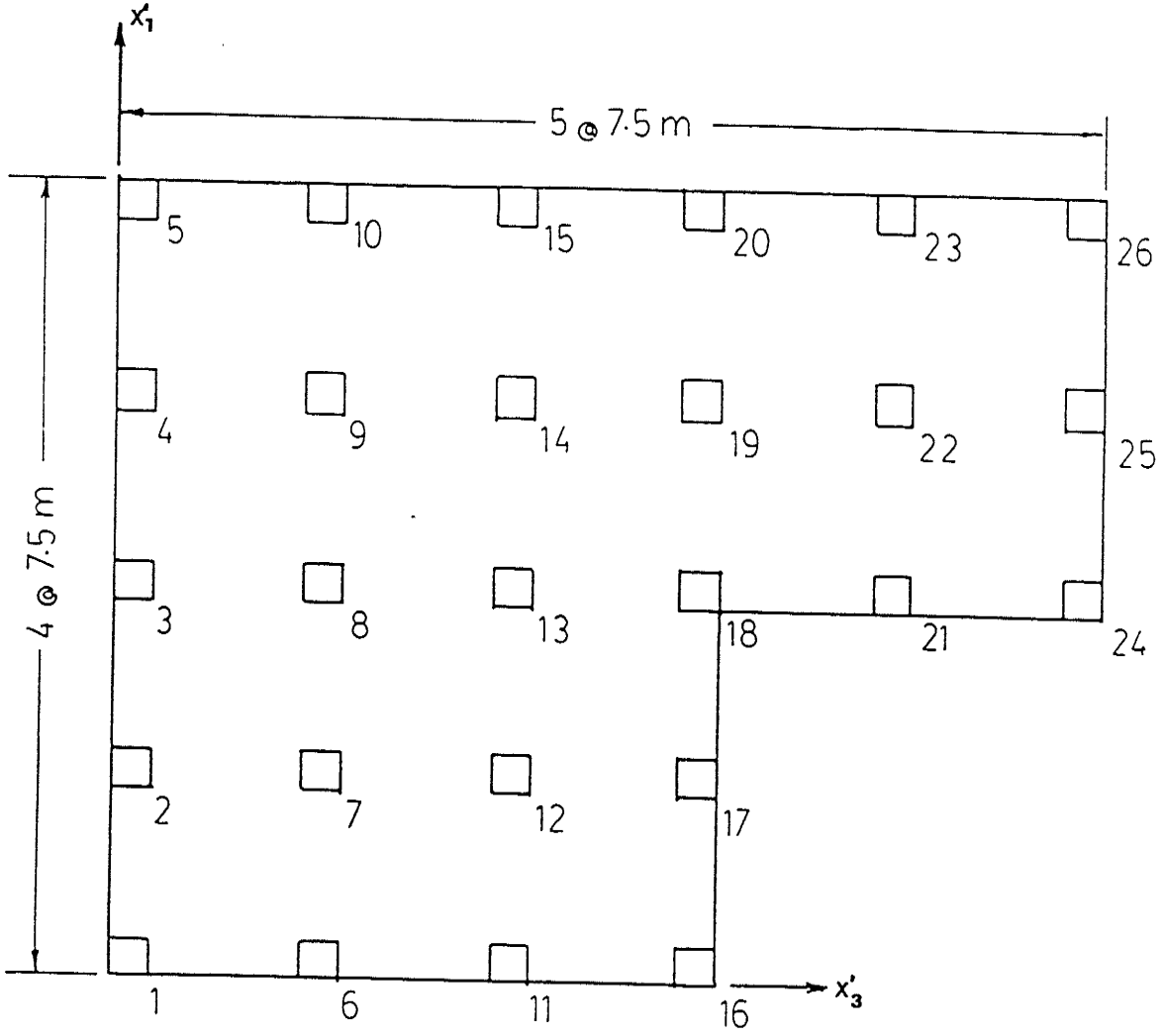

Figure B.2: Example Floor Plan

EXAMPLE

The following records generated the storey heights for the structure show in Figure B.3:

```
3     3
3.5
4     3
```

VI) Column Data

1) Heading Record

Field	Variable
1	'COLUMNS'
2	NCP

COLUMNS = label placed in field 1

NCP = number of column section property types

2) Section Property Records

One record for each section type, entered in order of increasing property number

Field	Variable
1	JX1
2	IX2
3	IX3
4	A
5	C

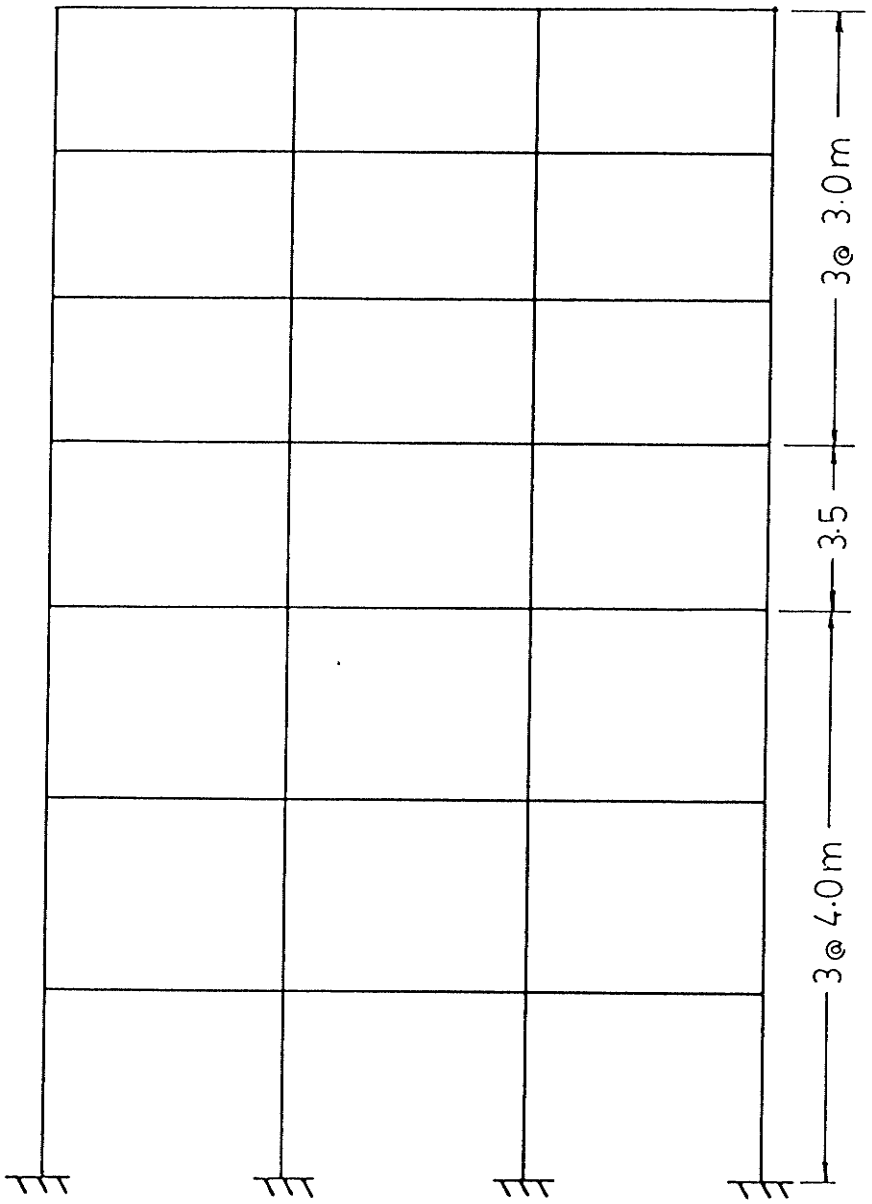

Figure B.3: Example Elevation

JX1 = St. Venant torsion constant (mm^4 or $inch^4$)

IX2 = second moment of area about the local X_2 axis (mm^4 or $inch^4$)

IX3 = second moment of area about the local X_3 axis (mm^4 or $inch^4$)

A = cross-sectional area (mm^2 or $inch^2$)

C = square column width (mm or inch)

3) Column Section Types

- use as many records as necessary
- omit this section if NCP=1

Field	Variable
1	IC
2	ICP
3	NCG
4	INCR

IC = column number

ICP = section type

NCG = number of columns generated

INCR = column increment

DEFAULTS

ICP = 1

NCG = 1

INCR = 1

NOTES

1) The column size is the average of the width and the depth of the column cross-section.

2) The program automatically numbers the columns and calculates their node incidences. Column I of storey J has upper and lower incidences U and L respectively where

$$L = J*(NCL+1)+1$$

$$U = L-(NCL+1)$$

Columns are numbered from the roof down, all columns on a given floor being numbered consecutively.

VII) Floor Data

Omit this section if no panel elements are required.

1) Heading Record

Field	Variable
1	'FLOOR'
2	NFP
3	NFG

FLOOR = label to be placed in field 1

NFP = number of floor property types

NFG = number of floor groups

DEFAULTS

NFP = 1

NFG = 1

2) Floor Property Records

- One record for each floor property type, entered in order of increasing property type

Field	Variable
1	t
2	E
3	ν
4	f_c'

t = floor thickness (mm or feet)

E = modulus of elasticity for floor (GPa or ksi)

ν = Poisson ratio for floor

f_c' = floor concrete strength (MPa or ksi)

DEFAULTS

E = 28 GPa or 4000 ksi

ν = 0.20

f_c' = 30 MPa or 4 ksi

3) Panel Incidence Records

Field	Variable
1	IPNL
2	A
3	B
4	C
5	D

6	NPG
7	INCR

IPNL = panel number

A = node a

B = node b

C = node c

D = node d

NPG = number of panels generated

INCR = node increment

DEFAULTS

NPG = 1

INCR = 1

4) Floor Property Records

- Omit this section if NFG=1

Field	Variable
1	IFLR
2	IFP
3	IFG
4	NFLG

IFLR = floor number

IFP = floor property type

IFG = floor group number

NFLG = number of floors generated

DEFAULT

IFP = 1

IFG = 1

NFLG = 1

NOTES

1) Only the elements on the roof are to be input. Elements in the lower floors are generated automatically.

2) Panels should be numbered in the direction of the building which has the fewest bays in order to minimize storage requirements.

3) When inputing the panel incidences, the nodes must be chosen so that the local coordinate system has the same orientation as the global system (Figure B.4).

4) Generally, the size of columns in a building increases in size from the roof down as the column loads increase. However, the size of columns may be constant over a number of storeys. Whenever the column-depth-to-plate-span ratio is the same or approximately the same, these floors should be grouped together. The program will calculate an average column-depth-to-plate-span ratio to be used for all panel elements in the floor group. This will reduce both run times and costs.

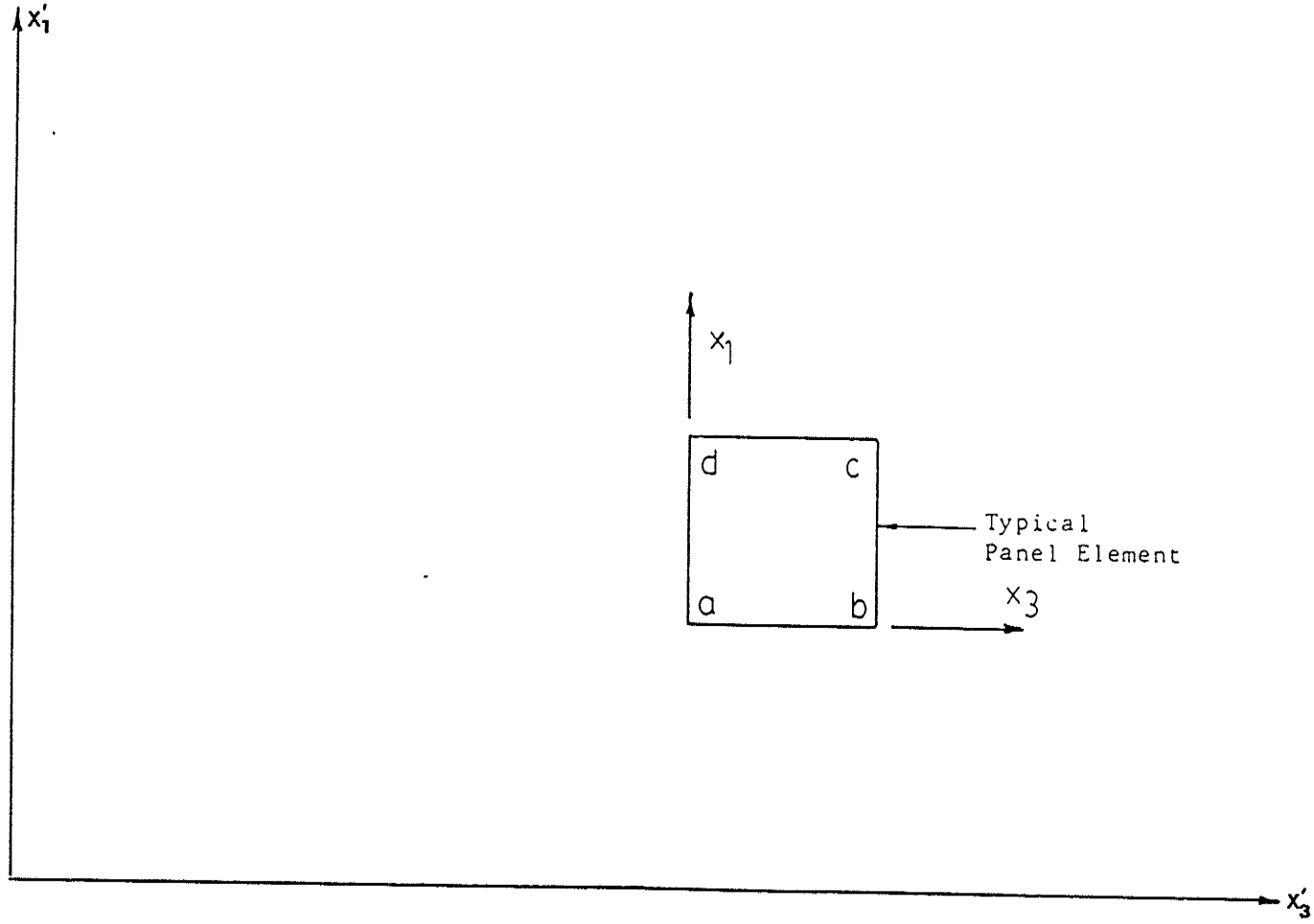

Figure B.4: Panel Coordinate System and Global System

5) All floors in a given floor group must have the same floor properties.

6) Floor groups are numbered consecutively from the roof down.

EXAMPLE

The following records generate the panels for the structure shown in Figure B.5:

1	1	5	6	2	3	1
4	5	9	10	6	3	1
7	9	13	14	10	3	1
10	13	17	18	14	3	1

Note that the panels are numbered in the direction of the fewest panels.

VIII) Shear wall Data

- Omit this section if no shear walls are used

1) Heading Record

Field	Variable
1	'WALLS'
2	NSWP

WALLS = label placed in Field 1

NSWP = number of shear wall property types

DEFAULTS

NSWP = 1

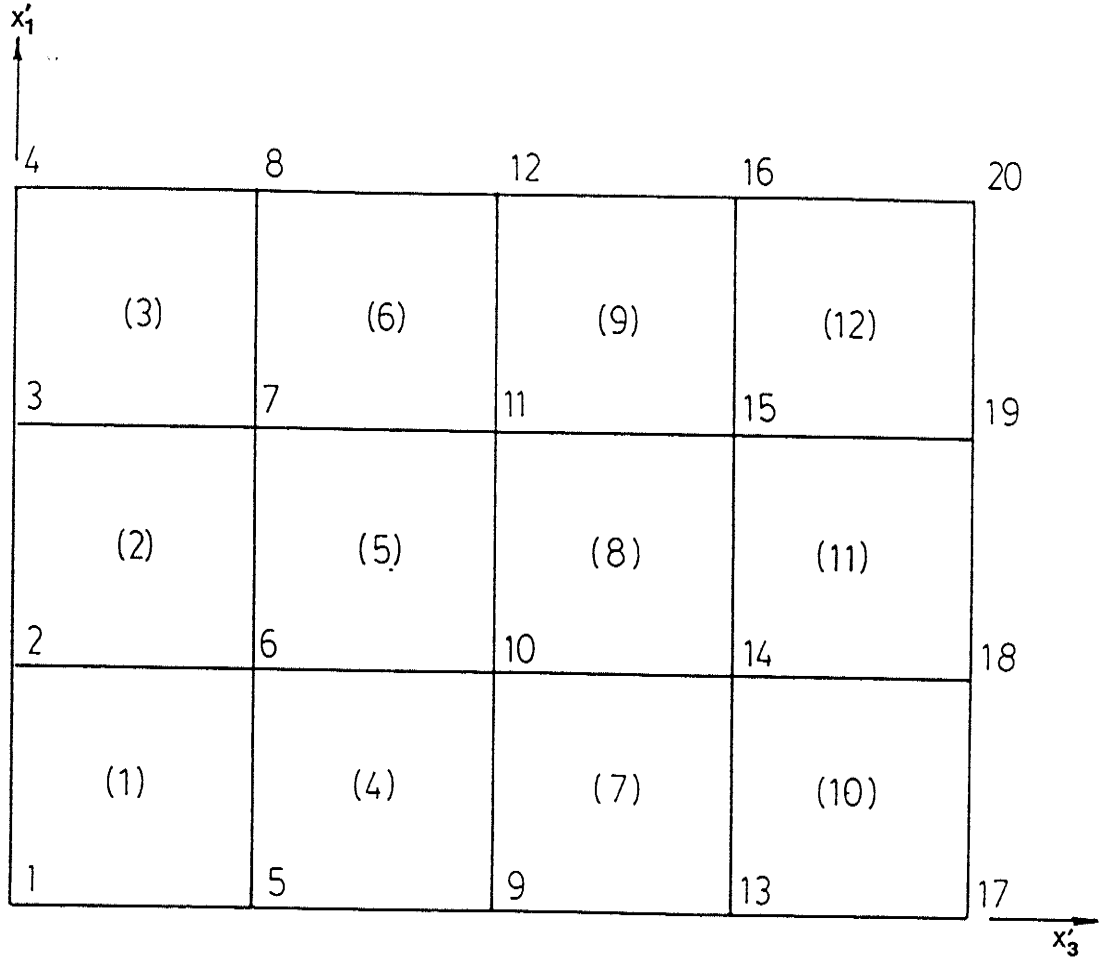

Figure B.5: Roof Joint Numbering

2) Shear Wall Property Records

One record for each property type, entered in order of increasing property type

Field	Variable
1	t
2	E
3	ν

t = shear wall thickness (mm or inch)

E = modulus of elasticity for shear wall (mm^4 or $inch^4$)

γ = Poisson ratio for shear wall

DEFAULTS

E = 28 GPa or 4000 ksi

ν = 0.2

3) Shear Wall Incidence Records

Field	Variable
1	A
2	B

A = node a

B = node b

4) Shear Wall Property Numbers

- Omit this section if NSWP = 1

Field	Variable
1	IW

2	ISWP
3	NWG
4	INCR

IW = shear wall number

ISWP = property number

NWG = number of shear walls generated

INCR = shear wall increment

DEFAULTS

ISWP = 1

NWG = 1

INCR = 1

NOTES

1) Shear walls are input for the top storey only. Walls in lower storeys are generated by the program.

2) Shear walls are numbered from roof down; walls in a given floor are numbered consecutively in the same order as they are input.

3) The local coordinate system for a typical shear wall is shown in Figure B.6.

IX) Load Data

1) Heading Record

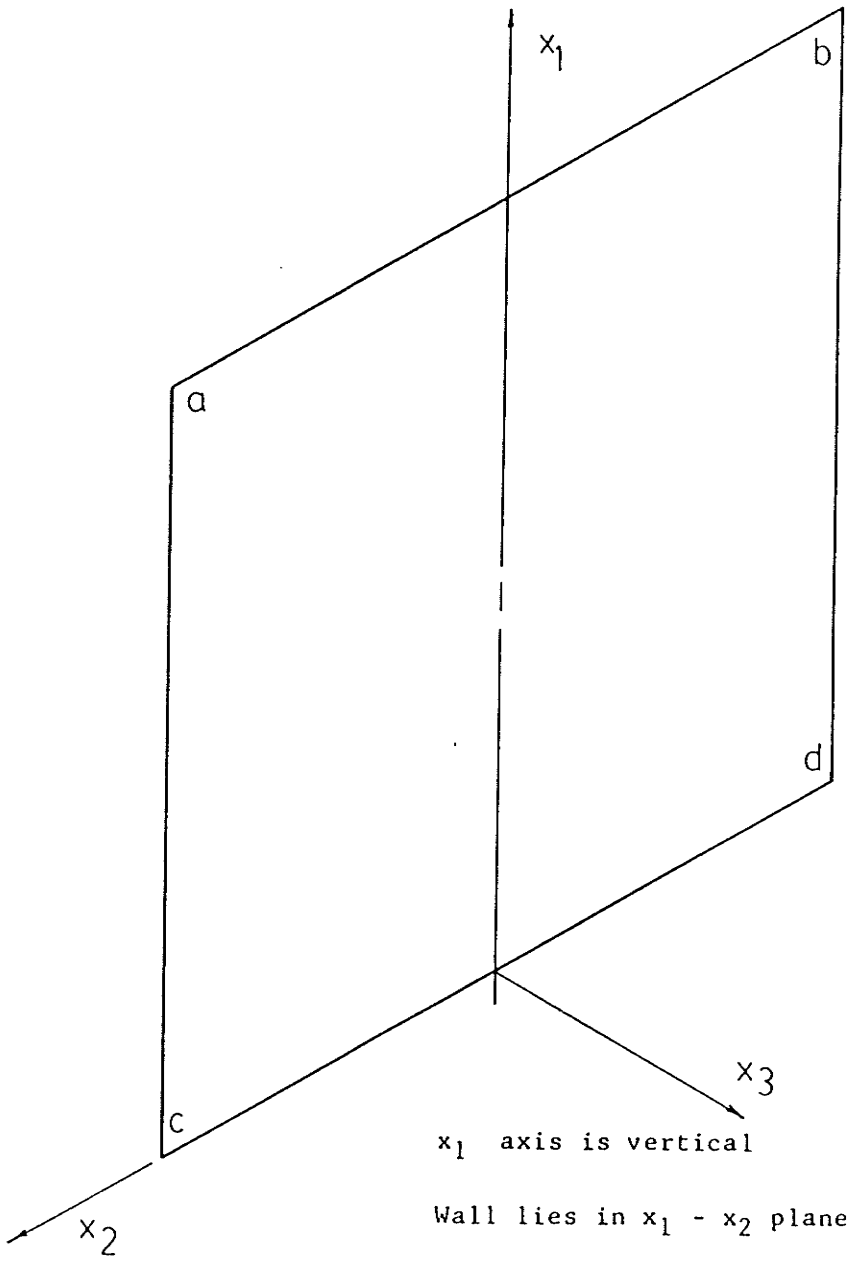

Figure B.6: Shear Wall Local Coordinate System

Field	Variable
1	'LOADS'

LOADS = label placed in Field 1

2) Load Description Records

2 records per loaded node

A) Location Record

Field	Variable
1	NODE
2	NG
3	INCR

NODE = node number

NG = number of nodes generated

INCR = node increment

DEFAULTS

If NG ≤ 1 and INCR=0; NG=1, INCR=1

If NG > 1 and INCR=0; INCR=NCL+1

B) Load Compobnents

Field	Variable
1	PX
2	PY
3	PZ
4	MX
5	MY
6	MZ

PX, PY, PZ = concentrated loads in global X'_1, X'_2, X'_3 directions respectively (kN or kips)

MX, MY, MZ = moment about the global X'_1, X'_2, X'_3 axes respectively (kN-m or foot-kips)

NOTES

1) A node may be referenced more than once to describe the loads at that node.

2) Loads placed on master nodes must not have any PY, MX or MZ components.

3) Loads are positive in the positive global directions. The right hand rule applies to all moments and rotations.

X) Plate-To-Column Connection Data

- Omit this section if the analysis is linear

1) Heading Record

Field	Variable
1	'CONNECTIONS'

CONNECTIONS = label placed in Field 1

2) Connection Property Records

- use as many records as necessary

Field	Variable
1	NFG

2	ROI
3	ROE
4	ROC
5	IGLL

NFG = number of floors to be generated

ROI = reinforcement ratio for interior plate-to-column connections

ROE = reinforcement ratio for edge plate-to-column connections

ROC = reinforcement ratio for corner plate-to-column connections

IGLL = gravity load level. For low gravity load level IGLL=1 for moderate gravity load level IGLL=2, and for high gravity load level IGLL=3.

DEFAULTS

NFG = 1

ROI = 0.01

ROE = 0.01

ROC = 0.01

IGLL = 2

NOTES

1) The total reinforcement ratio should be used (top and Bottom).

2) All connections of the same type have the same reinforcement ratio in a given floor.

XI) Program Mode

Field	Variable
1	PROGRAM MODE

If the word 'SOLVE' is placed in field 1, the program determines the node displacements and element end forces. If the word 'CHECK' is found or if the field is left blank, only the input data is generated. Thus the program can be run at high priority in the 'CHECK' mode until the input data has been debugged. It then can be run at low priority in the 'SOLVE' mode, resulting in significant savings.

Appendix C

TYPICAL PLATE PANEL STIFFNESS COEFFICIENTS

Table C.1 lists the expressions developed to describe floor plate panel stiffness coefficients $K_{1,2}$ through $K_{48,2}$ for column-depth-to-plate-span ratio of 1/8. It can be seen that some of the stiffness coefficients are influenced by one spring flexibility while others are influenced by two spring flexibilities. Similar expressions have been developed for all other stiffness coefficients of the plate panel.

It can be seen from Table C.1 that all stiffness coefficients relating degrees of freedom in different quarters of the plate panel, $K_{19,2}$ for instance, are independant of the eight spring flexibilities FS_1 through FS_8 and therefore are constant. The degrees of freedom I and J referred to in Table C.1 are illustrated in Figure 4.16.

TABLE C.1

Expressions Used For Stiffness Coefficients $K_{I,J}$

I	J	EXPRESSION
1	2	$-29.0 - 18.69\ EXP(-1400\ FS_1)$
2	2	$5.73 + 4.09\ EXP(-2000\ FS_1)$
3	2	$-1.73 - 0.486\ [EXP(-2000\ FS_1) + EXP(-2000\ FS_2)]$
4	2	0.01629
5	2	-0.0003
6	2	-0.00006
7	2	0.0071
8	2	0.00003
9	2	-0.00005
10	2	-0.0229
11	2	-0.00064
12	2	0.00006
13	2	$17.85 + 16.95\ EXP(-1800\ FS_1)$
14	2	$0.580 + 0.500\ EXP(-1800\ FS_1)$
15	2	$0.511 + 0.321\ EXP(-1800\ FS_1)$
16	2	$-0.111 - 0.063\ EXP(-1700\ FS_1)$
17	2	$-0.042 - 0.023\ EXP(-1700\ FS_1)$
18	2	$-0.012 - 0.013\ EXP(-1700\ FS_1)$
19	2	0.0456
20	2	0.0011
21	2	0.0029
22	2	0.0037
23	2	0.0013

Table C.1 continued

I	J	EXPRESSION
24	2	-0.00010
25	2	0.0089
26	2	0.0019
27	2	0.000
28	2	-0.0096
29	2	0.00071
30	2	0.00014
31	2	0.0094
32	2	0.00008
33	2	-0.0019
34	2	0.0127
35	2	0.00001
36	2	-0.0024
37	2	-0.0018
38	2	-0.00021
39	2	-0.00069
40	2	$7.24 + 3.42\ EXP(-1500\ FS_2)$
41	2	$-0.399 - 0.049\ [EXP(-1800\ FS_1) + EXP(-1800\ FS_2)]$
42	2	$-0.140 - 0.102\ [EXP(-1500\ FS_1) + EXP(-1500\ FS_2)]$
43	2	$-0.540 - 0.126\ EXP(-1500\ FS_2)$
44	2	$-0.009 - 0.002\ [EXP(-1300\ FS_1) + EXP(-1300\ FS_2)]$
45	2	$0.245 + 0.005\ [EXP(-1400\ FS_1) + EXP(-1400\ FS_2)]$
46	2	0.0061
47	2	-0.0035
48	2	0.00051